

KRISTOFOLAND VARAZO

The Underpotential Deposition and Surface Characterization of Metal and Chalcogenide Atomic Layers used in Electrochemical Atomic Layer Epitaxy (EC-ALE): Cadmium, Tellurium, and Sulfur
(Under the direction of JOHN L. STICKNEY)

The formation of high quality compound semiconductors is facilitated by controlling growth at the atomic level. Electrochemical atomic layer epitaxy (EC-ALE) has been developed to electrodeposit compound semiconductor thin films one atomic layer at a time, by the sequential underpotential deposition (UPD) of each element from a separate solution, in a cycle. Two important parameters for controlling growth during EC-ALE are the electrode potential and solution composition, which influence the deposit structure and stoichiometry. Studies of the first monolayer of a compound and its constituent elements are the most important; they form the interface between the substrate and deposit, which must accommodate any lattice mismatch, and can greatly influence the substrate morphology of the deposit as it grows. Surface sensitive techniques were used to study the structure and composition of cadmium, tellurium, and sulfur atomic layers, as well as cadmium telluride monolayers on Au(111): Auger electron spectroscopy (AES), low energy electron diffraction (LEED), X-ray photoelectron spectroscopy (XPS), and scanning tunneling microscopy (STM). CdTe formation using a two-step EC-ALE process resulted in the formation of $(\sqrt{7} \times \sqrt{7})R19.1^\circ$ and (3×3) structures with 1:1 and 2:1 stoichiometry, respectively. Both structures were formed using either cadmium or tellurium as a first layer on Au(111). Using a three-step procedure to form cadmium telluride produced the highest quality monolayer, relative to the two-step methods. Ordered cadmium atomic layers were electrodeposited at underpotentials on Au(111), where coadsorbed anions were structure determining, and

served to stabilize the layers from spontaneous oxidation during removal from solution. These layers can be used to form Cd-containing compound semiconductors such as CdTe, CdSe, or CdS using EC-ALE. Ordered sulfur atomic layers were formed on Au(111) from alkaline solutions of sulfide, thiosulfate, and thiourea. A range of solution compositions and electrode potentials were found where the same $1/3$ monolayer $(\sqrt{3} \times \sqrt{3})R30^\circ$ sulfur layer can form, which can be used in an EC-ALE cycle to form compound semiconductors such as ZnS, CdS, and CuInS₂.

INDEX WORDS: EC-ALE, cadmium telluride, cadmium, tellurium, sulfur, ultrahigh vacuum, Au(111), electrochemistry, AES, LEED, XPS, UHV-EC, underpotential deposition

THE UNDERPOTENTIAL DEPOSITION AND SURFACE CHARACTERIZATION
OF METAL AND CHALCOGENIDE ATOMIC LAYERS USED IN
ELECTROCHEMICAL ATOMIC LAYER EPITAXY (EC-ALE):
CADMIUM, TELLURIUM, AND SULFUR

by

KRISTOFOLAND VARAZO

B.S., The University of West Florida, 1993

A Dissertation Submitted to the Graduate Faculty
of The University of Georgia in Partial Fulfillment

of the

Requirements for the Degree

DOCTOR OF PHILOSOPHY

ATHENS, GEORGIA

2001

© 2001

Kristofoland Varazo

All Rights Reserved

THE UNDERPOTENTIAL DEPOSITION AND SURFACE CHARACTERIZATION
OF METAL AND CHALCOGENIDE ATOMIC LAYERS USED IN
ELECTROCHEMICAL ATOMIC LAYER EPITAXY (EC-ALE):
CADMIUM, TELLURIUM, AND SULFUR

by

KRISTOFOLAND VARAZO

Approved:

Major Professor: John L. Stickney

Committee: James L. Anderson
I. Jonathan Amster
Lionel A. Carreira
Thomas E. Johnson

Electronic Version Approved:

Gordhan L. Patel
Dean of the Graduate School
The University of Georgia
December 2001

DEDICATION

To Mande K. Thompson, whom I love, and my parents Harry and Helen Varazo, whose love and help have made this possible. I also dedicate this work to all those who were lost in the terrible tragedy that occurred September 11, 2001.

ACKNOWLEDGMENTS

This work required the help of many people. I owe so much thanks to Mandee Thompson, for her love and support. I also am grateful for the support my parents have provided. I would like to thank my major professor, John Stickney, for his patience, guidance, understanding, and support. He is a fine advisor, and none of this would have been possible without his help. I would also like to thank Drs. James L. Anderson, I. Jonathan Amster, Lionel A. Carreira, and James A. de Haseth for serving on my committee and offering their help. Of course, special acknowledgement needs to go to my coworkers over the years in the Stickney lab: Lisa Colletti, Thomas Sorenson, Robert Herrick, Billy Flowers, John Garvey, Lindell Ward, Raman Vaidyanathan, Marcus Lay, Mkhulu Mathe, Nattapong Srisook, and Madhi Muthuvel. Your opinions, ideas, and assistance have definitely left a big mark on this book. I also thank Brian Melkowits for being a good friend over the years. Finally, I would like to acknowledge Dr. Hiro and P. P. Malloy.

TABLE OF CONTENTS

	Page
ACKNOWLEDGEMENTS.....	v
CHAPTER	
1 INTRODUCTION AND LITERATURE REVIEW	1
Experimental Approaches.....	3
Literature Review.....	16
References.....	32
2 FORMATION OF THE FIRST MONOLAYERS OF CDTE ON AU(111) BY ELECTROCHEMICAL ATOMIC LAYER EPITAXY (EC-ALE): STUDIED BY LEED, AUGER, XPS, AND IN SITU STM.....	44
Abstract.....	45
Introduction.....	46
Experimental.....	48
Results.....	50
Discussion.....	70
Conclusions.....	89
Acknowledgements.....	90
References.....	90

3	CADMIUM UNDERPOTENTIAL DEPOSITION ON AU(111) FROM CHLORIDE, SULFATE, IODIDE, ACETATE, AND PERCHLORATE ELECTROLYTES: ANION INFLUENCE OF OBSERVED STRUCTURES STUDIED BY LEED, XPS, AND AUGER ELECTRON SPECTROSCOPY.....	95
	Abstract.....	96
	Introduction.....	97
	Experimental.....	99
	Results and Discussion	101
	Conclusions.....	159
	References.....	160
4	SULFUR ATOMIC LAYER FORMATION ON GOLD AS A FUNCTION OF POTENTIAL FROM SOLUTIONS OF SULFIDE, THIOSULFATE, THIOUREA, AND ETHANETHIOLATE: STUDIES BY LEED, XPS, AND AUGER ELECTRON SPECTROSCOPY	168
	Abstract.....	169
	Introduction.....	170
	Experimental.....	173
	Results and Discussion	175
	Conclusions.....	222
	References.....	223
5	CONCLUSIONS AND FUTURE STUDIES.....	235
	Future Studies	238
	References.....	240

CHAPTER 1

INTRODUCTION AND LITERATURE REVIEW

Controlling growth at the atomic level facilitates the synthesis of high quality compound semiconductors. Atomic layer epitaxy (ALE) is a technology used to produce thin films and single crystal layers, originally developed to improve the quality of zinc sulfide thin films in electroluminescent displays [1]. The term epitaxy is Greek for “arranged upon,” and refers to the formation of a crystalline layer on a crystalline substrate. The materials are produced one atomic layer at a time using self-limiting saturated surface reactions. The substrate temperature is the primary control during deposition, set at a value low enough to keep the monolayer of atoms or molecules on the surface until reaction in the next step, but high enough to remove any additionally deposited atoms or molecules. The completion of these two steps ideally forms one monolayer of the compound, and the process is repeated until the desired film thickness is reached.

Electrochemical atomic layer epitaxy (EC-ALE) is a method developed to electrodeposit compound semiconductors one monolayer at a time. It is the electrochemical paradigm of atomic layer epitaxy (ALE) or atomic layer deposition (ALD) [2-5]. Instead of substrate temperature, electrode potentials are used to control the deposition of individual atomic layers. The method is based on using surface-limited reactions where only two-dimensional growth occurs, and by alternating the deposition of each element the material is formed layer-by-layer. In electrodeposition surface-limited reactions occur during underpotential deposition (UPD) [6, 7], when an atomic layer of an element deposits onto a second element, copper on gold for example, at a potential more positive (under) than where bulk deposition of the first element occurs. The atomic layer forms as a result of the increased stability of the surface compound compared to

multiple layers of the first element. In EC-ALE, thin films are formed by sequential UPD of each element from a separate solution. The process is automated and can continue to produce a film with the desired film thickness.

This dissertation details the electrodeposition of cadmium, tellurium, and sulfur atomic layers on Au(111), as well as the formation of cadmium telluride monolayers. All of these studies are fundamental to understanding the EC-ALE process. The structure and composition of monolayers of the compound and the individual elements were studied by cyclic voltammetry and ultrahigh vacuum (UHV) based techniques such as Auger electron spectroscopy (AES), X-ray photoelectron spectroscopy (XPS), and low energy electron diffraction (LEED). Some thin layer electrochemical cell (TLEC) and scanning tunneling microscopy (STM) results are also discussed.

Experimental Approaches

The analytical techniques used here included cyclic voltammetry using thin-layer electrochemical cells (TLEC) and UHV-based electron spectroscopies following electrochemistry experiments carried out in an antechamber coupled to a surface analysis chamber. The methods are described below.

Thin Layer Electrochemical cells

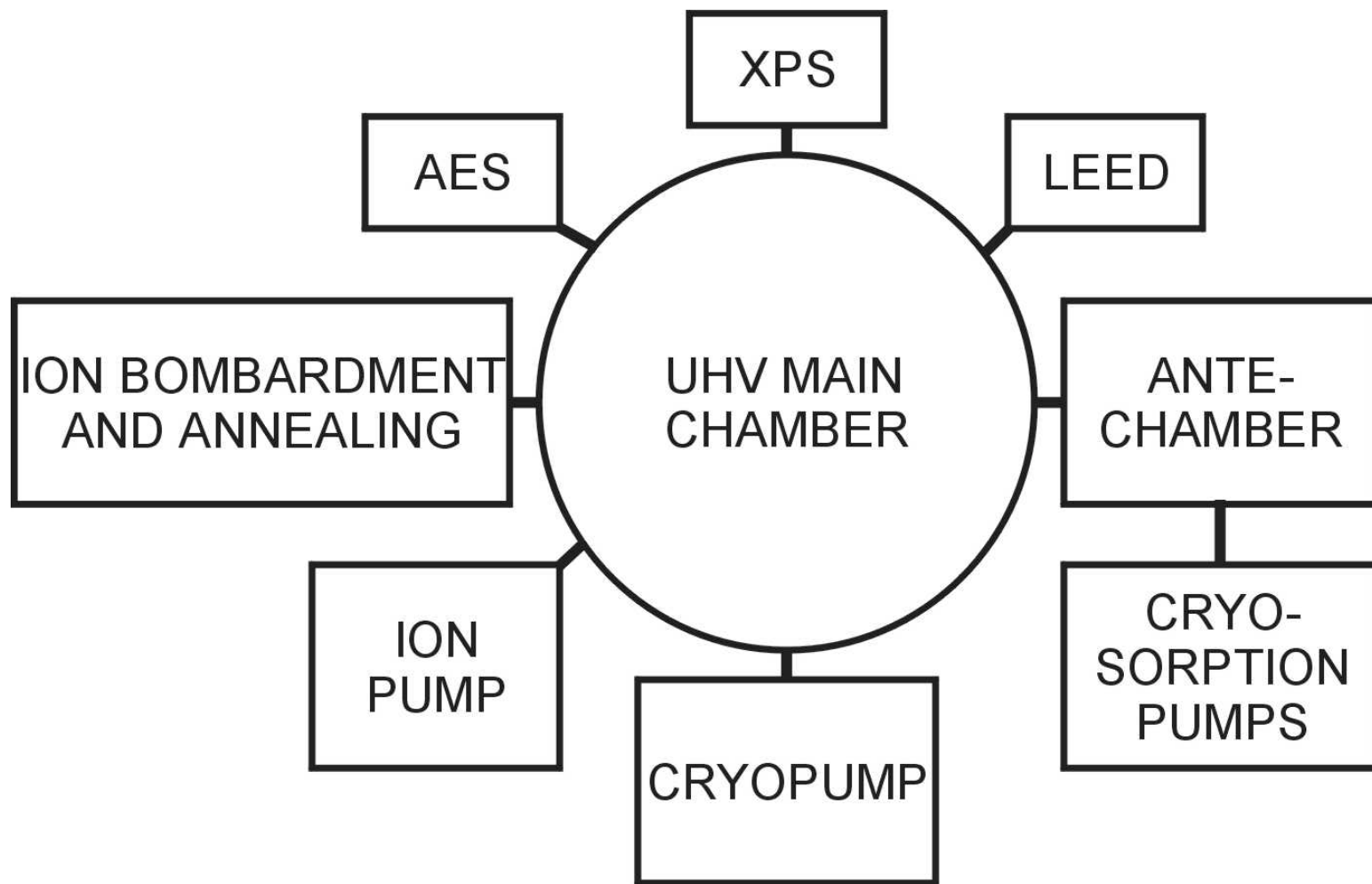
The thin layer electrochemical cell (TLEC) confines reactant species to within micrometers of the electrode surface [8]. Hubbard and Anson have written a comprehensive review of TLEC theory and practice [9]. The TLEC design used for these studies consists of a gold cylinder housed inside a glass cavity with a solution volume that is typically a few microliters. Solutions are expelled from the cavity by nitrogen

purging and enter the cavity by capillary action, allowing a quick and simple way to exchange the solution or rinse the electrode. The cell dimensions and volume provide species in solution direct access to the electrode surface, making the TLEC well suited for coulometric studies. Oxidation and reduction processes proceed to completion in dilute solutions, and quantitative coulometric analysis can be performed to determine the coverage of an element on the electrode surface. Additionally, the small volume of solution used minimizes the accumulation of solution-borne contaminants. Another important advantage of the TLEC is the ability to identify soluble and insoluble species. For example, if an electrochemical process produces an insoluble species on the electrode surface, rinsing out the solution will not remove the species, and its oxidation or reduction in a blank solution can still be observed. If a soluble species is generated, it is rinsed away and does not appear in a blank scan.

Ultrahigh Vacuum-Electrochemistry

Stickney et al. have reviewed ultrahigh vacuum-electrochemistry (UHV-EC) methodology used to study electrode surfaces [10-13]. Figure 1.1 shows a cartoon of the UHV system used in this work. Electrochemical experiments are performed in a stainless steel antechamber connected to the main surface analysis chamber through a gate valve. Before each experiment the single crystal electrode is cleaned in the UHV chamber by argon ion bombardment and subsequently annealed to repair surface damage. The cleanliness and order of the surface is determined by AES and LEED, respectively. The electrode is then transferred to the antechamber without exposure to air using sample manipulators, and the antechamber is isolated from the main chamber and backfilled with

Figure 1.1 Diagram of the ultrahigh vacuum system.

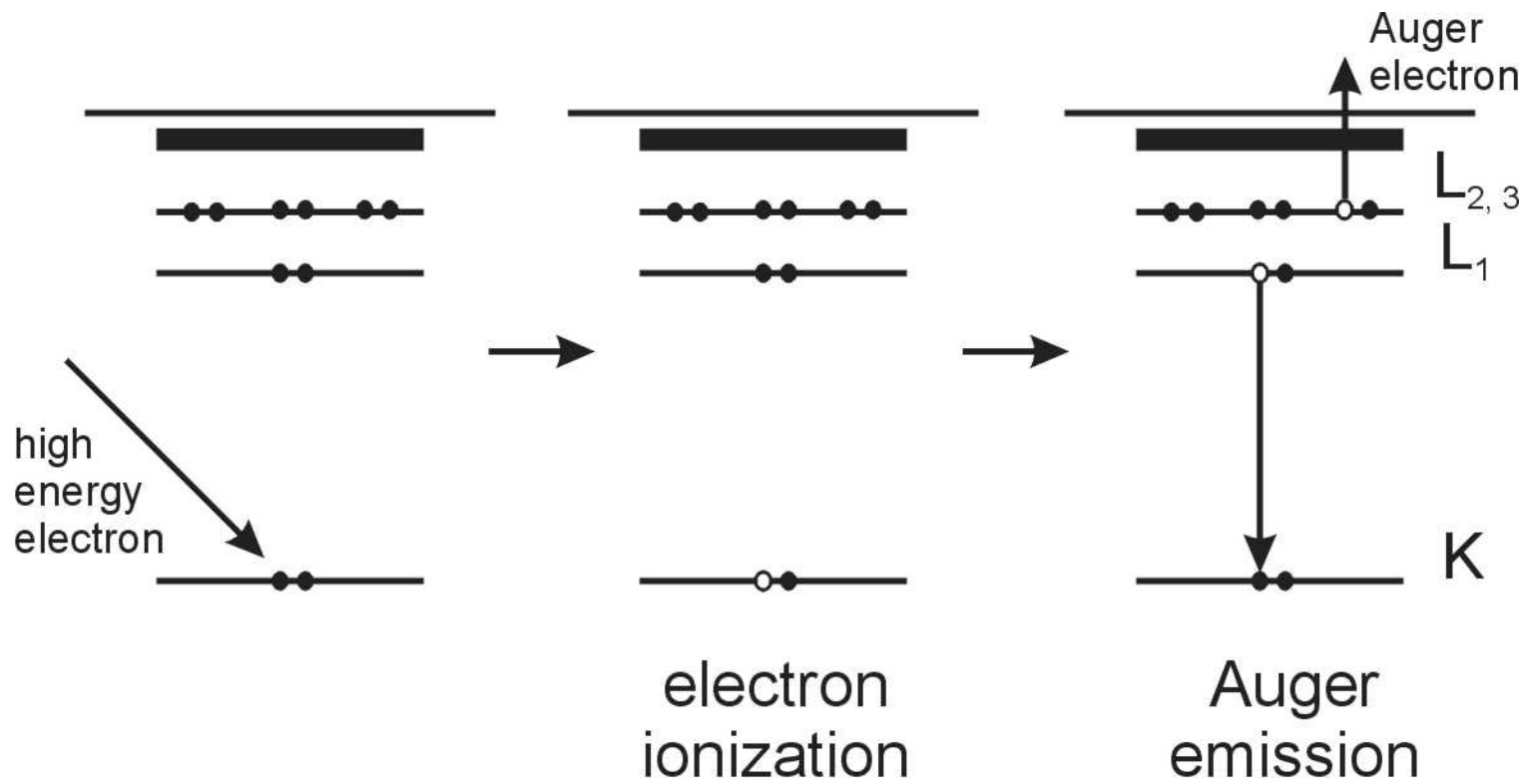


high purity argon. The glass cell containing the reference and auxiliary electrodes is introduced and the electrochemical experiment is performed. After concluding the experiment, the solution is drained and the cell removed. The antechamber is next isolated and pumped to medium vacuum using liquid nitrogen cooled cryosorption pumps and to ultrahigh vacuum pressure using a cryopump. The sample is then transferred back to the main chamber for surface analysis.

The base pressure of the UHV system used is 10^{-9} Torr, which is required to reproducibly prepare a clean surface that stays contamination-free for the duration of a surface characterization experiment. The low pressure also permits using electron spectroscopy techniques without undue interference from gas phase scattering. UHV pressures provide a mean free path for electrons of 5×10^5 m, much longer than the dimensions of the chamber [14]. This ensures that incident electrons are able to reach the sample, and electrons emitted from the sample can reach the detector.

Auger electron spectroscopy (AES) [15, 16] is a surface sensitive technique commonly used to identify the elements present on a surface. The process is shown schematically in Figure 1.2. An energetic electron beam, typically 3-5 kV, is used to produce a core hole in an atom. After ionization, the atom is in a highly excited state and can relax back to a lower energy state by either X-ray fluorescence or the emission of an Auger electron. The probability of Auger emission is overwhelmingly favored over X-ray fluorescence for K and L core levels [14]. These designations come from historic X-ray notation and refer to the 1s and 2s levels, respectively. An electron from a higher energy level fills the core hole, and the energy released is transferred to a second electron, which is ejected from the atom. This Auger electron has a measurable kinetic

Figure 1.2 The Auger process

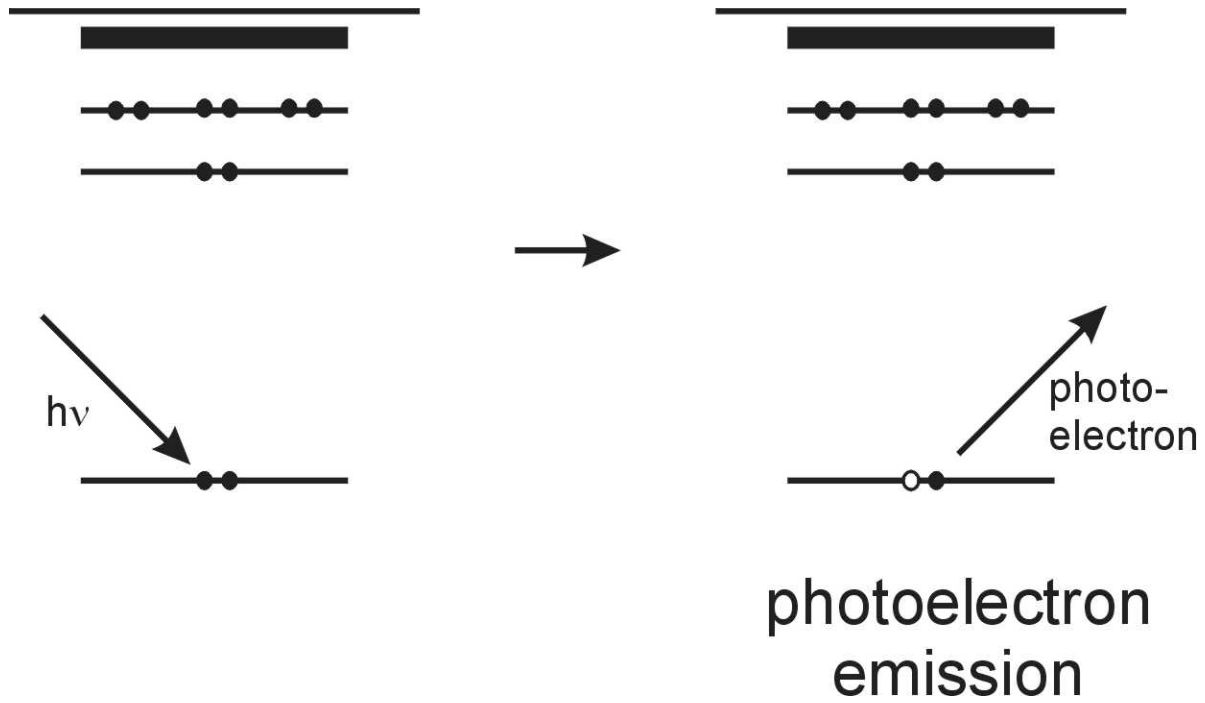


energy and is characteristic of the atom from which it is emitted. The initial ionization is not selective, and for heavier elements there are many combinations of core holes formed, electrons that fill the core hole, and emitted electrons. This yields a characteristic spectrum comprised of a series of peaks at different kinetic energies.

In X-ray photoelectron spectroscopy (XPS) [17-19], Al $K\alpha$ (1486.6 eV) or Mg $K\alpha$ (1253.6 eV) radiation is used to ionize an atom, leading to the emission of a core electron. The process is shown in Figure 1.3. The kinetic energy of the emitted photoelectron is measured using an electron energy analyzer, generating a photoelectron spectrum. The photoelectrons have a characteristic binding energy associated with the core level from which they come, and can be used to identify the elements present at a surface. The binding energy is equal to the incident X-ray energy less the electron kinetic energy. There is a small correction for the work function of the solid, since the binding energy is measured with respect to the Fermi level of the solid instead of the vacuum level [20].

The exact binding energy of an electron also depends on the formal oxidation state of the atom and the local chemical and physical environment. Changes in these cause small shifts in the peak positions known as chemical shifts [21]. The shifts are observable due to the high intrinsic resolution of the technique, because the core levels are discrete and have a well-defined energy. Atoms in higher positive oxidation states produce electrons with higher binding energies due to extra coulombic interaction between the photoelectron and the ion core [22]. This allows for the determination of the oxidation state of an element in addition to its identity, which provides additional information compared to AES.

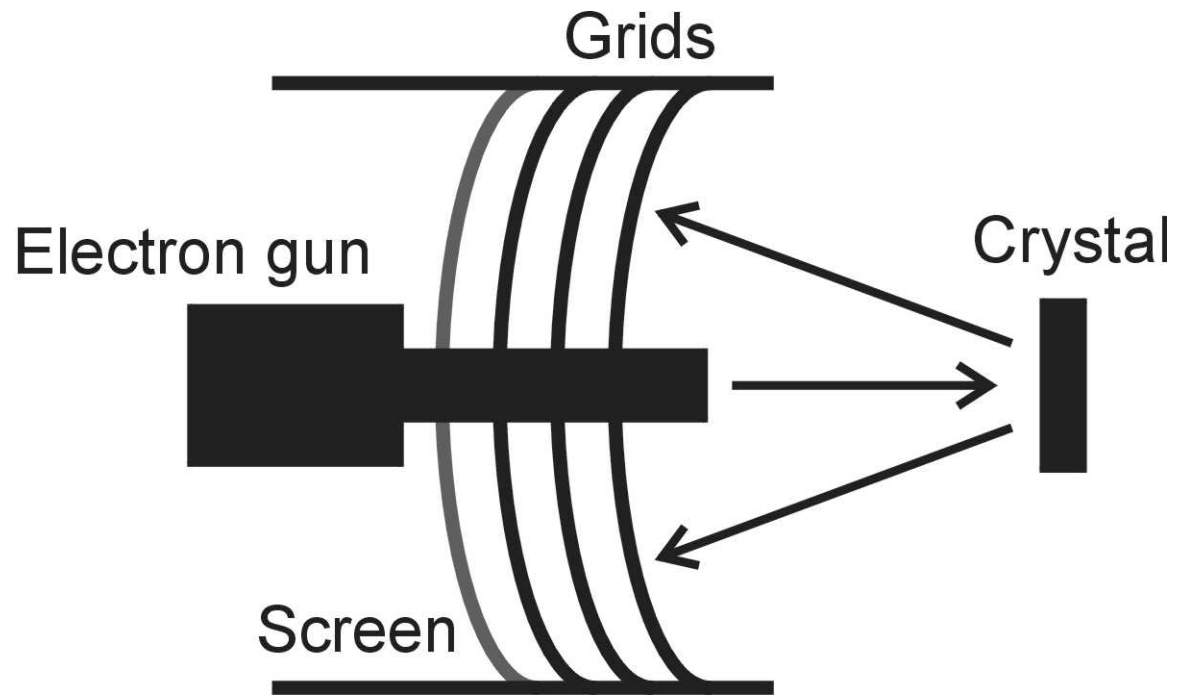
Figure 1.3 The X-ray photoelectron process



Low energy electron diffraction (LEED) is a method for determining two-dimensional surface structure. The experiment uses a low energy beam of electrons, typically 20-200 eV, which strikes a sample at normal incidence. The sample must be a single crystal with a well-ordered surface, and a representative experimental set-up is shown in Figure 1.4 [23]. Only elastically scattered electrons contribute to the backscattered electron diffraction pattern, and energy-filtering grids are placed in front of the fluorescent screen that displays the diffraction pattern to remove lower energy secondary electrons. Employing the principles of wave-particle duality, the electron beam can be considered a succession of electron waves incident normally on the surface. The waves are scattered by surface atoms that act as point scatterers. When the wavefront is backscattered by two adjacent atoms, there is a path difference in the distance the radiation must travel to reach the screen. If this path difference is equal to the product of the interatomic spacing and the angle between the incident and diffracted radiation, constructive interference occurs, producing the observed diffraction pattern [24]. The de Broglie relation gives the electron wavelength λ ; and $\lambda = h/p$, where h is Planck's constant and p is the electron momentum. The wavelengths of the electrons used in LEED are comparable to atomic spacing at the surface. The diffraction pattern reflects the symmetry of the surface structure and an inverse relationship to the size of the surface unit cell [25].

The structural analysis made using UHV-EC is considered an *ex situ* method, since the electrode must be removed from solution, a process called emersion, to be examined using AES, XPS, or LEED. This produces what is termed an emersion layer [26, 27], a thin film of solution on the electrode surface typically 10-30 μm in thickness

Figure 1.4 Diagram of the instrumentation for a LEED apparatus



[28]. It is important to use low concentrations that are millimolar or lower to avoid contributions from the bulk electrolyte, as demonstrated by Kolb and coworkers, who immersed gold single crystal electrodes from sufficiently dilute acid solutions [29]. The relationship between the structure of the solid liquid interface and what is observed in UHV must be established on a case-by-case basis [30]. The use of an in situ method such as scanning tunneling microscopy (STM) is invaluable in providing complementary information [31, 32]. UHV-EC can be helpful in determining the species present on a surface, but LEED generally provides only the unit cell with no information about the basis, the arrangement of the atoms within the unit cell. STM can be used to determine the positions of the atoms in the basis, but not their identity. Taken together, the use of ex situ and in situ techniques provides the best opportunity to obtain structural and compositional information on the particular system under study.

Literature Review

The topics reviewed here consist of the electrodeposition and surface characterization of cadmium, tellurium, and sulfur atomic layers on the low index planes of gold, concentrating on the (111) surface. Anion adsorption on gold surfaces will also be discussed. Studies of compound semiconductor formation by EC-ALE will be included, covering CdTe and other materials. Unless otherwise noted, the STM studies presented and discussed here were performed in situ.

Cadmium electrodeposition

Gewirth and coworkers performed the most detailed surface studies of cadmium underpotential deposition on Au(111) electrodes [33-35]. They used STM to investigate

the atomic structures formed by Cd UPD from sulfuric acid electrolyte. Three ordered adlattices were observed as a function of electrode potential in the UPD region, and each exhibited a linear banded morphology rotated 30° from the substrate lattice direction. The structures resembled reconstructed face-centered cubic (111) surfaces, suggesting that cadmium deposition facilitated the reconstruction of the Au(111) surface. It was not until their second study that they determined the influence of sulfate anions [34]. The ordered structures were not observed in supporting electrolyte that did not contain sulfate, and the sharp voltammetric peaks for cadmium UPD were replaced with a single broad deposition peak. They determined the coverages of cadmium and sulfate to be 0.66 ML and 0.23 ML, respectively, using potential-step chronocoulometry.

Gewirth and coworkers also studied cadmium UPD on Cu(111) using in situ atomic force microscopy (AFM). Using a perchlorate electrolyte, they observed a hexagonal adlattice with 0.343 nm spacing, and assigned it a (4X4)-Cd structure. Anion adsorption was believed not to occur because of the weakly adsorbing nature of perchlorate. When sulfate was used as the anion, no highly ordered structures were observed for cadmium UPD, suggesting that sulfate adsorption precluded obtaining clear AFM images [36].

An ex situ UHV-EC study of cadmium UPD on Cu(111) was performed by Stuhlmann et al. [37], where they identified a $(\sqrt{19} \times \sqrt{19})R23.4^\circ$ structure for cadmium UPD with 9/19 ML coverage. From XPS and low energy ion scattering spectroscopy (LEIS) they determined that coadsorbed chlorine was on top of the cadmium layer, serving to stabilize the open structure.

Alloy formation during cadmium electrodeposition on gold is an important process, and can obscure observation of UPD processes on gold [6]. Schultze and coworkers reported on the temperature and potential dependence of Cd/Au alloy formation as a function of time in 1974 [38, 39]. From cyclic voltammetry, they concluded that alloy formation began in the underpotential region, with a dependence on temperature and polarization times. For short times and low temperatures at large underpotentials, they did not observe the formation of a Cd/Au alloy.

Horányi and Inzelt conducted a more recent study using an electrochemical quartz crystal microbalance (EQCM) [40]. Their work also indicated that alloying occurred in the UPD region. Stripping the deposited cadmium was a slow process, as determined by the frequency response of the EQCM, and resulted in surface roughening. This was accompanied by changes in the amount of adsorbed perchlorate anions on the surface [41].

Vidu and Hara studied cadmium alloying at the Au(100) surface using electrochemical AFM [42-46]. Stripping cadmium deposited at potentials required to form bulk cadmium layers produced small pits covering nearly 30% of the Au surface. Applying a potential 400 mV more positive than the cadmium UPD stripping peak restored the surface. They proposed that the alloying process occurs through a place exchange mechanism, where cadmium atoms replace gold atoms in the lattice, and the pits observed by AFM were due to removing cadmium atoms from the gold lattice. They also observed a $(\sqrt{2} \times \sqrt{2})R45^\circ$ -Cd structure in the UPD region, and noted that it may correspond to an ordered alloy phase, but dissolution of the cadmium layer did not result

in pit formation. The alloying process is thermodynamically but not kinetically favored at room temperature due to the slow diffusion of surface atoms.

Anions are also known to affect alloy formation on gold, and Möller, Magnussen, and Behm examined the effect of chloride anions on copper UPD on Au(110) using in situ STM [47]. Prior to the formation of a (1X1)-Cu layer with full monolayer coverage, a (2X1) structure was observed in the presence of chloride. This structural transition was accompanied by surface roughening, producing gold islands and one-atom deep holes on the electrode surface. In the absence of chloride, no lower coverage structure was observed before the (1X1)-Cu adlayer was formed, and the electrode surface did not undergo any structural change in the UPD region. They concluded that anion induced Cu/Au surface alloying caused the surface roughening.

Anion adsorption

The presence of anions at an electrode surface is a fundamental aspect in studies of the liquid-solid electrolyte interface [6]. Anions form potential dependent ordered atomic layers, are capable of inducing structural changes in a crystalline surface, and influence the structure of electrodeposited metal layers by coadsorption [48]. The following section describes some work in the area of anion adsorption, particularly species that are present in the electrolytes employed for metal UPD.

Iodine adsorption on Au(111) from aqueous solution has been extensively studied by surface sensitive methods [49-54]. $(\sqrt{3} \times \sqrt{3})R30^\circ$ and $(5 \times \sqrt{3})$ unit cells corresponding to iodine atomic layers with 0.33 ML and 0.40 ML coverage, respectively, were observed using LEED and in situ STM [49, 55]. Gao and Weaver have observed in addition a high coverage incommensurate $(7 \times 7)R21.8^\circ$ structure [56], while Tao and Lindsay found a

(3×3) unit cell [53] using STM. Ocko et al. used in situ surface X-ray scattering (SXS) to show that iodine layers undergo electrocompression, a uniaxial compression of the iodine atoms as a function of potential [51]. Itaya and coworkers have investigated the same phenomenon using both LEED and STM, observing diffraction patterns with split spots for the iodine layers [54]. Interestingly, vapor deposited iodine layers on Au(111) also formed unit cells that produced diffraction patterns with the $\sqrt{3}$ spots split into arrangements of three and six [57]. The first structure observed was the 0.33 ML ($\sqrt{3}\times\sqrt{3}$) $R30^\circ$. Increasing the iodine coverage caused the fractional order $\sqrt{3}$ spots to split into a triplet, signifying a change in the unit cell. The highest coverage structure (0.48 ML) was unstable under UHV conditions, and degraded to the intermediate structure containing the triplet of spots.

Ordered chloride and bromide layers formed on Au(111) in aqueous solutions have been studied by in situ SXS [58]. An incommensurate hexagonal close-packed monolayer rotated 30° from the gold lattice was observed for both elements. The layers were also found to compress uniformly when an increasingly positive potential was applied. Obtaining in situ images of chlorine atomic layers on Au(111) by STM has proven difficult, as Uosaki and coworkers were not able to image an ordered chloride layer on this surface in a perchloric acid solution containing chloride ions [59]. Encouragingly, Cuesta and Kolb recently reported ordered chloride and bromide structures on Au(100) from solution in an STM study [60]. The STM micrographs for both elements revealed a distorted hexagonal structure that was comprised of a series of stripes. The distance between stripes decreased when the potential was made more positive, demonstrating that the halide layers undergo uniaxial compression, in excellent

agreement with the SXS data [61]. They found two unit cells for the bromide layers, a commensurate $c(\sqrt{2} \times \sqrt{2})R45^\circ$ and a uniaxially incommensurate $c(\sqrt{2} \times p)R45^\circ$ structure. Only the $c(\sqrt{2} \times p)R45^\circ$ structure was observed for chloride. Tao and Lindsay reported a $(\sqrt{3} \times \sqrt{3})R30^\circ$ -Br unit cell and two other higher coverage hexagonal structures with STM on Au(111) in NaBr solution [53]. An STM investigation of Au(110) in bromide electrolytes by Weaver and coworkers identified several ordered bromine structures [62]. They found (3×1) and (4×1) unit cells for bromine atomic layers with coverages of 0.66 ML and 0.75 ML, respectively, where the bromine atoms resided in the (110) troughs. Another 0.75 ML structure was observed with a hexagonal rather than square packing arrangement. Vapor phase dosing of chlorine on the (111) faces of rhodium, silver, and palladium produced a $(\sqrt{3} \times \sqrt{3})R30^\circ$ -Cl structure [63-65], which is closely related to the layers formed in solution. Kastanas and Koel have reported the formation of a dissociatively adsorbed chlorine layer on Au(111) with a coverage greater than one monolayer produced by gas beam dosing [66].

Sulfate adsorption on the crystalline faces of gold has also been studied, but to a lesser degree than halides. An early UHV study of Au(111) electrodes emersed from sulfuric acid solutions found a $(\sqrt{7} \times \sqrt{7})$ sulfate layer from LEED and AES experiments [67]. The same structure was observed independent of emersion potential, suggesting the presence of an emersed layer of sulfuric acid. Using STM, Magnussen et al. found a $(\sqrt{3} \times \sqrt{7})R19.1^\circ$ unit cell on Au(111) in sulfuric acid [68]. In their model they proposed a 0.40 ML coverage bisulfate layer. Sulfate adsorption occurs at high positive potentials, close to those required for gold oxidation, producing a sharp current spike in the

voltammetry, which has been attributed to a disorder-order phase transition [69, 70]. An infrared spectroscopy and STM study by Weaver and coworkers also found a $(\sqrt{3}\times\sqrt{7})R19.1^\circ$ structure on Au(111) [71]. They concluded that the layer consisted of sulfate molecules with 0.20 ML coverage and coadsorbed hydronium cations. The STM images revealed two types of maxima, or spots, with the larger ones corresponding to sulfate, and the smaller ones assigned to hydronium atoms. Similar STM images obtained for sulfate adsorption on Rh(111) led to the conclusion that the smaller maxima were coadsorbed water molecules [72]. A recent STM study of sulfate adsorption on Au(111) did not observe the $(\sqrt{3}\times\sqrt{7})R19.1^\circ$ structure using a neutral sulfate solution, suggesting that hydronium ions rather than water molecules are incorporated into the structure [70]. A UHV-EC study of sulfate adsorption on Au(111) [73] observed a diffuse $(\sqrt{3}\times\sqrt{3})R30^\circ$ pattern for adsorbed sulfate. They concluded that the sulfate layer does not desorb upon exposure to UHV conditions, and does not contain coadsorbed water or hydronium molecules. The absence of water or hydronium molecules may be why a different unit cell was formed.

The specific adsorption of anions can markedly affect the electrochemical and structural properties of metal electrode surfaces. They play a role in forming and lifting the reconstructions of Au(111) and Au(100) surfaces [74-77]. In acidic sulfate solutions an ordered sulfate structure forms, lifting the Au(100) hex reconstruction and transforming the surface to a (1X1) structure [69]. For Au(111) the $(\sqrt{3}\times\sqrt{3})$ herringbone reconstruction is lifted by the adsorption of bromide, chloride, or sulfate ions [78]. There are many instances in the literature where the coadsorption of anions during the underpotential deposition of metals has been demonstrated [6, 48, 79-84]. One example

is copper UPD on Au(111) [48, 85-96] where a $(\sqrt{3}\times\sqrt{3})R30^\circ$ unit cell has been observed that includes coadsorbed sulfate with a 2:1 ratio of copper to sulfate [93]. Cu UPD on Pt(111) [79, 97-100] is another example. Kolb and coworkers studied the effect of halides on copper UPD on Pt(111) [97], and found three different ordered layers over the entire UPD region using chloride solutions. The first structure observed was a $(\sqrt{3}\times\sqrt{3})R30^\circ$, which has been observed in sulfate electrolytes. XPS results indicated that sulfate was the predominant coadsorbed anion, and they concluded they had a Cu layer with adsorbed sulfate. The source of sulfate was the CuSO_4 salt used to prepare the solution. At more negative potentials, a (4×4) and a $(2\times\sqrt{3})$ were formed, and since a full copper layer was present, they concluded that the structures contained only chloride. They observed (7×7) and $c(7\times\sqrt{3})$ structures in bromide solutions. These results showed that the anions were structure determining, and they also found that anion adsorption added to the faradaic current in the voltammetry, making coverage determinations from simple coulometry inaccurate. Ross et al. reexamined copper UPD on Pt(111) in the presence of chloride using ex situ AES and LEED, and in situ anomalous SXS and rotating ring electrode techniques [101]. They also observed the (4×4) structure by LEED, but in combination with SXS they concluded that the unit cell consisted of both copper and chloride. The real space structure was a hexagonal unit cell with 0.58 ML coverage each for copper and chloride, and closely resembled the (111) plane of zincblende CuCl . There are still more examples, such as palladium and thallium electrodeposition on Au(111), which include coadsorbed chloride and bromide, respectively [102-104]. Radiotracer studies by Horanyi et al. have determined that

chloride and bisulfate anion adsorption accompanies zinc UPD on platinum [105, 106], and copper, cadmium, and silver on gold [41, 107, 108].

Tellurium Atomic Layers

Suggs and Stickney studied the electrodeposition of tellurium atomic layers on the low index planes of gold from acidic sulfate solutions containing TeO_2 using UHV-EC methodology [109, 110]. Tellurium UPD on Au(111) produced two different ordered structures. The first unit cell observed by LEED was a $(\sqrt{3}\times\sqrt{3})R30^\circ$ formed at potentials corresponding to the first tellurium UPD peak. A 0.33 ML (12X12)-Te structure was proposed to account for the $(\sqrt{3}\times\sqrt{3})R30^\circ$ pattern, since the diffraction spots at the $\sqrt{3}$ positions were split. This suggested that the pattern was not produced by a simple $(\sqrt{3}\times\sqrt{3})R30^\circ$ structure, but by one with a much larger unit cell. A second pattern, a (3X3), was observed after scanning to the second UPD peak. A 0.44 ML (3X3)-Te structure was proposed, with Te atoms forming dimer rows. They also used ex situ STM to study the surface structures formed during tellurium UPD on Au(111) [111]. STM images of the surface after depositing tellurium at potentials for the first UPD peak showed large rhombic unit cells of isolated tellurium atoms having dimensions consistent with the proposed (12X12) unit cell, forming rows rotated 30° with respect to the gold atoms and with 0.5 nm interatomic spacing, all indications of a $(\sqrt{3}\times\sqrt{3})R30^\circ$ unit cell. Closer inspection revealed slight variations in the spacing between atoms along the rows, and periodic disruptions such as missing atoms. They concluded that the variations in the atomic positions accounted for the large (12X12) periodicity. Imaging of the (3X3)-Te structure was difficult, as it quickly changed to the (12X12) after a few scans.

Hayden and Nandhakumar performed an STM study of Te UPD on the low index planes of gold, also using acidic TeO₂ solutions [112]. At potentials for the first UPD peak, they observed a structure with spacing close to (12X12) periodicity that possessed a regular pattern of point defects, and the measured interatomic spacing was 0.44 nm, in agreement with the earlier study. In contrast, they determined the coverage to be 0.42 ML, a value higher than previously reported [109, 111]. At potentials just beyond the second UPD peak, they observed a pseudomorphic (1X1)-Te structure with 0.90 ML coverage and 0.31 nm spacing, close to the lattice constant for Au(111). They did not obtain images of the (3X3)-Te structure. Interestingly, in their later STM study of CdTe formation on Au(111) by EC-ALE [113] they observed three domains of a missing row (3X3) structure with a coverage similar to the (12X12) layer when imaging in a solution containing 1 mM CdSO₄ and 10 mM H₂SO₄.

Tellurium atomic layers formed by vapor deposition on Au(111) have been studied using AES and LEED [114]. 99.999% purity elemental tellurium was evaporated from a conical tungsten filament source onto a Au(111) surface at room temperature. Two layers were observed by LEED; the first produced a $(\sqrt{3} \times \sqrt{3})R30^\circ$ pattern with split spots, and had a 0.16 nm nominal thickness. When the film thickness reached 0.17 nm to 0.20 nm, a (3X3) pattern was observed. Depositing additional tellurium caused the (3X3) unit cell to disappear, and a new ring pattern appeared. The atomic layers formed using vapor deposition appear to be the same structures observed using electrodeposition [109, 111], suggesting that EC-ALE is capable of forming the same quality of material as produced by ultrahigh vacuum methods.

Tellurium atomic layer electrodeposition from acidic TeO_2 solutions has even been studied with in situ AFM [115]. Ikemiya et al. observed a $(\sqrt{3}\times\sqrt{3})R30^\circ$ structure for the first tellurium UPD layer, with no indication of the long range periodicity of the (12×12) described by Suggs and Stickney [109, 111]. They successfully imaged the 0.44 ML (3×3) -Te structure reported previously [109, 111]. The formation of bulk tellurium layers was also studied, and the (3×3) structure persisted until approximately five monolayers were deposited. Beyond that amount, deposition resulted in the formation of two different rectangular lattices with different spacing, denoted as a $(3\times(3\sqrt{3}/2))$ -Te and a $c(3\times(3\sqrt{3}/2))$ -Te. Second harmonic generation (SHG) has also been used to study tellurium underpotential and bulk deposition on polycrystalline and Au(111) by monitoring changes in the surface rotational anisotropy [116-118].

The most recent report of electrodeposited tellurium atomic layers on Au(111) provides additional data on this well-studied system [119]. Using STM, the first tellurium structure imaged was a 0.33 ML $(\sqrt{3}\times\sqrt{3})R30^\circ$ structure with an array of domain walls, having (13×13) periodicity. Scanning to more negative potentials caused the structure to change to a less symmetric one, where the domain walls formed rhombi. During the second UPD peak a 0.36 ML $(\sqrt{7}\times\sqrt{13})R19.1^\circ$ -Te unit cell was observed prior to the formation of the (3×3) -Te structure. Forming the higher coverage structures induced a roughening transition, where 40% of the gold surface had pits one atom deep. To account for pit formation, a mechanism was proposed that was similar to the pitting caused by the self-assembly of alkanethiols [120].

Sulfur atomic layers

The characterization of sulfur atomic layers on Au(111) with STM has been studied by several groups. Sulfide oxidation on Au(111) electrodes was studied by Weaver et al. using STM [121]. With potential control in aqueous 0.1 M NaClO₄, 4 mM HClO₄, and 1 mM Na₂S, between -0.4 and -0.1 V (vs. SCE) they observed a ($\sqrt{3}\times\sqrt{3}$)R30° lattice consisting of monomeric sulfur atoms in threefold hollow binding sites, with 1/3 ML coverage. At more negative potentials the Au(111) surface was imaged, indicating that sulfur atoms were desorbed from the surface. At more positive potentials, above -0.1 V, the formation of rectangular eight member sulfur rings (S₈) was predominant. Using surface-enhanced Raman spectroscopy (SERS) [122], they found additional evidence for the existence of S₈ rings, as well as the formation of polysulfides during the formation of bulk sulfur layers. The production of polymeric sulfur species was prevented using sulfide concentrations below 1 mM. In the cyclic voltammetry, there was a small oxidation peak that they ascribed to the oxidation of an adsorbed SH⁻ species at the electrode surface. SERS data showed that the observed bands at 270- and 310-cm⁻¹ were likely due to metal-monoatomic sulfur stretching. The ($\sqrt{3}\times\sqrt{3}$)R30° lattice has also been observed for ordered layers of alkanethiols on Au(111) [123], making the study of sulfur atomic layers important in understanding the formation of self-assembled monolayers (SAMs) [123-132]. Sulfur atomic layer formation on Au(111) has been studied by other groups, namely Shannon et al., who used the layers for the EC-ALE formation of CdS and ZnS compound semiconductors [133-135]. Salvarezza et al. also observed the structures reported by Weaver and coworkers [136-138].

Sulfur oxidative UPD on Ag(111) electrodes has been studied by Foresti and coworkers, who used STM and cyclic voltammetry to determine the structure and coverage of sulfur layers [139]. In alkaline Na₂S solutions, they obtained images for two different structures. At negative potentials, between -1.1 V and -0.9 V (vs. SCE), a ($\sqrt{3} \times \sqrt{3}$)R30° structure was observed with 1/3 ML sulfur coverage, which also forms on Au(111) surfaces. At more positive potentials, a ($\sqrt{7} \times \sqrt{7}$)R19.1° structure was observed, with 3/7 (0.44) ML coverage. The STM micrographs showed a triplet of sulfur atoms at each lattice site. An electrochemical investigation by White et al. also reported a ($\sqrt{7} \times \sqrt{7}$)R19.1° unit cell on Ag(111), but the sulfur coverage determined by EQCM measurements was 0.52 ML [140].

Compound Semiconductors formed by EC-ALE

EC-ALE methodology has been used to form CdS, ZnS, ZnSe, and CdTe on Ag(111) by Foresti et al. [141-144]. They were the first research group to use Ag single crystal substrates for the EC-ALE process. For CdS deposits, coulometric stripping analysis found the stoichiometry to be 1:1, and a ($\sqrt{7} \times \sqrt{7}$)R19.1° unit cell was observed by STM. They proposed a structure containing 1/7 ML coverage each of cadmium and sulfur [142]. In a more recent study using X-ray photoelectron diffraction (XPD) and XPS [145], they determined that the deposit was cadmium-terminated, possessing a wurzite structure with the (0001) plane parallel to the substrate plane. XPS showed that the stoichiometry was 1:1, in agreement with previous coulometric measurements. Stripping analysis of ZnS, ZnSe, and CdTe deposits also showed 1:1 stoichiometry, indicating compound formation [141, 143, 144].

CdSe formation on Au(111) by EC-ALE has been studied using UHV-EC and STM [146-150]. CdSe monolayers were formed by first depositing a UPD layer of selenium on the clean gold surface, followed by cadmium UPD. Two different selenium structures were formed at underpotentials, one with a $(\sqrt{3}\times\sqrt{3})R30^\circ$ $1/3$ ML coverage unit cell, and a close-packed layer of square eight-member selenium rings with $8/9$ ML coverage. Cadmium UPD on the selenium atomic layers produced a (3×3) -CdSe structure, observed by STM, with $4/9$ ML coverage of each element. A $(\sqrt{7}\times\sqrt{7})R19.1^\circ$ -CdSe structure was observed in ex situ experiments using LEED.

Demir and Shannon used EC-ALE to grow CdS monolayers on Au(111) [133, 134]. Using STM they monitored the structural changes that accompanied compound formation. The first atomic layer deposited was a 0.33 ML $(\sqrt{3}\times\sqrt{3})R30^\circ$ -S structure. When cadmium was electrodeposited on the sulfur layer, they observed a (3×3) unit cell, and the monolayer formed was atomically flat over the micrometer scale. They proposed a slightly distorted zincblende structure with an interatomic spacing 4% larger than bulk crystalline CdS. They continued their work using EC-ALE methodology to grow ZnS monolayers on Au(111) [151]. An atomic layer of zinc was deposited on top of a 0.33 ML $(\sqrt{3}\times\sqrt{3})R30^\circ$ -S layer. XPS experiments showed that a layer of sulfate was coadsorbed with the zinc layer. The sulfate was removed chemically by immersion in a sulfide solution, where HS^- ions displaced sulfate, and formed ZnS. STM images revealed a six-fold symmetric structure with sulfur bond distances of 0.37 nm, close to the sulfur spacing for wurtzite ZnS. They determined that a $2:\sqrt{7}$ supercell with a small lattice mismatch of $+0.13\%$ was formed. A complete EC-ALE cycle formed ZnS nanocrystallites randomly across Au(111) terraces. They also reported the formation of a

CdS/HgS heterojunction by EC-ALE [152]. Yoneyama and coworkers have also studied EC-ALE formation of CdS and ZnS on Au(111) [153-155], but did not perform atomic level investigations.

The formation of CdTe monolayers on the low index planes of gold has been studied ex situ and in situ [110, 111, 113]. UHV-EC studies by Suggs and Stickney found $(\sqrt{7}\times\sqrt{7})R19.1^\circ$ and (3×3) unit cells on Au(111) [110]. The layers were formed by cadmium deposition on an existing tellurium atomic layer. The same $(\sqrt{7}\times\sqrt{7})R19.1^\circ$ and (3×3) structures were formed depositing cadmium on either the first or second tellurium UPD atomic layer. Depositing cadmium at potentials close to the beginning of bulk deposition formed the (3×3) . In their subsequent ex situ STM study of this system [111], they obtained images of the $(\sqrt{7}\times\sqrt{7})R19.1^\circ$ structure. They proposed a model structure where cadmium atoms resided on top of two Te atoms, with Cd-Cd distances similar to the Cd-Cd distance (0.46 nm) in a (100) monolayer of zinc blende CdTe. The same bonding geometry was used to construct models for the (110) and (100) planes.

Hayden and Nandhakumar performed the second STM study of CdTe formation by EC-ALE on gold [113]. CdTe monolayers were formed by depositing cadmium on a (12×12) -Te atomic layer. They only obtained in situ images of the hexagonal (3×3) structure. The average Cd-Cd spacing was 0.44 nm, a slight compression compared to the Cd-Cd distance in a CdTe(111) bulk lattice. Cadmium deposition did not disrupt the large and atomically flat terraces of the substrate, indicating that three-dimensional growth did not occur. They concluded that the (3×3) structure was not associated with bulk cadmium deposition, and a stoichiometric monolayer was formed.

The formation and characterization of individual atomic layers of the elements used to form compound semiconductors by EC-ALE has facilitated the production of thin films of the materials. Early studies using TLE electrodes were successful in forming CdTe [156] and CdS [157] deposits. Five EC-ALE cycles were completed for CdS, and the coverages for cadmium and sulfur were determined to be 0.45 ML each. In 1995, the first report of using an automated EC-ALE process to form CdTe deposits more than ten monolayers thick was made [158]. The thin films were grown on polycrystalline gold substrates using a special thin layer flow cell coupled to a computer controlled solution delivery system. Deposits were formed using as many as 150 cycles. Results from inductively coupled plasma atomic emission spectrometry (ICP-AES) and electron probe microanalysis (EPMA) showed the desired 1:1 stoichiometry, but the deposits exhibited a rough morphology due to elemental tellurium and CdTe particles on the surface. There were also bubbles in the deposition cell and gasket effects that adversely affected the morphology. Changing the deposition program and apparatus hardware improved the deposit morphology. In a later study [159], the deposition cell was changed to a modified H-cell employing a thick layer design to overcome the problems with the gasket and bubbles encountered with the first generation flow cell. The optimal deposition potentials for cadmium and tellurium during CdTe thin film growth were systematically investigated. When the cadmium deposition potential was too positive CdTe did not form, and when the potential was too negative bulk cadmium was deposited, leading to three-dimensional growth of Cd-enriched CdTe films. At intermediate potentials, there was a plateau where good quality deposits formed. CdSe and CdS thin films have also been formed with the same deposition system [160]. Grazing incidence X-ray diffraction

(XRD) experiments showed that the films, which were grown on Au-coated Si(100) substrates, had a cubic structure with a predominant (111) orientation. Scanning electron microscopy (SEM) showed that thin films formed using less than 200 cycles were smooth, but with 500 or more cycles the morphology degraded, as particulates and crystallites became increasingly prevalent on the surface. Excess chalcogenide was believed to cause of the surface roughening. Villegas and Napolitano constructed a continuous flow system based on a wall-jet design to produce high quality CdTe thin films [161]. Energy dispersive X-ray analysis indicated stoichiometric growth, and scanning electron microscopy (SEM) results showed that the film morphology followed the orientation of the substrate, indicative of epitaxial growth. Transmission electron microscopy (TEM) revealed atomic domains between 10 and 100 nm in size. The use of EC-ALE methodology continues to grow, as there are recent reports of forming III-V compound semiconductors such as InAs and InAs/InSb superlattices on gold [162, 163].

References

1. T. Suntola, Mater. Sci. Rep. 4 (1989) 261.
2. T. F. Kuech, P. D. Dapkus, and Y. Aoyagi, Atomic Layer Growth and Processing, Materials Research Society, Pittsburgh, 1991.
3. C. H. L. Goodman and M. V. Pessa, J. Appl. Phys. 60 (1986) R65.
4. M. A. Tischler and S. M. Bedair, J. Cryst. Growth 77 (1986) 89.
5. L. Niinisto and M. Leskela, Thin Solid Films 225 (1993) 130.

6. D. M. Kolb, in: H. Gerischer and C. W. Tobias (Eds.), *Advances in Electrochemistry and Electrochemical Engineering*, Wiley & Sons, New York, 1978, p. 125.
7. K. Juttner and W. J. Lorenz, *Z. Phys. Chem. (Wiesbaden)* 122 (1980) 163.
8. A. T. Hubbard, *CRC Crit. Rev. Anal. Chem.* 3 (1973) 201.
9. A. T. Hubbard and F. C. Anson, *Electroanal. Chem.* 4 (1970) 129.
10. M. P. Soriaga, D. A. Harrington, J. L. Stickney, and A. Wieckowski, in: B. E. Conway, J. O. Bockris, and R. E. White (Eds.), *Modern Aspects of Electrochemistry*, Plenum Press, New York, 1995, p. 1.
11. D. M. Kolb, *Z. Phys. Chem. Neue Fol.* 154 (1987) 179.
12. D. M. Kolb, *J. Vac. Sci. Technol., A* 4 (1986) 1294.
13. D. M. Kolb, *Angew. Chem., Int. Ed. Engl.* 40 (2001) 1162.
14. D. Briggs and M. P. Seah, eds., *Practical Surface Analysis*, John Wiley and Sons, Ltd., Chichester, 1983.
15. P. Auger, *Surf. Sci.* 48 (1975) 1.
16. P. Auger, *J. Phys., Colloq.* (1987) C9.
17. C. Nordling, E. Sokolowski, and K. Siegbahn, *Phys. Rev.* 105 (1957) 1676.
18. T. A. Carlson, *X-ray Photoelectron Spectroscopy*, Dowden Hutchinson & Ross, Stroudsburg, Pa., 1978.
19. S. Hagstrom, C. Nordling, and K. Siegbahn, *Phys. Letters* 9 (1964) 235.
20. J. F. Moulder, W. F. Stickle, P. E. Soble, and K. D. Bomben, *Handbook of X-ray Photoelectron Spectroscopy*, Perkin-Elmer Corporation, Eden Prairie, 1992.

21. T. L. Barr, MODERN ESCA The Principles and Practice of X-Ray Photoelectron Spectroscopy, CRC Press, Inc., Boca Raton, 1994.
22. K. Siegbahn, C. Nordling, G. Johansson, J. Hedman, P. F. Heden, K. Hamrin, U. Gelius, T. Bergmark, L. O. Werme, R. Manne, and Y. Baer, ESCA [Electron Spectroscopy for Chemical Analysis] Applied to Free Molecules, 1970.
23. L. C. Feldman and J. W. Mayer, Fundamentals of Surface and Thin Film Analysis, PTR Prentice-Hall, Englewood Cliffs, 1986.
24. L. J. Clarke, Surface Crystallography- An Introduction to Low Energy Electron Diffraction, John Wiley and Sons, Chichester, 1985.
25. G. Ertl and J. Küppers, Low Energy Electrons and Surface Chemistry, VCH Publishers, Weinheim, 1985.
26. W. N. Hansen, C. L. Wang, and T. W. Humphreys, J. Electroanal. Chem. Interfacial Electrochem. 93 (1978) 87.
27. F. T. Wagner and P. N. Ross, Jr., J. Electrochem. Soc. 130 (1983) 1789.
28. P. N. Ross and F. T. Wagner, Adv. Electrochem. Electrochem. Eng. 13 (1985) 69.
29. M. S. Zei, G. Lehmpfuhl, and D. M. Kolb, Surf. Sci. 221 (1989) 23.
30. P. N. Ross, in: J. Lipkowski and P. N. Ross (Eds.), Structure of Electrified Interfaces, VCH Publishers, Inc., New York, 1993, p. 35.
31. M. P. Soriaga, K. Itaya, and J. L. Stickney, in: W. J. Lorenz and W. Plieth (Eds.), Electrochemical Nanotechnology: In-situ Local Probe Techniques at Electrochemical Interfaces, Wiley-VCH, Weinheim, 1998, p. 56.
32. J. Inukai, Y. Osawa, M. Wakisaka, K. Sashikata, Y. G. Kim, and K. Itaya, J. Phys. Chem. B 102 (1998) 3498.

33. J. C. Bondos, A. A. Gewirth, and R. G. Nuzzo, *J. Phys. Chem.* 100 (1996) 8617.
34. B. K. Niece and A. A. Gewirth, *Langmuir* 13 (1997) 6302.
35. S. J. Hsieh and A. A. Gewirth, *Langmuir* 16 (2000) 9501.
36. M. H. Ge and A. A. Gewirth, *Surf. Sci.* 324 (1995) 140.
37. C. Stuhlmann, Z. Park, C. Bach, and K. Wandelt, *Electrochim. Acta* 44 (1998) 993.
38. J. W. Schultze, F. D. Koppitz, and M. M. Lohrengel, *Ber. Bunsenges. Phys. Chem.* 78 (1974) 1253.
39. J. W. Schultze, F. D. Koppitz, and M. M. Lohrengel, *Ber. Bunsenges. Phys. Chem.* 78 (1974) 693.
40. G. Inzelt and G. Horanyi, *J. Electroanal. Chem.* 491 (2000) 111.
41. G. Horanyi, *J. Solid State Electrochem.* 4 (2000) 177.
42. R. Vidu and S. Hara, *J. Electroanal. Chem.* 475 (1999) 171.
43. R. Vidu and S. Hara, *Surf. Sci.* 452 (2000) 229.
44. R. Vidu and S. Hara, *J. Vac. Sci. Technol., B* 17 (1999) 2423.
45. R. Vidu and S. Hara, *Electrochemistry* 67 (1999) 1240.
46. R. Vidu and S. Hara, *Scr. Mater.* 41 (1999) 617.
47. F. A. Moller, O. M. Magnussen, and R. J. Behm, *Phys. Rev. B: Condens. Matter* 51 (1995) 2484.
48. E. Herrero, L. J. Buller, and H. D. Abruna, *Chem. Rev.* 101 (2001) 1897.
49. B. G. Bravo, S. L. Michelhaugh, M. P. Soriaga, I. Villegas, D. W. Suggs, and J. L. Stickney, *J. Phys. Chem.* 95 (1991) 5245.
50. R. L. McCarley and A. J. Bard, *J. Phys. Chem.* 95 (1991) 9618.

51. B. M. Ocko, G. M. Watson, and J. Wang, *J. Phys. Chem.* 98 (1994) 897.
52. T. Yamada, N. Batina, and K. Itaya, *J. Phys. Chem.* 99 (1995) 8817.
53. N. J. Tao and S. M. Lindsay, *J. Phys. Chem.* 96 (1992) 5213.
54. T. Yamada, N. Batina, and K. Itaya, *Surf. Sci.* 335 (1995) 204.
55. W. Haiss, J. K. Sass, X. Gao, and M. J. Weaver, *Surf. Sci.* 274 (1992) L593.
56. X. P. Gao and M. J. Weaver, *J. Am. Chem. Soc.* 114 (1992) 8544.
57. S. A. Cochran and H. H. Farrell, *Surf. Sci.* 95 (1980) 359.
58. O. M. Magnussen, B. M. Ocko, R. R. Adzic, and J. X. Wang, *Phys. Rev. B: Condens. Matter* 51 (1995) 5510.
59. S. Ye, C. Ishibashi, and K. Uosaki, *Langmuir* 15 (1999) 807.
60. A. Cuesta and D. M. Kolb, *Surf. Sci.* 465 (2000) 310.
61. B. M. Ocko, O. M. Magnussen, J. X. Wang, and T. Wandlowski, *Phys. Rev. B* 53 (1996) R7654.
62. S. Z. Zou, X. P. Gao, and M. J. Weaver, *Surf. Sci.* 452 (2000) 44.
63. A. G. Shard, V. R. Dhanak, and A. Santoni, *Surf. Sci.* 429 (1999) 279.
64. A. G. Shard and V. R. Dhanak, *J. Phys. Chem. B* 104 (2000) 2743.
65. A. G. Shard, V. R. Dhanak, and A. Santoni, *Surf. Sci.* 445 (2000) 309.
66. G. N. Kastanas and B. E. Koel, *Appl. Surf. Sci.* 64 (1993) 235.
67. M. S. Zei, D. Scherson, G. Lehmpfuhl, and D. M. Kolb, *J. Electroanal. Chem.* 229 (1987) 99.
68. O. M. Magnussen, J. Hagebock, J. Hotlos, and R. J. Behm, *Faraday Discuss.* (1992) 329.
69. M. Kleinert, A. Cuesta, L. A. Kibler, and D. M. Kolb, *Surf. Sci.* 430 (1999) L521.

70. A. Cuesta, M. Kleinert, and D. M. Kolb, *Phys. Chem. Chem. Phys.* 2 (2000) 5684.
71. G. J. Edens, X. P. Gao, and M. J. Weaver, *J. Electroanal. Chem.* 375 (1994) 357.
72. L. J. Wan, S. L. Yau, and K. Itaya, *J. Phys. Chem.* 99 (1995) 9507.
73. P. Mrozek, M. Han, Y. E. Sung, and A. Wieckowski, *Surf. Sci.* 319 (1994) 21.
74. X. P. Gao, A. Hamelin, and M. J. Weaver, *Phys. Rev. Lett.* 67 (1991) 618.
75. X. P. Gao, A. Hamelin, and M. J. Weaver, *J. Chem. Phys.* 95 (1991) 6993.
76. D. M. Kolb, *Prog. Surf. Sci.* 51 (1996) 109.
77. D. M. Kolb, in: J. Lipkowsky and P. N. Ross (Eds.), *Structure of Electrified Interfaces*, VCH Publishers, Inc., New York, 1993, p. 65.
78. D. M. Kolb and J. Schneider, *Electrochim. Acta* 31 (1986) 929.
79. R. Gomez, H. S. Yee, G. M. Bommarito, J. M. Feliu, and H. D. Abruna, *Surf. Sci.* 335 (1995) 101.
80. L. J. Buller, E. Herrero, R. Gomez, J. M. Feliu, and H. D. Abruna, *J. Chem. Soc., Faraday Trans.* 92 (1996) 3757.
81. M. Wilms, P. Broekmann, M. Krufft, Z. Park, C. Stuhlmann, and K. Wandelt, *Surf. Sci.* 404 (1998) 83.
82. H. D. Abruna, J. M. Feliu, J. D. Brock, L. J. Buller, E. Herrero, J. Li, R. Gomez, and A. Finnefrock, *Electrochim. Acta* 43 (1998) 2899.
83. P. Broekmann, M. Wilms, M. Krufft, C. Stuhlmann, and K. Wandelt, *J. Electroanal. Chem.* 467 (1999) 307.
84. L. J. Buller, E. Herrero, R. Gomez, J. M. Feliu, and H. D. Abruna, *J. Phys. Chem. B* 104 (2000) 5932.

85. Y. Nakai, M. S. Zei, D. M. Kolb, and G. Lehmpfuhl, *Ber. Bunsenges. Phys. Chem.* 88 (1984) 340.
86. M. S. Zei, Y. Nakai, D. M. Kolb, and G. Lehmpfuhl, *Acta Crystallogr., Sect. A* 40 (1984) C387.
87. M. S. Zei, G. Qiao, G. Lehmpfuhl, and D. M. Kolb, *Ber. Bunsenges. Phys. Chem.* 91 (1987) 349.
88. O. M. Magnussen, J. Hotlos, R. J. Nichols, D. M. Kolb, and R. J. Behm, *Phys. Rev. Lett.* 64 (1990) 2929.
89. R. J. Nichols, D. M. Kolb, and R. J. Behm, *J. Electroanal. Chem.* 313 (1991) 109.
90. O. M. Magnussen, J. Hotlos, G. Bettel, D. M. Kolb, and R. J. Behm, *J. Vac. Sci. Technol., B* 9 (1991) 969.
91. N. Batina, T. Will, and D. M. Kolb, *Faraday Discuss.* (1992) 93.
92. W. Haiss, D. Lackey, J. K. Sass, H. Meyer, and R. J. Nichols, *Chem. Phys. Lett.* 200 (1992) 343.
93. Z. C. Shi and J. Lipkowski, *J. Electroanal. Chem.* 365 (1994) 303.
94. M. F. Toney, J. N. Howard, J. Richer, G. L. Borges, J. G. Gordon, and O. R. Melroy, *Phys. Rev. Lett.* 75 (1995) 4472.
95. J. Hotlos, O. M. Magnussen, and R. J. Behm, *Surf. Sci.* 335 (1995) 129.
96. J. Zhang, Y. E. Sung, P. A. Rikvold, and A. Wieckowski, *J. Chem. Phys.* 104 (1996) 5699.
97. R. Michaelis, M. S. Zei, R. S. Zhai, and D. M. Kolb, *J. Electroanal. Chem.* 339 (1992) 299.
98. N. Markovic and P. N. Ross, *Langmuir* 9 (1993) 580.

99. P. N. Ross and N. Markovic, *Langmuir* 10 (1994) 976.
100. N. M. Markovic, C. A. Lucas, H. A. Gasteiger, and P. N. Ross, *Surf. Sci.* 372 (1997) 239.
101. N. M. Markovic, H. A. Gasteiger, C. A. Lucas, I. M. Tidswell, and P. N. Ross, *Surf. Sci.* 335 (1995) 91.
102. L. A. Kibler, M. Kleinert, R. Randler, and D. M. Kolb, *Surf. Sci.* 443 (1999) 19.
103. J. X. Wang, I. K. Robinson, and R. R. Adzic, *Surf. Sci.* 413 (1998) 374.
104. R. R. Adzic and J. X. Wang, *J. Phys. Chem. B* 102 (1998) 6305.
105. G. Horanyi and A. Aramata, *J. Electroanal. Chem.* 434 (1997) 201.
106. A. Aramata, S. Taguchi, T. Fukuda, M. Nakamura, and G. Horanyi, *Electrochim. Acta* 44 (1998) 999.
107. G. Horanyi, E. M. Rizmayer, and P. Joo, *J. Electroanal. Chem.* 152 (1983) 211.
108. G. Horanyi and A. Wieckowski, *J. Electroanal. Chem.* 294 (1990) 267.
109. D. W. Suggs and J. L. Stickney, *J. Phys. Chem.* 95 (1991) 10056.
110. D. W. Suggs and J. L. Stickney, *Surf. Sci.* 290 (1993) 362.
111. D. W. Suggs and J. L. Stickney, *Surf. Sci.* 290 (1993) 375.
112. B. E. Hayden and I. S. Nandhakumar, *J. Phys. Chem. B* 101 (1997) 7751.
113. B. E. Hayden and I. S. Nandhakumar, *J. Phys. Chem. B* 102 (1998) 4897.
114. S. Nagashima, *Appl. Surf. Sci.* 145 (1999) 73.
115. N. Ikemiya, D. Iwai, K. Yamada, R. Vidu, and S. Hara, *Surf. Sci.* 369 (1996) 199.
116. I. Yagi, S. Nakabayashi, and K. Uosaki, *J. Phys. Chem. B* 102 (1998) 2677.
117. I. Yagi, S. Nakabayashi, and K. Uosaki, *Surf. Sci.* 406 (1998) 1.

118. I. Yagi, J. M. Lantz, S. Nakabayashi, R. M. Corn, and K. Uosaki, *J. Electroanal. Chem.* 401 (1996) 95.
119. T. A. Sorenson, K. Varazo, D. W. Suggs, and J. L. Stickney, *Surf. Sci.* 470 (2001) 197.
120. G. E. Poirier, *Langmuir* 13 (1997) 2019.
121. X. P. Gao, Y. Zhang, and M. J. Weaver, *J. Phys. Chem.* 96 (1992) 4156.
122. X. P. Gao, Y. Zhang, and M. J. Weaver, *Langmuir* 8 (1992) 668.
123. C. A. Widrig, C. A. Alves, and M. D. Porter, *J. Am. Chem. Soc.* 113 (1991) 2805.
124. R. G. Nuzzo and D. L. Allara, *J. Am. Chem. Soc.* 105 (1983) 4481.
125. R. G. Nuzzo, B. R. Zegarski, and L. H. Dubois, *J. Am. Chem. Soc.* 109 (1987) 733.
126. M. D. Porter, T. B. Bright, D. L. Allara, and C. E. D. Chidsey, *J. Am. Chem. Soc.* 109 (1987) 3559.
127. C. D. Bain, E. B. Troughton, Y. T. Tao, J. Evall, G. M. Whitesides, and R. G. Nuzzo, *J. Am. Chem. Soc.* 111 (1989) 321.
128. G. M. Whitesides, *Sci. Am.* 273 (1995) 146.
129. G. E. Poirier and E. D. Pylant, *Science* 272 (1996) 1145.
130. A. Ulman, *Chem. Rev.* 96 (1996) 1533.
131. N. Bowden, A. Terfort, J. Carbeck, and G. M. Whitesides, *Science* 276 (1997) 233.
132. G. E. Poirier, *Chem. Rev.* 97 (1997) 1117.
133. U. Demir and C. Shannon, *Langmuir* 10 (1994) 2794.
134. U. Demir and C. Shannon, *Langmuir* 12 (1996) 6091.

135. A. Gichuhi, B. E. Boone, U. Demir, and C. Shannon, *J. Phys. Chem. B* 102 (1998) 6499.
136. G. Andreasen, C. Vericat, M. E. Vela, and R. C. Salvarezza, *J. Chem. Phys.* 111 (1999) 9457.
137. H. Martin, C. Vericat, G. Andreasen, A. H. Creus, M. E. Vela, and R. C. Salvarezza, *Langmuir* 17 (2001) 2334.
138. C. Vericat, G. Andreasen, M. E. Vela, and R. C. Salvarezza, *J. Phys. Chem. B* 104 (2000) 302.
139. G. D. Aloisi, M. Cavallini, M. Innocenti, M. L. Foresti, G. Pezzatini, and R. Guidelli, *J. Phys. Chem. B* 101 (1997) 4774.
140. D. W. Hatchett and H. S. White, *J. Phys. Chem.* 100 (1996) 9854.
141. M. Innocenti, G. Pezzatini, F. Forni, and M. L. Foresti, *J. Electrochem. Soc.* 148 (2001) C357.
142. M. L. Foresti, G. Pezzatini, M. Cavallini, G. Aloisi, M. Innocenti, and R. Guidelli, *J. Phys. Chem. B* 102 (1998) 7413.
143. F. Forni, M. Innocenti, G. Pezzatini, and M. L. Foresti, *Electrochim. Acta* 45 (2000) 3225.
144. G. Pezzatini, S. Caporali, M. Innocenti, and M. L. Foresti, *J. Electroanal. Chem.* 475 (1999) 164.
145. T. Cecconi, A. Atrei, U. Bardi, F. Forni, M. Innocenti, F. Loglio, M. L. Foresti, and G. Roviada, *J. Electron Spectrosc. Relat. Phenom.* 114 (2001) 563.
146. T. E. Lister, L. P. Colletti, and J. L. Stickney, *Isr. J. Chem.* 37 (1997) 287.

147. T. E. Lister, R. D. Herrick, and J. L. Stickney, *Abstr. Pap. Am. Chem. Soc.* 208 (1994) 128.
148. T. E. Lister, B. M. Huang, and J. L. Stickney, *Abstr. Pap. Am. Chem. Soc.* 210 (1995) 188.
149. T. E. Lister and J. L. Stickney, *Appl. Surf. Sci.* 107 (1996) 153.
150. T. E. Lister and J. L. Stickney, *Abstr. Pap. Am. Chem. Soc.* 212 (1996) 151.
151. A. Gichuhi, C. Shannon, and S. S. Perry, *Langmuir* 15 (1999) 5654.
152. A. Gichuhi, B. E. Boone, and C. Shannon, *Langmuir* 15 (1999) 763.
153. T. Torimoto, A. Obayashi, S. Kuwabata, H. Yasuda, H. Mori, and H. Yoneyama, *Langmuir* 16 (2000) 5820.
154. T. Torimoto, S. Nagakubo, M. Nishizawa, and H. Yoneyama, *Langmuir* 14 (1998) 7077.
155. T. Torimoto, A. Obayashi, S. Kuwabata, and H. Yoneyama, *Electrochem. Commun.* 2 (2000) 359.
156. B. W. Gregory, M. L. Norton, and J. L. Stickney, *J. Electroanal. Chem.* 293 (1990) 85.
157. L. P. Colletti, D. Teklay, and J. L. Stickney, *J. Electroanal. Chem.* 369 (1994) 145.
158. B. M. Huang, L. P. Colletti, B. W. Gregory, J. L. Anderson, and J. L. Stickney, *J. Electrochem. Soc.* 142 (1995) 3007.
159. L. P. Colletti and J. L. Stickney, *J. Electrochem. Soc.* 145 (1998) 3594.
160. L. P. Colletti, B. H. Flowers, and J. L. Stickney, *J. Electrochem. Soc.* 145 (1998) 1442.

161. I. Villegas and P. Napolitano, *J. Electrochem. Soc.* 146 (1999) 117.
162. T. L. Wade, L. C. Ward, C. B. Maddox, U. Happek, and J. L. Stickney, *Electrochem. Solid State Lett.* 2 (1999) 616.
163. T. L. Wade, R. Vaidyanathan, U. Happek, and J. L. Stickney, *J. Electroanal. Chem.* 500 (2001) 322.

CHAPTER 2

FORMATION OF THE FIRST MONOLAYERS OF CDTE ON AU(111) BY ELECTROCHEMICAL ATOMIC LAYER EPITAXY (EC-ALE): STUDIED BY LEED, AUGER, XPS, AND IN SITU STM¹

¹K. Varazo, M.D. Lay, T.A. Sorenson, J.L. Stickney. Submitted to J. Electroanal. Chem., 07/19/01.

Abstract

The two-step alternated electrodeposition of Cd and Te atomic layers to form CdTe monolayers, electrochemical atomic layer epitaxy (EC-ALE), was studied on Au(111) using Auger electron spectroscopy (AES), low energy electron diffraction (LEED), in situ scanning tunneling microscopy (STM), and X-ray photoelectron spectroscopy (XPS). Well ordered $(\sqrt{7}\times\sqrt{7})R19.1^\circ$ -CdTe and (3X3)-CdTe structures were formed using either Te or Cd as the first layer, and model structures are proposed for both. STM images suggest that previously proposed hexagonal structures based on a plane of zinc blende CdTe may be incorrect. A chain structure is suggested to account for the $(\sqrt{7}\times\sqrt{7})R19.1^\circ$, based on $3/7$ (0.43) ML each of Cd and Te. The (3X3)-CdTe structure results from the deposition of a CdTe sandwich: first an atomic layer of Cd on Au, followed by a layer of Te, and then a second Cd layer. Based on this three layer model for the (3X3), a three step deposit was formed, starting with Cd, then Te, and finally Cd. This resulted in an excellent quality LEED pattern, suggesting a well-ordered (3X3)-CdTe deposit and strongly supporting the proposed model. The importance of deposit stoichiometry was also investigated using STM, which indicated that too low a coverage in the first atomic layer resulted in cluster formation and the degradation of surface morphology.

Introduction

II-VI compound semiconductors are an important group of materials, used in a wide variety of optoelectronic devices: detectors [1, 2], solar cells [3-5], and photovoltaics [6]. High quality thin film deposits are usually the result of excellent control over the growth process, generally at the nanometer scale. This is currently achieved using high temperature vacuum based methods such as molecular beam epitaxy (MBE) [7] and metalorganic vapor phase epitaxy (MOVPE) [8], where the substrate temperature is the primary control during deposition. A number of ambient pressure methods such as chemical bath deposition (CBD) and electrodeposition have also been used to form thin films of these materials. Compound electrodeposition has been well reviewed by a number of workers [9-13].

Electrochemical atomic layer epitaxy (EC-ALE) is a method developed to electrodeposit compound semiconductors one monolayer at a time [13, 14]. It is the electrochemical paradigm of atomic layer epitaxy (ALE) or atomic layer deposition (ALD) [15-18]. Instead of substrate temperature, electrode potential is used to control the deposition of individual atomic layers. The method is based on using surface-limited reactions, where only two-dimensional growth occurs, and the material is formed layer-by-layer. In electrodeposition, surface-limited reactions are generally referred to as underpotential deposition (UPD) [19-23], where an atomic layer of an element deposits onto a second element, copper on gold for example, at a potential prior to (under) that required for bulk deposition of the first element. The atomic layer forms as a result of the free energy of formation for the surface compound. In EC-ALE, thin films are formed by the sequential UPD of each element from a separate solution, in a cycle. The process is

automated and continues until the desired film thickness is reached. Several groups have prepared thin films of II-VI compound semiconductors using EC-ALE, such as CdTe, CdSe, CdS, ZnS, and ZnSe on gold and silver substrates [24-31]. In addition, deposits of the III-V compounds InAs and InSb have recently been formed, as well as a superlattice [32, 33].

The EC-ALE formation of CdTe on the low index planes of gold has been studied by ultrahigh vacuum electrochemistry (UHV-EC) [34], ex situ scanning tunneling microscopy (STM) [35], and in situ STM [36]. Well-ordered structures were formed on each low index plane. Two different structures were observed with low energy electron diffraction (LEED) on the Au(111) face, a $(\sqrt{7} \times \sqrt{7})R19.1^\circ$ -CdTe and a (3X3)-CdTe, but STM results varied. Until recently, the $(\sqrt{7} \times \sqrt{7})R19.1^\circ$ -CdTe unit cell was only observed by ex situ STM [35] and the images were of a poor quality, while the (3X3)-CdTe structure had been observed using in situ STM by Hayden and Nandhakumar [36]. Both STM studies formed CdTe by first depositing Te on the Au surface, followed by Cd deposition. Cd was not used as the first layer due to fears that a first monolayer of Cd might spontaneously oxidize during solution exchange, as some oxygen was always observed in the resulting Auger spectra [34]. Recent studies of Cd UPD from different electrolytes suggest that the oxygen was due to coadsorbed sulfate [37].

This paper presents a UHV-EC study [38] of CdTe formation on Au(111) by EC-ALE. The effect of stoichiometry on the structures formed was examined using Auger electron spectroscopy (AES), X-ray photoelectron spectroscopy (XPS), LEED, and in situ STM. The first layer is the most important, as it is the interface between the substrate and deposit. There is a 6% lattice mismatch between Au(111) and zinc blende

CdTe (discussed later in this paper). Studies of the structure and composition of the first compound monolayer are essential, since the first monolayer accommodates the transition from the chemistry of the Au substrate to that of CdTe. The structure of the first monolayer can influence the morphology of thicker deposits.

Experimental

The UHV-EC studies were performed using an ultrahigh vacuum (UHV) surface analysis chamber connected directly to an antechamber containing an electrochemical cell [39]. Surface analysis instrumentation included a cylindrical mirror analyzer for Auger electron spectroscopy (AES) (Perkin-Elmer 11-010 Auger system), reverse-view optics for low energy electron diffraction (LEED) (Princeton model 11-020), an X-ray source (VG Scientific) and hemispherical analyzer (Leybold-Heraeus) for X-ray photoelectron spectroscopy (XPS), as well as an ion bombardment cage for sputter cleaning substrates. The base pressure of the chamber was 10^{-9} Torr, maintained with an ion pump and cryopump. The electrochemistry antechamber was stainless steel and connected to the main chamber through a gate valve, allowing direct sample transfer into and out of the analysis chamber without exposure to atmosphere.

Auger spectra were collected using 3 keV ionizing electrons. XPS spectra were obtained using Al K α X-rays (1486.6 eV). The Au 4f_{7/2} peak (83.98 eV) was used for calibration [40]. Images of the LEED patterns were obtained using a Kodak digital camera (Model DC290).

The Au(111) single crystal used (MaTecK GmbH) was a 99.999% pure disc 1 cm in diameter and 2 mm thick. Prior to each electrochemical experiment, the crystal was

cleaned by argon ion bombardment (8.5×10^{-5} Torr) for 30 minutes, followed by annealing with a resistively heated tungsten filament. Surface cleanliness and order were confirmed using AES and LEED, respectively.

Electrochemical experiments were carried out using a Pyrex glass cell, housed in the stainless steel antechamber. The potentiostat was based on conventional operational amplifier circuitry, and was built in-house. A gold wire (Wilkinson Company) served as the auxiliary electrode. All potentials were measured against a Ag/AgCl (3 M NaCl) reference electrode (Bioanalytical systems). Solutions were delivered into the cell from pressurized Pyrex bottles. All experiments were conducted in an atmosphere of high purity argon (BOC).

The Au(111) electrodes used for in-situ STM studies were either Au(111) single crystals or vapor deposited gold films on either glass or mica. Before each experiment the substrate was cleaned using concentrated nitric acid followed by annealing in a high purity hydrogen (99.999%, BOC) flame, resulting in an array of Au(111) facets. A Digital Instruments Nanoscope III electrochemical STM was used, and the STM head was calibrated using highly ordered pyrolytic graphite (HOPG). The electrochemical cell used for STM contained a compartment for the Ag/AgCl (3 M NaCl) reference electrode and a Au wire auxiliary, and was connected to the substrate compartment via a small solution trough [41]. The tungsten tips were prepared by etching in freshly prepared 1 M KOH at 12 V AC. The tips were then coated with polyethylene to reduce the tip area exposed to solution.

All solutions were prepared with ultrapure water (18 M Ω) obtained from a Nanopure filtration system (Barnstead), fed from the house distilled water supply. The

cadmium solution was composed of 0.2 mM CdCl₂ (99.998% Puratronic Alfa Aesar) and 1 mM HCl (Baker analyzed A.C.S. reagent). The pH 2.2 tellurium solution contained 0.25 mM TeO₂ (99.9995% Puratronic Alfa Aesar) and 20 mM H₂SO₄ (Baker analyzed A.C.S. reagent). A second alkaline tellurium solution, pH 9.4, consisting of 0.20 mM TeO₂, 0.20 mM KCl (Baker analyzed reagent grade), and 0.40 mM KOH (Baker analyzed reagent grade) was used to deposit Te on existing Cd atomic layers.

Results

The studies described here involved depositing CdTe monolayer structures in a two-step process. In the first two sets of experiments Te was first electrodeposited on Au(111), followed by Cd. In the second two sets Cd was deposited first, followed by Te (Table 1).

CdTe Electrodeposition- Te first

UPD of Te on Au(111) from acidic solutions has been studied ex situ in detail using LEED [42] and STM [35], and in situ using STM [43, 44]. In addition, Te deposition on Au(111) has been studied using atomic force microscopy (AFM) and second harmonic generation (SHG) [45-49]. Figure 2.1 displays the cyclic voltammogram of a Au(111) electrode in a solution containing 0.20 mM TeO₂ and 10 mM H₂SO₄ (pH 2). Several ordered structures are formed as a function of potential and coverage during the course of Te UPD.

Table 2.1 A-D, Elemental coverages and structures for CdTe deposits. A) Te deposition first at 0.15 V, followed by Cd deposition; B) Te deposition first at 0.10 V, followed by Cd deposition; C) Cd deposition first at -0.60 V, followed by Te deposition; D) Cd deposition first at -0.70 V, followed by Te deposition.

Table 2.1A Te, Cd, and Cl Coverages with Structures for CdTe Deposits; Te Deposition first at 0.15 V, Followed by Cd Deposition

Cd Deposition Potential/V	Te Coverage/ML	Cd Coverage/ML	Cl Coverage/ML	LEED Pattern
-0.40	0.33	0.18	0.33	(13X13) Clear
-0.50	0.33	0.40	0.37	($\sqrt{7}\times\sqrt{7}$)R19.1° Clear
-0.60	0.33	0.50	0.50	(3X3) Diffuse
-0.70	0.33	0.65	0.65	(3X3) Diffuse
-0.80	0.33	0.95	0.72	($\sqrt{3}\times\sqrt{3}$)R30° Diffuse
-0.90	0.33	0.93	0.65	($\sqrt{3}\times\sqrt{3}$)R30° Diffuse
-1.0	0.33	0.99	0.69	($\sqrt{3}\times\sqrt{3}$)R30°

Table 2.1B Te, Cd, and Cl Coverages with Structures for CdTe Deposits; Te Deposition First at 0.10 V, Followed by Cd Deposition

Cd Deposition Potential/V	Te Coverage/ML	Cd Coverage/ML	Cl Coverage/ML	LEED Pattern
-0.40	0.44	0.20	0.06	Clear ($\sqrt{7} \times \sqrt{7}$)R19.1°
-0.50	0.44	0.40	0.15	Clear ($\sqrt{7} \times \sqrt{7}$)R19.1°
-0.60	0.44	0.52	0.21	Clear (3X3)
-0.70	0.44	0.82	0.71	Clear (3X3)
-0.80	0.44	1.2	0.76	Diffuse ($\sqrt{3} \times \sqrt{3}$)R30°
-0.90	0.44	1.2	0.59	Diffuse ($\sqrt{3} \times \sqrt{3}$)R30°
-1.0	0.44	1.2	0.75	Diffuse ($\sqrt{3} \times \sqrt{3}$)R30°

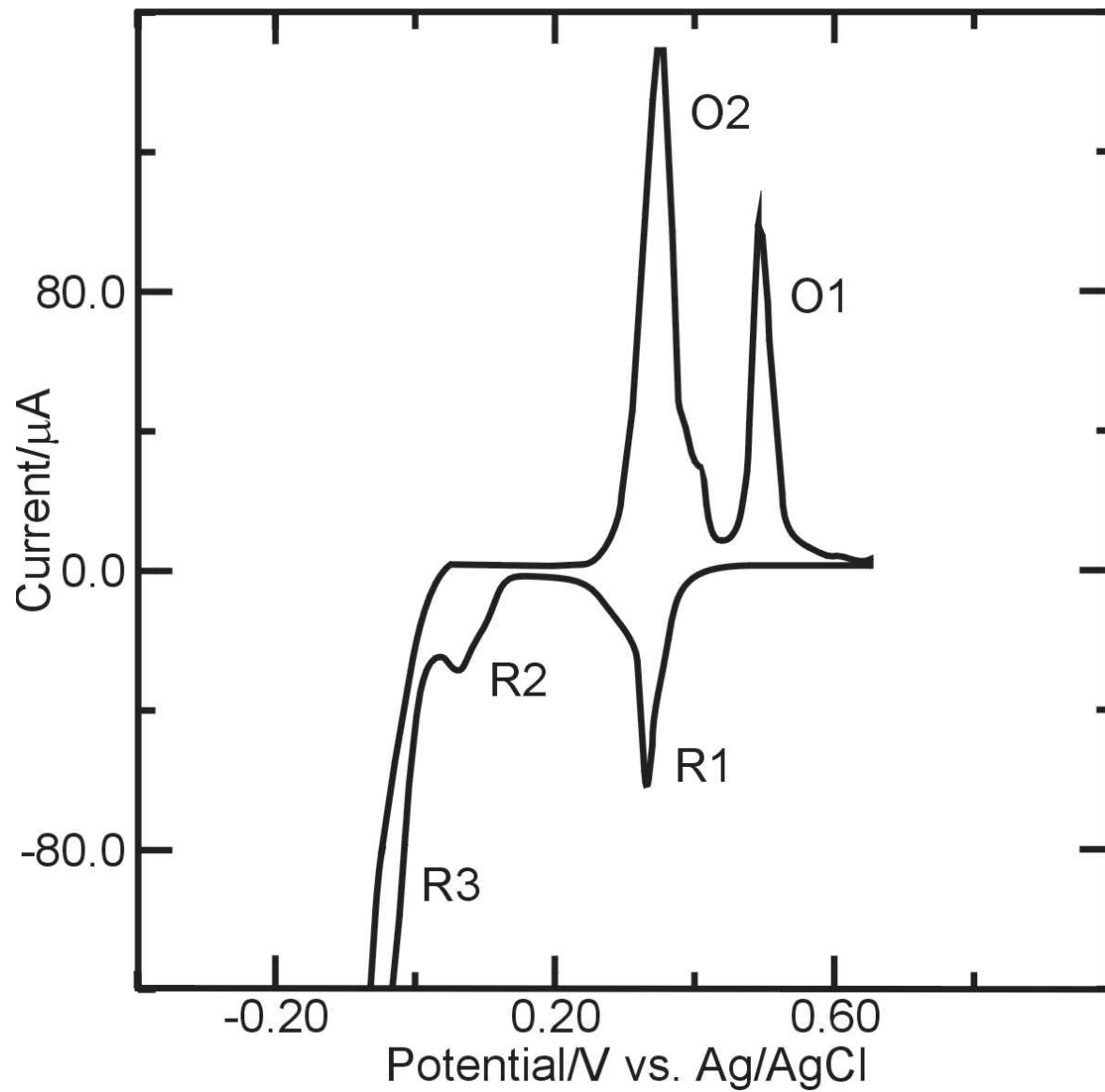
Table 2.1C Cd, Te, Cl, K, and Te Oxide Coverages with Structures for CdTe Deposits;
Cd Deposition First at -0.60 V, Followed by Te Deposition

Te Deposition Potential/V	Cd Coverage/ML	Te Coverage/ML	Cl Coverage/ML	K Coverage/ML	Te oxide Coverage/ML	LEED Pattern
-0.60	0.28	0.48	0.10	0.09	0.40	Diffuse intensity Clear
-0.70	0.28	0.36	0.03	0.13	0.10	($\sqrt{7} \times \sqrt{7}$)R19.1° Clear
-0.80	0.28	0.40	0.05	0.14	0.10	($\sqrt{7} \times \sqrt{7}$)R19.1° Diffuse
-0.90	0.28	0.51	0.04	0.16	0	($\sqrt{7} \times \sqrt{7}$)R19.1° Diffuse
-0.95	0.28	0.58	0.05	0.10	0	($\sqrt{7} \times \sqrt{7}$)R19.1°
-1.0	0.28	0.67	0.05	0.15	0	(1X1)
-1.1	0.28	0.80	0.04	0.17	0	(1X1)
-1.2	0.28	0.73	0.05	0.21	0	(1X1)

Table 2.1D Cd, Te, Cl, K, and Te Oxide Coverages with Structures for CdTe Deposits;
Cd Deposition First at -0.70 V, Followed by Te Deposition

Te Deposition Potential/V	Cd Coverage/ML	Te Coverage/ML	Cl Coverage/ML	K Coverage/ML	Te oxide Coverage/ML	LEED Pattern
-0.70	0.48	0.38	0.09	0.09	0.60	Diffuse intensity Very diffuse ($\sqrt{7} \times \sqrt{7}$)R19.1°
-0.80	0.48	0.44	0.09	0.10	0.40	and (3X3) spots
-0.90	0.48	0.55	0.06	0.15	0	Diffuse (3X3)
-1.0	0.48	0.77	0.06	0.12	0	Very diffuse (3X3)
-1.1	0.48	0.81	0.06	0.24	0	Very diffuse ($\sqrt{7} \times \sqrt{7}$)R19.1°
-1.2	0.48	1.07	0.05	0.26	0	(1X1)
-1.3	0.48	0.87	0.05	0.25	0	(1X1)

Figure 2.1 Cyclic voltammogram of the Au(111) electrode in 0.20 mM TeO_2 and 20 mM H_2SO_4 (pH 2). Scan rate = 5 mV/s

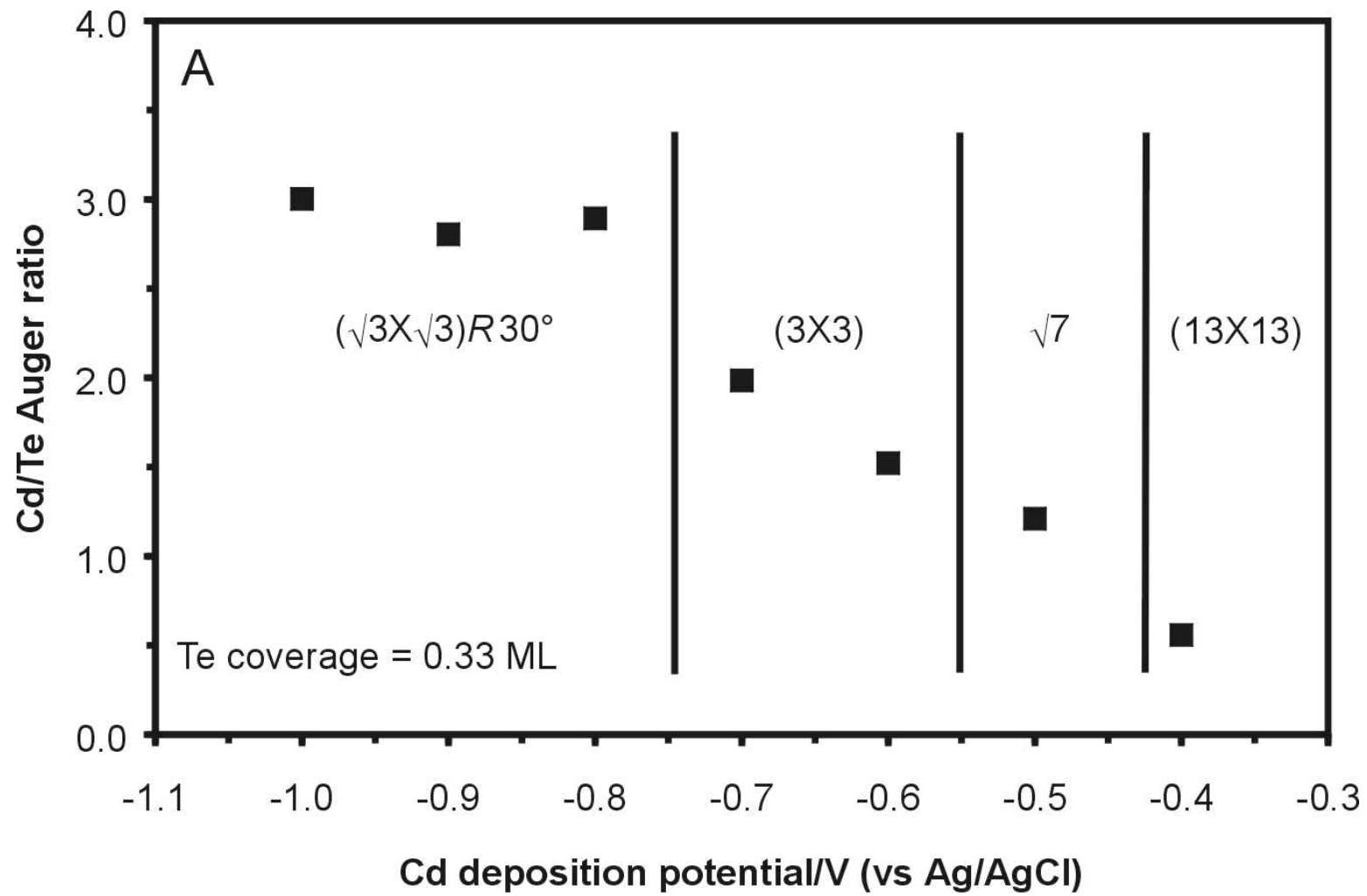


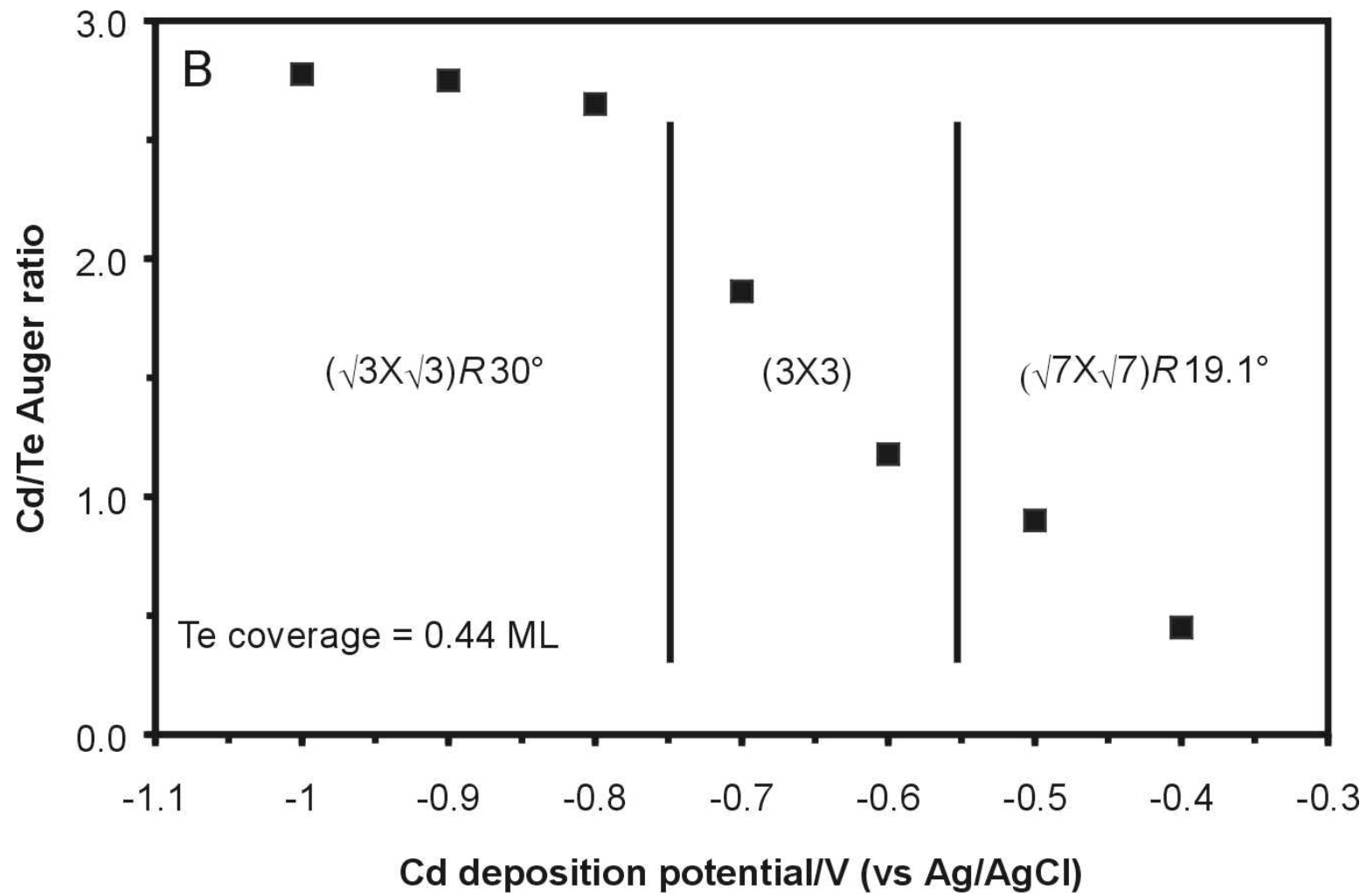
The first set of studies involved depositing Te onto the clean and ordered Au(111) electrode by immersing into the pH 2 TeO_2 solution at 0.40 V, scanning negative to 0.15 V and emersing (removing the deposit from solution) near peak R1 (Figure 2.1), resulting in the formation of a $1/3$ ML coverage (13X13)-Te structure [43]. The coverages are defined relative to the number of Au substrate surface atoms, with a ratio of 1.0 being a full monolayer (ML). Cd was then deposited from a 0.20 mM CdCl_2 solution containing 1 mM HCl (pH 3) for two minutes at a series of controlled potentials.

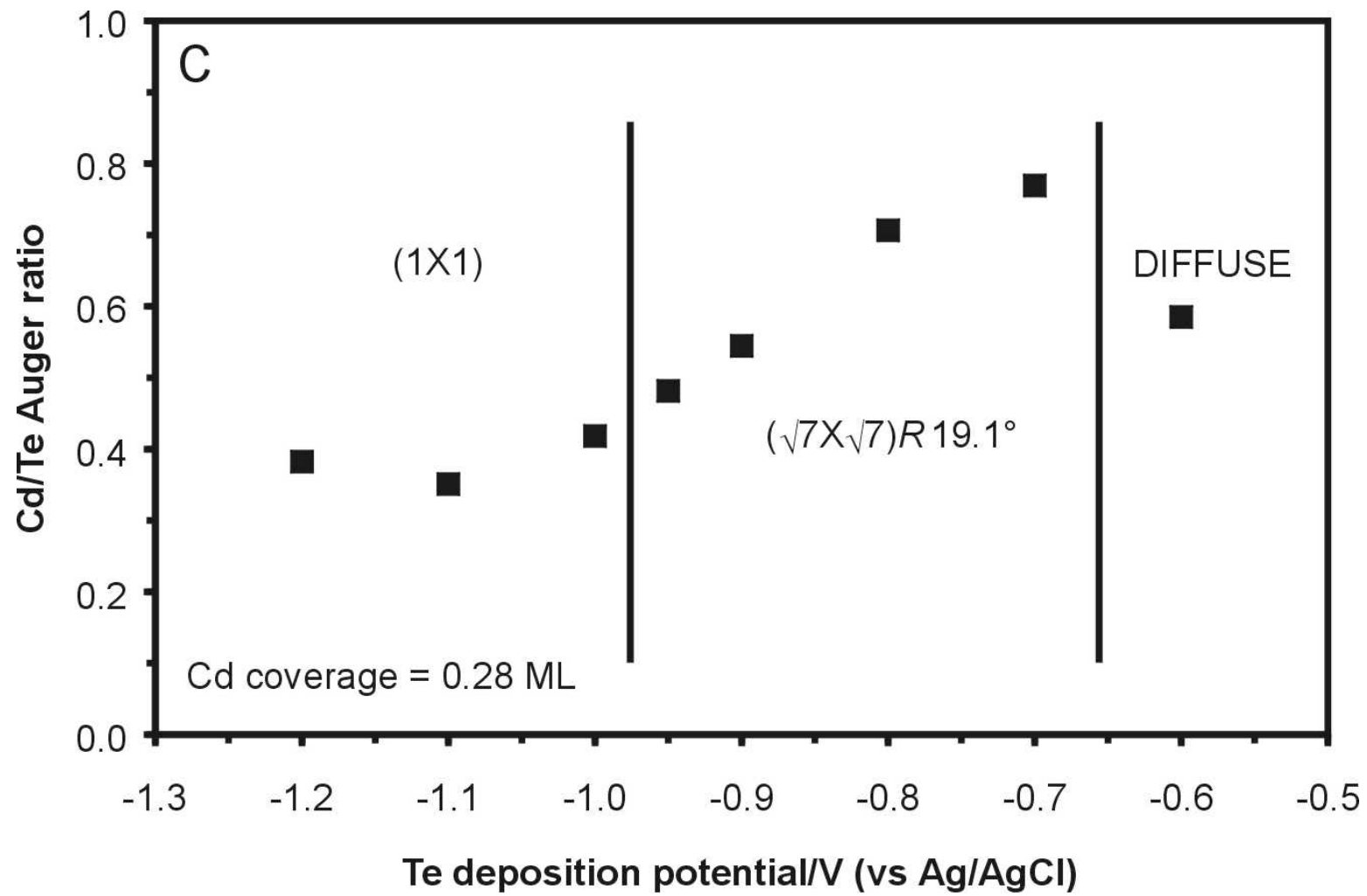
Figure 2.2A is a plot of the elemental Cd/Te ratios as a function of the potential used to deposit the Cd atomic layer, between -0.4 V and -1.0 V. The ratios in Figure 2.2A were obtained from Auger peak heights and adjusted for the elemental sensitivities in order to reflect the deposit stoichiometry. Table 1A lists the coverages of Cd, Te, and Cl to provide a clear picture of the surface composition.

LEED patterns from the deposit formed at -0.40 V showed no significant change in the diffraction pattern for the initial (13X13)-Te unit cell, and a low Cd/Te ratio, 0.5. It has been shown that Cd deposition on substrates coated with a Te atomic layer occurs at a more negative potential than on bare gold [34] or silver [50] substrates. This suggests that Cd is more stable on bare gold than on gold covered by an atomic layer of Te; however, Cd still deposits at an underpotential on a Te coated surface. At -0.50 V, a $(\sqrt{7}\times\sqrt{7})R19.1^\circ$ pattern was observed with a Cd/Te ratio of 1.2 (Figure 2.3A), while at -0.60 V and -0.70 V a (3X3) pattern was observed, with ratios of 1.5 and 2.0, respectively (Figure 2.3B). Cd deposition at -0.80 V and more negative potentials resulted in a $(\sqrt{3}\times\sqrt{3})R30^\circ$ structure (not shown) with Cd/Te ratios near 3.0.

Figure 2.2A-D Cd/Te ratios as a function of deposition potential for the second element deposited in a two-step process. A) Cd deposition on a $1/3$ (0.33) ML (13X13)-Te atomic layer deposited at 0.15 V; B) Cd deposition on a $4/9$ (0.44) ML (3X3)-Te atomic layer deposited at 0.10 V; C) Te deposition on 0.28 ML of Cd deposited at -0.60 V; D) Te deposition on 0.48 ML of Cd deposited at -0.70 V.







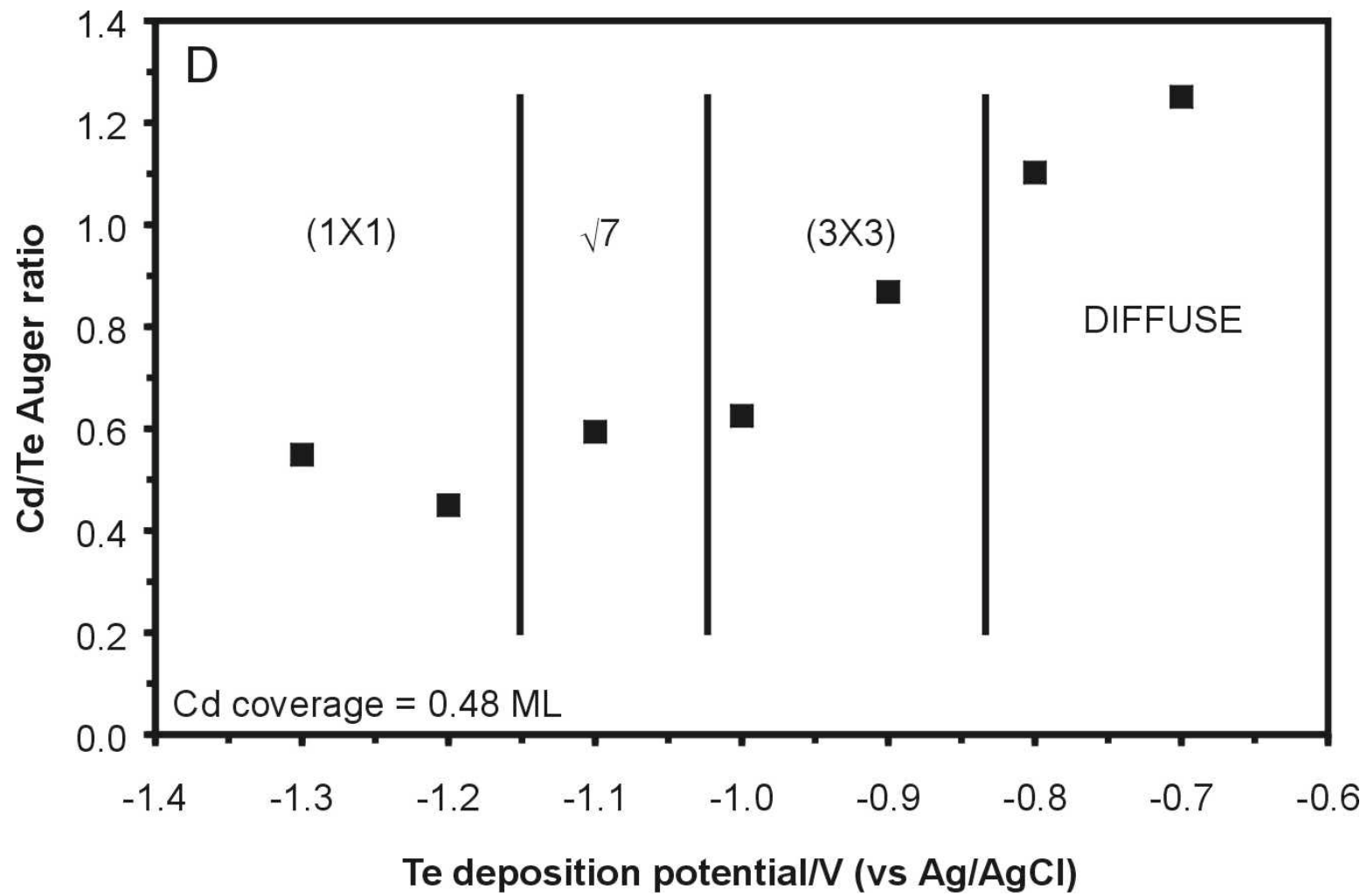
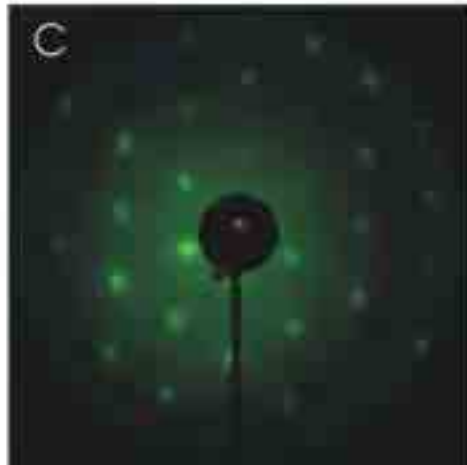
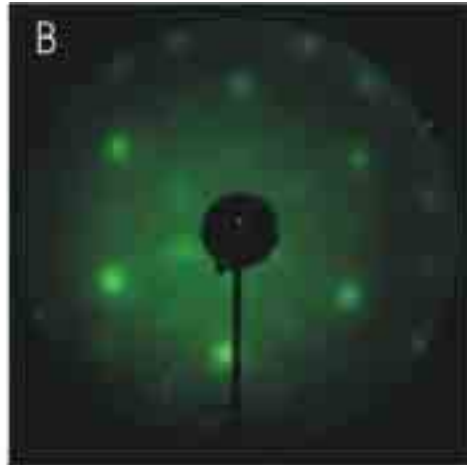
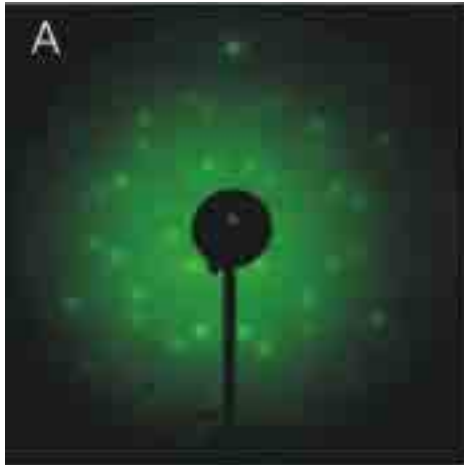


Figure 2.3 LEED patterns observed for CdTe monolayer formation. A) $(\sqrt{7} \times \sqrt{7})R19.1^\circ$ -CdTe formed using a two-step process, Cd first at -0.60 V, and then Te at -0.80 V, electron energy 75.4 eV; B) (3×3) -CdTe formed using a two-step process, Cd first at -0.70 V and then Te at -0.90 V, electron energy 52.3 eV; C) (3×3) -CdTe formed in a three-step process, Cd first at -0.60 V, Te second at -0.70 V, and finally Cd at -0.60 V, electron energy 48.5 eV.



This sequence of two-step deposits was then repeated using a higher initial Te coverage, corresponding to a (3X3) structure at 4/9 (0.44) ML coverage [43]. The Te atomic layer was formed by scanning to 0.10 V, and emersing. This potential corresponds to R2 (Figure 2.1), a small reduction feature appearing as a shoulder on the bulk Te reduction wave R3. Cd was again deposited at a series of potentials, and the Cd/Te ratios are plotted in Figure 2.2B. Table 2.1B lists the elemental coverages. Cd deposition at -0.40 V and -0.50 V resulted in the $(\sqrt{7} \times \sqrt{7})R19.1^\circ$ structure, with Cd/Te ratios of 0.4 and 0.9, respectively. Deposition at -0.60 V and -0.70 V resulted in formation of the (3X3) structure (Figure 2.3B), with Cd/Te ratios of 1.2 and 1.9, respectively. Again, Cd deposition at potentials more negative than -0.70 V formed the $(\sqrt{3} \times \sqrt{3})R30^\circ$ structure, with Cd/Te ratios near 3.

CdTe Electrodeposition-Cd first

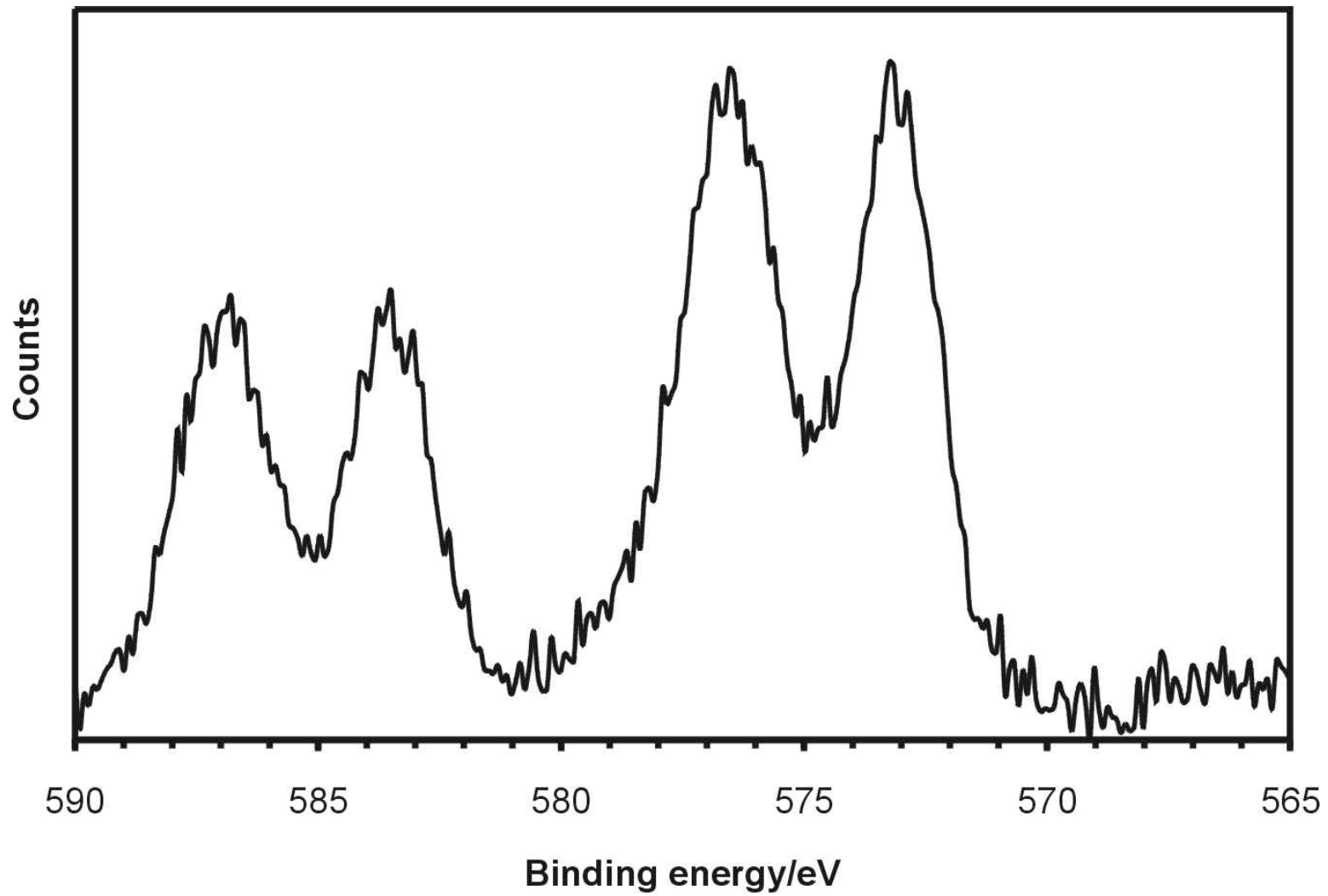
CdTe monolayer structures were also formed in two-steps, where Cd was electrodeposited first. The clean, ordered Au(111) electrode was immersed at 0.40 V in 0.20 mM CdCl₂ and 1 mM HCl, and the potential was scanned to -0.60 V. The crystal was then emersed under potential control, resulting in 0.3 ML of Cd, estimated from Auger spectroscopy. The Cd coverages were based on AES sensitivity factors [51] and studies of Cl on Au(111), from which a 1/3 coverage $(\sqrt{3} \times \sqrt{3})R30^\circ$ -Cl structure was used as a calibration point [37]. An ordered $(p \times \sqrt{3})R30^\circ$ -Cl structure on Au(111) has been reported by Magnussen et al., from in situ X-ray scattering experiments (SXS) [52]. Coulometric measurements in this lab indicated a charge for Cd UPD at -0.6 V of $170 \mu\text{C}/\text{cm}^2$, after background subtraction, corresponding to 0.3 ML. Previous thin-layer

electrode (TLE) studies of Cd UPD on gold from acidic sulfate solutions yielded a Cd coverage closer to 0.2 ML [53].

To allow reductive deposition of a Te atomic layer on top of an existing Cd atomic layer in a second step, a basic Te solution was required: 0.20 mM TeO₂, 0.20 mM KCl and 0.40 mM KOH (pH 9.4). The higher pH shifted Te UPD negative of the potential for Cd dissolution, allowing reductive deposition of both Cd and Te in successive steps. Te was deposited by controlled potential immersion of the Cd coated Au electrode for two minutes in the Te solution, at a series of potentials. Figure 2.2C displays the elemental Cd/Te Auger ratios for CdTe layers as a function of the Te deposition potential. At the most positive potential, -0.60 V, no ordered LEED pattern was observed. AES evinced some oxygen on the surface, and XPS analysis suggested the presence of a tellurium oxide (Table 2.1C). Figure 2.4 shows the Te 3d spectrum, with an elemental tellurium peak at 573 eV, and a significant peak at ~576 eV, indicating the presence of a tellurium oxide species [40], given the solution composition. However, the peak may indicate the presence of tellurite, tellurate, or both, as their Te 3d_{5/2} peaks are difficult to resolve. Between -0.70 V and -0.90 V, the ($\sqrt{7} \times \sqrt{7}$)R19.1° structure was again observed, with Cd/Te ratios between 0.5 and 0.8. The best quality diffraction patterns were observed at the higher Cd/Te ratios, 0.8. Te deposition more negative than -0.90 V produced only a diffuse (1X1).

In a second series of Cd first two-step experiments, Cd was deposited at -0.7 V, resulting in nearly twice as much Cd, 0.5 ML for the first atomic layer. Figure 2.2D displays the elemental Cd/Te ratios as a function of the potentials used to deposit Te. For Te deposited at -0.70 V and -0.80 V, no ordered structures were observed, due to

Figure 2.4 Te 3d XPS spectrum for Te deposition at -0.60 V on Cd deposited at -0.60 V.



tellurium oxide adsorption (Table 2.1D). Between -0.90 V and -1.0 V the (3X3) was observed, with Cd/Te ratios of 0.6 and 0.9. In the previous Cd first series (Figure 2.2C), the (3X3) pattern was not observed, although it was observed in both Te first series, at higher Cd coverages (Figures 2.2A and 2.2B). At -1.1 V, very faint spots, characteristic of a $(\sqrt{7}\times\sqrt{7})R19.1^\circ$ pattern, were observed at a Cd/Te ratio of 0.6. Beyond -1.1 V only a diffuse (1X1) was observed.

Discussion

As noted, the first studies of this system [34, 35] indicated the presence of both the (3X3) and the $(\sqrt{7}\times\sqrt{7})R19.1^\circ$ structures in two-step depositions. A model structure was proposed for the $(\sqrt{7}\times\sqrt{7})R19.1^\circ$ at that time, where the Cd atoms were placed in twofold sites between Te atoms on the Au(111) surface, based on the assumption that the structure was related to a (100) monolayer of zinc blende CdTe. Both elements were believed to be present at 3/7 (0.43) ML coverage. Subsequent X-ray diffraction measurements of 200 cycle thin films indicated that CdTe, CdSe, and CdS deposit preferentially with their (111) plane parallel to the Au(111) surface [26]. Graphs of Auger signals vs. the Cd deposition potential used for the second step [34] indicated the Cd coverage for the (3X3) was almost twice that for Te, while for the $(\sqrt{7}\times\sqrt{7})R19.1^\circ$ the Cd and Te coverages were nearly equal. No structure was proposed for the (3X3) at that time.

A (3X3) structure was subsequently observed with STM by Shannon et al. [30] after deposition of a monolayer of CdS, formed by first depositing S and then Cd on

Au(111). They proposed a structure equivalent to a (111) monolayer of zinc blende CdS superimposed on the Au(111) surface, with a 4% expansion of the lattice constant.

Results similar to those for CdTe were later obtained for two-step CdSe monolayer deposits [13, 27], where LEED patterns for a $(\sqrt{7}\times\sqrt{7})R19.1^\circ$ and a (3X3) were again observed. The low Auger sensitivity for Se [51] prevented quantitative coverage measurements by AES. Quantitative Cd coulometry was also problematic, due to large, ill-defined background currents in the voltammetry. At that time it was assumed that the Cd and Se coverages were equal in the $(\sqrt{7}\times\sqrt{7})R19.1^\circ$ and equal in the (3X3). Additionally, the coverages for the two structures were assumed to be very similar, $3/7$ (0.43) ML for each element in the $(\sqrt{7}\times\sqrt{7})R19.1^\circ$ and $4/9$ (0.44) ML each in the (3X3). The proposed structures were based on the crystalline structure of zinc blende CdSe, as suggested in the model by Shannon for CdS [30]. A (111) monolayer of zinc blende CdSe was superimposed on the Au(111) surface to account for both structures. At that time, the (3X3) structure was not considered to be composed of more than a monolayer of CdSe. Instead, a single monolayer of CdSe was superimposed on the Au(111) substrate, creating a 2:3 lattice match, where two times the Cd-Cd distance from zinc blende CdSe was matched with three times the Au-Au distance on Au(111). The resulting lattice mismatch was relatively small, about 1%. The structure proposed for the $(\sqrt{7}\times\sqrt{7})R19.1^\circ$ was essentially the same, but rotated 19.1° , with the lattice constant expanded by 1%. Hayden and Nandhakumar proposed a similar (3X3)-CdTe structure based on in situ STM and UHV-EC studies of CdTe deposition [36]. In their study they did not image the $(\sqrt{7}\times\sqrt{7})R19.1^\circ$ structure observed by LEED in earlier work [34], and concluded that it was a result of the emersion process and did not exist in solution.

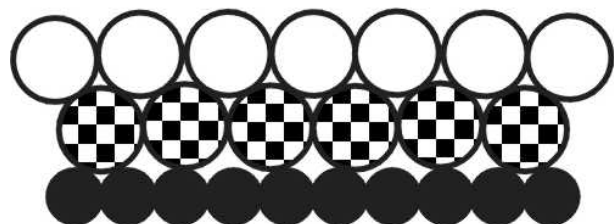
The two-step studies described in the results section above were developed to provide a more detailed picture of the conditions needed to optimally form the $(\sqrt{7}\times\sqrt{7})R19.1^\circ$ and (3×3) CdTe structures. Examination of the graphs in Figure 2.2 and the data in Table 2.1 reveals several trends. Figure 2.2A displays the graph of Cd/Te ratios after Cd deposition on the $1/3$ ML (13×13) -Te structure [43]. At -0.4 V, LEED shows only the (13×13) pattern, as insufficient Cd was deposited to form a significant amount of CdTe. At -0.5 V the Cd/Te ratio was 1.2, and the $(\sqrt{7}\times\sqrt{7})R19.1^\circ$ LEED pattern was observed, suggesting a 1:1 stoichiometry. Deposition at -0.6 V and -0.7 V resulted in formation of the (3×3) structure, with Cd/Te ratios between 1.5 and 2. At still higher Cd coverages, the $(\sqrt{3}\times\sqrt{3})R30^\circ$ was formed. From Figure 2.2A it is clear that the two structures differ significantly in Cd coverage, with the (3×3) having almost twice that of the $(\sqrt{7}\times\sqrt{7})R19.1^\circ$. In addition, the coverages of Te and Cd were essentially equal in the $(\sqrt{7}\times\sqrt{7})R19.1^\circ$. Given the symmetry of the unit cell, and that the initial Te coverage was $\sim 1/3$ ML, the probable Cd and Te coverages were $2/7$ (0.29) ML or $3/7$ (0.43) ML.

In Figure 2.2B the initial coverage of Te was 0.44 ML, and the $(\sqrt{7}\times\sqrt{7})R19.1^\circ$ was evident at -0.4 V and -0.5 V, with Cd/Te ratios just under 1. At -0.6 V and -0.7 V the (3×3) was formed with ratios just below 2, and the $(\sqrt{3}\times\sqrt{3})R30^\circ$ was again formed at more negative potentials and the ratio approached 3. Previous model structures considered the (3×3) as resulting from equal coverages of Cd and the chalcogenide [13, 27, 30, 34-36], which is inconsistent with the present results. A model that accounts for the higher Cd coverage in the (3×3) , and is consistent with previous STM images consists of a deposit three atomic layers thick (Figure 2.5B); a first atomic layer of Cd,

Figure 2.5 Side view models for the CdTe monolayer deposits.

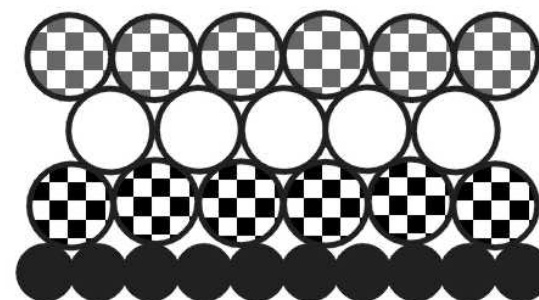
A) $(\sqrt{7} \times \sqrt{7})R19.1^\circ$ -CdTe; B) (3×3) -CdTe.

A



CdTe-Au(111)
 $(\sqrt{7} \times \sqrt{7})R19.1^\circ$

B



CdTe-Au(111)-(3X3)

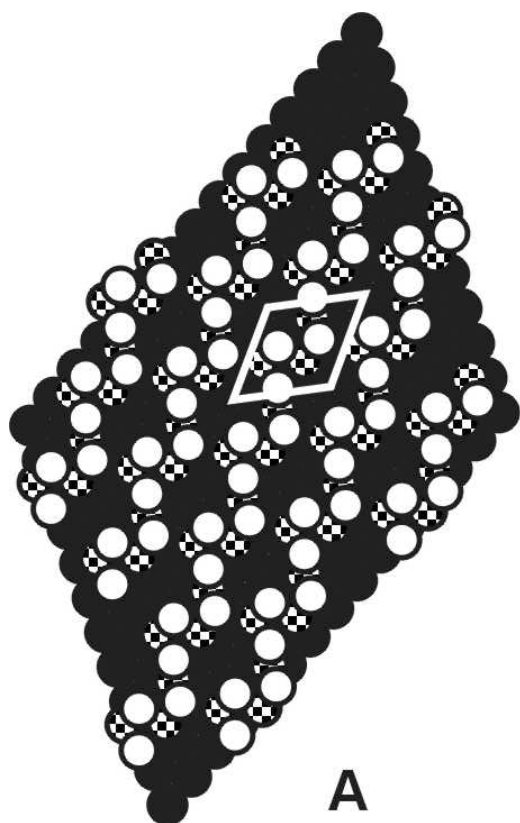


then one of Te, and then Cd again. This model raises questions as to how Cd can be deposited under an atomic layer of Te, but that is not an unknown phenomenon. For instance, it has been clearly shown that metals such as Ag and Cu can be deposited under an adsorbed layer of halogen atoms on Pt surfaces [54]. As noted above, Cd UPD on Au occurs at a larger underpotential than when deposited on Te-coated Au, suggesting the greater affinity of Cd for the Au surface than for Te. In addition, it is well known that Cd forms alloys with Au at underpotentials [55-58]. It is thus proposed that Cd is more stable than Te as the first atomic layer on Au in the formation of CdTe monolayers, suggesting that Cd place exchanges with the Te.

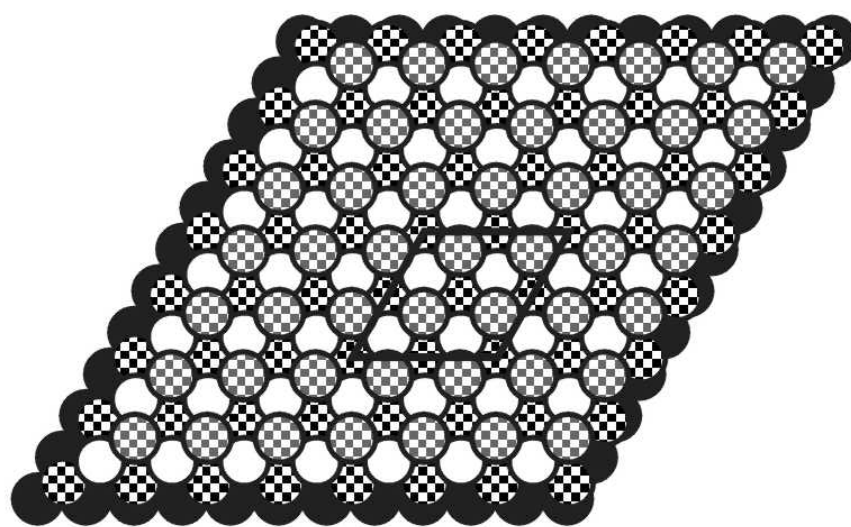
Given that Cd can deposit under the Te, previously proposed models can be modified to explain the (3X3) structure by adding a top layer of Cd atoms (Figure 2.6A). That is, the structure is still a slice of zinc blende CdTe superimposed on the Au(111) surface, but consists of 1.5 ML of CdTe, instead of 1.0 ML, clearly explaining the 2:1 ratio of Cd/Te. The optimal Te coverage would be 4/9 (0.44) ML, while the optimal Cd coverage would be 8/9 (0.88) ML. STM images of the (3X3)-CdTe structure (Figure 2.7) are consistent with the symmetry and interatomic spacing in the proposed structure (Figure 2.6A).

Recently proposed structures for the $(\sqrt{7}\times\sqrt{7})R19.1^\circ$ suggested a monolayer of zinc blende CdTe superimposed on Au(111) [13, 27], essentially the first two atomic layers of the structure shown in Figure 2.6A but rotated 19.1° , with Cd and Te coverages of 3/7 (0.43) ML each. STM images of such a structure should look very similar to the (3X3) shown in Figure 2.7, but rotated 19.1° . Recent in situ STM images of the $(\sqrt{7}\times\sqrt{7})R19.1^\circ$ (Figure 2.8), however, clearly show a periodic array of darker spots, or

Figure 2.6 CdTe model structures. The substrate layer consists of black circles. A) (3X3)-CdTe model structure. The first Cd layer consists of circles with a black and white checkered pattern, the Te layer consists of white circles, and the final Cd layer consists of circles with a grey and white checkered pattern; B) $(\sqrt{7} \times \sqrt{7})R19.1^\circ$ -CdTe model structure. The Cd layer consists of circles with a black and white checkered pattern, and the Te layer consists of white circles.



A



B

Figure 2.7 STM micrograph of (3X3)-CdTe. Scan size is 20 nm x 20 nm.

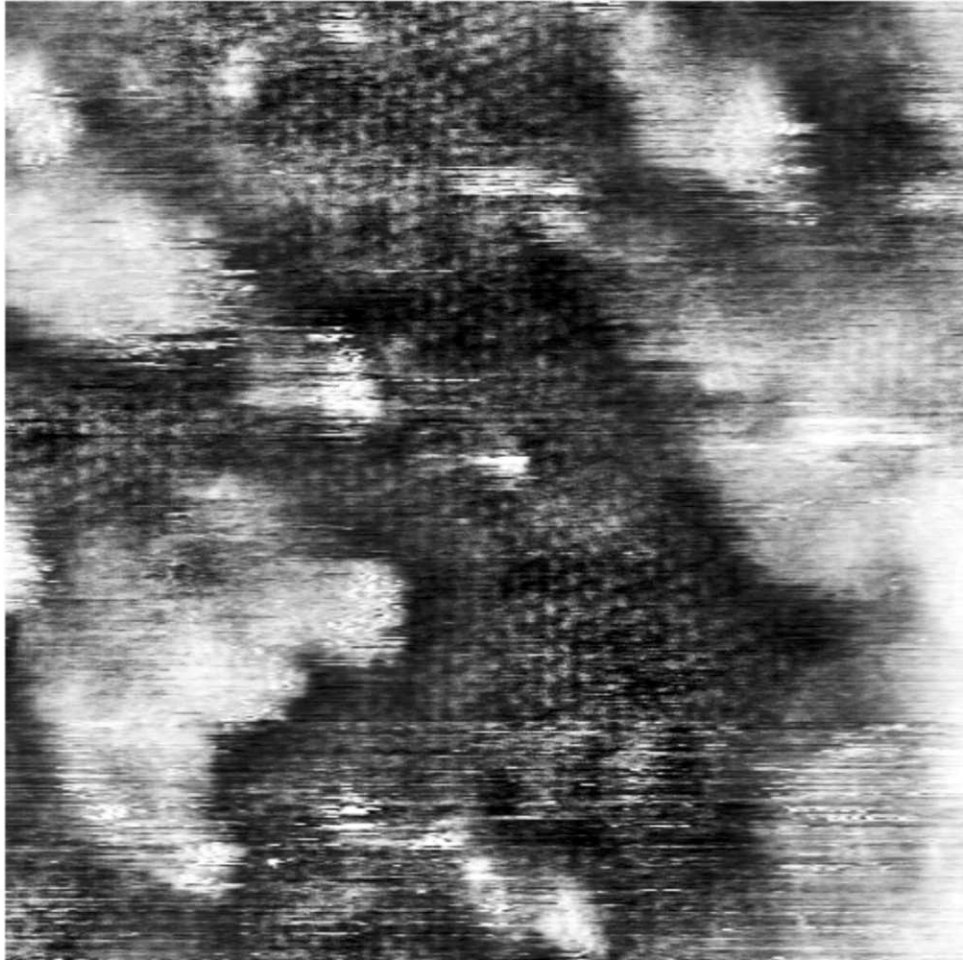
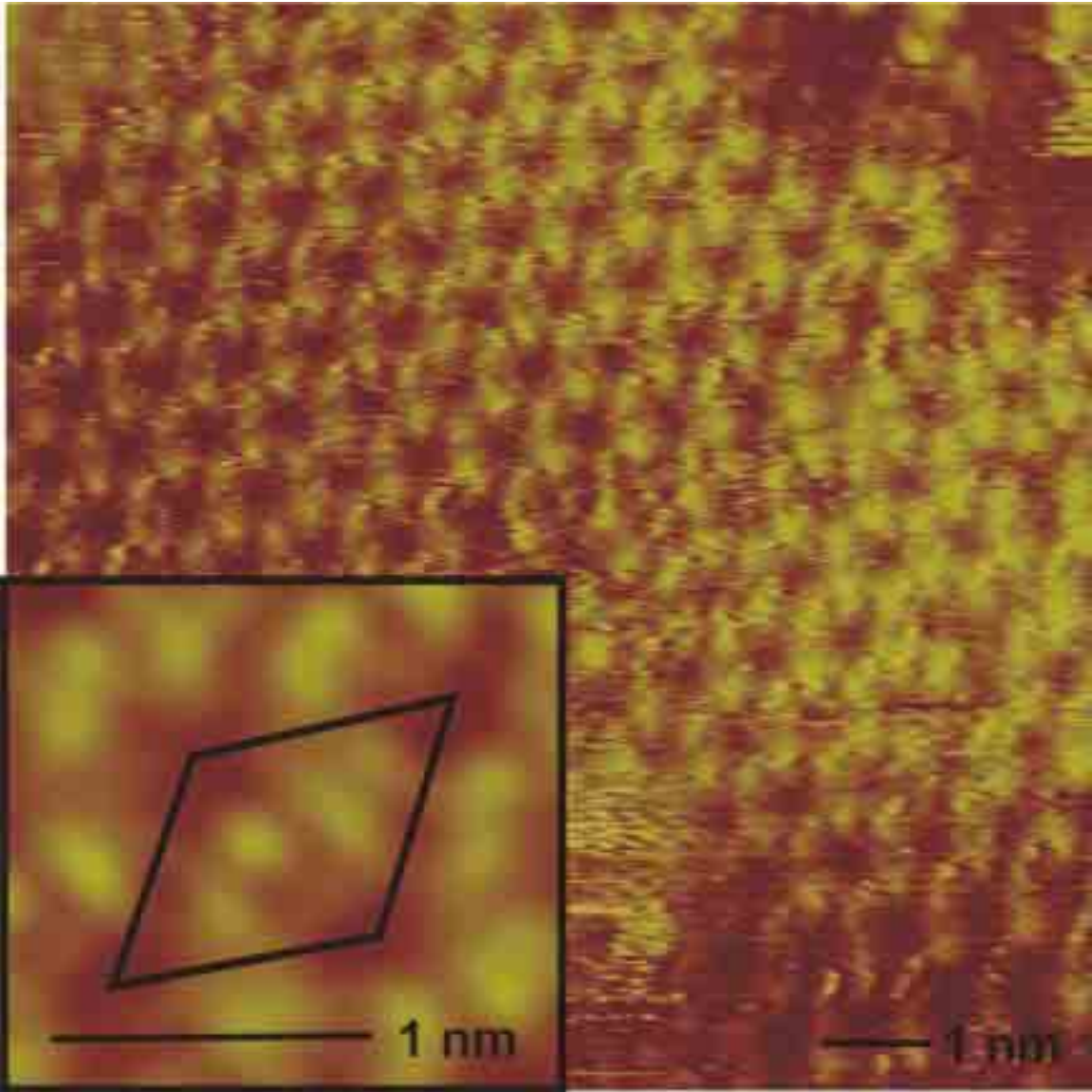


Figure 2.8 STM micrograph of $(\sqrt{7} \times \sqrt{7})R19.1^\circ$ -CdTe. Scan size is 10 nm x 10 nm.



holes. The holes create a simple $(\sqrt{7}\times\sqrt{7})R19.1^\circ$ lattice, suggesting a structure composed of 1/7 ML coverage of each element as the simplest basis for the unit cell. However, the idea of 1/7 ML coverage of each element is at odds with the coverage data. A model which results in the $(\sqrt{7}\times\sqrt{7})R19.1^\circ$ array of darker spots and maintains a 3/7 ML coverage of both elements with the Cd atoms on the Au surface, is shown in Figure 2.6B. The inset in Figure 2.8 is a section of an image that was significantly filtered, and suggests features consistent with the structure proposed in Figure 2.6B.

The data in Figure 2.2C, obtained by depositing 0.28 ML of Cd in the first step followed by Te deposition at a series of potentials, and the data listed in Table 2.1C are consistent with the above models. The first point, at -0.6 V, for Te deposition resulted in a diffuse LEED pattern, the result of adsorbed tellurite, TeO_3^{2-} (Table 2.1C), and probable disruption of the previously deposited Cd structure, as Te UPD begins. At -0.7 V, a good quality $(\sqrt{7}\times\sqrt{7})R19.1^\circ$ was observed with a Cd/Te ratio near 0.8. Given that the model structure (Figure 2.6B) suggests Cd and Te coverages of 0.43 ML each, and only 0.28 ML of Cd was initially deposited, some of the surface is probably covered with Te UPD. This would result in a Cd/Te ratio less than one, as observed. As more Te is deposited the Cd/Te ratio drops to below 0.5, and the $(\sqrt{7}\times\sqrt{7})R19.1^\circ$ pattern becomes increasingly diffuse, until a diffuse (1X1) is observed at potentials below -0.95 V. The best $(\sqrt{7}\times\sqrt{7})R19.1^\circ$ LEED pattern was observed for the deposits with Cd/Te ratios closest to 1, and the pattern becomes diffuse as excess Te is deposited, consistent with the proposed model (Figure 2.6B). It is also understandable that no (3X3) was observed in this set of studies, Figure 2.2C, as there was not even enough Cd to form a full monolayer of the $(\sqrt{7}\times\sqrt{7})R19.1^\circ$ structure.

In Figure 2.2D, the initial coverage of Cd was 0.48 ML. As Te was deposited, diffuse LEED patterns were again observed at -0.7 V and -0.8 V, although very faint indications of both $(\sqrt{7}\times\sqrt{7})R19.1^\circ$ and (3X3) patterns were evident. These surface structures were probably transitions, where some Te was deposited and disrupted the initial Cd structure, but the CdTe structures were not yet well formed. In addition, there is evidence of some tellurite species present at these more positive potentials (Table 2.1D). At -0.9 V, a (3X3) was clearly evident, but not of a high quality, as many of the LEED spots were barely visible. The ratio was near 0.8, suggesting that there was again a significant excess of Te, even starting with 0.5 ML of Cd. With the deposition of more Te at -1.0V, the ratio drops to 0.6, and the LEED pattern became very diffuse, with only a few spots evident. At -1.1V, a diffuse (1X1) was evident with some faint indications of $\sqrt{7}$ spots. It is not presently clear why a $(\sqrt{7}\times\sqrt{7})R19.1^\circ$ structure would be forming with such high coverages of Cd and Te.

Based on the above results, and specifically the proposed structures in Figure 2.6, a three-step experiment was performed. The idea was to form the (3X3) structure (Figure 2.6A) by first depositing 0.44 ML of Cd, followed by 0.44 ML of Te, and finally 0.44 ML of Cd again. The first two-steps of the three-step procedure produced a high quality $(\sqrt{7}\times\sqrt{7})R19.1^\circ$ pattern, while the third step converted the surface structure to the (3X3). Figure 2.3C is the LEED pattern observed after the three-step deposit, while Figure 2.3B is one of the best (3X3) structures formed using a two-step deposition. The difference in quality between the two is striking, suggesting that a much higher quality (3X3) deposit resulted from the three-step process, relative to the two-step process. In addition, this

procedure clearly shows how the increase in Cd coverage induced formation of the (3X3) from the $(\sqrt{7}\times\sqrt{7})R19.1^\circ$.

Figure 2.9 shows two sequential large-scale in situ STM images. The first is of a Au(111) surface coated with the 1/3 ML coverage (13X13)-Te structure in a solution containing 0.20 mM CdSO₄ and 1 mM H₂SO₄ at a potential prior to Cd UPD. The potential was switched midway through the second image, and in the upper half of Figure 2.9B, a series of clusters is visible during CdTe deposition. Figure 2.10 shows two sequential images taken in the Cd²⁺ solution, the first is of a non-atomically resolved $(\sqrt{7}\times\sqrt{7})R19.1^\circ$ -CdTe deposit, formed by depositing Cd on the 1/3 ML coverage (13X13)-Te structure. In the second image, the potential was shifted positive to strip Cd from the deposit, leaving only the (13X13)-Te layer on the surface (the bottom half of Figure 2.10B). Evidence for the (13X13) lattice can be seen in the hexagonal pattern at the bottom of Figure 2.10B. The bright clusters evident on the surface in Figure 2.9B and the upper part of Figure 2.10B are presumed to be similar. Given that the initial Te coverage was 1/3 (0.33) ML, and that an optimal $(\sqrt{7}\times\sqrt{7})R19.1^\circ$ -CdTe structure involves 3/7 (0.43) ML of both Cd and Te, this structure should only cover about 3/4 of the surface. This then suggests that Cd UPD will cover the remaining surface. It is proposed here that the clusters evident in both sets of STM images (Figures 2.9 and 2.10) are patches of Cd UPD. Hayden and Nandhakumar also observed similar patches during the EC-ALE formation of CdTe on Au(100) [36]. There are several reasons why these patches may appear brighter than the surrounding $(\sqrt{7}\times\sqrt{7})R19.1^\circ$ -CdTe structure. First, these images were obtained in a sulfate electrolyte, and it is known that Cd UPD occurs with the coadsorption of sulfate anions [59-61], thickening the Cd UPD domains. The

Figure 2.9 Large-scale STM micrographs of a (13X13)-Te atomic layer before and after Cd deposition. A) (13X13)-Te atomic layer at 0.10 V in 0.20 mM CdSO₄ with 1 mM H₂SO₄; B) Cd deposition at -0.40 V in 0.20 mM CdSO₄ with 1 mM H₂SO₄. The potential was changed from 0.10 V to -0.40 V midway through the image.

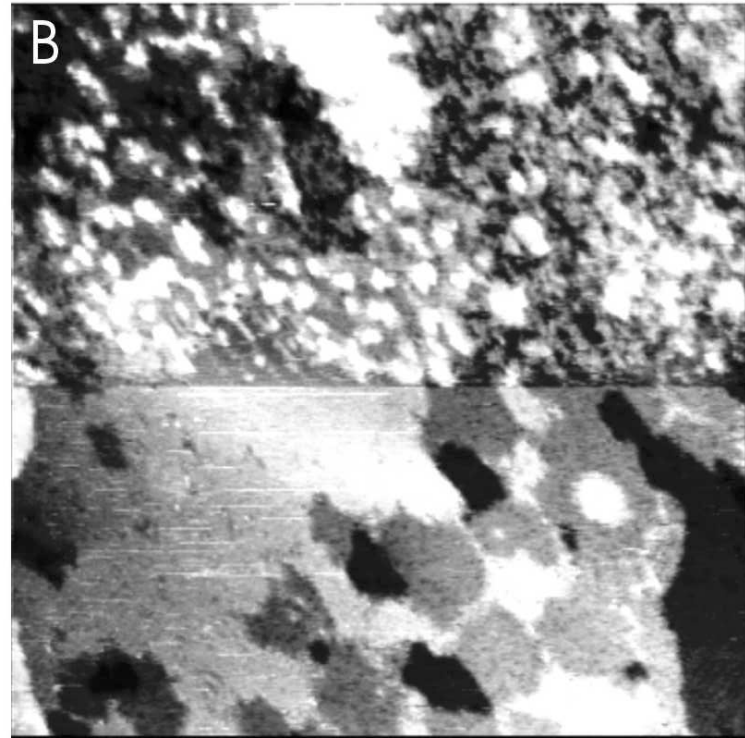
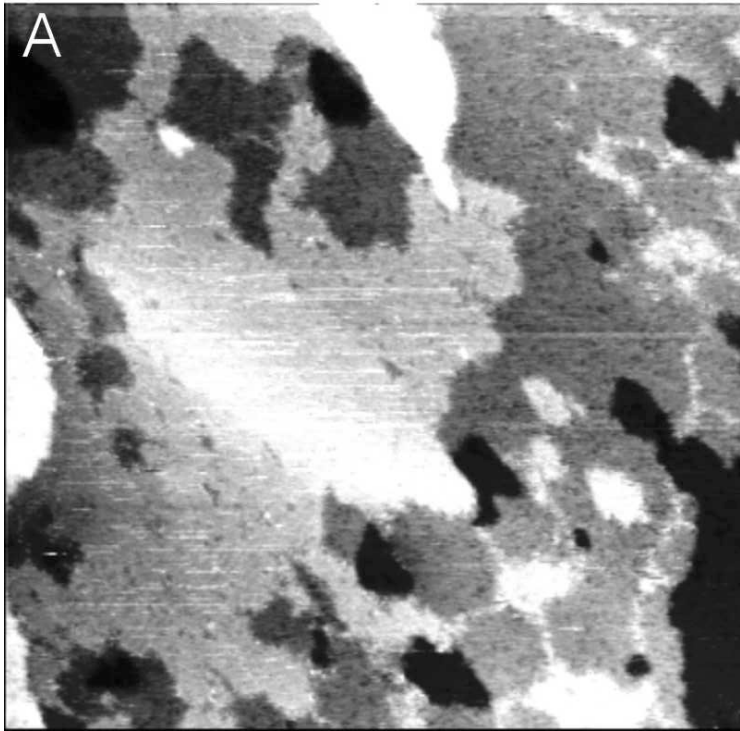
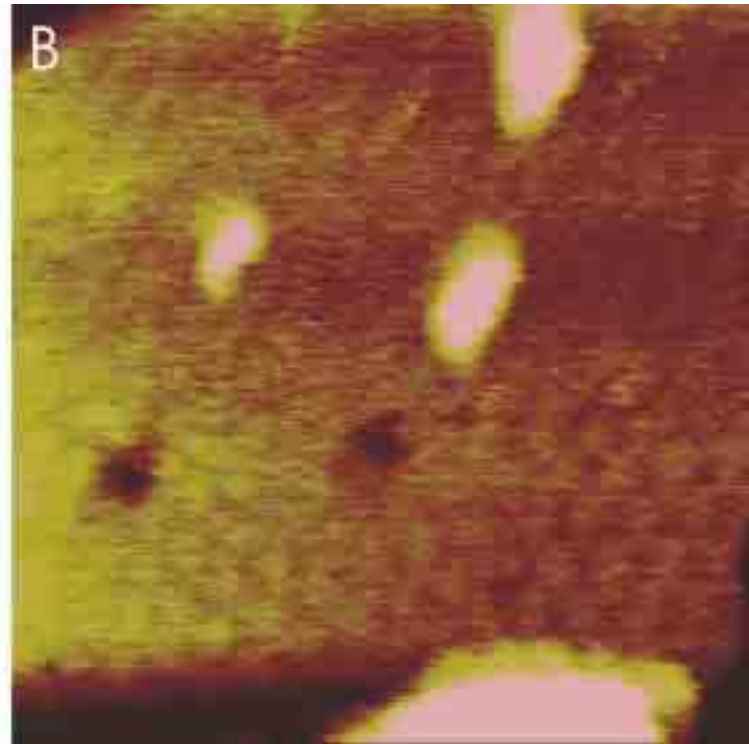
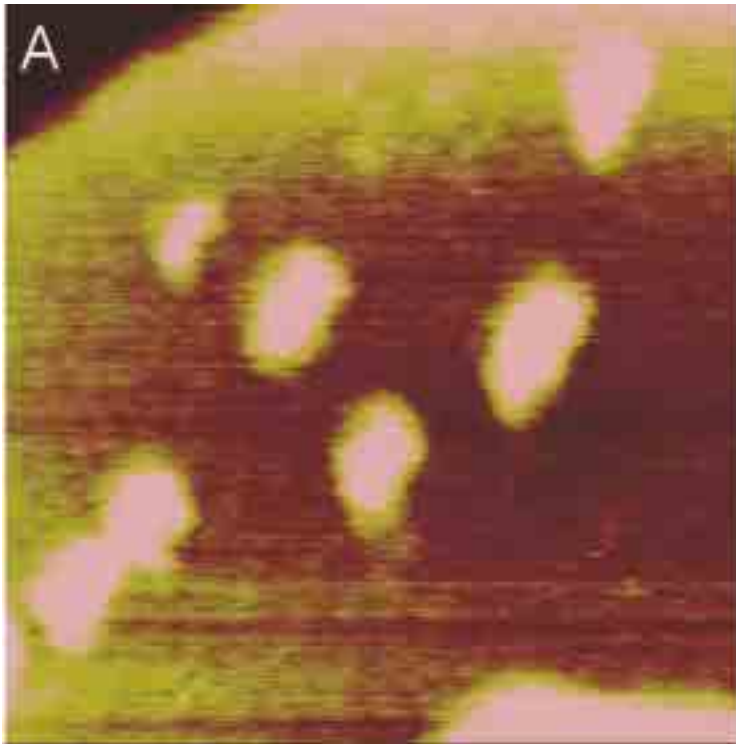


Figure 2.10 STM micrographs of Cd deposition and stripping on a (13X13)-Te atomic layer. A) Cd deposition at -0.50 V using 0.20 mM CdSO₄ in 1 mM H₂SO₄; B) Cd stripping at -0.30 V in 0.20 mM CdSO₄ with 1 mM H₂SO₄. Scan size is 50 nm x 50 nm, and the Z-range is 0.40 nm.



brightness of the areas may be due to an electronic effect, as there is evidence that the first monolayer of compound has an electronic structure closer to bulk CdTe than an atomic layer of Cd or Te on Au, and tunneling may be more difficult on the CdTe domains under the conditions used, while Cd UPD would behave as a normal metal surface, and appear brighter. Finally, the first image in Figure 2.10 shows a number of these brighter clusters. When Cd was stripped from the surface, the Te (13×13) was revealed, along with some pits. The pit locations coincided with the positions of the clusters, suggesting that the clusters contained Cd UPD, and when the Cd was stripped, the bare Au was revealed. The pits appeared to fill in fairly rapidly, as the surrounding Te atoms diffused back to fill the voids.

Conclusions

Atomic layers of CdTe were electrodeposited on Au(111) by alternately depositing atomic layers of Cd and Te, using EC-ALE. Two structures, a $(\sqrt{7}\times\sqrt{7})R19.1^\circ$ -CdTe and a (3×3) -CdTe, were observed. Both structures were formed starting with Cd or Te. Structures have been proposed for both which differ significantly from previously proposed models, based on coverage measurements and in-situ STM images. The (3×3) appears to adopt a sandwich structure, with an atomic layer of Te between the atomic layer of Cd in contact with the Au surface and the topmost Cd layer. The (3×3) was thus only observed when significant Cd was present. The (3×3) was prepared using either a two-step or three-step process, however, the highest quality structure was formed using the latter. Stoichiometry appears to be an important factor in determining the structure and morphology of the resulting deposit. From AES, the

stoichiometric ratios are 1:1 for the $(\sqrt{7} \times \sqrt{7})R19.1^\circ$ -CdTe and 2:1 for the (3X3)-CdTe.

In addition, clusters are formed on the deposit if the coverage of the first atomic layer is too low, and the desired structure does not completely cover the surface.

Acknowledgements

The National Science Foundation, Division of Materials Research, and the University of Georgia Research Foundation have provided support for this work, and we gratefully appreciate their assistance.

References

1. A. M. D. Ede, E. J. Morton, and P. DeAntonis, Nucl. Instrum. Methods Phys. Res., Sect. A 458 (2001) 7.
2. T. Ozaki, Y. Iwase, H. Takamura, and M. Ohmori, Nucl. Instrum. Methods Phys. Res., Sect. A 380 (1996) 141.
3. N. W. Duffy, L. M. Peter, R. L. Wang, D. W. Lane, and K. D. Rogers, Electrochim. Acta 45 (2000) 3355.
4. L. M. Peter and R. L. Wang, Electrochem. Commun. 1 (1999) 554.
5. J. Tousekova, D. Kindl, and J. Tousek, Thin Solid Films 293 (1997) 272.
6. S. A. Gamboa, P. J. Sebastian, X. Mathew, H. Nguyen-Cong, and P. Chartier, Sol. Energy Mater. 59 (1999) 115.
7. A. T. S. Wee, Z. C. Feng, H. H. Hng, K. L. Tan, R. F. C. Farrow, and W. J. Choyke, J. Phys.: Condens. Matter 7 (1995) 4359.

8. K. Maruyama, H. Nishino, T. Okamoto, S. Murakami, T. Saito, Y. Nishijima, M. Uchikoshi, M. Nagashima, and H. Wada, *J. Electron. Mater.* 25 (1996) 1353.
9. G. F. Fulop and R. M. Taylor, *Ann. Rev. Mater. Sci.* 15 (1985) 197.
10. K. Rajeshwar, *Adv. Mater.* 4 (1992) 23.
11. G. Hodes, in: I. Rubinstein (Ed.), *Physical Electrochemistry*, Marcel Dekker, New York, 1995, p. 515.
12. R. K. Pandey, S. N. Sahu, and S. Chandra, *Handbook of Semiconductor Electrodeposition*, Marcel Dekker, Inc., New York, 1996.
13. J. L. Stickney, in: I. Rubenstein (Ed.), *Electroanalytical Chemistry*, Marcel Dekker, New York, 1999, p. 75.
14. B. W. Gregory, D. W. Suggs, and J. L. Stickney, *J. Electrochem. Soc.* 138 (1991) 1279.
15. C. H. L. Goodman and M. V. Pessa, *J. Appl. Phys.* 60 (1986) R65.
16. T. F. Kuech, P. D. Dapkus, and Y. Aoyagi, *Atomic Layer Growth and Processing*, Materials Research Society, Pittsburgh, 1991.
17. S. Bedair, *Atomic Layer Epitaxy*, Elsevier, Amsterdam, 1993.
18. L. Niinisto and M. Leskela, *Thin Solid Films* 225 (1993) 130.
19. D. M. Kolb, in: C. W. Tobias (Ed.), *Advances in Electrochemistry and Electrochemical Engineering*, John Wiley, New York, 1978, p. 125.
20. B. W. Gregory and J. L. Stickney, *J. Electroanal. Chem.* 300 (1991) 543.
21. R. R. Adzic, in: H. Gerischer and C. W. Tobias (Eds.), *Advances in Electrochemistry and Electrochemical Engineering*, 1984, p. 159.
22. K. Juttner and W. J. Lorenz, *Z. Phys. Chem. (Wiesbaden)* 122 (1980) 163.

23. A. A. Gewirth and B. K. Niece, *Chem. Rev.* 97 (1997) 1129.
24. M. L. Foresti, G. Pezzatini, M. Cavallini, G. Aloisi, M. Innocenti, and R. Guidelli, *J. Phys. Chem. B* 102 (1998) 7413.
25. G. Pezzatini, S. Caporali, M. Innocenti, and M. L. Foresti, *J. Electroanal. Chem.* 475 (1999) 164.
26. L. P. Colletti, B. H. Flowers, and J. L. Stickney, *J. Electrochem. Soc.* 145 (1998) 1442.
27. T. E. Lister, L. P. Colletti, and J. L. Stickney, *Isr. J. Chem.* 37 (1997) 287.
28. T. E. Lister and J. L. Stickney, *Appl. Surf. Sci.* 107 (1996) 153.
29. T. E. Lister, R. D. Herrick, and J. L. Stickney, *Abstr. Pap. Am. Chem. Soc.* 208 (1994) 128.
30. U. Demir and C. Shannon, *Langmuir* 10 (1994) 2794.
31. T. Torimoto, A. Obayashi, S. Kuwabata, H. Yasuda, H. Mori, and H. Yoneyama, *Langmuir* 16 (2000) 5820.
32. T. L. Wade, L. C. Ward, C. B. Maddox, U. Happek, and J. L. Stickney, *Electrochem. Solid State Lett.* 2 (1999) 616.
33. T. L. Wade, R. Vaidyanathan, U. Happek, and J. L. Stickney, *J. Electroanal. Chem.* 500 (2001) 322.
34. D. W. Suggs and J. L. Stickney, *Surf. Sci.* 290 (1993) 362.
35. D. W. Suggs and J. L. Stickney, *Surf. Sci.* 290 (1993) 375.
36. B. E. Hayden and I. S. Nandhakumar, *J. Phys. Chem. B* 102 (1998) 4897.
37. K. Varazo, M. D. Lay, and J. L. Stickney, University of Georgia, Athens, GA, 2000.

38. M. P. Soriaga, *Prog. Surf. Sci.* 39 (1992) 325.
39. M. P. Soriaga, D. A. Harrington, J. L. Stickney, and A. Wieckowski, in: B. E. Conway, J. O. Bockris, and R. E. White (Eds.), *Modern Aspects of Electrochemistry*, Plenum Press, New York, 1995, p. 1.
40. J. F. Moulder, W. F. Stickle, P. E. Soble, and K. D. Bomben, *Handbook of X-ray Photoelectron Spectroscopy*, Perkin-Elmer Corporation, Eden Prairie, 1992.
41. D. W. Suggs and A. J. Bard, *J. Am. Chem. Soc.* 116 (1994) 10725.
42. D. W. Suggs and J. L. Stickney, *J. Phys. Chem.* 95 (1991) 10056.
43. T. A. Sorenson, K. Varazo, D. W. Suggs, and J. L. Stickney, *Surf. Sci.* 470 (2001) 197.
44. B. E. Hayden and I. S. Nandhakumar, *J. Phys. Chem. B* 101 (1997) 7751.
45. N. Ikemiya, D. Iwai, K. Yamada, R. Vidu, and S. Hara, *Surf. Sci.* 369 (1996) 199.
46. N. Ikemiya, K. Yamada, and S. Hara, *J. Vac. Sci. Technol., B* 14 (1996) 1369.
47. I. Yagi, J. M. Lantz, S. Nakabayashi, R. M. Corn, and K. Uosaki, *J. Electroanal. Chem.* 401 (1996) 95.
48. I. Yagi, S. Nakabayashi, and K. Uosaki, *Surf. Sci.* 406 (1998) 1.
49. I. Yagi, S. Nakabayashi, and K. Uosaki, *J. Phys. Chem. B* 102 (1998) 2677.
50. F. Forni, M. Innocenti, G. Pezzatini, and M. L. Foresti, *Electrochim. Acta* 45 (2000) 3225.
51. L. E. Davis, N. C. MacDonald, P. W. Palmberg, G. E. Riach, and R. E. Weber, *Handbook of Auger Electron Spectroscopy*, Physical Electronics Division, Perkin-Elmer Corporation, Eden Prairie, Minnesota, 1978.

52. O. M. Magnussen, B. M. Ocko, R. R. Adzic, and J. X. Wang, *Phys. Rev. B: Condens. Matter* 51 (1995) 5510.
53. B. W. Gregory, M. L. Norton, and J. L. Stickney, *J. Electroanal. Chem.* 293 (1990) 85.
54. J. L. Stickney, S. D. Rosasco, and A. T. Hubbard, *J. Electrochem. Soc.* 131 (1984) 260.
55. J. W. Schultze, F. D. Koppitz, and M. M. Lohrengel, *Ber. Bunsenges. Phys. Chem.* 78 (1974) 693.
56. R. Vidu and S. Hara, *J. Electroanal. Chem.* 475 (1999) 171.
57. G. Horanyi, *J. Solid State Electrochem.* 4 (2000) 177.
58. G. Inzelt and G. Horanyi, *J. Electroanal. Chem.* 491 (2000) 111.
59. B. K. Niece and A. A. Gewirth, *Langmuir* 13 (1997) 6302.
60. J. C. Bondos, A. A. Gewirth, and R. G. Nuzzo, *J. Phys. Chem.* 100 (1996) 8617.
61. S. J. Hsieh and A. A. Gewirth, *Langmuir* 16 (2000) 9501.

CHAPTER 3

CADMIUM UNDERPOTENTIAL DEPOSITION ON AU(111) FROM CHLORIDE, SULFATE, IODIDE, ACETATE, AND PERCHLORATE ELECTROLYTES: ANION INFLUENCE OF OBSERVED STRUCTURES STUDIED BY LEED, XPS, AND AUGER ELECTRON SPECTROSCOPY¹

¹K. Varazo, M.D. Lay, J.L. Stickney, to be submitted to Surface Science.

Abstract

Cd electrodeposition on Au(111) in chloride, sulfate, iodide, acetate, and perchlorate solutions has been studied using cyclic voltammetry, Auger electron spectroscopy (AES), low energy electron diffraction (LEED), and X-ray photoelectron spectroscopy (XPS). Surface analysis demonstrated that Cd UPD and Cd-Au alloy formation occurred with the coadsorption of anions. The voltammetric behavior of Cd electrodeposition in perchlorate solutions differed from all the others studied, apparently affected by the weak adsorption behavior of perchlorate. Emersion from chloride or iodide electrolyte revealed no oxygen by AES, and XPS showed that the oxygen present after emerging from acetate, sulfate, and perchlorate electrolytes was due to anions. LEED experiments revealed different ordered structures for Cd UPD that depended upon the identity of the coadsorbed anion. The observed patterns were due to scattering from both cadmium and the anion, as shown by rinsing experiments demonstrating that an anion can be rinsed away and replaced by another to form a different structure. For Cd UPD from the chloride electrolyte, a $(\sqrt{7} \times \sqrt{7})R19.1^\circ$ structure was observed, and a $(\sqrt{3} \times \sqrt{3})R30^\circ$ for Cd UPD from sulfate, acetate, and perchlorate. What appeared to be a (6×6) was observed for Cd UPD from iodide electrolyte. The Cd layers did not appear to undergo spontaneous oxidation upon loss of potential control and emersion, and the anions appeared to form a protective overlayer. Electrochemical atomic layer epitaxy (EC-ALE) is the electrochemical analog of atomic layer epitaxy (ALE), a method used to form compound semiconductors one layer at a time, in a cycle. Cd atomic layers can be used in an EC-ALE cycle to form CdTe, CdS, CdSe, and HgCdTe materials.

Introduction

The formation of well-ordered atomic layers on metal substrates is an important process from a fundamental and technological viewpoint [1, 2]. In electrochemical systems, underpotential deposition (UPD) is a phenomenon in which an element deposits on a foreign metal substrate at potentials more positive than the reversible Nernst potential [3-5]. The structure of metal layers formed by UPD is influenced by the substrate identity, orientation, applied potential, and presence of specifically adsorbed anions [3, 6, 7]. Two of the most studied systems are Cu UPD on Au(111) [8-15] and Pt(111) [16-20], where the effect of anions has been clearly demonstrated by marked changes in the voltammetric behavior and structures formed.

Likewise, anion adsorption at metal surfaces is an important phenomenon, dependent on the potential and capable of changing the structure of a metal surface. In situ scanning tunneling microscopy (STM) has shown that anions induce the removal of Au(111) and Au(100) surface reconstructions [21-24]. Ordered chlorine, bromine, and iodine layers on Au(111) have been characterized by in situ (STM) [25-28] and X-ray scattering (SXS) [29-31]. Ordered sulfate structures have also been observed with in situ STM [32-34]. Hubbard and coworkers used iodine layers on Pt(111) electrodes to protect the metal surface during silver [35], copper [36], and lead [37] electrodeposition.

Electrodeposited Cd atomic layers on single crystal gold surfaces may have uses in materials research. Gewirth and coworkers have identified a catalytically active Cd layer on Au(111) for nitrate reduction, applicable to waste remediation and detection [38]. Au-Cd alloys can be used as ohmic contacts for semiconductor materials [39]. Cd atomic layers are also a central step in the formation of compound semiconductors using

electrochemical atomic layer epitaxy (EC-ALE) [40-43], an analog of atomic layer epitaxy (ALE) developed for the formation of compound semiconductors one monolayer at a time. Using surface-limited reactions, only two-dimensional growth is allowed as the materials are formed layer-by-layer. In EC-ALE, the individual elements are deposited at underpotentials, where an atomic layer forms as a result of the increased stability of the surface compound formed compared to formation of multiple layers of the element. Thin films are formed by sequential UPD of each element from a separate solution, in a cycle. The process can be automated and continued until the desired film thickness is reached. Several groups have used EC-ALE to prepare II-VI compound semiconductors, such as CdTe, Cd Se, CdS, ZnS, and ZnSe on gold and silver substrates [44-50]. Recently, deposits of the III-V compounds InAs and InSb have been formed, as well as a superlattice of them [51, 52].

Cd UPD has been studied on polycrystalline and (111) gold surfaces [38, 53-68]. Gewirth and coworkers have performed detailed in situ STM and chronocoulometry studies of Cd UPD on Au(111) from sulfate electrolytes [38, 59, 60]. In the UPD region, they observed a series of ordered adlattices exhibiting a long-range linear morphology, rotated 30° with respect to the gold lattice. From chronocoulometry they found that the layer contained Cd and coadsorbed sulfate. No ordered structures were formed in the absence of sulfate. Previous radiotracer studies of Cd UPD on Au also demonstrated the presence of sulfate [67, 68].

Earlier, ex situ studies of Cd UPD on the low index planes of gold suggested that Cd was spontaneously oxidized upon emersion (removal from solution), as significant amounts of oxygen were observed on the surface [69]. However, an ex situ study of Cd

UPD on Cu(111) by Wandelt et al. [70] identified the formation of a $(\sqrt{19}\times\sqrt{19})R23.4^\circ$ Cd UPD structure that included coadsorbed chlorine, and oxygen was not evident.

This study presents a UHV-EC study [71] of Cd UPD on Au(111) from different electrolyte solutions: chloride, sulfate, iodide, acetate, and perchlorate. The structures and compositions of the atomic layers formed were characterized by Auger electron spectroscopy (AES), X-ray photoelectron spectroscopy (XPS), and low energy electron diffraction (LEED). The results demonstrate the dependence of surface structure on electrode potential and anions present in solution.

Experimental

The UHV-EC [72] studies were performed using an ultrahigh vacuum (UHV) surface analysis chamber connected directly to an antechamber containing an electrochemical cell. The UHV system included a cylindrical mirror analyzer for Auger electron spectroscopy (AES) (Perkin-Elmer 11-010 Auger system), reverse-view optics for low energy electron diffraction (LEED) (Princeton model 11-020), an X-ray source (VG Scientific) and hemispherical analyzer (Leybold-Heraeus) for X-ray photoelectron spectroscopy (XPS), and an ion bombardment cage for sputter cleaning substrates. The base pressure of the chamber was 10^{-9} Torr, maintained with an ion and cryopump. The electrochemistry antechamber was stainless steel and connected to the main chamber through a gate valve, allowing direct sample transfer into and out of the analysis chamber without exposure to atmosphere. Auger spectra were collected using 3 keV ionizing electrons. XPS spectra were obtained using Al $K\alpha$ X-rays (1486.6 eV), and the Au $4f_{7/2}$

peak (83.98 eV) was used for calibration [73]. LEED pattern images were collected using a Kodak digital camera (Model DC290).

The Au(111) single crystal used (99.999% MaTecK GmbH) was a disc 1 cm in diameter and 2 mm thick. Before each electrochemical experiment, the crystal was cleaned by argon ion bombardment (8.5×10^{-5} Torr) for 30 minutes, followed by annealing with a resistively heated tungsten filament. Surface cleanliness and order were confirmed using AES and LEED, respectively.

All solutions were prepared with ultrapure water ($18 \text{ M}\Omega\text{-cm}$) obtained from a Nanopure filtration system (Barnstead), fed from the house-distilled water supply. The chloride and sulfate based cadmium solutions were prepared using 0.20 mM CdCl_2 (99.998% Puratronic Alfa Aesar) in 1 mM HCl (Baker analyzed A.C.S. reagent) (pH 3.0) and 0.20 mM CdSO_4 (99.999% Aldrich) in 1 mM H_2SO_4 (Baker analyzed A.C.S. reagent) (pH 3.0), respectively. The iodide solution was prepared with 0.20 mM CdCl_2 (99.998% Puratronic Alfa Aesar) in 1 mM HI (J. T. Baker reagent) (pH 3.0), and 0.20 mM $\text{Cd}(\text{ClO}_4)_2$ (G. Frederick Smith chemical company reagent) in 1 mM HClO_4 (J. T. Baker ULTREX) (pH 3.0) for the perchlorate electrolyte. The acetate solution contained 0.20 mM CdSO_4 (99.999% Aldrich) in a 0.40 mM sodium acetate (Baker A.C.S. reagent) and 0.40 mM acetic acid (Baker analyzed A.C.S. reagent) (pH 4.85) solution. All experiments were conducted at room temperature.

The electrochemistry experiments were carried out using a Pyrex glass cell housed in a stainless steel antechamber [72] coupled directly to the main surface analysis chamber. The potentiostat was based on conventional operational amplifier circuitry, and built in house. A gold wire (Wilkinson Company) served as the auxiliary electrode, and

all potentials were measured against a Ag/AgCl (3 M NaCl) reference electrode (Bioanalytical systems). Solutions were delivered into the cell from pressured Pyrex bottles, and experiments were conducted in an atmosphere of high purity argon (BOC).

Results and Discussion

Cadmium electrodeposition from chloride electrolyte

Figure 3.1 shows the cyclic voltammogram for the clean and annealed Au(111) crystal in a solution containing 0.20 mM CdCl₂ and 1 mM HCl (pH 3). Scanning negative from 0.30 V there is a small shoulder, before peak R1, at -0.30 V. Peaks R1 and O1 are due to Cd underpotential deposition (UPD) and stripping [57, 60, 65, 74]. The charge for peak R1, after background subtraction is 170 mC/cm², corresponding to 0.3 ML of Cd. The coverage is defined relative to the number of Au substrate surface atoms, with a ratio of 1.0 being a full monolayer (ML). Previous thin layer electrochemical cell (TLEC) studies using 0.05 M CdSO₄ in 0.05 M H₂SO₄ (pH 1.5) suggested 0.22 ML for Cd UPD on polycrystalline gold [57]. Continuing in the negative direction, reduction feature R2 at -0.56 V exists as a shoulder on the large reduction wave R3. Peaks O2 and R2 are related, as are O3 and R3. R2/R3 are due to Cd-Au alloy formation and O2/O3 to alloy stripping, which has been shown to occur at potentials more positive than the reversible Cd deposition potential [66, 74, 75]. The charge for R3 was greater than for O3 because of concomitant hydrogen evolution. Bulk Cd stripping was not observed even at the most negative potentials studied. Investigations of Cd electrodeposition in sulfuric acid evidenced Cd bulk stripping just positive of the Cd formal potential, near -0.80 V (vs. Ag/AgCl) [38, 57]. The absence of this peak in

Figure 3.1 Cyclic voltammogram of the Au(111) electrode in 0.20 mM CdCl₂ and 1 mM HCl (pH 3). Scan rate = 5 mV/s

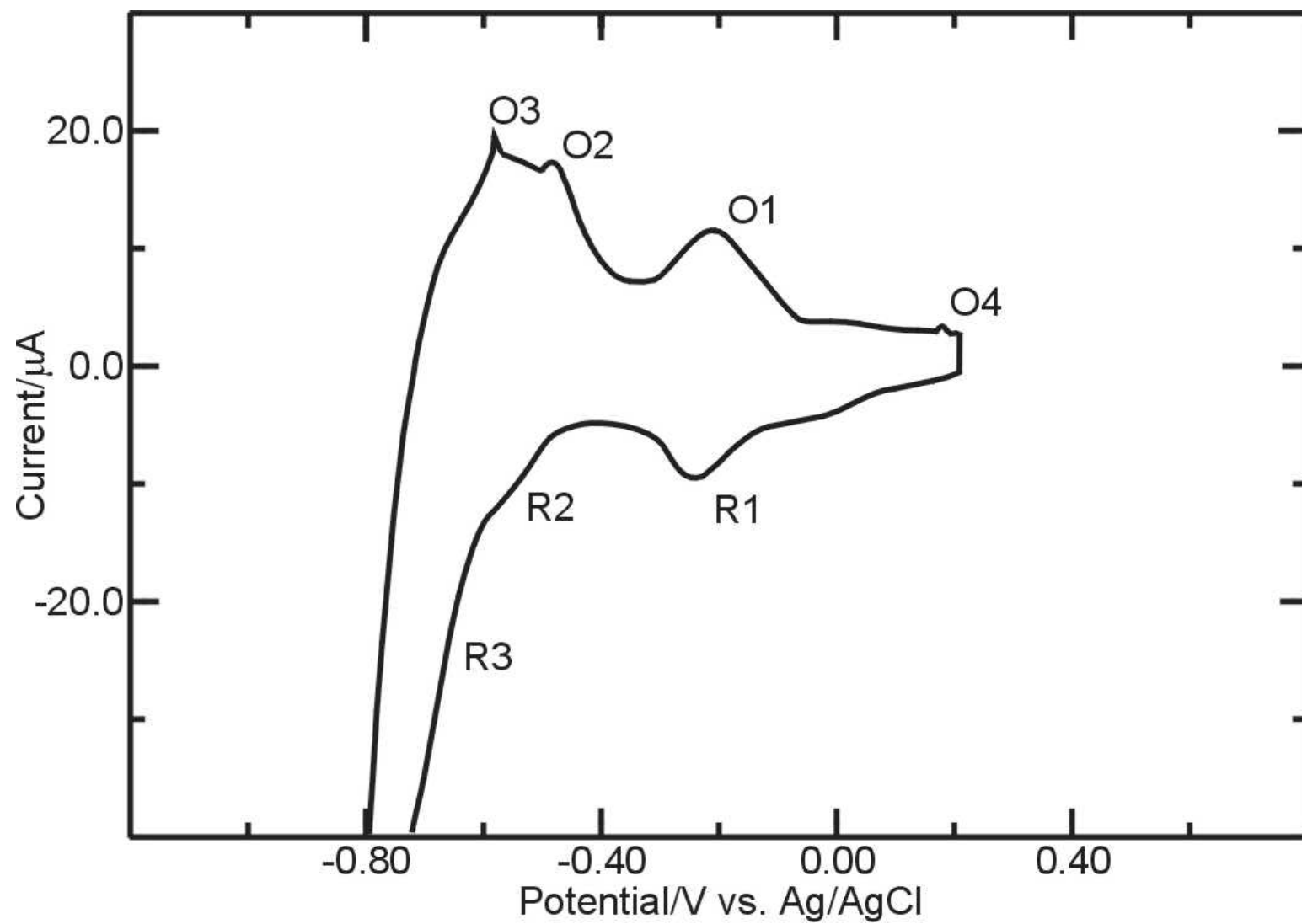


Figure 3.1 may be due to the low concentration of Cd, as the studies in sulfuric acid were performed with much higher Cd concentrations. Jovic and Jovic have shown that when using higher Cd concentrations, the bulk Cd stripping peak can be observed [75]. Cd deposition at -0.70 V and more negative, followed by Cd stripping, increased the charge under all the oxidation peaks including the Cd UPD stripping peak, due to the slow kinetics of alloy stripping [68]. A similar change in the Cd UPD stripping peak was observed for bulk Cd stripping from a Cu(111) electrode [70]. Finally, the small peak O4 at 0.20 V has been associated with the lifting of the Au(111) reconstruction [23, 76]. Cyclic voltammetry of the Au crystal in 1 mM HCl without Cd (not shown) also exhibits a small peak at 0.20 V, supporting that the oxidation feature is not due to Cd, but involves Cl.

After Cd electrodeposition the surface was analyzed using AES and XPS. The AES spectrum for the electrode emersed at -0.40 V (Figure 3.2) shows transitions for Cd (376 eV), Cl (181 eV), and gold (69 eV) only. For all the immersion experiments in 0.20 mM CdCl₂ and 1 mM HCl (pH 3), oxygen was not detected by AES, suggesting that the Cd monolayers were not oxidized upon emersion. The Cl 2p and Cd 3d XPS spectra obtained after emersing the electrode at -0.40 V are shown in figures 3.3 and 3.4, respectively. The Cl 2p_{3/2} peak at 198.0 eV is within the range for metal chlorides such as TiCl₄ (198.2 eV) [77] and HgCl₂ (198.7 eV) [78]. The Cd 3d_{5/2} peak at 404.7 eV is lower than bulk Cd (405.1 eV) [73], which may be due to Cd bonding to Au, since for CdTe the Cd peak is shifted to lower binding energies (404.9 eV) [79, 80]. From in situ extended X-ray absorption fine structure (EXAFS), X-ray standing wave (XSW), and electrochemical studies of Cu UPD on Pt(111), Abruna and coworkers found that in the

Figure 3.2 Auger spectrum of the Au(111) surface after emersion at -0.40 V from 0.20 mM CdCl₂ and 1 mM HCl (pH 3).

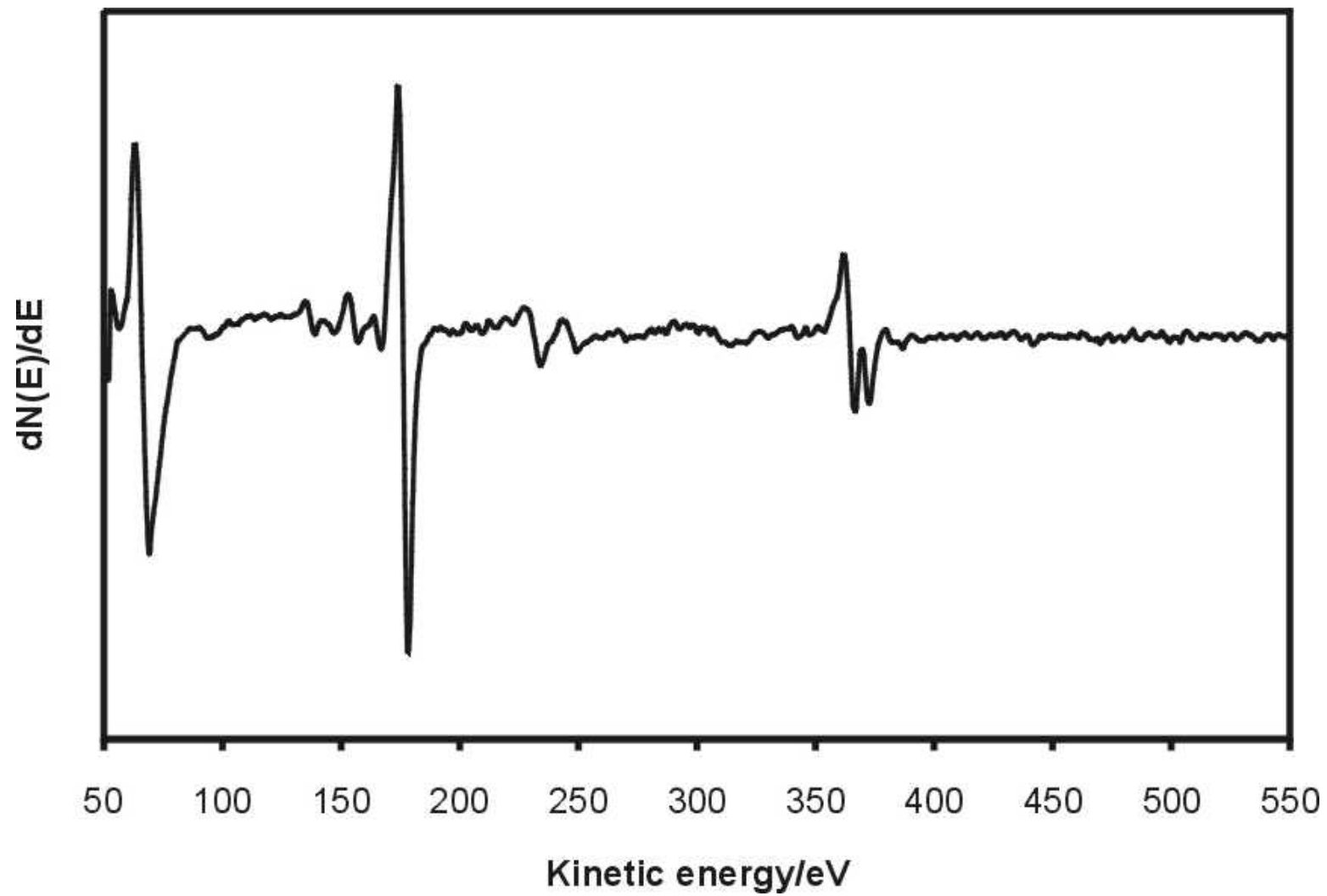


Figure 3.3 Chlorine 2p XPS spectrum of the Au(111) surface after emersion at -0.40 V from 0.20 mM CdCl₂ and 1 mM HCl (pH 3).

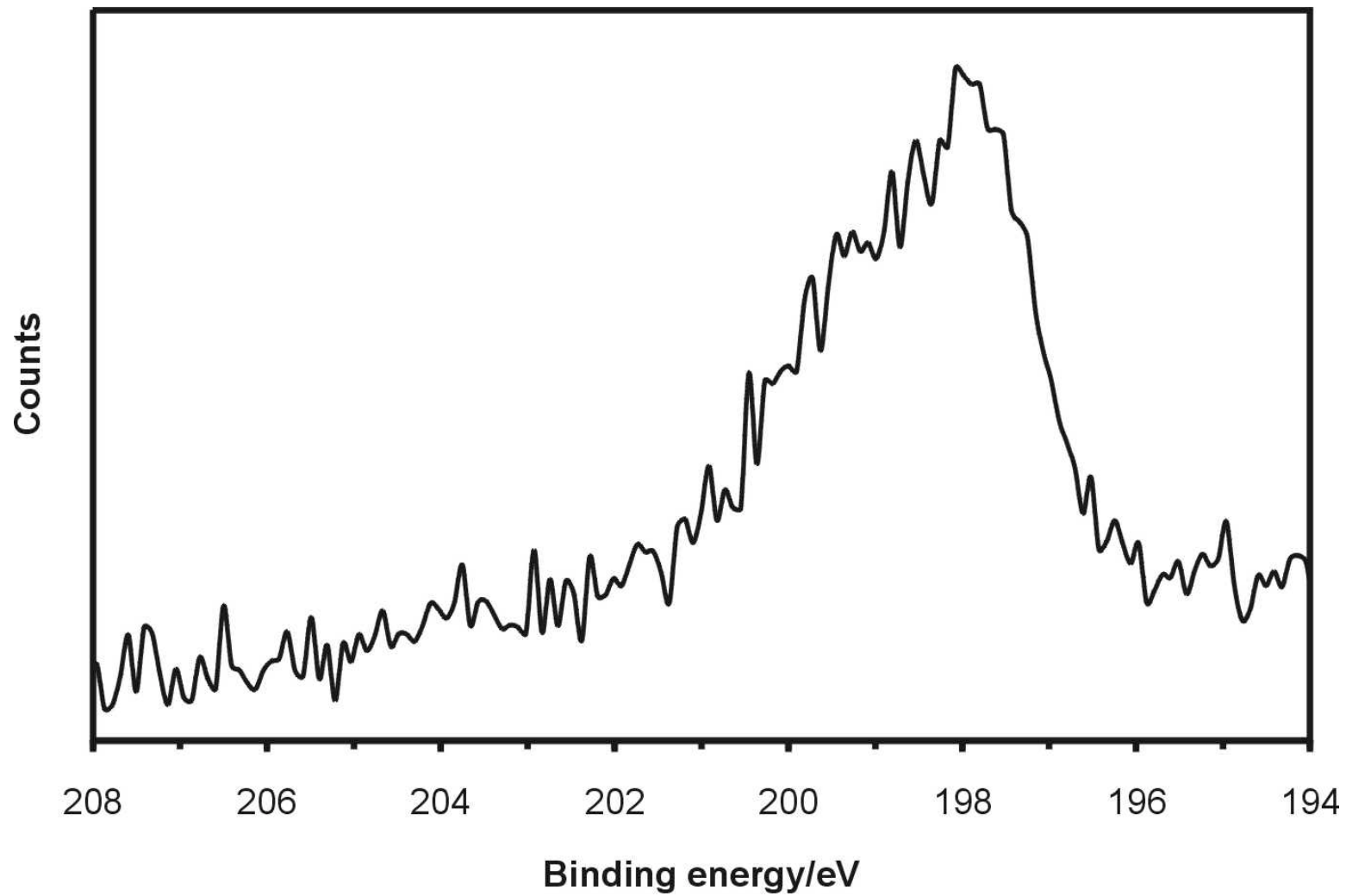
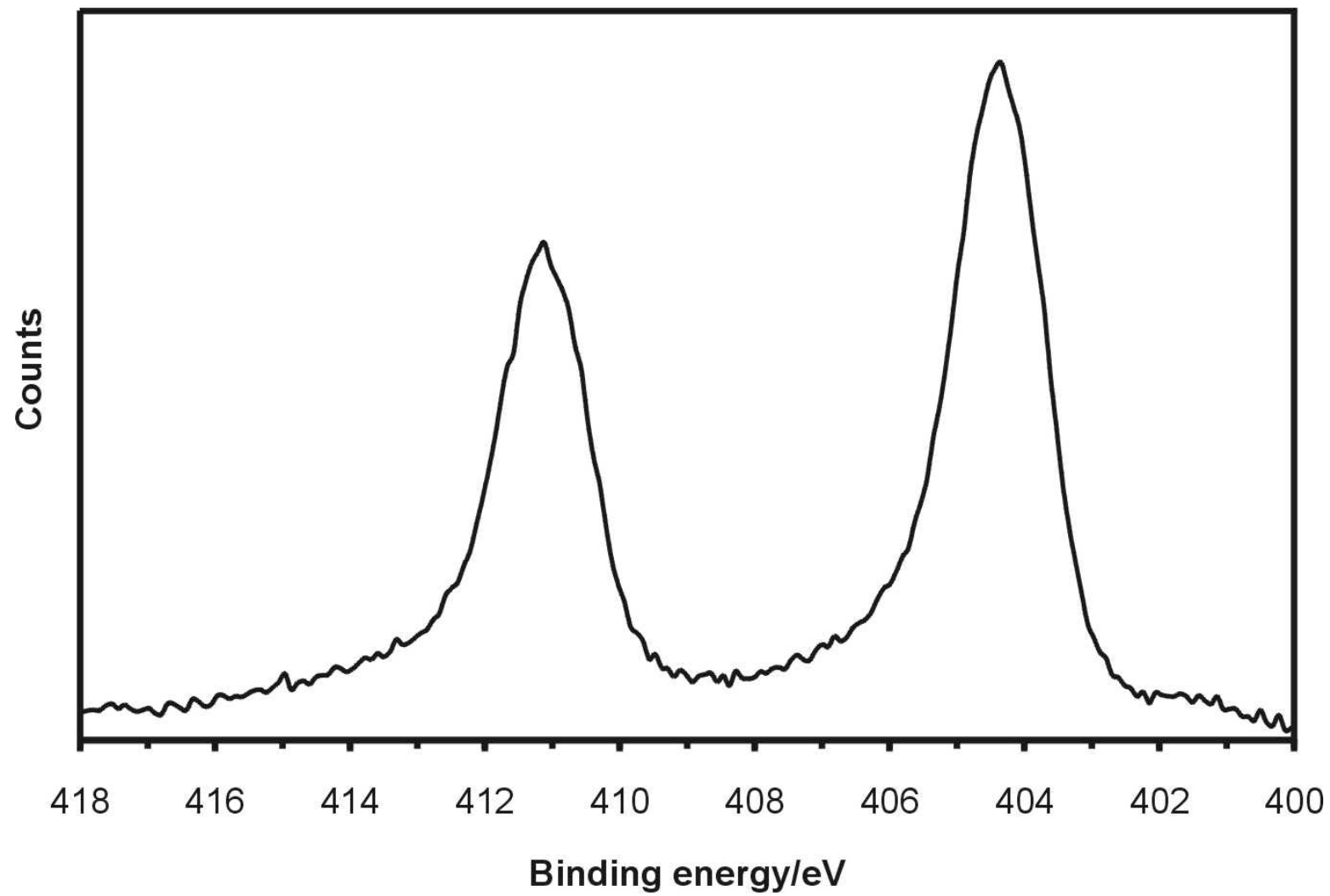


Figure 3.4 Cadmium 3d XPS spectrum of the Au(111) surface after emersion at -0.40 V from 0.20 mM CdCl₂ and 1 mM HCl (pH 3).



presence of chloride, oxygen was not present in the copper layer, and that the chloride acted as a protective layer precluding oxygen adsorption [19].

Figure 3.5 shows a graph of the Cd/Au and Cl/Au Auger ratios as a function of the immersion potential, and Figure 3.6A-B shows the LEED patterns obtained. At potentials prior to Cd UPD, some Cl was found on the surface with only a residual Cd signal. The Cl signal began to increase with the onset of Cd UPD. LEED experiments revealed a faint $(\sqrt{7}\times\sqrt{7})R19.1^\circ$ unit cell after emersing the electrode at -0.08 V. The same structure was observed at potentials for R1 at -0.30 V and -0.40 V, where the Cd/Au ratio was higher and the pattern contained much sharper and clearer spots, indicating a higher quality structure (Figure 3.6A). The Cd/Au ratio reached a plateau value between -0.30 V and -0.40 V, expected for a surface-limited reaction [41, 81]. At -0.60 V the Cd/Au ratio increased, and a diffuse $(\sqrt{3}\times\sqrt{3})R30^\circ$ unit cell was observed. Diffraction spots from the $(\sqrt{7}\times\sqrt{7})R19.1^\circ$ were still visible however, indicating that the surface structure was in transition at this potential. At -0.70 V and potentials more negative the Cd/Au ratio increased still further, and only the $(\sqrt{3}\times\sqrt{3})R30^\circ$ pattern was visible (Figure 3.6B). Below -0.80 V, bulk Cd deposition takes place [38, 57], as suggested by the dramatic increase in the Cd/Au ratio. These structures have not been previously reported, but an ex situ study of Cd UPD on Cu(111) by Wandelt et al. from chloride electrolytes found a $9/19$ ML Cd $(\sqrt{19}\times\sqrt{19})R23.1^\circ$ structure containing coadsorbed Cl, and a different structure for bulk Cd deposition [70]. The Cd and Cl coverages as a function of immersion potential were determined using AES sensitivity factors [82] and a $1/3$ ML Cl $(\sqrt{3}\times\sqrt{3})R30^\circ$ structure formed on Au(111) at 0.80 V from 1 mM HCl, as a model (Figure 3.6E), and those values are listed in Table 3.1. In the Cd

Figure 3.5 Cd/Au and Cl/Au Auger ratios as a function of immersion potential from 0.20 mM CdCl₂ and 1 mM HCl (pH 3).

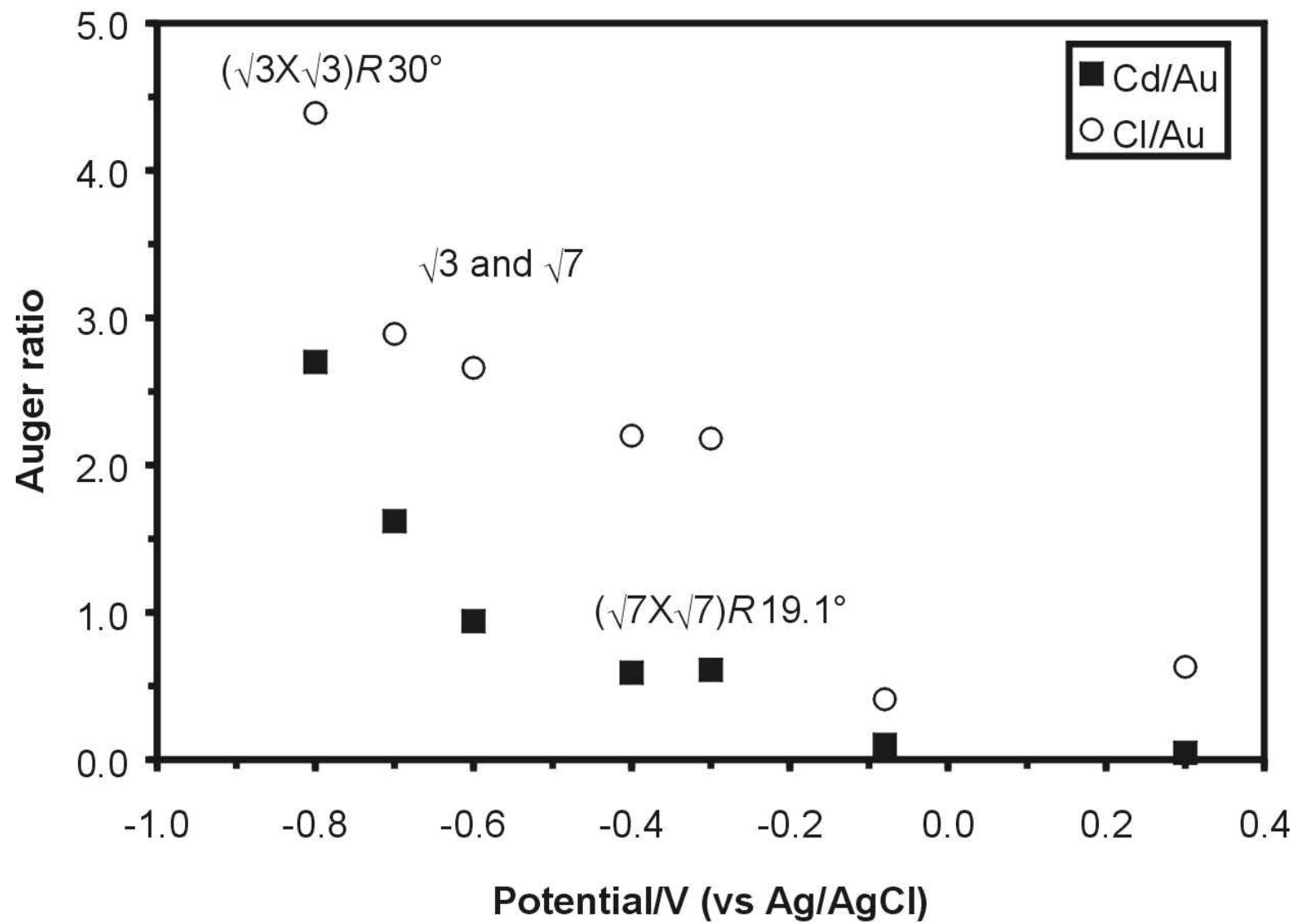


Figure 3.6 LEED patterns for Cd electrodeposition and Cl adsorption. A) -0.40 V, 0.20 mM CdCl₂ and 1 mM HCl (pH 3), ($\sqrt{7} \times \sqrt{7}$)R19.1°, electron energy 43.1 eV; B) -0.80 V, 0.20 mM CdCl₂ and 1 mM HCl (pH 3), ($\sqrt{3} \times \sqrt{3}$)R30°, electron energy 53.0 eV; C) -0.40 V, 0.20 mM CdSO₄ and 1 mM H₂SO₄ (pH 3), ($\sqrt{3} \times \sqrt{3}$)R30°, electron energy 47.2 eV; D) -0.80 V, 0.20 mM CdSO₄ and 1 mM H₂SO₄ (pH 3), hexagonal pattern, electron energy 22.4 eV; E) 0.85 V, 1 mM HCl (pH 3), ($\sqrt{3} \times \sqrt{3}$)R30°, electron energy 48.1 eV.

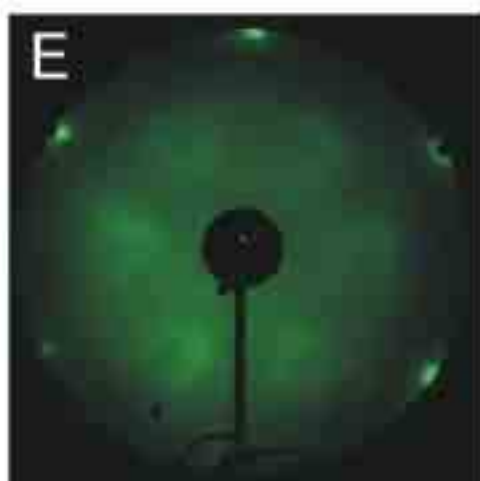
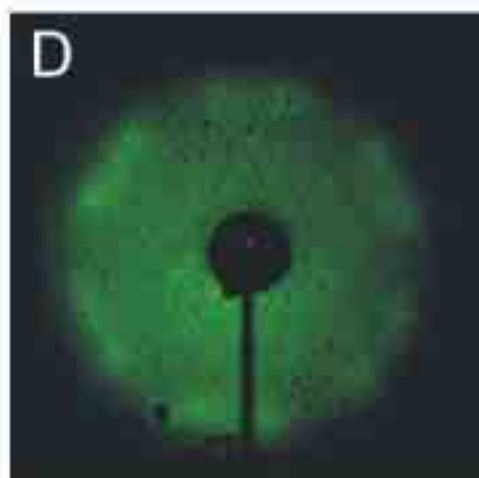
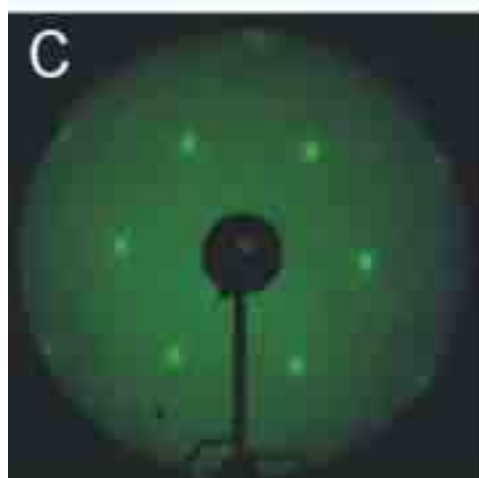
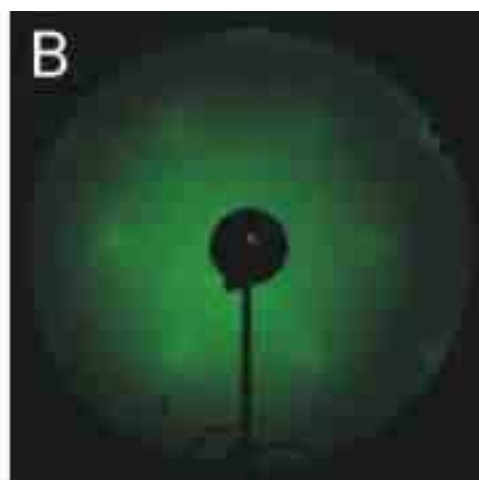
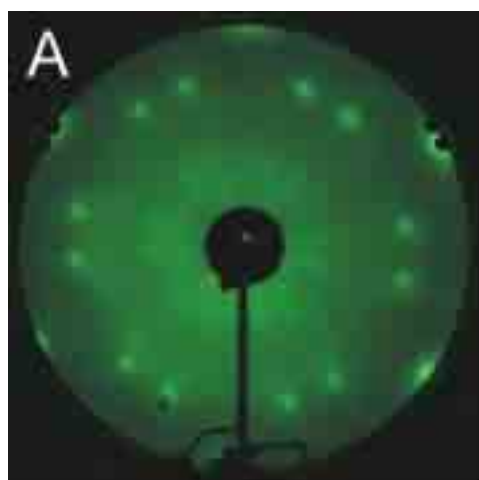


Table 3.1 Cadmium and chlorine coverages as a function of immersion potential from 0.20 mM CdCl₂ and 1 mM HCl (pH 3).

Potential/V	Cd coverage/ML	Cl coverage/ML
0.30	0.014	0.18
-0.080	0.029	0.12
-0.30	0.18	0.64
-0.40	0.17	0.65
-0.60	0.28	0.78
-0.70	0.48	0.85
-0.80	0.80	1.3

UPD region, the Cd coverage appears to be about 1/7 (0.14) ML, and the Cl coverage close to 4/7 (0.57) ML. The Cd coverage is lower than expected compared to the coulometry results, but a 1/7 ML coverage for Cd UPD on sulfur layers to form CdS on Ag(111) has been reported by Foresti et al. [44]. At potentials near Cd bulk deposition, the Cd coverage increased to 0.80 ML, and the Cl coverage to 1.3 ML, a value similar to that reported for a Cl layer resulting from Cl₂ dosing in vacuum on Au(111) [83]. The discrepancy between the Cd coverage values determined from AES and coulometry may arise from different sources. One is the effect of anions on the voltammetry, where Kolb et al. have shown that chloride or bromide adsorption during Cu UPD on Pt(111) added to the faradaic current in the voltammetry, making coverage determinations from simple coulometry inaccurate [16]. Also, there is the effect of alloy formation. The presence of Cl atoms could facilitate alloy formation, as suggested by Möller et al., who reported that Cl ions induce surface alloying during Cu UPD on Au(111) [84]. For Cd-Au alloy formation in the UPD region [55, 62-68, 74], a turnover process has been proposed where Cd atoms place exchange with Au atoms at the surface and the alloyed phase extends below the surface [63, 68]. Cd atoms present in the alloy may not be detected as easily by AES, causing a low Cd signal.

The increase in the level of Cl as additional Cd was deposited suggests that Cl was bound to Cd and not gold. To determine the nature of the Cl bonding, the clean and ordered electrode was immersed at -0.40 V in 1 mM HCl, a potential where the $(\sqrt{7} \times \sqrt{7})R19.1^\circ$ structure containing Cd and Cl forms in the Cd²⁺/Cl⁻ solution. AES indicated no Cl on the surface, and a (1 x 1) was observed by LEED, suggesting the clean Au(111) surface. These results agree well with other studies of anion adsorption on

UPD metal layers. Studies of Cd UPD on Cu(111) found Cl adsorbed on top of the Cd layer [70, 75], and also for Cu UPD on Au(111) [13] and Pt(111) [19]. Sulfate and chloride have been found to specifically adsorb during Cu UPD on Au(111) [8, 9, 12, 85-87] and Bi UPD on gold [88].

To determine how Cd and Cl comprise the unit cell structure, rinsing experiments were performed. The $(\sqrt{7} \times \sqrt{7})R19.1^\circ$ structure was formed by immersing the electrode at -0.40 V in 0.20 mM CdCl₂ and 1 mM HCl (pH 3) (Figure 3.7A). The crystal was then emersed under potential control, and subsequently rinsed at -0.40 V in 0.20 mM CdSO₄ and 1 mM H₂SO₄. AES showed essentially no Cl, but sulfur and oxygen were present (Figure 3.7B), and the LEED pattern observed was a $(\sqrt{3} \times \sqrt{3})R30^\circ$. There was essentially no change in the Cd signal, indicating no Cd was removed or deposited. The results clearly demonstrate that both Cd and the anion produced the diffraction pattern, and changing the anion changes the surface structure. Ross and coworkers, studying Cu UPD on Pt(111) in Cl electrolytes, found a (4X4) structure by LEED, and using SXS methods they determined that diffraction pattern was due to both Cu and Cl in the unit cell [89]. The rinsing experiments show that the $(\sqrt{7} \times \sqrt{7})R19.1^\circ$ pattern is not due to the Cd layer only or the Cl layer only, but both Cd and Cl.

Cadmium deposition from sulfate electrolyte

Cadmium UPD on gold from sulfuric acid solutions has been studied by electrochemical and situ scanning probe techniques [38, 57, 59, 60, 62-65]. Figure 3.8 shows a voltammogram of the Au(111) electrode in 0.20 mM CdSO₄ and 1 mM H₂SO₄ (pH 3). The broad peak centered at -0.16 V corresponds to Cd UPD, including the smaller peak at -0.40 V [59, 60]. The increase in reductive current beginning at -0.50 V

Figure 3.7 Cd UPD rinsing experiments. A) Cd UPD at -0.40 V from 0.20 mM CdCl₂ and 1 mM HCl (pH 3); B) After rinsing the electrode containing UPD Cd and Cl at -0.40 V in 0.20 mM CdSO₄ in 1 mM H₂SO₄ (pH 3).

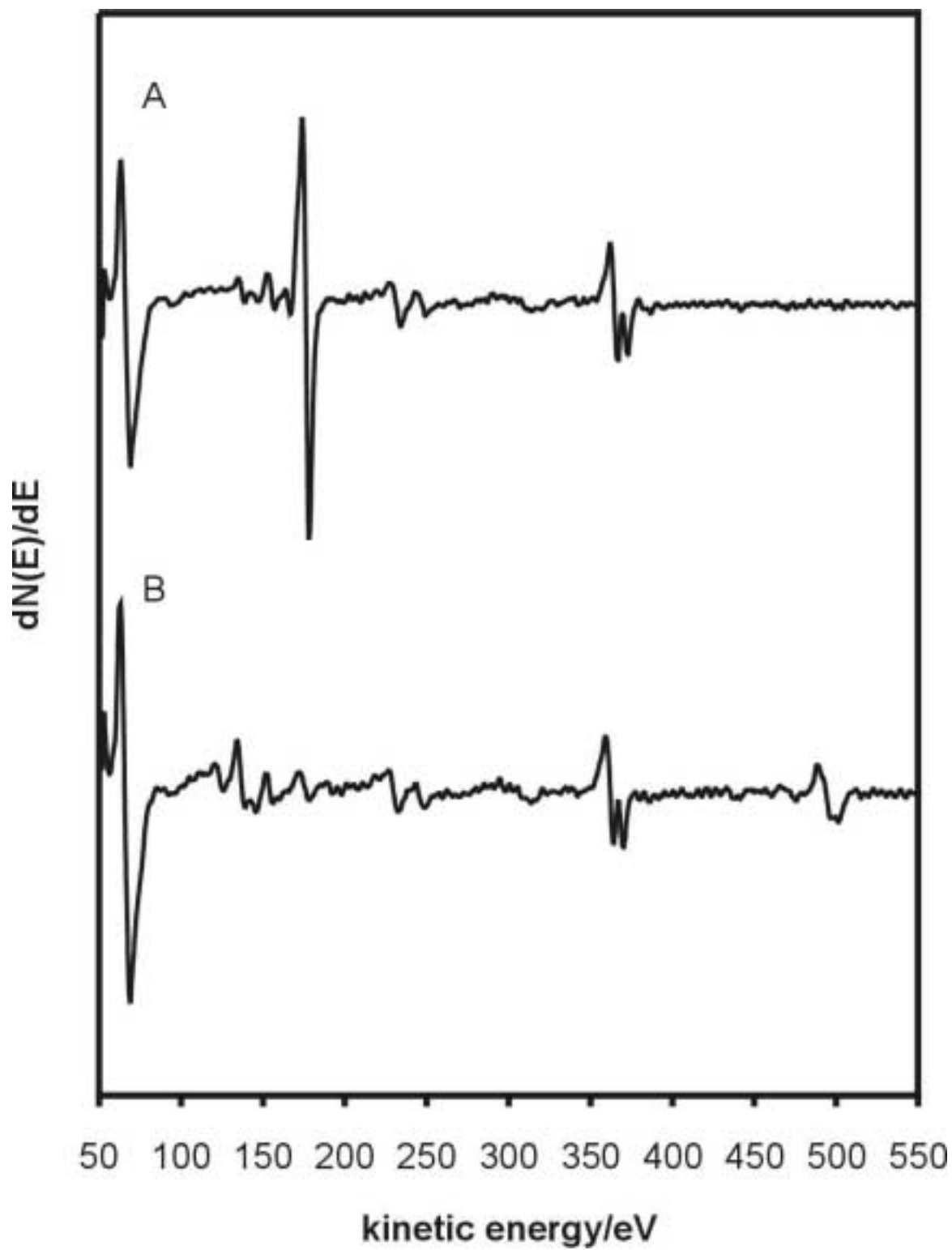
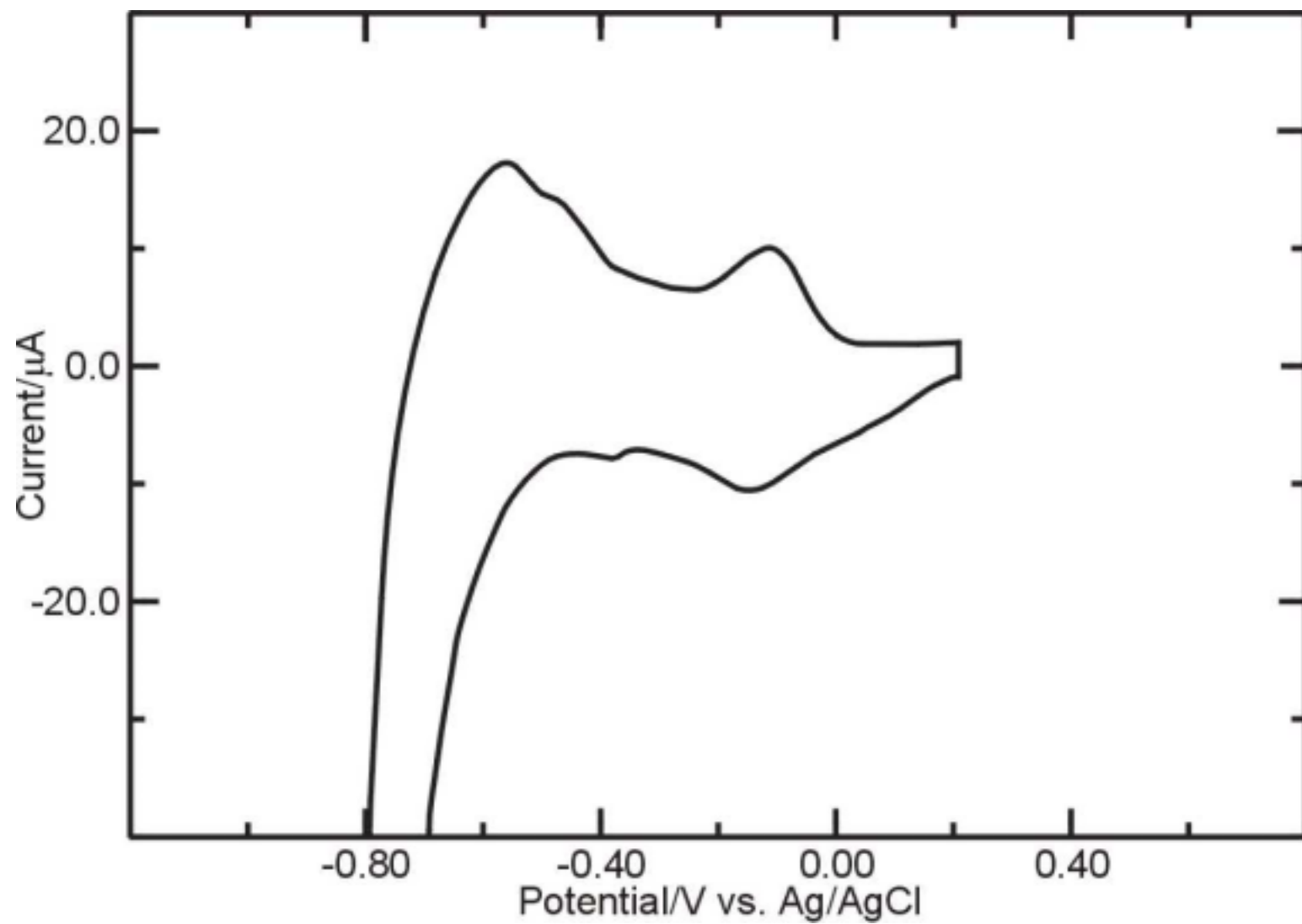


Figure 3.8 Cyclic voltammogram of the Au(111) electrode in 0.20 mM CdSO₄ and 1 mM H₂SO₄ (pH 3). Scan rate = 5 mV/s



is again due to formation of a Cd-Au alloy and proton reduction. Reversing the scan at -0.80 V removes the alloy from the surface, producing a broad oxidation feature comprised of two overlapping peaks at -0.56 V and -0.48 V, and the Cd UPD layer desorbs at -0.16 V. Vidu and Hara obtained similar voltammetry for Cd on Au(100) in sulfuric acid solution [62-65]. AES of the surface after Cd UPD evinced cadmium (376 eV), sulfur (150 eV), and O (503 eV) on the surface (Figure 3.9), indicative of sulfate coadsorption. XPS results confirmed that sulfate was present, based on the binding energies of the S 2p (168.6 eV) and O 1s (531.5 eV) peaks (Figures 3.10 and 3.11, respectively), which are consistent with sulfate [90, 91]. Figure 3.12 shows the Cd/Au Auger ratio as a function of immersion potential. Between -0.40 V and -0.50 V the ratio was constant, and a $(\sqrt{3} \times \sqrt{3})R30^\circ$ pattern was observed by LEED (Figure 3.6C), denoting a surface structure rotated 30° from the underlying gold substrate. In the same potential region, in situ STM studies of Cd UPD by Gewirth and coworkers observed a structure consisting of linear bands rotated 30° from the Au(111) lattice directions [59, 60]. At increasingly negative potentials the Cd/Au ratio markedly increased as alloy formation began, and LEED revealed a hexagonal pattern at -0.70 V and -0.80 V (Figure 3.6D) that was not rotated with respect to the integral beams. At potentials near bulk Cd deposition on Au(100), a (1X1) Cd layer was observed by in situ atomic force microscopy (AFM) [63]. Using potential-step chronocoulometry, it has been shown that the ordered structures observed for Cd UPD on Au(111) by in situ STM are due to a layer of Cd and sulfate [60], and sulfate coadsorption has been demonstrated by radiotracer studies of Cd UPD on Au [85]. Additionally, Cu UPD on Au(111) forms a $(\sqrt{3} \times \sqrt{3})R30^\circ$ structure containing Cu and sulfate [12, 92].

Figure 3.9 Auger spectrum of the Au(111) surface after emersion at -0.60 V from 0.20 mM CdSO₄ and 1 mM H₂SO₄ (pH 3).

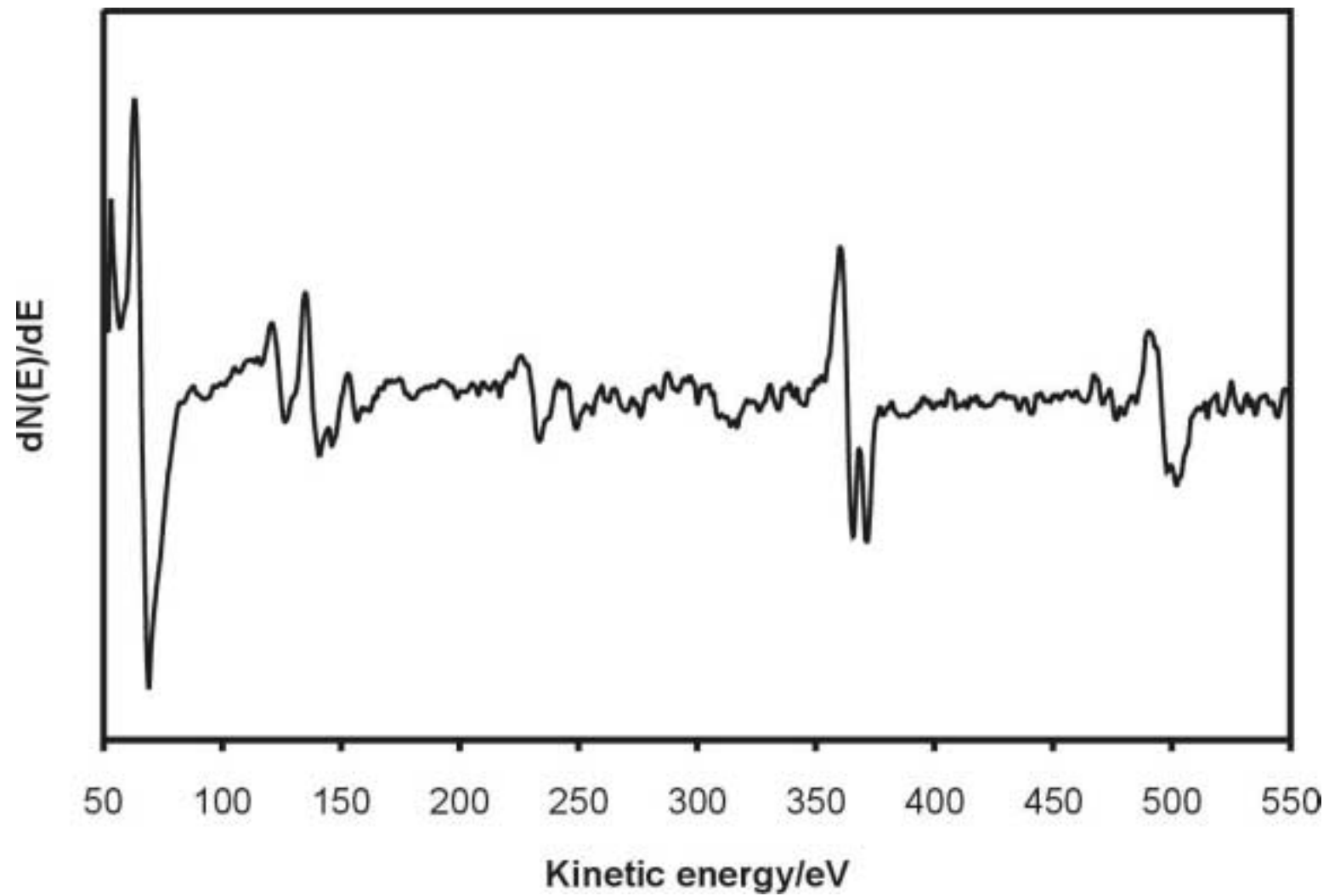


Figure 3.10 Sulfur 2p XPS spectrum of the Au(111) surface after emersion at -0.60 V from 0.20 mM CdSO₄ and 1 mM H₂SO₄ (pH 3).

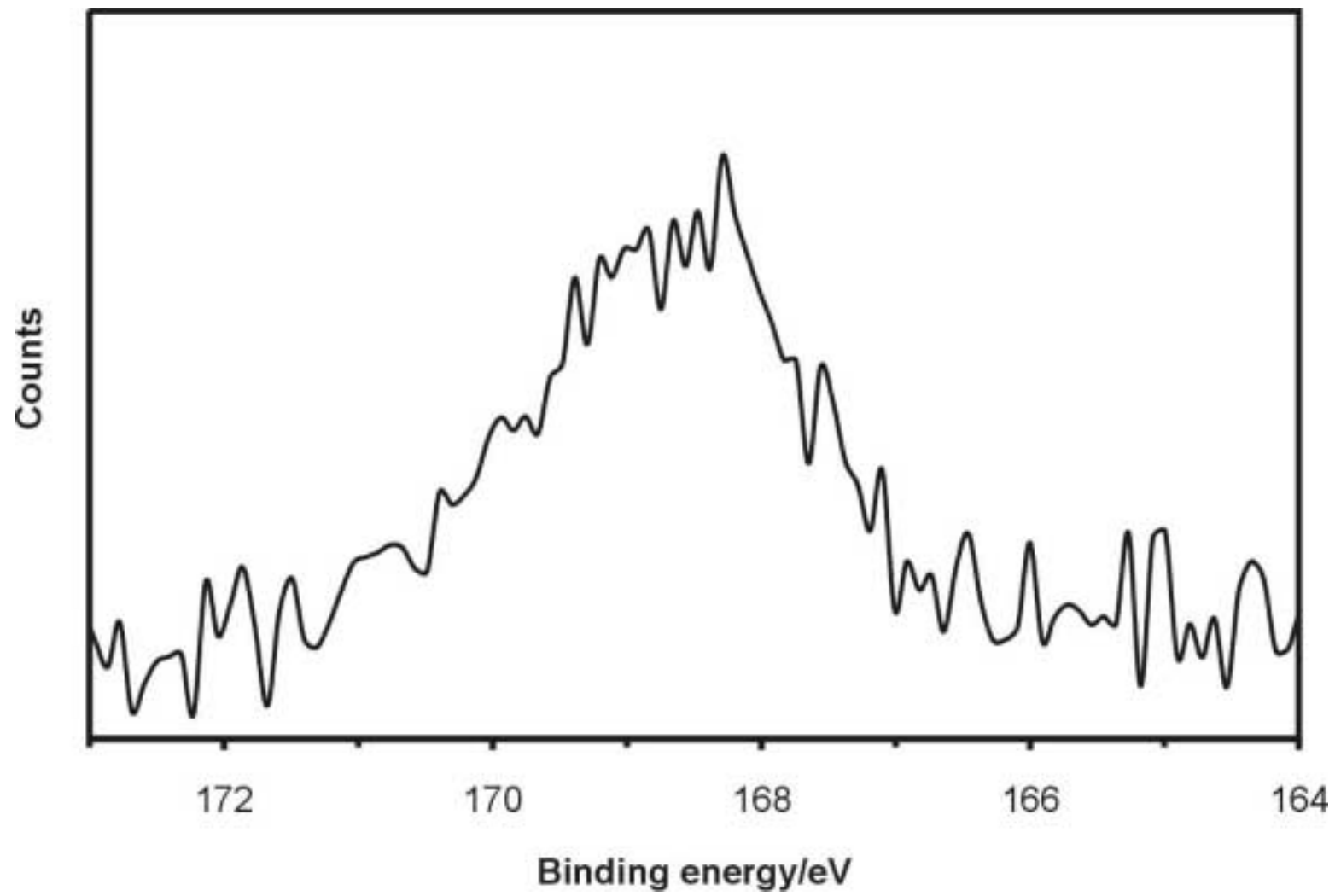


Figure 3.11 Oxygen 1s XPS spectrum of the Au(111) surface after emersion at -0.60 V from 0.20 mM CdSO₄ and 1 mM H₂SO₄ (pH 3).

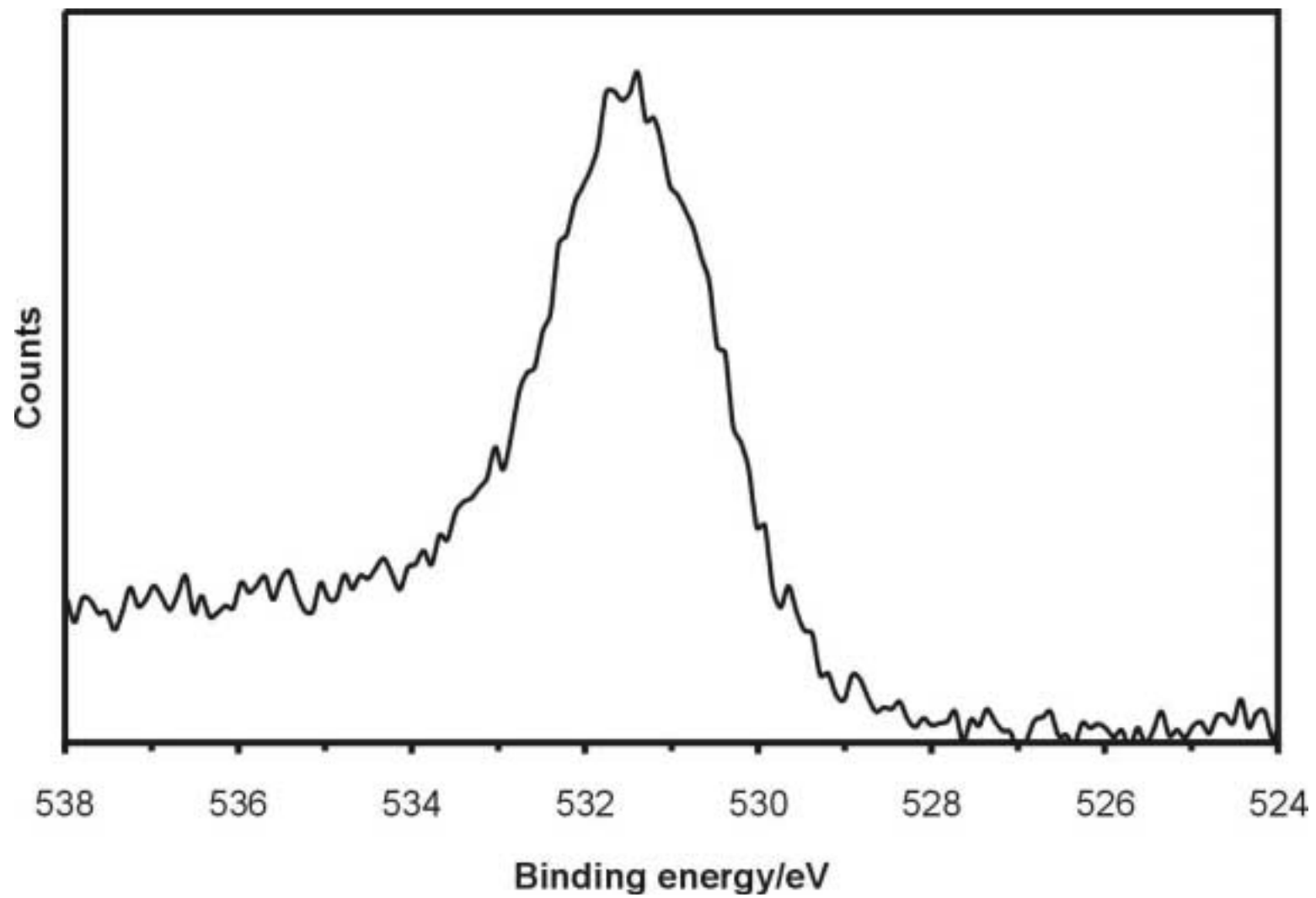
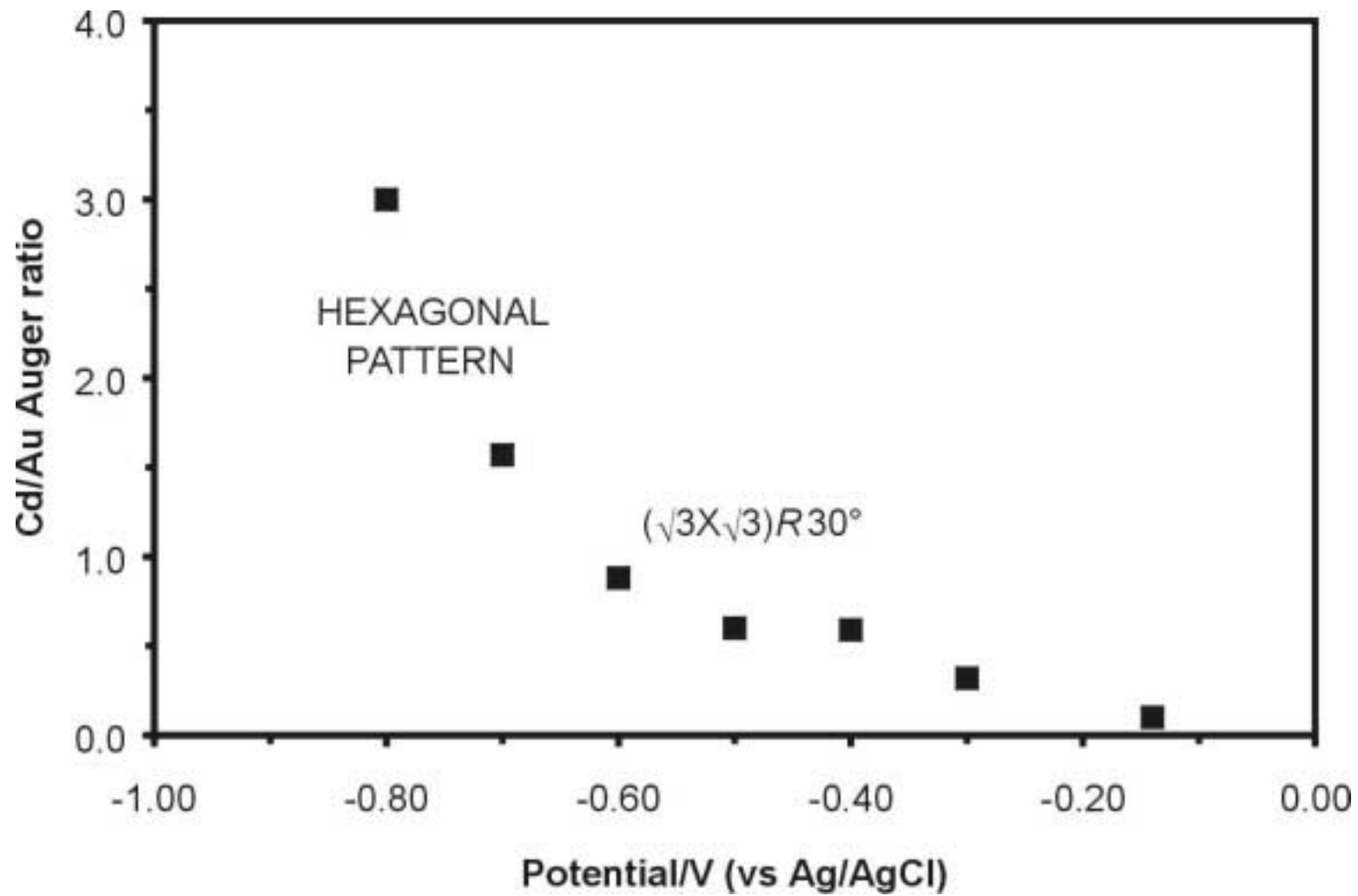


Figure 3.12 Cd/Au Auger ratio as a function of immersion potential from 0.20 mM CdSO₄ and 1 mM H₂SO₄ (pH 3).



Cadmium electrodeposition from iodide electrolyte

The electrodeposition of Cd was also studied in iodide containing solutions, and the voltammogram for the Au(111) electrode in 0.20 mM CdCl₂ and 1 mM HI is shown in Figure 3.13. The electrochemical behavior at positive potentials is the same as 1 mM HI, and the same ordered iodine structures are formed [93-97]. Scanning negative from 0 V, there is a sharp reduction peak at -0.36 V, and a with a corresponding oxidation peak at -0.28 V, Cd UPD and stripping. The average charge for the oxidation and reduction peaks is 170 $\mu\text{C}/\text{cm}^2$, which corresponds to a 0.3 ML Cd coverage. At -0.50 V there are two small features resembling current spikes, which have reversible oxidation counterparts. At more negative potentials the reduction current increases, caused by Cd-Au alloy formation and proton reduction. Reversing the scan at -0.80 V results in two partially resolved oxidation peaks as well as an increase in the area near the Cd UPD stripping peak, all due to alloy stripping.

The electrode surface was examined by AES, XPS, and LEED after emersion at different points in the voltammogram. AES indicated only iodide at all potentials, as no chlorine was present. The iodine 3d_{5/2} peak in the XPS spectrum (Figure 3.14), centered at 619.2 eV, is in excellent agreement with CdI [79], suggesting the formation of a metal-halide surface compound [13, 89, 98-100]. Figure 3.15 shows the Cd and I coverages as a function of potential from 0.20 mM the CdCl₂ and 1 mM HI solution. The iodine coverage was based on the measured Auger iodine peak height for a 0.40 ML ($5 \times \sqrt{3}$) iodine layer deposited at 0 V and the 1/3 ML ($\sqrt{3} \times \sqrt{3}$)R30° iodine structure deposited at -0.75 V from 1 mM HI [93-97]. Using both structures as a calibration gave virtually the same iodine coverage values. The Cd coverage was based on AES sensitivity factors

Figure 3.13 Cyclic voltammogram of the Au(111) electrode in 0.20 mM CdCl₂ and 1 mM HI (pH 3). The solid black line is the first scan, and the dotted black line is the second scan. Scan rate = 5 mV/s

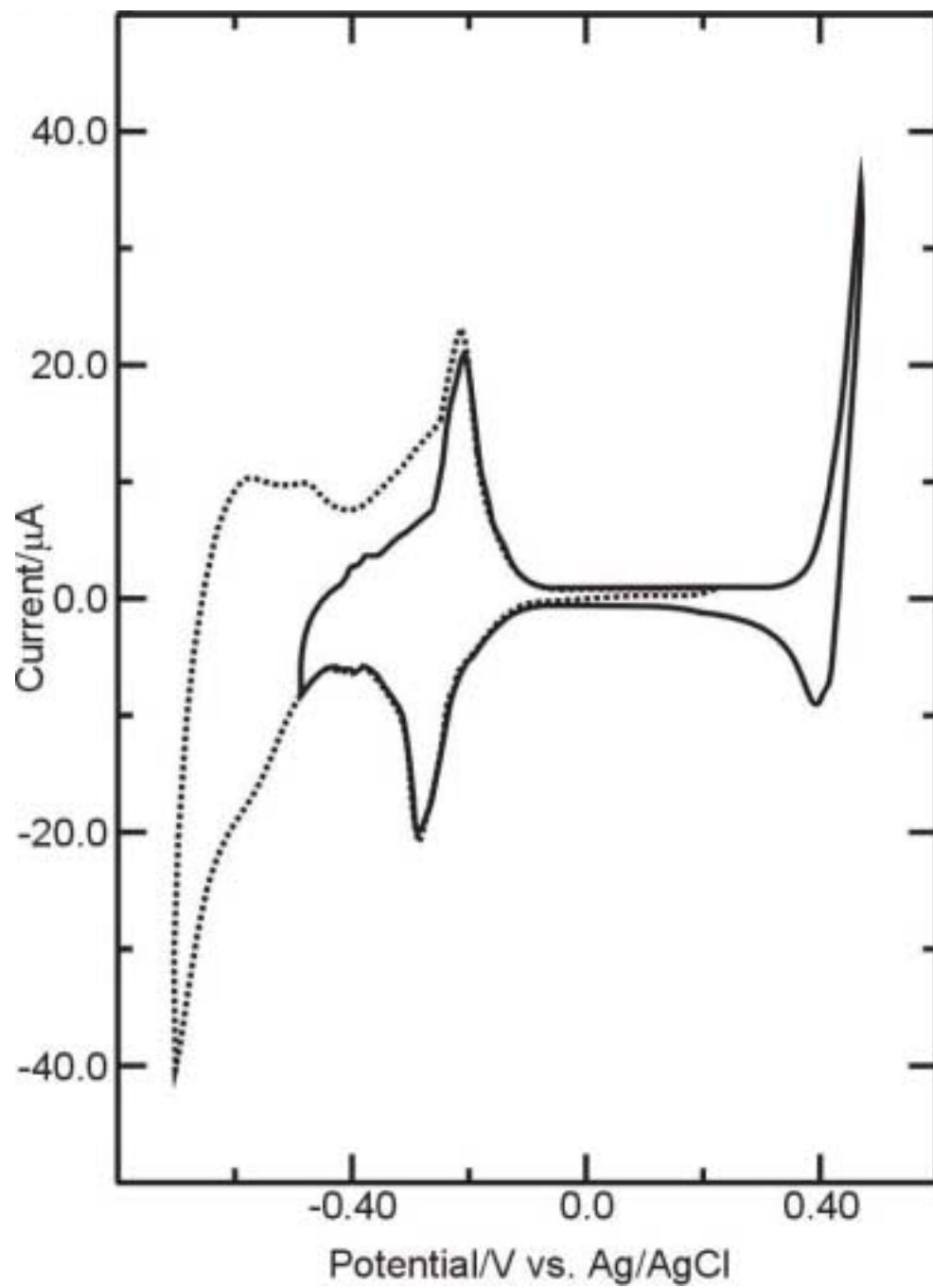


Figure 3.14 Iodine 3d XPS spectrum of the Au(111) surface after immersion at -0.50 V from 0.20 mM CdCl₂ and 1 mM HI (pH 3).

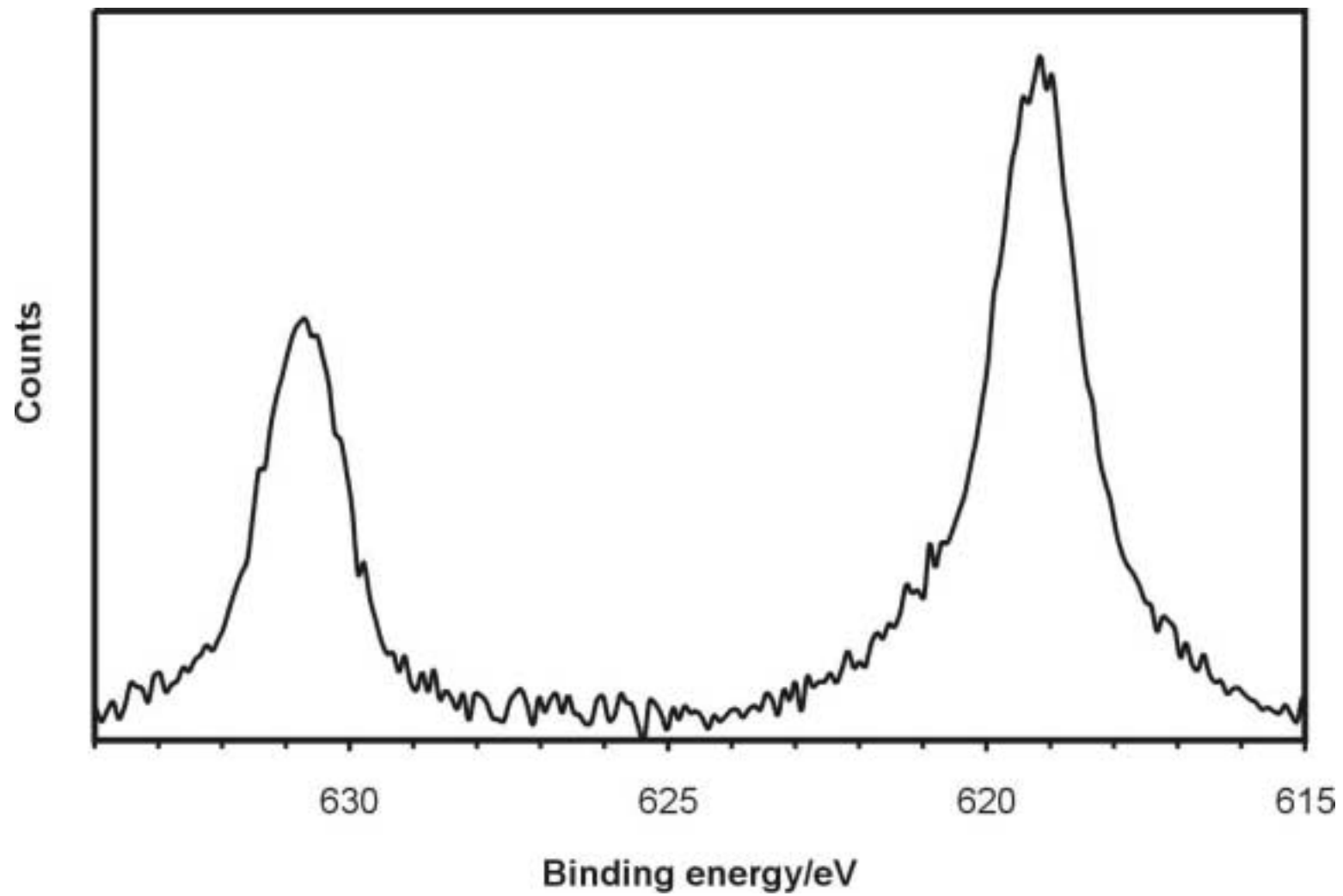
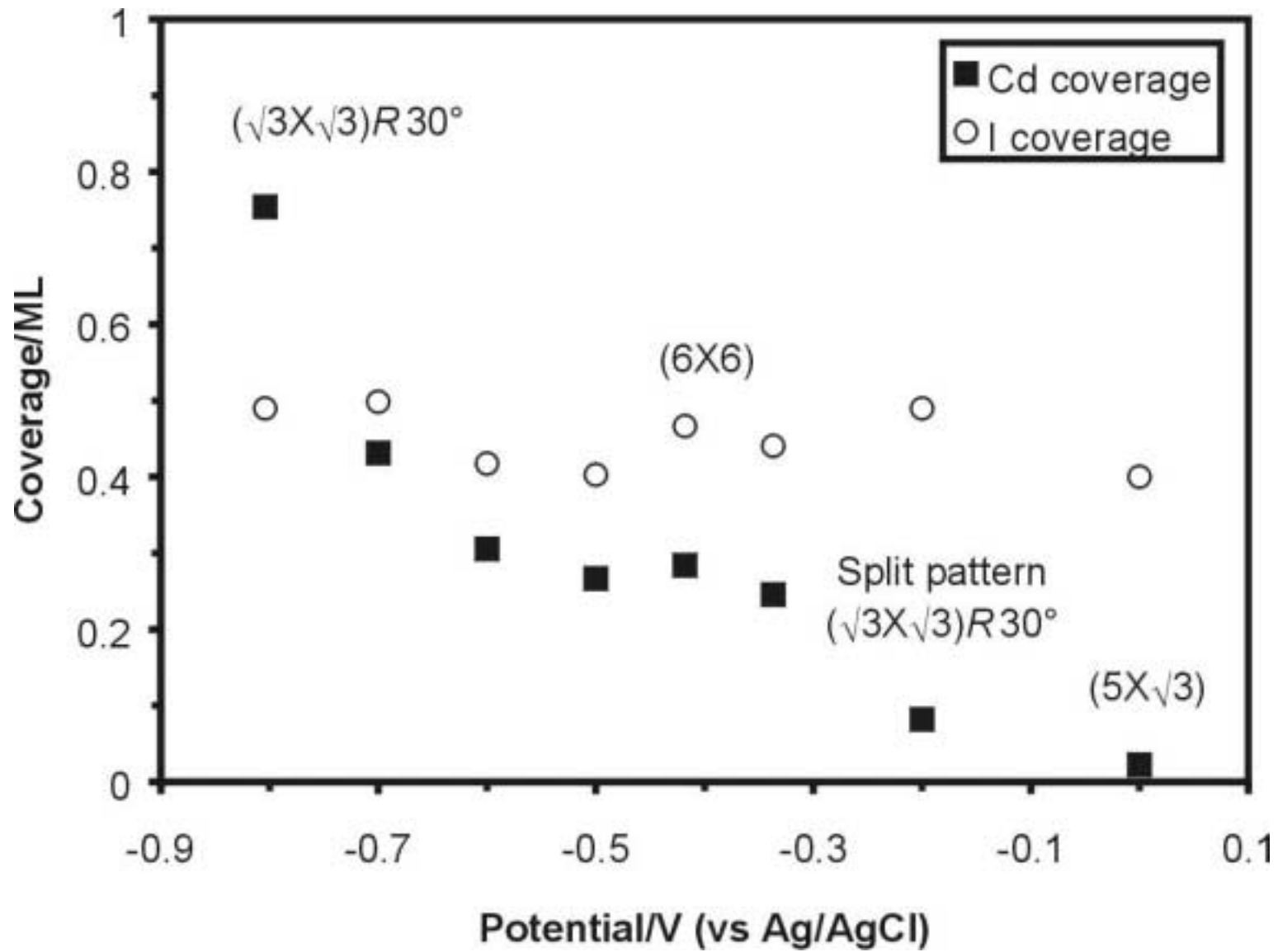


Figure 3.15 Cadmium and iodine coverages as a function of immersion potential from 0.20 mM CdCl₂ and 1 mM HI (pH 3).

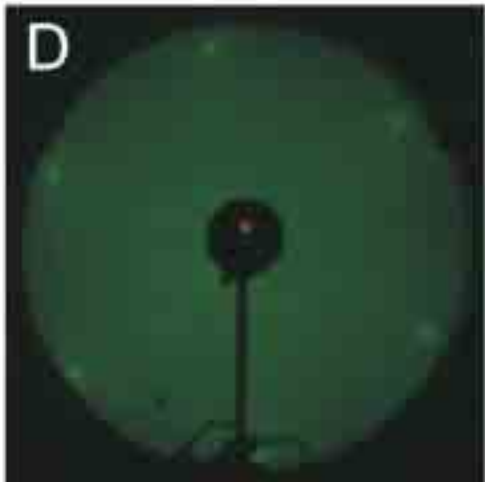
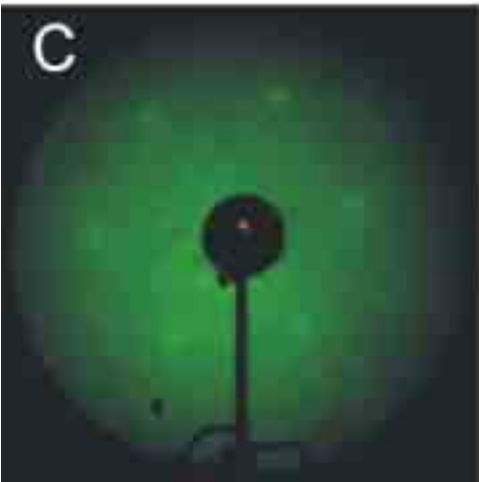
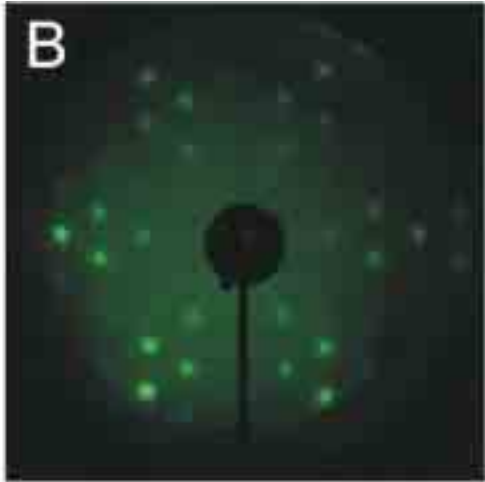
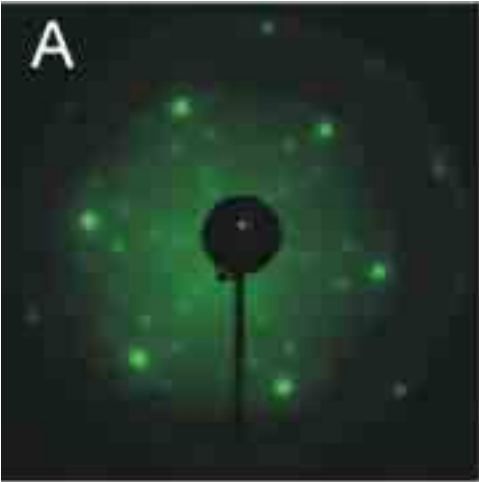


[82] between -0.30 V and -0.60 V, corresponding to the plateau in Cd coverage, 0.28 ML, and has the characteristics of a (6X6) unit cell (Figure 3.16A-B). Coadsorption of halides with Cu UPD on Pt(111) and Au(111) has resulted in (n x n) structures (where n = 3-7), observed by in situ STM and ex situ LEED [10, 16, 98]. At -0.80 V a $(\sqrt{3} \times \sqrt{3})R30^\circ$ structure was observed, similar to iodine atomic layers on Au(111), but the iodine layer is on top of a layer of Cd at this potential. Itaya et al. found that a $c(p \times \sqrt{3})R30^\circ$ iodine structure was formed on a (1X1) Cu layer electrodeposited on Pt(111) [101]. The existence of a similar iodine layer cannot be determined due to the diffuseness of the LEED pattern.

Over the entire potential range, the iodine coverage was essentially constant at 0.45 ML, indicating that iodine was not displaced during Cd deposition, although the surface underwent structural changes. In studies of lead, copper, and silver electrodeposition on iodine-covered Pt(111) surfaces, AES showed that the iodine signal did not diminish in size as additional metal was deposited, while the substrate signal steadily vanished. It was clearly shown that iodine was always the outermost layer, residing on top of the metal [35-37]. In situ STM studies have also concluded that iodine is the top layer for Cu UPD layers on Pt(111) [102] and Au(111) [100].

In a study of Cd electrodeposition on mercury from a perchlorate solution, it was found that the addition of iodide accelerated the deposition process, demonstrating an example of anion-induced adsorption [103], where metal adsorption is promoted by an anion that is specifically adsorbed on the electrode and forms complexes with the metal cation [104-107]. The same phenomenon is occurring here, and may serve to explain the

Figure 3.16 LEED patterns obtained for Cd electrodeposition from iodide and acetate electrolytes. A) -0.50 V, 0.20 mM CdCl₂ and 1 mM HI (pH 3), (6X6) pattern, electron energy 50.0 eV; B) -0.50 V, 0.20 mM CdCl₂ and 1 mM HI (pH 3), (6X6) pattern, electron energy 34.9 eV; C) -0.40 V, 0.20 mM CdSO₄ in 0.40 mM sodium acetate/0.40 mM acetic acid (pH 4.85), ($\sqrt{3} \times \sqrt{3}$)R30°, electron energy 43.1 eV; D) -0.60 V, 0.20 mM CdSO₄ in 0.40 mM sodium acetate/0.40 mM acetic acid (pH 4.85), (1X1), electron energy 38.0 eV.



sharper Cd UPD and stripping peaks in the voltammetry (Figure 3.13). This can also be thought of as formation of a surface compound, with the potential shift resulting from the free energy of formation of the compound.

Cd UPD from acetate electrolyte

The electrodeposition of Cd on Au from acetate containing solutions has been previously studied [55, 108]. The voltammetry for the Au(111) electrode in 0.20 mM CdSO₄ and 0.40 mM sodium acetate/0.40 mM acetic acid (pH 4.85) is shown in Figure 3.17. Cd deposition begins with the reductive current increase at 0.16 V, producing a shoulder that leads into a reduction peak at -0.20 V, due to Cd UPD. The reduction starting at -0.60 V results in Cd-Au alloy formation [55]. Alloy stripping occurs in a broad peak centered at -0.44 V, with Cd UPD stripping at -0.08 V. An Auger spectrum of the surface after emersing the electrode at -0.60 V shows cadmium (376 eV) and oxygen (503 eV) on the surface (Figure 3.18). A carbon peak (272 eV) was difficult to discern due to nearby gold (255 eV) and cadmium (277 eV) transitions [82], but XPS analysis showed that carbon was present (Figure 3.19). The carbon 1s spectrum contained two peaks, one at (287.7 eV) and the other at (284.2 eV). The higher binding energy peak agrees well with carbonyl species [109-111], but the second peak is close to elemental carbon (284.3 eV) [73]. A UHV adsorption study of acetic acid on Pt(111) observed two carbon 1s peaks, with the higher binding energy peak being attributed to the carboxyl group [112]. Figure 3.20 shows the Cd/Au and O/Au Auger ratios for a series of immersion experiments, and Figure 3.16C-D shows the observed LEED patterns. At -0.40 V, after the Cd UPD peak, a $(\sqrt{3} \times \sqrt{3})R30^\circ$ unit cell was observed (Figure 3.16C), and at -0.60 V a (1X1) was visible (Figure 3.16D). A (1X1) Cd structure

Figure 3.17 Cyclic voltammogram of the Au(111) electrode in 0.20 mM CdSO₄ in 0.40 mM sodium acetate/0.40 mM acetic acid (pH 4.85). Scan rate = 5 mV/s

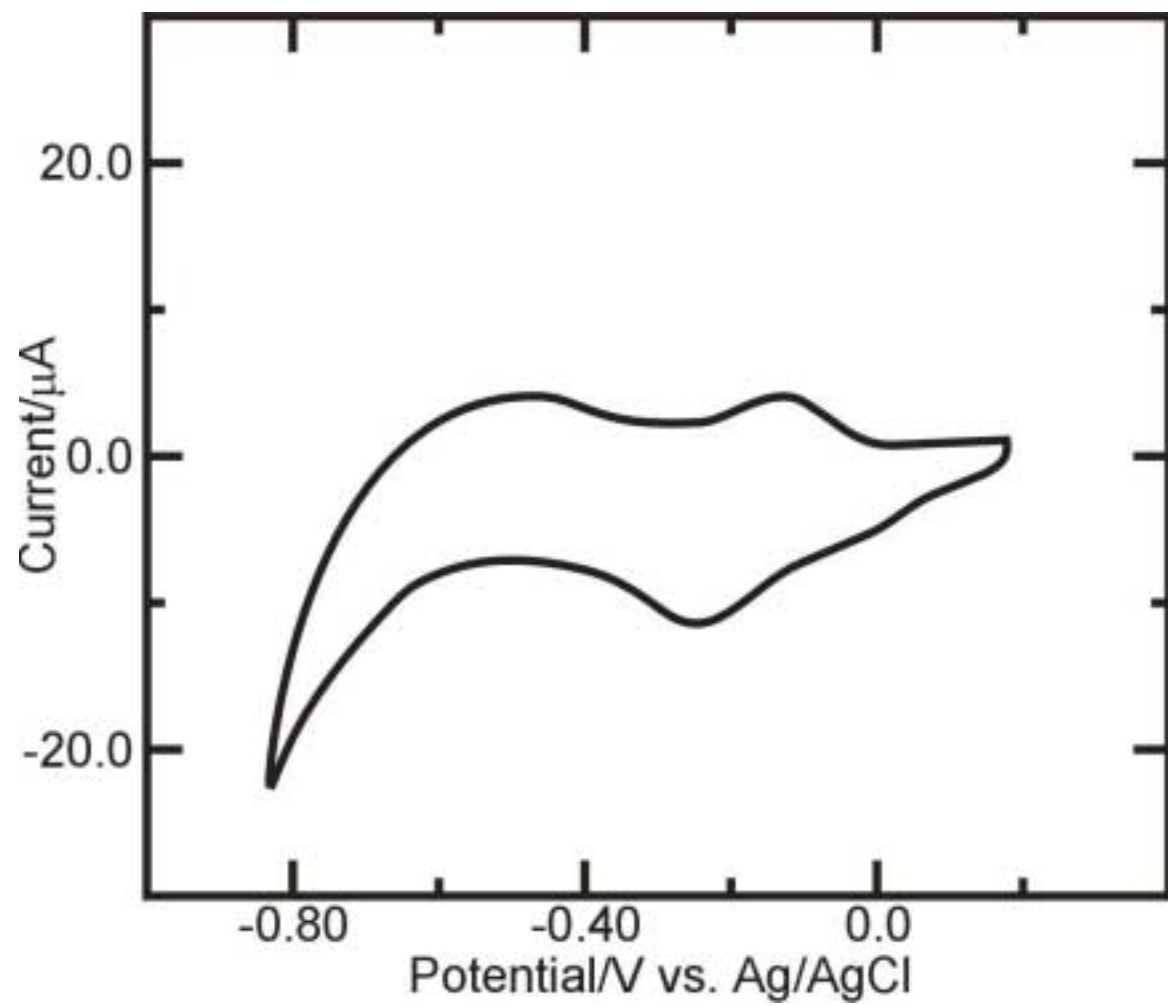


Figure 3.18 Auger spectrum of the Au(111) surface after emersion at -0.60 V from 0.20 mM CdSO₄ in 0.40 mM sodium acetate/0.40 mM acetic acid (pH 4.85).

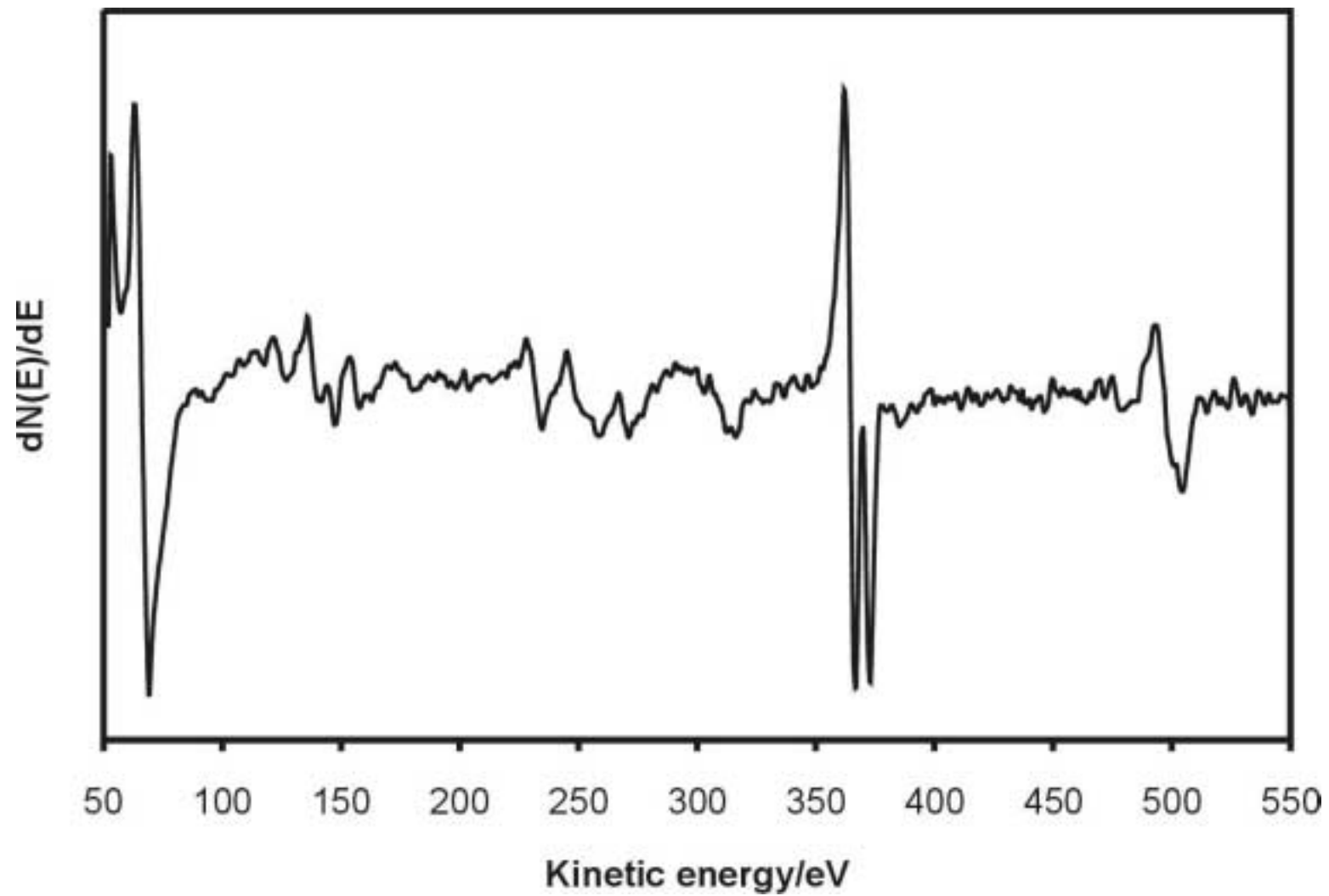


Figure 3.19 Carbon 1s XPS spectrum of the Au(111) surface after emersion at -0.60 V from 0.20 mM CdSO₄ in 0.40 mM sodium acetate/0.40 mM acetic acid (pH 4.85).

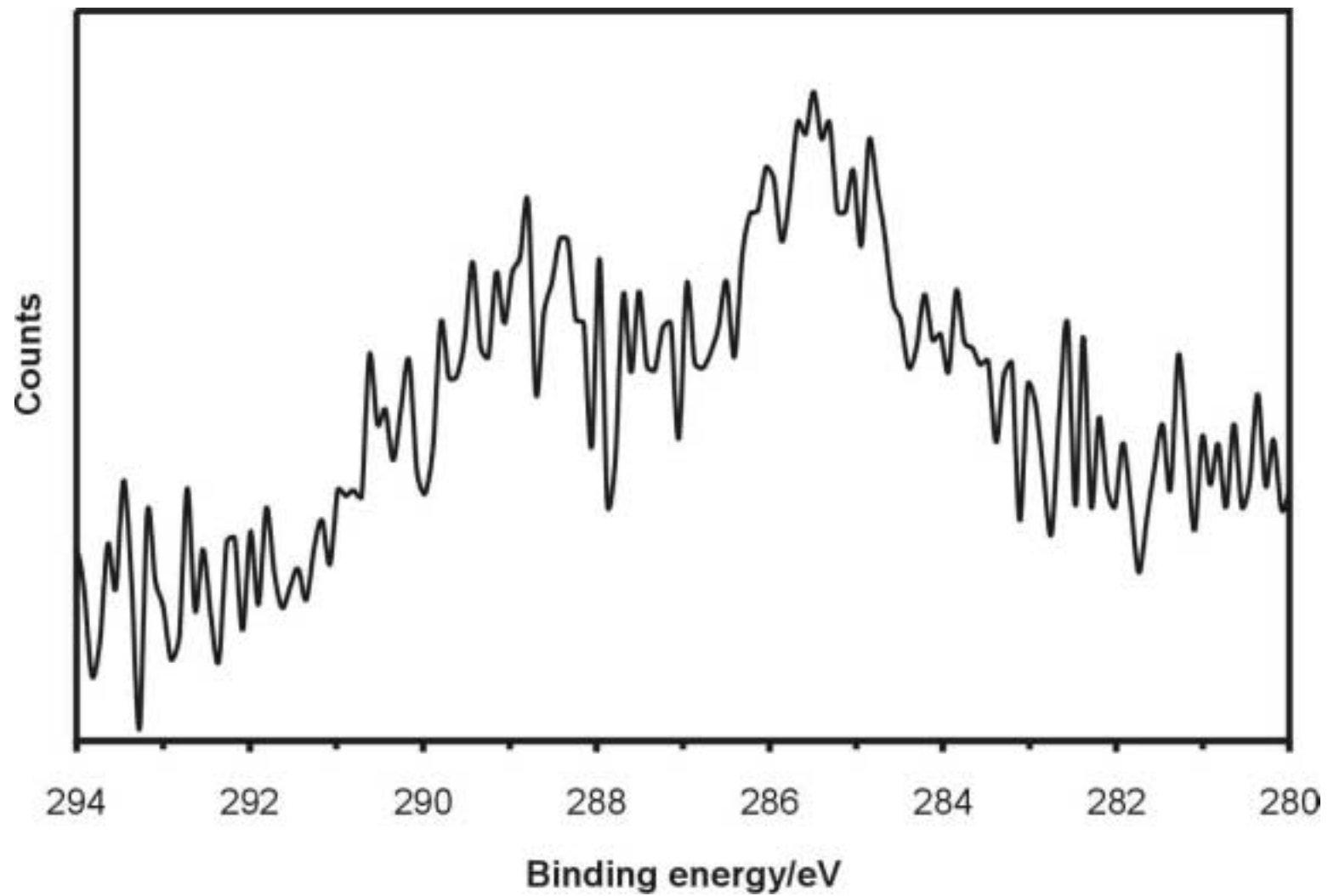
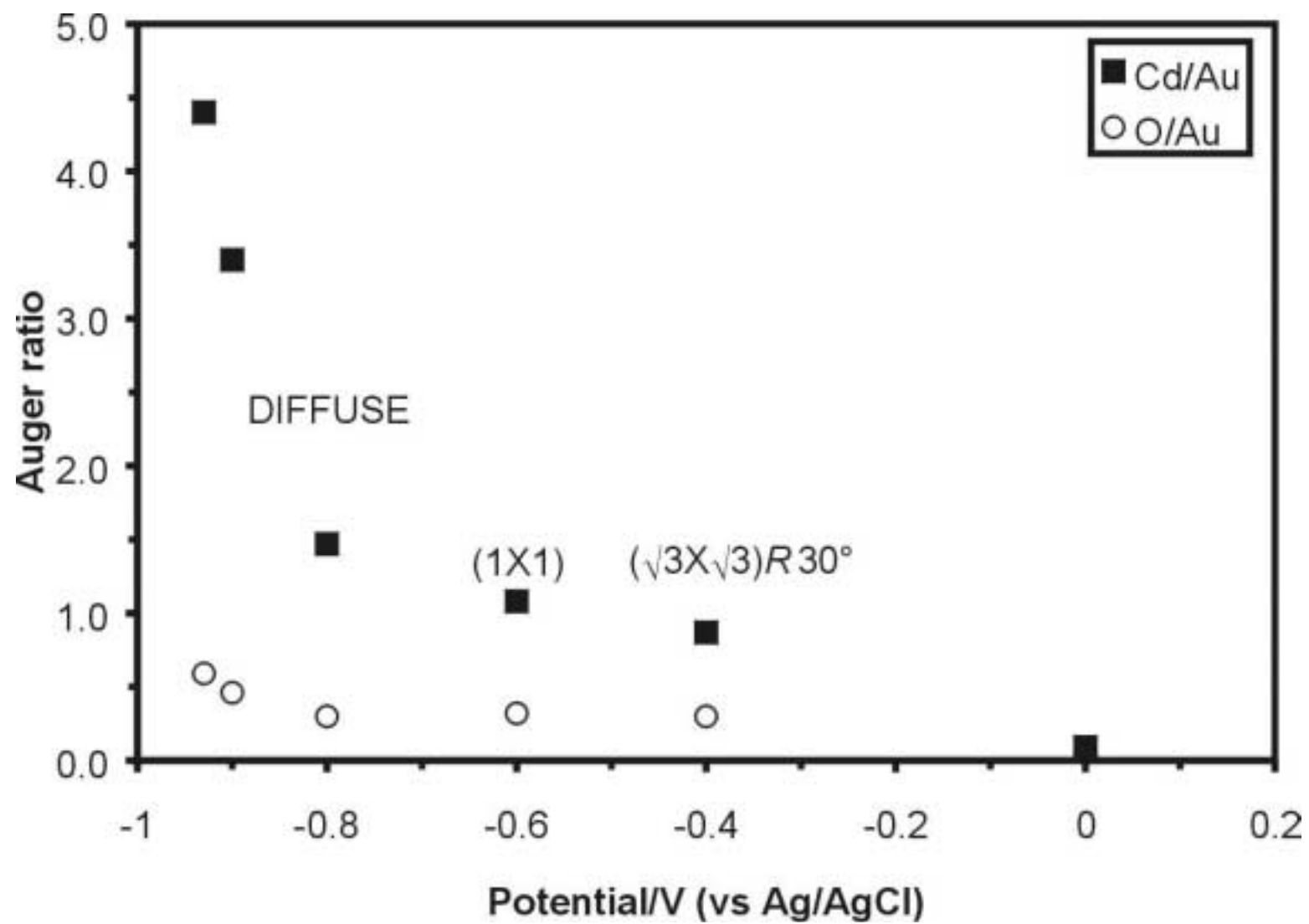


Figure 3.20 Cd/Au and O/Au Auger ratios as a function of immersion potential from 0.20 mM CdSO₄ in 0.40 mM sodium acetate/0.40 mM acetic acid (pH 4.85)



has been reported by Hsieh and Gewirth during Cd UPD from sulfuric acid solutions on Au(111) [38]. At more negative potentials, the Cd/Au ratio increased steeply, and no ordered LEED patterns were visible. The O/Au was constant between -0.40 V and -0.80 V, only increasing at -0.90 V, and was indicative of the amount of adsorbed acetate.

Cd UPD from perchlorate electrolyte

Figure 3.21 shows a voltammogram of the Au(111) electrode in 0.20 mM $\text{Cd}(\text{ClO}_4)_2$ in 1 mM HClO_4 (pH 3.0). The voltammetry in perchlorate electrolyte is different from all the other electrolytes studied, in that there are no separate alloy and UPD Cd stripping peaks (Figures 3.1, 3.8, and 3.13). Scanning negative from the rest potential at 0.32 V, there is a shallow, broad reduction peak centered at -0.30 V consistent with Cd UPD. The shape of the peak indicates that the UPD process is kinetically hindered [9], and Behm et al. have observed the same voltammetric behavior for Cu UPD in perchloric acid solution [13]. The increase in reductive current at -0.60 V is due to Cd-Au alloy formation and proton reduction. Upon reversing the scan direction no oxidative current flows until -0.30 V, producing two closely spaced peaks. Inzelt and Horanyi have reported that alloy formation begins during Cd UPD in perchloric acid electrolytes from EQCM measurements [68], as have Vidu and Hara for Cd UPD on Au(100) from sulfuric acid solutions [64, 65].

Emersion experiments were performed after the first reduction peak at -0.40 V and at -0.80 V. In both cases the Auger spectra showed chlorine (181 eV) and oxygen (503 eV) on the surface (Figure 3.22), suggesting adsorbed perchlorate. XPS results (Figure 3.23) confirmed that perchlorate was present, based on the high binding energy for the chlorine $2p_{3/2}$ peak (206.8 eV), which agrees well with NaClO_4 (208.5 eV) [113].

Figure 3.21 Cyclic voltammogram of the Au(111) electrode in 0.20 mM Cd(ClO₄)₂ in 1 mM HClO₄ (pH 3.0). Scan rate = 5 mV/s

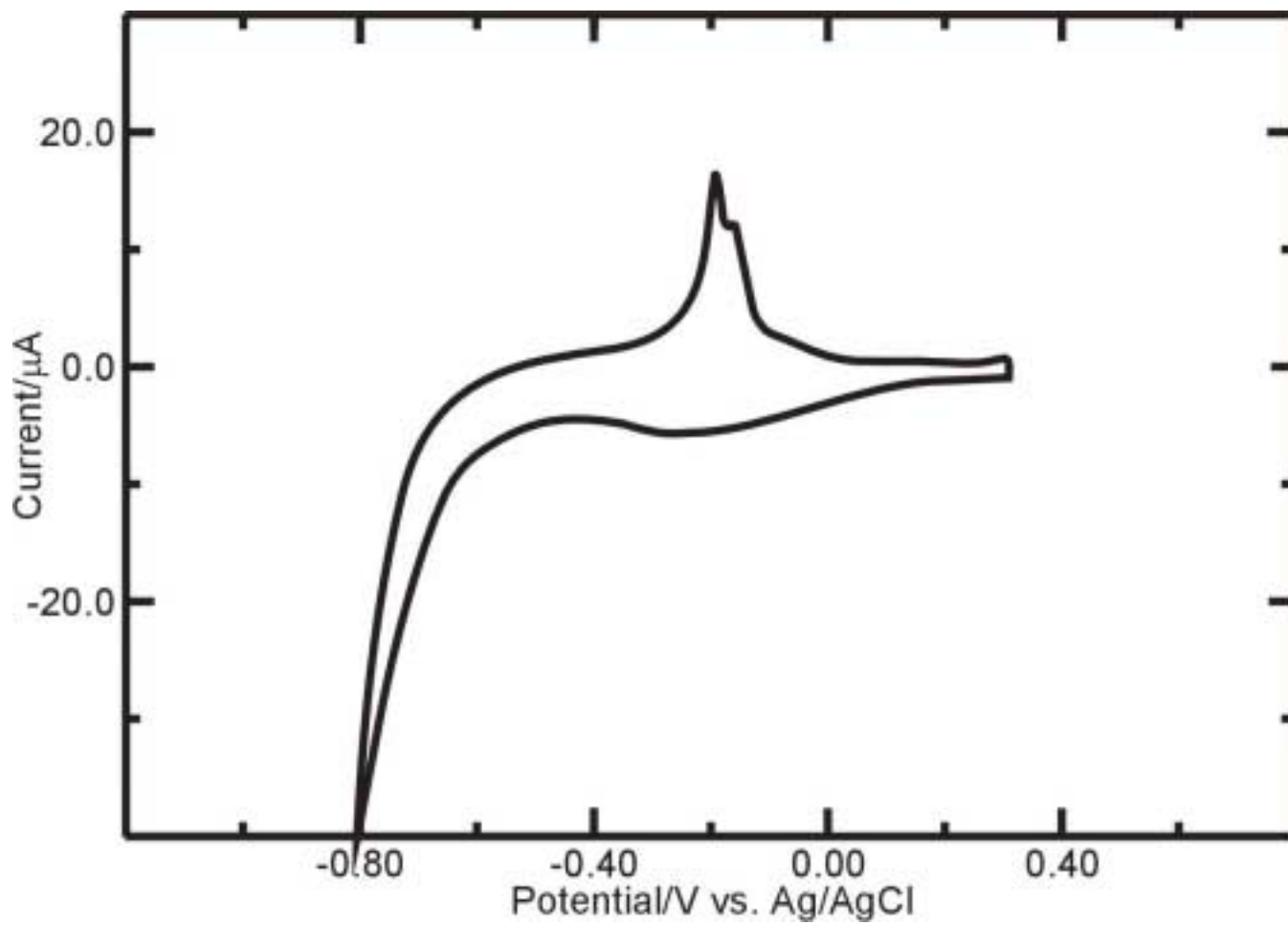


Figure 3.22 Auger spectrum of the Au(111) surface after emersion at -0.80 V from 0.20 mM Cd(ClO₄)₂ in 1 mM HClO₄ (pH 3.0).

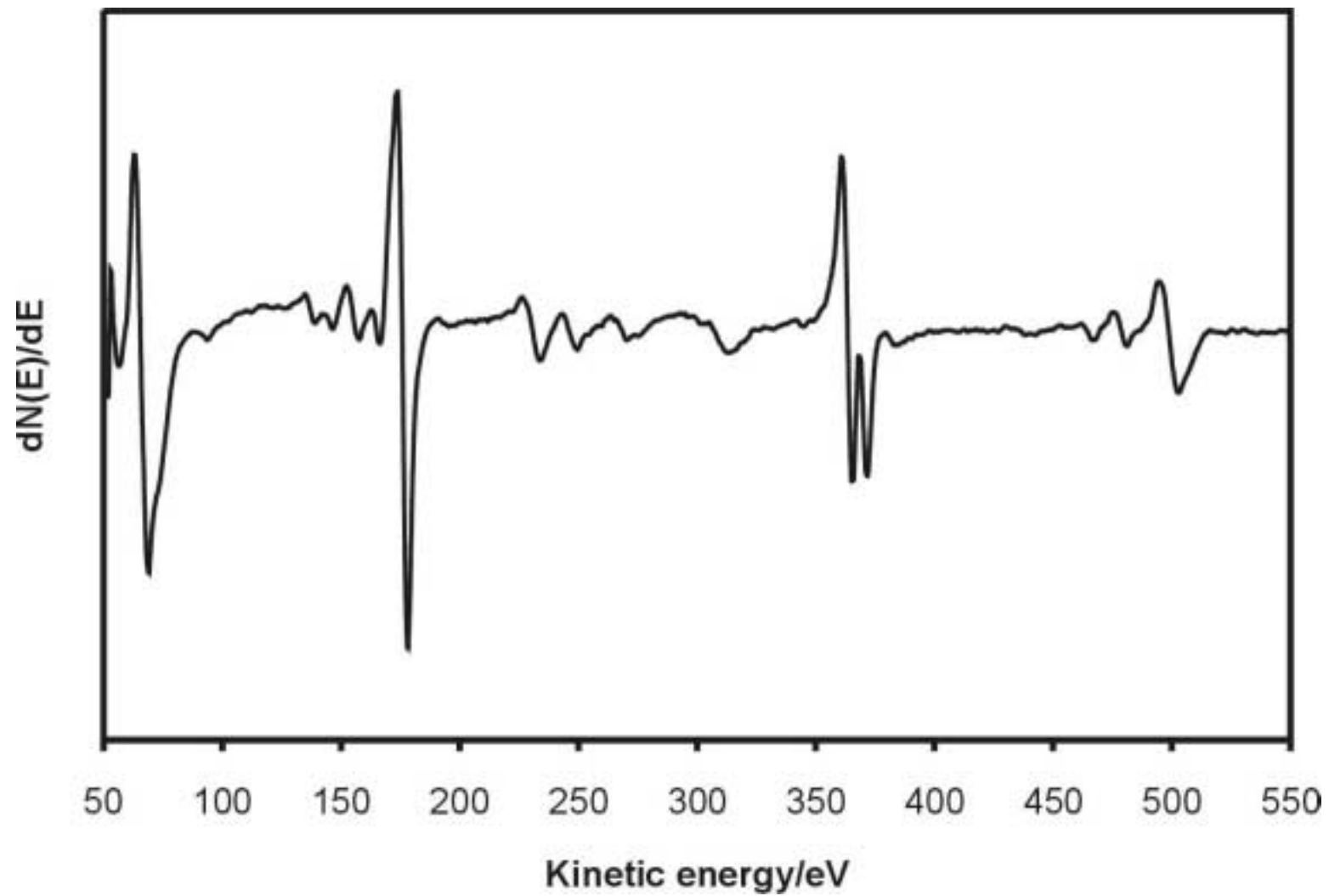
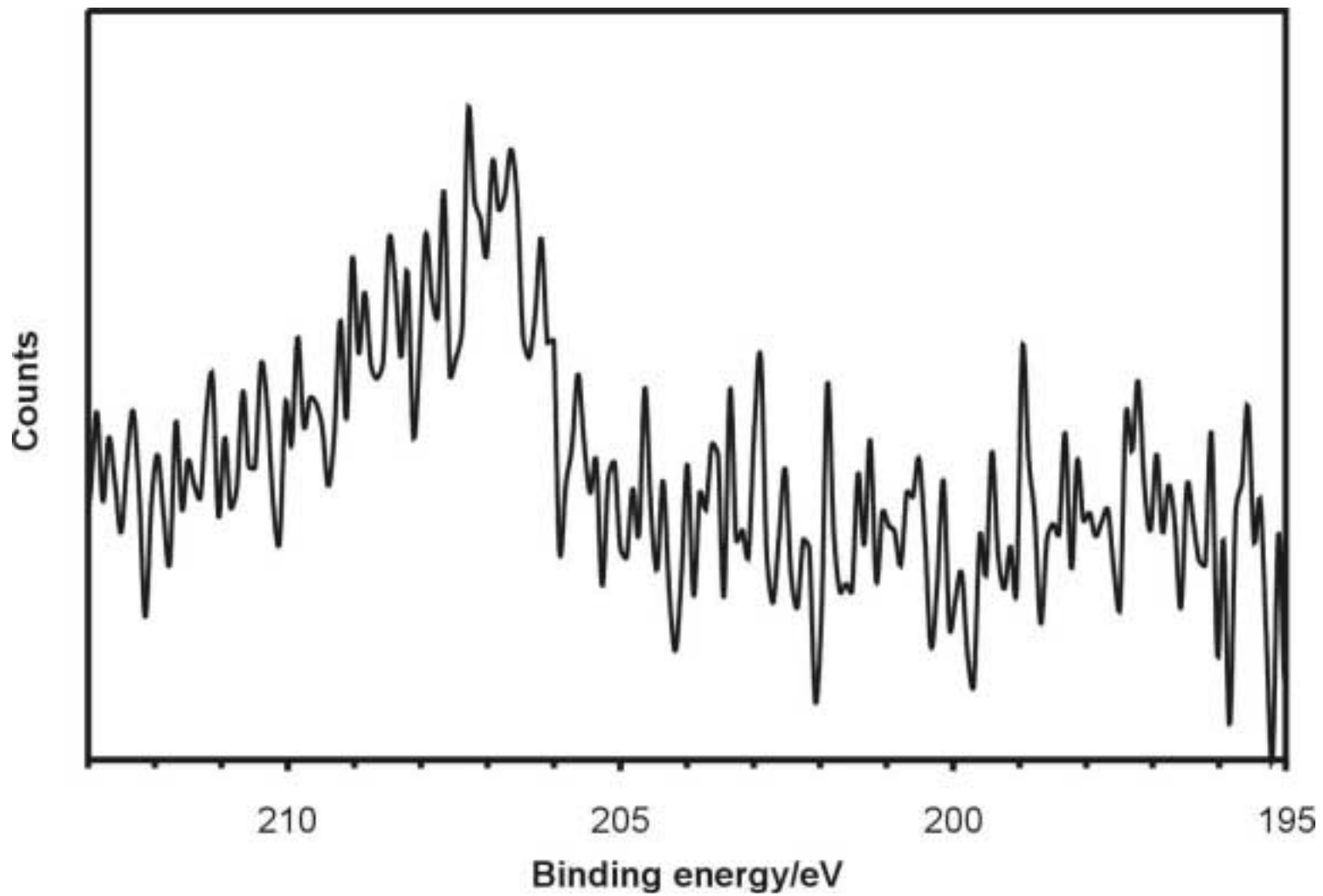


Figure 3.23 Chlorine 2p XPS spectrum of the Au(111) surface after emersion at -0.80 V from 0.20 mM $\text{Cd}(\text{ClO}_4)_2$ in 1 mM HClO_4 (pH 3.0)



In their in situ STM studies, Behm et al. have shown that chloride was coadsorbed with Cu during UPD on Au(111) from perchlorate solutions containing trace amounts of chloride, but could not definitely state whether perchlorate was adsorbed [13]. LEED experiments showed a faint $(\sqrt{3}\times\sqrt{3})R30^\circ$ pattern at -0.40 V, which disappeared after approximately 10 seconds. AES of the surface after LEED showed no change in the cadmium, chlorine, and oxygen levels, suggesting that the surface was only disordered by the electron beam. The evanescent nature of the structure may be due to the weakly adsorbing nature of perchlorate anions [114], which would not be present at negative potentials except for coadsorption with Cd [67, 68]. No diffraction pattern was visible for emersion at -0.80 V. Electrochemical quartz crystal microbalance (EQCM) studies by Deakin and Melroy [58] found that during Cd UPD the frequency shift corresponded to the formation of a Cd atomic layer with less than a full monolayer coverage, consistent with the $(\sqrt{3}\times\sqrt{3})R30^\circ$ pattern observed at -0.40 V.

Conclusions

Cd electrodeposition on Au(111) in chloride, sulfate, iodide, acetate, and perchlorate solutions has been studied. The voltammetric behavior of Cd electrodeposition in perchlorate solutions differed from all the others studied, probably due to its tendency to be weakly adsorbed. AES and XPS demonstrated that Cd UPD as well as Cd-Au alloy formation occurred with the coadsorption of anions. Emersion from chloride or iodide electrolyte revealed no oxygen by AES, and the oxygen present after emersion from acetate and perchlorate electrolytes was found by XPS to be due to acetate or perchlorate, respectively. Different LEED patterns were observed for Cd UPD, and

depended upon the identity of the coadsorbed anion. The observed patterns were due to scattering from both cadmium and the anion, as shown by rinsing experiments demonstrating that an anion can be rinsed away and replaced by another to form a different structure. The Cd layers do not appear to undergo spontaneous oxidation upon loss of potential control and emersion, as once thought by this group, and the anions appear to form a protective overlayer.

References

1. R. R. Adzic, *Isr. J. Chem.* 18 (1979) 166.
2. G. A. Somorjai, *Chemistry in Two Dimensions: Surfaces*, Cornell University Press, London, 1981.
3. D. M. Kolb, in: H. Gerischer and C. W. Tobias (Eds.), *Advances in Electrochemistry and Electrochemical Engineering*, Wiley & Sons, New York, 1978, p. 125.
4. K. Juttner and W. J. Lorenz, *Z. Phys. Chem. (Wiesbaden)* 122 (1980) 163.
5. R. R. Adzic, in: H. Gerischer and C. W. Tobias (Eds.), *Advances in Electrochemistry and Electrochemical Engineering*, 1984, p. 159.
6. P. Broekmann, M. Wilms, M. Krufft, C. Stuhlmann, and K. Wandelt, *J. Electroanal. Chem.* 467 (1999) 307.
7. M. Wilms, P. Broekmann, M. Krufft, Z. Park, C. Stuhlmann, and K. Wandelt, *Surf. Sci.* 404 (1998) 83.
8. Y. Nakai, M. S. Zei, D. M. Kolb, and G. Lehmpfuhl, *Ber. Bunsenges. Phys. Chem.* 88 (1984) 340.

9. M. S. Zei, G. Qiao, G. Lehmpfuhl, and D. M. Kolb, *Ber. Bunsenges. Phys. Chem.* 91 (1987) 349.
10. O. M. Magnussen, J. Hotlos, R. J. Nichols, D. M. Kolb, and R. J. Behm, *Phys. Rev. Lett.* 64 (1990) 2929.
11. W. Haiss, D. Lackey, J. K. Sass, H. Meyer, and R. J. Nichols, *Chem. Phys. Lett.* 200 (1992) 343.
12. Z. C. Shi and J. Lipkowski, *J. Electroanal. Chem.* 365 (1994) 303.
13. J. Hotlos, O. M. Magnussen, and R. J. Behm, *Surf. Sci.* 335 (1995) 129.
14. J. Zhang, Y. E. Sung, P. A. Rikvold, and A. Wieckowski, *J. Chem. Phys.* 104 (1996) 5699.
15. E. Herrero, L. J. Buller, and H. D. Abruna, *Chem. Rev.* 101 (2001) 1897.
16. R. Michaelis, M. S. Zei, R. S. Zhai, and D. M. Kolb, *J. Electroanal. Chem.* 339 (1992) 299.
17. N. Markovic and P. N. Ross, *Langmuir* 9 (1993) 580.
18. P. N. Ross and N. Markovic, *Langmuir* 10 (1994) 976.
19. R. Gomez, H. S. Yee, G. M. Bommarito, J. M. Feliu, and H. D. Abruna, *Surf. Sci.* 335 (1995) 101.
20. N. M. Markovic, C. A. Lucas, H. A. Gasteiger, and P. N. Ross, *Surf. Sci.* 372 (1997) 239.
21. X. P. Gao, A. Hamelin, and M. J. Weaver, *Phys. Rev. Lett.* 67 (1991) 618.
22. X. P. Gao, A. Hamelin, and M. J. Weaver, *J. Chem. Phys.* 95 (1991) 6993.
23. D. M. Kolb, *Prog. Surf. Sci.* 51 (1996) 109.

24. D. M. Kolb, in: J. Lipkowski and P. N. Ross (Eds.), *Structure of Electrified Interfaces*, VCH Publishers, Inc., New York, 1993, p. 65.
25. N. Batina, M. Kunitake, and K. Itaya, *J. Electroanal. Chem.* 405 (1996) 245.
26. L. Huang, P. Zeppenfeld, S. Horch, and G. Comsa, *J. Chem. Phys.* 107 (1997) 585.
27. A. Cuesta and D. M. Kolb, *Surf. Sci.* 465 (2000) 310.
28. S. Z. Zou, X. P. Gao, and M. J. Weaver, *Surf. Sci.* 452 (2000) 44.
29. J. Wang, G. M. Watson, and B. M. Ocko, *Physica A* 200 (1993) 679.
30. B. M. Ocko, G. M. Watson, and J. Wang, *J. Phys. Chem.* 98 (1994) 897.
31. O. M. Magnussen, B. M. Ocko, R. R. Adzic, and J. X. Wang, *Phys. Rev. B: Condens. Matter* 51 (1995) 5510.
32. G. J. Edens, X. P. Gao, and M. J. Weaver, *J. Electroanal. Chem.* 375 (1994) 357.
33. A. Cuesta, M. Kleinert, and D. M. Kolb, *Phys. Chem. Chem. Phys.* 2 (2000) 5684.
34. M. Kleinert, A. Cuesta, L. A. Kibler, and D. M. Kolb, *Surf. Sci.* 430 (1999) L521.
35. J. L. Stickney, S. D. Rosasco, D. Song, M. P. Soriaga, and A. T. Hubbard, *Surf. Sci.* 130 (1983) 326.
36. J. L. Stickney, S. D. Rosasco, and A. T. Hubbard, *J. Electrochem. Soc.* 131 (1984) 260.
37. J. L. Stickney, D. A. Stern, B. C. Schardt, D. C. Zapien, A. Wieckowski, and A. T. Hubbard, *J. Electroanal. Chem.* 213 (1986) 293.
38. S. J. Hsieh and A. A. Gewirth, *Langmuir* 16 (2000) 9501.
39. P. C. Searson, *Sol. Energy Mater.* 27 (1992) 377.
40. C. H. L. Goodman and M. V. Pessa, *J. Appl. Phys.* 60 (1986) R65.

41. T. F. Kuech, P. D. Dapkus, and Y. Aoyagi, *Atomic Layer Growth and Processing*, Materials Research Society, Pittsburgh, 1991.
42. M. A. Tischler and S. M. Bedair, *J. Cryst. Growth* 77 (1986) 89.
43. L. Niinisto and M. Leskela, *Thin Solid Films* 225 (1993) 130.
44. M. L. Foresti, G. Pezzatini, M. Cavallini, G. Aloisi, M. Innocenti, and R. Guidelli, *J. Phys. Chem. B* 102 (1998) 7413.
45. G. Pezzatini, S. Caporali, M. Innocenti, and M. L. Foresti, *J. Electroanal. Chem.* 475 (1999) 164.
46. L. P. Colletti, B. H. Flowers, and J. L. Stickney, *J. Electrochem. Soc.* 145 (1998) 1442.
47. T. E. Lister, L. P. Colletti, and J. L. Stickney, *Isr. J. Chem.* 37 (1997) 287.
48. T. E. Lister and J. L. Stickney, *Appl. Surf. Sci.* 107 (1996) 153.
49. T. E. Lister, R. D. Herrick, and J. L. Stickney, *Abstr. Pap. Am. Chem. Soc.* 208 (1994) 128.
50. U. Demir and C. Shannon, *Langmuir* 10 (1994) 2794.
51. T. L. Wade, L. C. Ward, C. B. Maddox, U. Happek, and J. L. Stickney, *Electrochem. Solid State Lett.* 2 (1999) 616.
52. T. L. Wade, R. Vaidyanathan, U. Happek, and J. L. Stickney, *J. Electroanal. Chem.* 500 (2001) 322.
53. E. Schmidt and H. R. Gygax, *J. Electroanal. Chem.* 12 (1966) 300.
54. D. M. Kolb, M. Przasnyski, and H. Gerischer, *J. Electroanal. Chem. Interfacial Electrochem.* 54 (1974) 25.

55. J. W. Schultze, F. D. Koppitz, and M. M. Lohrengel, *Ber. Bunsenges. Phys. Chem.* 78 (1974) 1253.
56. K. Takamura, F. Watanabe, and T. Takamura, *Electrochim. Acta* 26 (1981) 979.
57. B. W. Gregory, M. L. Norton, and J. L. Stickney, *J. Electroanal. Chem.* 293 (1990) 85.
58. M. R. Deakin and O. Melroy, *J. Electroanal. Chem. Interfacial Electrochem.* 239 (1988) 321.
59. J. C. Bondos, A. A. Gewirth, and R. G. Nuzzo, *J. Phys. Chem.* 100 (1996) 8617.
60. B. K. Niece and A. A. Gewirth, *Langmuir* 13 (1997) 6302.
61. M. C. dos Santos and S. A. S. Machado, *J. Braz. Chem. Soc.* 9 (1998) 211.
62. R. Vidu and S. Hara, *Scr. Mater.* 41 (1999) 617.
63. R. Vidu and S. Hara, *J. Vac. Sci. Technol., B* 17 (1999) 2423.
64. R. Vidu and S. Hara, *Electrochemistry* 67 (1999) 1240.
65. R. Vidu and S. Hara, *J. Electroanal. Chem.* 475 (1999) 171.
66. R. Vidu and S. Hara, *Surf. Sci.* 452 (2000) 229.
67. G. Horanyi, *J. Solid State Electrochem.* 4 (2000) 177.
68. G. Inzelt and G. Horanyi, *J. Electroanal. Chem.* 491 (2000) 111.
69. D. W. Suggs and J. L. Stickney, *Surf. Sci.* 290 (1993) 375.
70. C. Stuhlmann, Z. Park, C. Bach, and K. Wandelt, *Electrochim. Acta* 44 (1998) 993.
71. M. P. Soriaga, *Prog. Surf. Sci.* 39 (1992) 325.

72. M. P. Soriaga, D. A. Harrington, J. L. Stickney, and A. Wieckowski, in: B. E. Conway, J. O. Bockris, and R. E. White (Eds.), *Modern Aspects of Electrochemistry*, Plenum Press, New York, 1995, p. 1.
73. J. F. Moulder, W. F. Stickle, P. E. Soble, and K. D. Bomben, *Handbook of X-ray Photoelectron Spectroscopy*, Perkin-Elmer Corporation, Eden Prairie, 1992.
74. J. W. Schultze, F. D. Koppitz, and M. M. Lohrengel, *Ber. Bunsenges. Phys. Chem.* 78 (1974) 693.
75. V. D. Jovic and B. M. Jovic, *J. Serb. Chem. Soc.* 66 (2001) 345.
76. S. Ye, C. Ishibashi, and K. Uosaki, *Langmuir* 15 (1999) 807.
77. C. Moustydesbuquoit, J. Riga, and J. J. Verbist, *J. Chem. Phys.* 79 (1983) 26.
78. R. D. Seals, Alexander, L. T. Taylor, and J. G. Dillard, *Inorg. Chem.* 12 (1973) 2485.
79. S. W. Gaarenstroom and N. Winograd, *J. Chem. Phys.* 67 (1977) 3500.
80. T. S. Sun, S. P. Buchner, and N. E. Byer, *J. Vac. Sci. Technol.* 17 (1980) 1067.
81. L. P. Colletti, D. Teklay, and J. L. Stickney, *J. Electroanal. Chem.* 369 (1994) 145.
82. L. E. Davis, N. C. MacDonald, P. W. Palmberg, G. E. Riach, and R. E. Weber, *Handbook of Auger Electron Spectroscopy*, Physical Electronics Industries, Inc., Eden Prairie, 1976.
83. G. N. Kastanas and B. E. Koel, *Appl. Surf. Sci.* 64 (1993) 235.
84. F. Moller, O. M. Magnussen, and R. J. Behm, *Electrochimica Acta* 40 (1995) 1259.
85. G. Horanyi, E. M. Rizmayer, and P. Joo, *J. Electroanal. Chem.* 152 (1983) 211.

86. D. M. Kolb, *Z. Phys. Chem. Neue Fol.* 154 (1987) 179.
87. P. Zelenay, L. M. Ricejackson, A. Wieckowski, and J. Gawlowski, *Surf. Sci.* 256 (1991) 253.
88. B. K. Niece and A. A. Gewirth, *Langmuir* 12 (1996) 4909.
89. N. M. Markovic, H. A. Gasteiger, C. A. Lucas, I. M. Tidswell, and P. N. Ross, *Surf. Sci.* 335 (1995) 91.
90. D. S. Zingg and D. M. Hercules, *J. Phys. Chem.* 82 (1978) 1992.
91. N. H. Turner, J. S. Murday, and D. E. Ramaker, *Anal. Chem.* 52 (1980) 84.
92. M. F. Toney, J. N. Howard, J. Richer, G. L. Borges, J. G. Gordon, and O. R. Melroy, *Phys. Rev. Lett.* 75 (1995) 4472.
93. B. G. Bravo, S. L. Michelhaugh, M. P. Soriaga, I. Villegas, D. W. Suggs, and J. L. Stickney, *J. Phys. Chem.* 95 (1991) 5245.
94. X. P. Gao and M. J. Weaver, *J. Am. Chem. Soc.* 114 (1992) 8544.
95. W. Haiss, J. K. Sass, X. Gao, and M. J. Weaver, *Surf. Sci.* 274 (1992) L593.
96. T. Yamada, N. Batina, and K. Itaya, *Surf. Sci.* 335 (1995) 204.
97. T. Yamada, N. Batina, and K. Itaya, *J. Phys. Chem.* 99 (1995) 8817.
98. H. Matsumoto, I. Oda, J. Inukai, and M. Ito, *J. Electroanal. Chem.* 356 (1993) 275.
99. I. M. Tidswell, C. A. Lucas, N. M. Markovic, and P. N. Ross, *Phys. Rev. B* 51 (1995) 10205.
100. A. Martinez-Ruiz, J. Valenzuela-Benavides, L. M. de la Garza, and N. Batina, *Surf. Sci.* 476 (2001) 139.

101. J. Inukai, Y. Osawa, M. Wakisaka, K. Sashikata, Y. G. Kim, and K. Itaya, *J. Phys. Chem. B* 102 (1998) 3498.
102. J. Inukai, Y. Osawa, and K. Itaya, *J. Phys. Chem. B* 102 (1998) 10034.
103. Y. M. Loshkarev, A. A. Rysakov, and V. F. Vargalyuk, *Sov. Electrochem.* 11 (1975) 1256.
104. F. C. Anson, *Anal. Chem.* 38 (1966) 54.
105. G. W. Odom and R. W. Murray, *Anal. Chem.* 39 (1967) 51.
106. J. H. Christie, R. A. Osteryoung, and F. C. Anson, *J. Electroanal. Chem.* 13 (1967) 236.
107. F. C. Anson and D. J. Barclay, *Anal. Chem.* 40 (1968) 1791.
108. D. W. Suggs and J. L. Stickney, *Surf. Sci.* 290 (1993) 362.
109. U. Gelius, P. F. Heden, J. Hedman, B. J. Lindberg, R. Manne, R. Nordberg, C. Nordling, and K. Siegbahn, *Phys. Scr.* 2 (1970) 70.
110. E. Desimoni, G. I. Casella, A. Morone, and A. M. Salvi, *Surf. Interface Anal.* 15 (1990) 627.
111. E. Desimoni, G. I. Casella, and A. M. Salvi, *Carbon* 30 (1992) 521.
112. P. Baumann, G. Pirug, D. Reuter, and H. P. Bonzel, *Surf. Sci.* 335 (1995) 186.
113. W. E. Morgan, W. J. Stec, and J. R. Vanwazer, *J. Am. Chem. Soc.* 95 (1973) 751.
114. F. Silva and A. Martins, *J. Electroanal. Chem.* 467 (1999) 335.

CHAPTER 4

SULFUR ATOMIC LAYER FORMATION ON GOLD AS A FUNCTION OF POTENTIAL FROM SOLUTIONS OF SULFIDE, THIOSULFATE, THIOUREA, AND ETHANETHIOLATE: STUDIES BY LEED, XPS, AND AUGER ELECTRON SPECTROSCOPY¹

¹K. Varazo, M.D. Lay, J.L. Stickney, to be submitted to Langmuir.

Abstract

The electrodeposition of sulfur atomic layers on polycrystalline gold and Au(111) surfaces from alkaline solutions of sulfide, thiosulfate, thiourea, and ethanethiolate was studied using a thin layer electrochemical cell (TLEC) and UHV-EC techniques: Auger electron spectroscopy (AES), low energy electron diffraction (LEED), and X-ray photoelectron spectroscopy (XPS). Oxidative sulfur underpotential deposition (UPD) was demonstrated in sulfide and thiosulfate solutions, and the sulfur coverage was determined as a function of potential. After oxidative sulfur UPD, the coverage was constant, and a $(\sqrt{3}\times\sqrt{3})R30^\circ$ unit cell was observed by LEED, corresponding to a $1/3$ ML of sulfur. At potentials near bulk sulfur deposition, a 0.50 ML $(1\times\sqrt{3})$ structure was observed from both sulfide and thiosulfate solutions. AES and XPS data showed no evidence for sulfur oxidation after emersion from solution. Thiourea appears to decompose upon adsorbing on the gold surface, as no carbon or nitrogen was detected in the AES spectra, and a $1/3$ ML $(\sqrt{3}\times\sqrt{3})R30^\circ$ sulfur layer was observed. AES and XPS experiments indicated that ethanethiolate layers underwent partial decomposition, and a complex $(\sqrt{3}\times\sqrt{3})R30^\circ$ split-spot pattern with some (3×3) intensity was observed. Electrochemical atomic layer epitaxy (EC-ALE) is the electrochemical analog of atomic layer epitaxy (ALE), a method used to produce thin films of materials one monolayer at a time, in a cycle. This study suggests that sulfur atomic layer formation from alkaline solutions of sulfide, thiosulfate, and thiourea is possible, offering a range of solution composition and electrode potentials for use in an EC-ALE cycle to form compound semiconductors such as ZnS, CdS, and CuInS₂.

Introduction

The formation of sulfur atomic layers on single crystal surfaces has been widely studied, and numerous metals have been used: Au [1-9], Pt [10-17], Ni [18-21], Rh [22-24], Pd [25-29], and Ru [30-34], among others. Sulfur atomic layers play an important role in catalysis [35-38] and corrosion processes [39, 40], and are used in the electrochemical formation of sulfur containing compound semiconductor thin films [5, 41-49]. The formation of alkanethiol self-assembled monolayers (SAMs) on gold substrates involves sulfur bonding, and is an important, extensively studied process [50-59]. A range of ordered sulfur atomic layer structures have been deposited as a function of the sulfur coverage from the gas phase and from aqueous media using electrodeposition.

Somorjai et al. performed AES, LEED and STM studies of sulfur layers on the Rh(111) surface [24]. Ordered sulfur structures were obtained by gas phase deposition at room temperature followed by substrate heating. Sharp LEED patterns were obtained for a number of unit cells with increasing sulfur coverage: $(\sqrt{3}\times\sqrt{3})R30^\circ$, $c(\sqrt{3}\times 7)\text{rect}$, $c(4\times 2)$, (4×4) , and (7×7) . The lowest coverage was a $1/3$ ML $(\sqrt{3}\times\sqrt{3})R30^\circ$, while the highest coverage atomic layer structure was a $3/4$ ML (7×7) . Somorjai and coworkers also examined sulfur structures on Pt(111) by LEED and STM [60], where they observed a $1/4$ ML (2×2) , $1/3$ ML $(\sqrt{3}\times\sqrt{3})R30^\circ$, and a $3/7$ ML $c(7\times\sqrt{3})\text{rect}$.

Sulfur layers have also been formed from aqueous solutions, such as the study of sulfur layer formation on Pt(111) by Wieckowski et al. [16, 17]. Exposing the Pt crystal to a 1 mM Na_2S solution at open circuit produced the sulfur layers, which were then stripped in sulfuric acid, and yielded a number of ordered structures dependent on the

amount of sulfur oxidized to sulfate. Using LEED and AES, they observed a full coverage (1X1) prior to stripping any deposited sulfur. After one cycle in sulfuric acid a $1/2$ ML c(2X2) was observed, and after two cycles a $1/3$ ML ($\sqrt{3}\times\sqrt{3}$)R30°.

Sulfur layer deposition on Ag(111) from aqueous Na₂S has been studied by Foresti and coworkers [61]. Prior to bulk deposition of sulfur, they observed two ordered structures by in situ scanning tunneling microscopy (STM), a $1/3$ ML ($\sqrt{3}\times\sqrt{3}$)R30° and a $3/7$ ML ($\sqrt{7}\times\sqrt{7}$)R19°. Hatchett and White also investigated sulfur electrodeposition on Ag(111) with EQCM and STM [62, 63].

The characterization of sulfur atomic layers on Au(111) with STM has been studied by several groups. Sulfide oxidation on Au(111) electrodes was studied by Weaver et al. using STM [4]. In acidic solutions containing 1 mM Na₂S, they observed a $1/3$ ML ($\sqrt{3}\times\sqrt{3}$)R30° unit cell between -0.4 and -0.1 V (vs. SCE), with the sulfur atoms in threefold hollow binding sites. At more negative potentials the Au(111) surface was imaged, indicating that sulfur atoms were desorbed from the surface. At potentials above -0.1 V the formation of a structure composed of rectangular eight-member sulfur rings (S₈) predominated. Using surface-enhanced Raman spectroscopy (SERS) they found additional evidence for the existence of S₈ rings and polysulfides at the onset of bulk sulfur layer formation [64]. Demir and Shannon have also observed the ($\sqrt{3}\times\sqrt{3}$)R30° unit cell on Au(111) [5], as have Salvarezza et al. [7-9].

The structure of self-assembled monolayers (SAMs), formed from solutions of alkanethiols in ethanol also exhibits a ($\sqrt{3}\times\sqrt{3}$)R30° lattice [54], and bonding is through the sulfur head group. The sulfide ion is the simplest sulfur species, and studies of sulfur

atomic layers formed by it may provide insight into the mechanism of more complex systems, such as SAMs [50-59].

Electrochemical atomic layer epitaxy (EC-ALE) is a method developed to electrodeposit compound semiconductors one monolayer at a time [65, 66]. It is the electrochemical analog of atomic layer epitaxy (ALE) or atomic layer deposition (ALD) [67-70]. The method is based on using surface-limited reactions, where only two-dimensional growth occurs to form materials layer-by-layer. In electrodeposition, surface-limited reactions are generally referred to as underpotential deposition (UPD) [65, 71-74], where an atomic layer of an element deposits onto a second element, copper on gold for example, at a potential prior to (under) that required for bulk deposition of the first element. The atomic layer forms as a result of the free energy of formation for the surface compound. In EC-ALE, thin films are formed by the sequential UPD of each element from a separate solution, in a cycle. The process is automated and continues until the desired film thickness is reached. Several groups have prepared thin films of CdS and ZnS compound semiconductors using EC-ALE [5, 41-49, 75]. CdTe, CdSe, and ZnSe have also been prepared [76-85], and there are recent reports of the EC-ALE formation of the III-V compounds InSb and InAs, as well as superlattices of these compounds [86, 87].

The work presented here describes a UHV-EC [88] and thin layer electrochemical cell (TLEC) [89, 90] study of sulfur atomic layer formation on polycrystalline gold and Au(111) using aqueous solutions of sulfide, thiosulfate, thiourea, and ethanethiolate. The structure and composition the layers were characterized using Auger electron spectroscopy (AES), low energy electron diffraction (LEED), X-ray photoelectron

spectroscopy (XPS), and a TLEC. The electrochemical behavior and suitability of the different sulfur precursors have been evaluated, as the formation of sulfur atomic layers is a central step in the EC-ALE formation of compound semiconductors.

Experimental

The thin layer electrochemical cell (TLEC) used in these studies contained a polycrystalline gold annealed and polished rod, having a 0.123 in. diameter and 0.46 in. in length [89-91]. The Au rod was fitted into the TLEC cavity so that the glass walls were within 0.001 in. of the Au electrode, creating a volume of 3.0 μL . Two holes at the bottom of the TLEC cavity provide a path for solution to enter and exit the cavity and provide ionic conductivity. Solution enters the TLEC by capillary action and is expelled by purging the cavity with nitrogen gas. The TLEC was used in an H-cell fitted with a Teflon thermometer adapter. The Pyrex glass H-cell has a separate compartment for the reference and auxiliary electrodes separated by a fine glass frit from the working electrode compartment. Separate H-cells were used for each solution. The potentiostat used was based on a conventional op-amp design. A Ag/AgCl reference electrode (1.0 M NaCl) was used, and the auxiliary electrode was a gold wire (Wilkinson Company).

The sulfur containing solutions were prepared fresh before each experiment, and were purged with nitrogen prior to adding the sulfur precursor. Baker reagent grade sulfuric acid was used to prepare solutions for cleaning the Au electrode and for stripping experiments. Baker Analyzed $\text{Na}_2\text{S}\cdot 9\text{H}_2\text{O}$ and $\text{Na}_2\text{S}_2\text{O}_3$ were used as sulfur sources, and KOH and K_2SO_4 (Baker Analyzed) were used to adjust the pH and electrolyte levels.

The solutions were then purged with nitrogen prior to each experiment. For the UHV-EC studies, K_2S (99.9 %) (Atomergic Chemicals), $Na_2S_2O_3$ (Baker analyzed reagent), thiourea (A.C.S. reagent), and sodium ethanethiolate (Aldrich, technical) were used as received. KOH was added to the thiosulfate, thiourea, and ethanethiolate solutions to adjust the pH.

All solutions were prepared using water from a Nanopure water filtration system fed from the house-distilled water line that produced water with a resistivity greater than $18\text{ M}\Omega\text{-cm}$, and all experiments were conducted at room temperature.

The polycrystalline Au electrode was prepared before each experiment by electrochemical cleaning using $1.0\text{ M H}_2\text{SO}_4$. The cleaning cycle consisted of alternating the working electrode potential between -0.50 V and 1.40 V . At each potential the electrode was rinsed 10 times, and the protocol was repeated three times. During a rinse, the solution in the TLEC cavity was expelled by a flow of nitrogen, and stopping the flow drew in a new aliquot of solution by capillary action. A cyclic voltammogram was obtained after the cleaning procedure to assess electrode surface cleanliness.

The Au(111) single crystal used (MaTeck GmbH) was a 99.999% pure disc 1 cm in diameter and 2 mm thick. Before each electrochemical experiment, the crystal was cleaned by argon ion bombardment ($8.5 \times 10^{-5}\text{ Torr}$) for 30 minutes, followed by annealing with a resistively heated tungsten filament. Surface cleanliness and order were confirmed using AES and LEED, respectively.

The UHV-EC studies were performed using an ultrahigh vacuum (UHV) surface analysis chamber connected directly to an antechamber containing an electrochemical cell [92]. The UHV system included a cylindrical mirror analyzer for Auger electron

spectroscopy (AES) (Perkin-Elmer 11-010 Auger system), reverse-view optics for low energy electron diffraction (LEED) (Princeton model 11-020), an X-ray source (VG Scientific) and hemispherical analyzer (Leybold-Heraeus) for X-ray photoelectron spectroscopy (XPS), and an ion bombardment cage for sputter cleaning substrates. The base pressure of the chamber was 10^{-9} Torr, maintained with an ion pump and cryopump. The electrochemistry antechamber was stainless steel and connected to the main chamber through a gate valve, allowing direct sample transfer into and out of the analysis chamber without exposure to atmosphere.

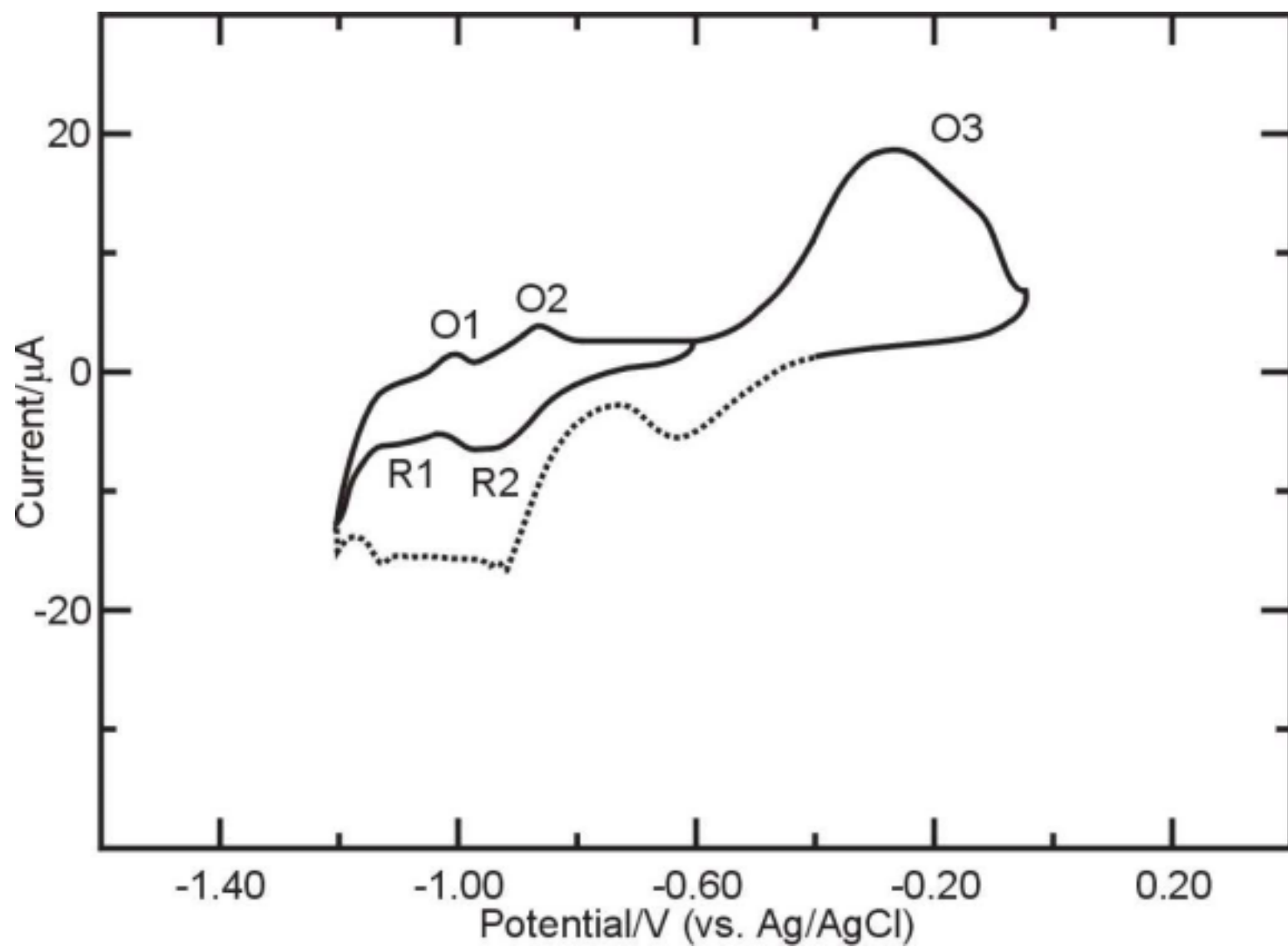
Auger spectra were collected using 3 keV ionizing electrons. To prevent electron beam damage of the deposited sulfur layers [93-95], low beam currents and single sweeps were used. XPS spectra were obtained using Al $K\alpha$ X-rays (1486.6 eV). The Au $4f_{7/2}$ peak (83.98 eV) was used for calibration [96]. Images of the LEED patterns were obtained using a Kodak digital camera (Model DC290).

Results and Discussion

Sulfide Voltammetry

The electrochemistry of sulfide on noble metal electrodes has been extensively studied [61, 63, 64, 97-108]. Previous TLEC investigations of sulfur layer electrodeposition on polycrystalline gold from alkaline sulfide solutions by this group [109] used an 11 mM Na_2S solution containing 0.5 M NaClO_4 (pH 11). Sulfide voltammetry in the present study was performed in 1 mM Na_2S with 0.10 M K_2SO_4 and 0.10 M KOH (pH 12.8). Figure 4.1 shows a cyclic voltammogram of the clean gold electrode in this solution. The two pKa values for H_2S are ≈ 7 and 15 [110], suggesting

Figure 4.1 Cyclic voltammogram of the polycrystalline gold electrode in 1 mM Na₂S with 0.10 M K₂SO₄ and 0.10 M KOH (pH 12.8). Scan rate = 5 mV/s. The first sweep is the solid black line, and the second is the black dotted line.



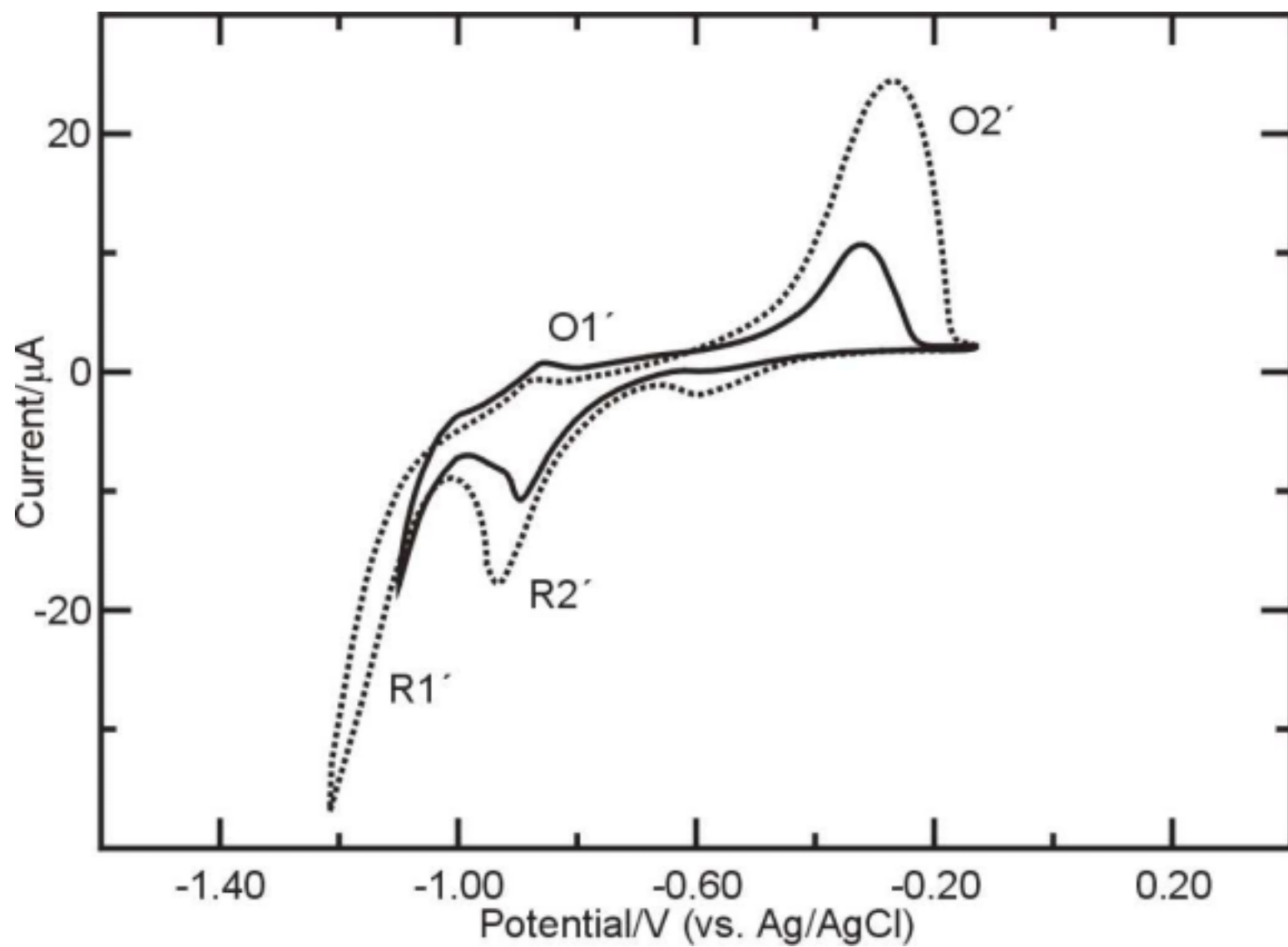
the sulfur species present in solution is SH^- . Scanning negative from the open circuit potential, -0.60 V, a reduction feature is visible at -0.94 V (R2), followed by a second smaller reduction peak at -1.1 V (R1). The charge for the reduction peaks is $100 \mu\text{C}/\text{cm}^2$, which corresponds to desorption of approximately 1/3 ML of sulfur, in a two-electron process. The coverage is defined relative to the number of Au substrate surface atoms, where a ratio of 1.0 is a full monolayer (ML), meaning one sulfur for each Au atom. Scanning further negative, there is an increase in reductive current corresponding to solvent decomposition [106]. Upon reversing the scan direction, two small oxidation peaks are visible, with the first at -1.0 V (O1) and the second at -0.86 V (O2). The peaks R1 and O1 appear to be related, as well as R2 and O2. The peak separation is ~ 80 mV for both redox couples. The voltammetric features O1 and O2 appear to result in the oxidative underpotential deposition (UPD) of sulfur, while R1 and R2 are due to the reductive stripping of UPD sulfur from the electrode [64, 103, 106-109, 111]. Scanning further positive, there is a larger oxidation process (O3) that begins at -0.60 V and continues until 0 V, and is due to the oxidation of sulfide in solution to form bulk sulfur [64, 106, 108, 109]. Reversing the scan direction at 0 V produces a new reduction feature at -0.60 V that was not present during the initial scan in the negative direction. The peak appears to result from the reduction of a sulfur species produced during the large oxidation process, probably the reduction of sulfur and polysulfides formed during O3. In studies of sulfur deposition using a gold rotating ring disc electrode (RRDE), Buckley and Woods found that polysulfides were formed as intermediates during the oxidation of sulfide to sulfur and during the reductive dissolution of sulfur [106]. Scanning negative beyond -0.60 V, there is significantly more reduction occurring than in the initial sweep,

consisting of a peak at -0.92 V and a small shoulder at -1.1 V. The increase in reduction current in this potential range appears to be due to further reduction of bulk sulfur and polysulfide layers, deposited during peak O3 [64, 106, 108, 109]. The value of the open circuit potential suggests that oxidative sulfur UPD from a sulfide solution occurs spontaneously upon immersion [109], probably with a concomitant reduction of protons to hydrogen gas. Thus, the initial reductive sweep served to strip the UPD sulfur layer from the surface. Similar processes have been observed for the halides on different metals, such as the spontaneous oxidative adsorption of I^- on gold [112] and platinum [113, 114], and Cl^- and Br^- on copper [115-117], silver [118-120], and platinum [114].

Thiosulfate Voltammetry

Thiosulfate electrochemistry was carried out in solutions containing 6 mM $Na_2S_2O_3$, 0.10 M K_2SO_4 , and 0.10 M KOH (pH 12.7). The alkaline pH was used to prevent thiosulfate decomposition [121-123]. The rest potential for a clean gold electrode immersed in the thiosulfate solution was -0.23 V, and Figure 4.2 shows the cyclic voltammogram. Scanning negative from the open circuit potential a reduction peak, R2', is visible at -0.90 V (first sweep, solid line). The measured charge for the peak was $110 \mu C/cm^2$, corresponding to reductive dissolution of about 1/3 ML of sulfur. This result is consistent with the reductive stripping of sulfur UPD seen for peaks R2 and R1 over the same potential region in the sulfide solution (Figure 4.1). Scanning further negative, the reduction peak is followed by a steep increase in reductive current labeled R1' that begins at -1.0 V, and appears to be due to solvent reduction [106]. Upon reversing the scan, a small oxidation peak (O1') is observed at -0.88 V, slightly positive

Figure 4.2 Cyclic voltammogram of the polycrystalline gold electrode in 6 mM $\text{Na}_2\text{S}_2\text{O}_3$ with 0.10 M K_2SO_4 and 0.10 M KOH (pH 12.7). Scan rate = 5 mV/s. The first sweep is the solid black line, and the second is the black dotted line.



of the potential for the reduction feature near -0.90 V, and is believed to be due to the underpotential deposition of sulfur. It is interesting that the sulfide voltammetry in Figure 4.1 shows two small oxidation peaks while thiosulfate shows only one. Scanning further positive, there is a second oxidation process ($O2'$) that begins at -0.60 V and continues until -0.20 V, and is apparently due to the bulk oxidation of sulfide. On the second sweep in the negative direction (the dotted line), a new reduction feature was visible at -0.60 V, and observed only after scanning positive past $O2'$. It appears that this peak is similar to that observed for the second cycle in sulfide (Figure 4.1), the reduction of polysulfides formed by the oxidation process at -0.30 V [106]. Scanning further negative, the reduction peak at -0.90 V increased in size, and shifted to a more negative potential. This charge is due to reduction of bulk sulfur deposited at -0.30 V, and may include polysulfide formation. The charge was $210 \mu\text{C}/\text{cm}^2$ for bulk sulfur oxidation, and $200 \mu\text{C}/\text{cm}^2$ for reduction of bulk sulfur to sulfide, suggesting that the sulfur was quantitatively deposited. The large reduction wave at -1.00 V was present, and the extent of reduction increased as the scan went more negative. Scanning back in the positive direction $O1'$ at -0.88 V was again present, but did not change in size. The constant peak area is consistent with sulfur UPD, a surface limited process. Peak $O2'$ at -0.30 V however, increased dramatically in area after scanning to a more negative potential before reversing the scan direction. The reduction process $R1'$ appears to also include thiosulfate reduction to sulfide in addition to solvent decomposition, producing additional sulfide to be oxidized to bulk sulfur. The oxidation of sulfide to form bulk sulfur, $O2'$, occurs at the same potential in the sulfide solution, -0.30 V. Colletti and coworkers have shown that the large oxidation peak at -0.30 V (Figure 4.1) was due to the deposition of

insoluble elemental sulfur on the electrode surface by performing rinsing experiments with a TLEC [109]. Similar experiments were performed here. After depositing bulk sulfur at -0.30 V, the thiosulfate solution was exchanged for a blank solution containing only 0.10 M K_2SO_4 and 0.10 M KOH (pH 12.7) at -0.10 V. Upon completing another cycle, O_2' was still present, showing that insoluble bulk sulfur was deposited on the electrode. A related experiment was performed to identify the sulfur species undergoing oxidation at -0.30 V. After sulfur UPD the solution was exchanged for 0.10 M K_2SO_4 and 0.10 M KOH (pH 12.7) at -0.65 V, and the scan was continued in the positive direction to 0 V. Peak O_2' was absent, and only charging current was evident, demonstrating that the sulfur species oxidized at -0.30 V was soluble, sulfide, and was rinsed out of the TLE cavity, precluding bulk sulfur deposition.

The average oxidation state for the sulfur atoms in a thiosulfate molecule is $+2$, so sulfide can be produced by its reduction [124]. As mentioned above, the reduction process occurring at -1.0 V is believed to include thiosulfate reduction to sulfide, and O_2' is not visible if the scan direction is reversed after the reduction peak at -0.90 V but before the reduction beginning at -1.0 V. It appears that a layer of sulfur is spontaneously deposited on the gold surface at the rest potential, and may be caused by the catalytic decomposition of thiosulfate at the gold surface, as reported by Freund et al. [125] and others [126, 127]. Under acidic conditions, thiosulfate undergoes hydrolysis to form elemental sulfur and bisulfite ion [121, 128, 129], suggesting a lack of stability. The open circuit potential in the thiosulfate solution is ~ 400 mV more positive than in the corresponding sulfide solution, -0.23 V versus -0.60 V, respectively. For the sulfide solution, the rest potential is negative of the potential for bulk sulfide oxidation, while for

thiosulfate the rest potential is at the same potential for bulk oxidation of sulfide. This shows that on the Au electrode in the thiosulfate solution at open circuit, there is no sulfide present to oxidize, and no redox species to block a shift in the potential.

Quantitative Stripping of Sulfur Layers in Acid

On gold, sulfur is irreversibly oxidized to sulfate in a six-electron process in acid media at positive potentials corresponding to Au oxide formation [100, 102, 105, 109, 130]. To determine the sulfur layer coverage, sulfur layers were oxidized to sulfate in 1 M sulfuric acid, and the charges were corrected for concomitant gold oxidation. The coverage measurements were made relative to the number of surface gold atoms. The surface area was 1.2 cm^2 , and the roughness factor of 1.9 was determined from the amount of surface oxide formed [131, 132]. A series of controlled potential immersion experiments was conducted in 1 mM solutions of sulfide and thiosulfate containing 0.10 M K_2SO_4 and 0.10 M KOH (pH 12.8). A typical experiment began with rinsing the clean Au electrode in the blank solution 10-15 times at -1.30 V to remove any acid remaining from the cleaning cycle. The potential chosen was sufficiently negative to reduce any protons to hydrogen gas, since the glass walls of the TLEC can act as a buffer at high pH [109]. The blank solution was then flushed from the TLE cavity, and the cell filled with a sulfide or thiosulfate solution, under potential control for 60 seconds. The solution was then expelled and the cell rinsed with blank at the same potential. The cell was then filled with 1 M H_2SO_4 at 0 V and the potential scanned positive to 1.40 V (Figure 4.3). Sulfur is irreversibly oxidized to sulfate at potentials greater than 0.80 V [100, 102, 105, 109, 130]. A second sweep was performed to ensure that all of the sulfur on the electrode was removed and to determine the charge for gold oxide formation. The

procedure was repeated for a range of potentials, from -1.40 V to 0.40 V, for both thiosulfate and sulfide. Figure 4.3 shows the linear stripping voltammetry for the electrode in 1 M H₂SO₄ after sulfur layer deposition at -0.30 V (A), -0.50 V (B) and -1.10 V (C), as described above. Sulfur oxidation began prior to gold oxide formation and continued until 1.40 V. The clean gold scan was obtained during the second sweep (solid line). The largest stripping charges were observed for sulfur deposited at -0.30 V (A), corresponding to 1.1 ML, consistent with bulk sulfur deposition [64, 103, 106-108, 111, 133]. At -0.50 V (B), the onset of bulk sulfide oxidation, the sulfur coverage was 0.41 ML, while at -1.10 V (C) the coverage was 0.10 ML, a value higher than expected since sulfur should be desorbed from the surface at this potential [100]. A study of sulfur UPD on Ag(111) by Foresti et al. found that sulfur remained on the surface as low as -1.3 V (vs Ag/AgCl) by in situ STM, which revealed sulfur atoms at surface defects [61]. Another STM study on Ag suggested SH⁻ ions were present at -1.35 V on stepped Ag(110) surfaces [63].

Figure 4.4 shows the sulfur coverage as a function of the potential used to deposit sulfur from 1 mM sulfide and 1 mM thiosulfate solutions containing 0.10 M K₂SO₄ and 0.10 M KOH (pH 12.8), after stripping the sulfur layers in 1 M H₂SO₄. For the sulfide experiments there is a plateau between -0.60 V and -0.90 V, in the region where oxidative sulfur UPD occurs (Figure 4.1). From -0.50 V to -0.20 V, the coverage increases sharply, corresponding to bulk sulfur deposition [64, 103, 106-108, 111, 133] and polysulfides [106]. At potentials more positive than -0.20 V the coverage appears to decrease, possibly due to an increase in the formation of soluble polysulfides by reaction of the

Figure 4.3 Linear stripping voltammetry of sulfur layers in 1 M H₂SO₄. Scan rate = 5 mV/s. The solid line is for the clean Au electrode. Stripping curves for sulfur deposited from 1 mM Na₂S with 0.10 M K₂SO₄ and 0.10 M KOH (pH 12.8) at the following potentials: A) -0.30 V; B) -0.50 V; C) -1.1 V.

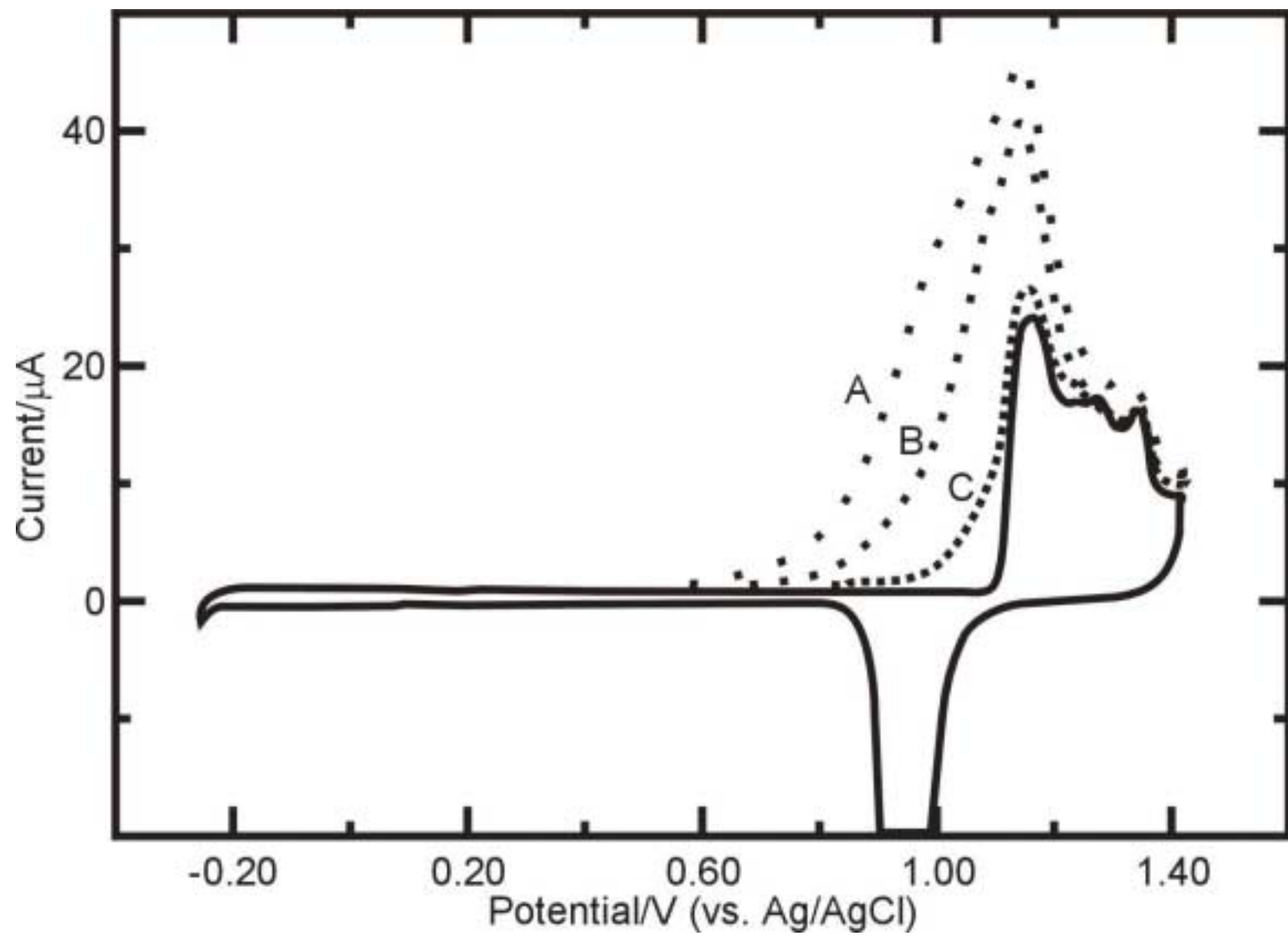
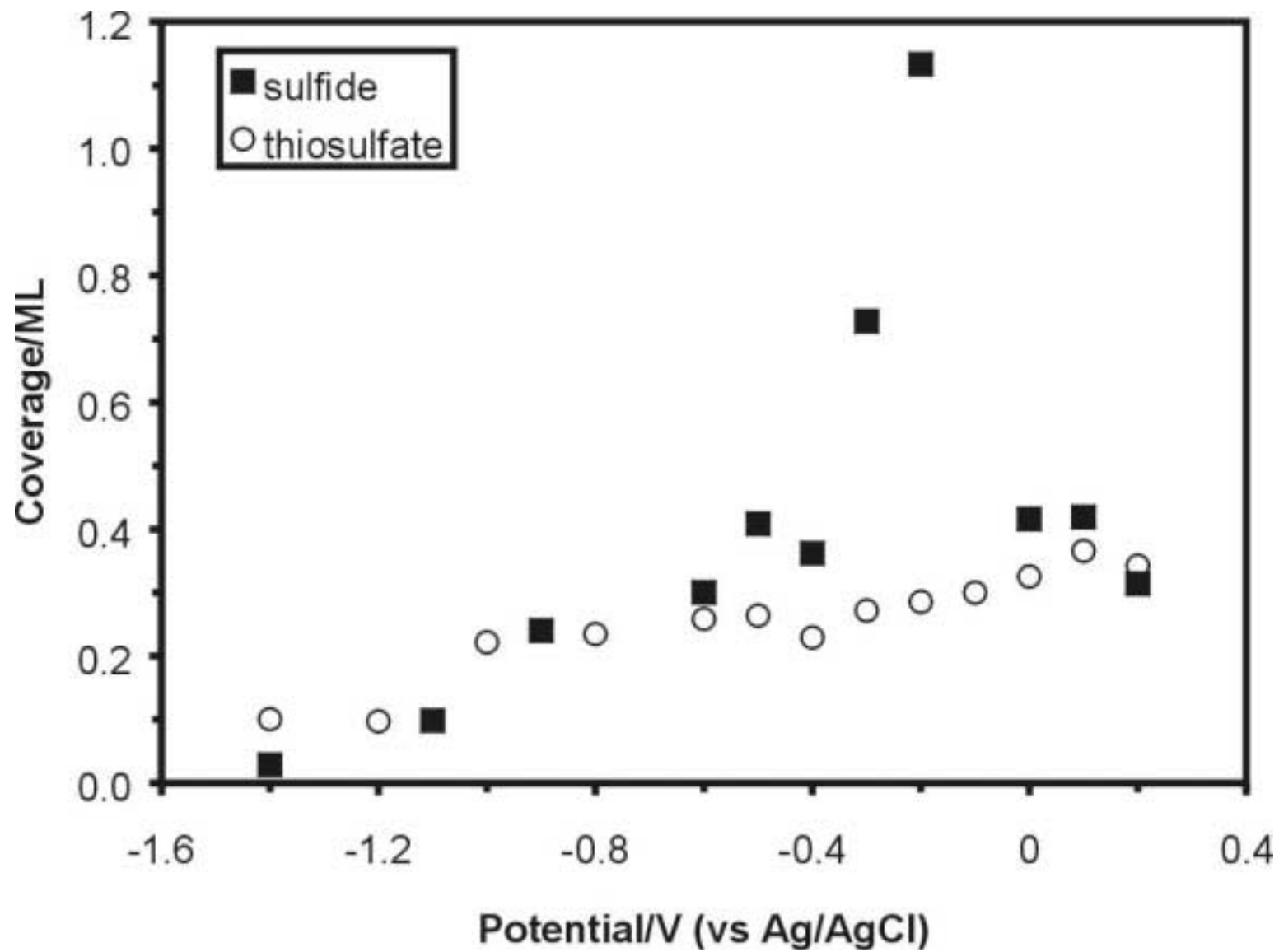


Figure 4.4 Graph of sulfur coverage as function of immersion potential from 1 mM Na₂S with 0.10 M K₂SO₄ and 0.10 M KOH (pH 12.8), and 1 mM Na₂S₂O₃ with 0.10 M K₂SO₄ and 0.10 M KOH (pH 12.7).



sulfur layer with sulfide [98, 106] or possibly the initiation of sulfur oxidation to sulfate [100]. At -1.1 V and negative, the sulfur coverage drops close to zero, as expected.

The potential range over which thiosulfate yielded a plateau in sulfur coverage spanned over a volt. At potentials more negative than -1.2 V, the coverage approached zero. The sulfur coverage was somewhat higher at these potentials, relative to sulfide, possibly related to thiosulfate reduction to sulfide at these potentials (Figure 4.2). Bulk sulfur layers were not obtained from the thiosulfate experiments at more positive potentials as no excursions were made to potentials where thiosulfate could be reduced to sulfide.

UHV-EC Studies Using Sulfide

A series of sulfur electrodeposition experiments was performed using UHV-EC techniques [92]. For the sulfide studies, a 0.20 mM K_2S solution (pH 9.8) was used with no other supporting electrolyte, to avoid electrolyte crystallization on the electrode surface upon removal from solution (emersion) [134]. The clean and ordered Au(111) crystal was immersed in the 0.20 mM K_2S solution for two minutes and then emersed under potential control at potentials between -1.20 V and 0.40 V. After pumping down the antechamber to UHV pressures, the crystal was transferred to the main chamber for analysis. Figure 4.5 is a graph of the S/Au and K/Au Auger ratios as a function of the immersion potential, and Table 4.1 lists approximate sulfur and potassium coverages and observed LEED patterns. Experiments performed at -1.00 V revealed little adsorbed sulfur, 0.13 ML, which decreased to zero at -1.20 V. This is expected, as UPD sulfur is reduced to sulfide at these potentials [109]. LEED experiments showed a (1X1) pattern

Figure 4.5 Graph of S/Au and K/Au Auger ratios as a function of immersion potential for the Au(111) electrode in 0.20 mM K₂S (pH 9.8).

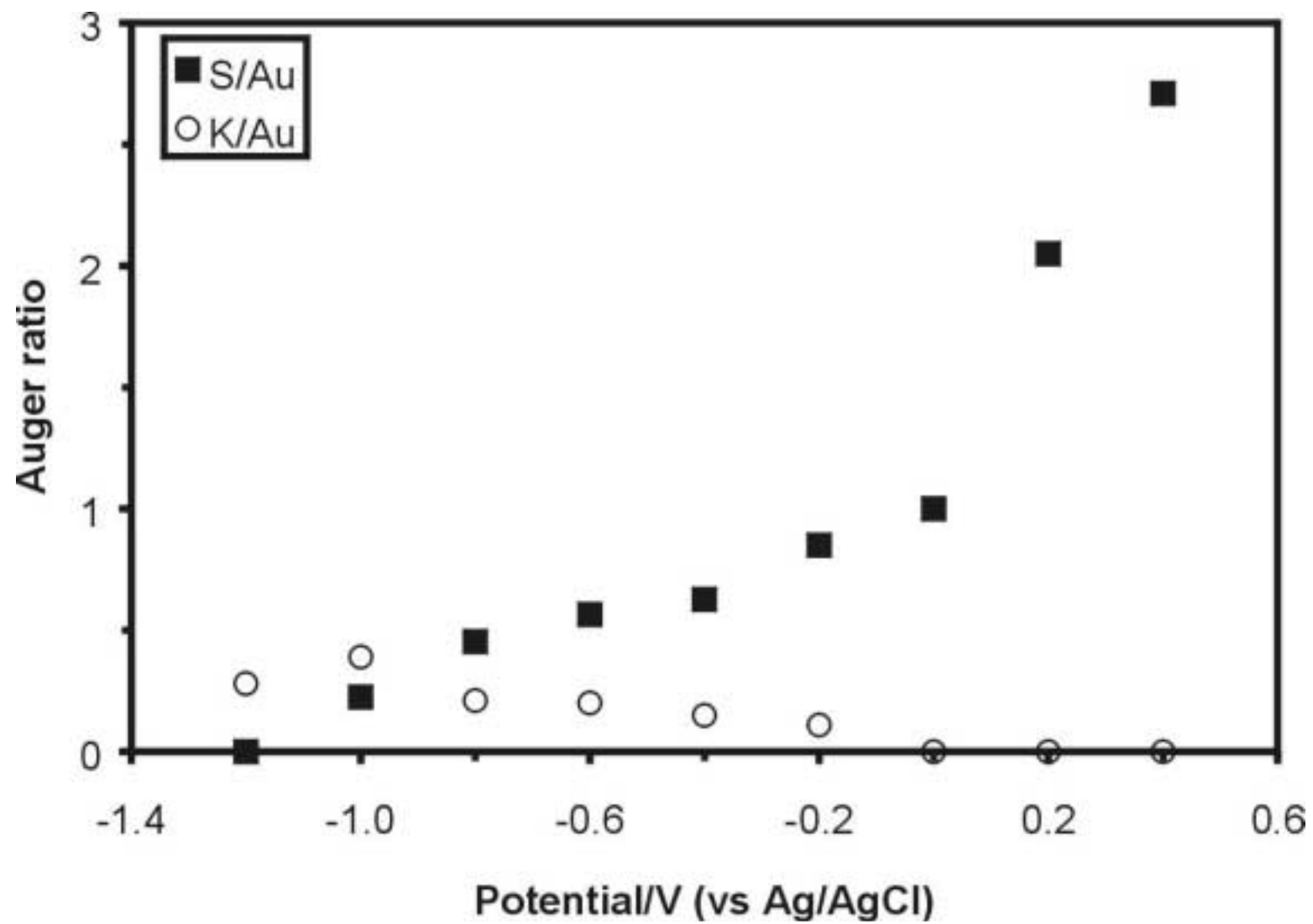


Table 4.1 Sulfur coverages, potassium coverages, and LEED patterns as a function of immersion potential from 0.20 mM K_2S (pH 9.8).

Potential/V	Sulfur Coverage/ML	Potassium Coverage/ML	LEED Pattern
0.40	1.60	0	(2X2)
0.20	1.21	0	(2X2)
0	0.59	0	(2X2)
-0.20	0.50	0.06	(2X2)
-0.40	0.37	0.09	$(\sqrt{3} \times \sqrt{3})R30^\circ$
-0.60	0.33	0.12	$(\sqrt{3} \times \sqrt{3})R30^\circ$
-0.80	0.27	0.12	$(\sqrt{3} \times \sqrt{3})R30^\circ$
-1.0	0.13	0.23	(1X1)
-1.2	0	0.17	(1X1)

similar to those obtained for the clean gold surface before immersion, consistent with the absence of adsorbed sulfur.

Between -0.80 V and -0.40 V, the S/Au ratio was constant, and a $(\sqrt{3}\times\sqrt{3})R30^\circ$ diffraction pattern was visible, corresponding to 1/3 ML sulfur coverage (Figure 4.6A). The same structure has been observed on Au(111) using in situ STM by several workers [5, 7, 8, 44, 135, 136], as well as on Ag(111) [41, 61] and Pt(111) [16, 17] from aqueous solutions of Na₂S. The $(\sqrt{3}\times\sqrt{3})R30^\circ$ sulfur structure has also been formed by vapor phase deposition on Pt(111) [10, 12, 60, 137], Rh(111) [24], and Pd(111) [28, 29]. STM studies indicate that sulfur is bound in threefold hollow sites [4], and a model structure is shown in Figure 4.7A, with the sulfur atoms drawn at their van der Waals diameter [138].

Immersion experiments performed between -0.20 V and 0.40 V revealed a single LEED pattern, a diffuse (2X2) or a (1X $\sqrt{3}$), which has not been previously reported (Figure 4.6B). The diffuseness of the pattern suggested some disorder, so the crystal was gently annealed, which produced a complex pattern (Figure 4.6C). AES showed that the S/Au ratio was in between the (2X2) and $(\sqrt{3}\times\sqrt{3})R30^\circ$ values, suggesting that annealing desorbed some sulfur, and further annealing produced the 1/3 coverage $(\sqrt{3}\times\sqrt{3})R30^\circ$. The structure producing the LEED pattern in Figure 4.6C was not observed by electrodeposition alone. The S/Au ratio for the (2X2) is higher than for the $(\sqrt{3}\times\sqrt{3})R30^\circ$ structure, corresponding to 0.50 ML at -0.20 V and 0 V (Table 4.1). A c(2X2) structure with a 1/2 ML sulfur coverage, formed by electrodeposition on Pt(111) has been reported by Wieckowski et al. [16, 17]. A proposed structure for the 1/2 ML sulfur (2X2) layer on Au(111), also with sulfur atoms in threefold hollow sites, is shown in Figure 4.7B. This

Figure 4.6 LEED patterns obtained for the Au(111) electrode upon emersion from 0.20 mM K_2S (pH 9.8). A) $(\sqrt{3} \times \sqrt{3})R30^\circ$ at -0.40 V, 51.2 eV electron beam energy; B) (2X2) at 0 V, 58.0 eV electron beam energy; C) after annealing the (2X2) structure, 56.3 eV electron beam energy.

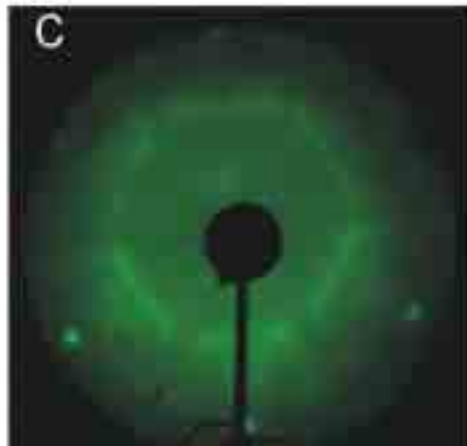
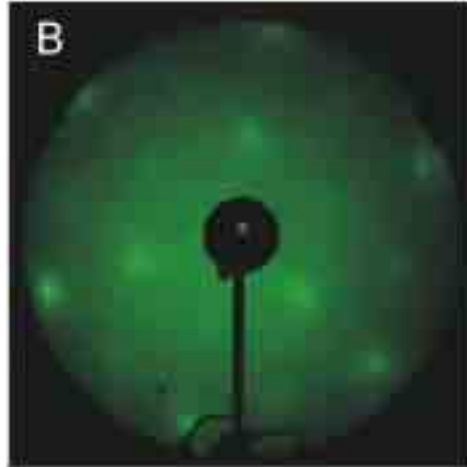
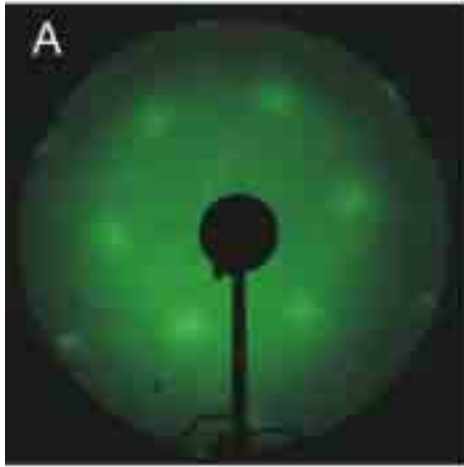
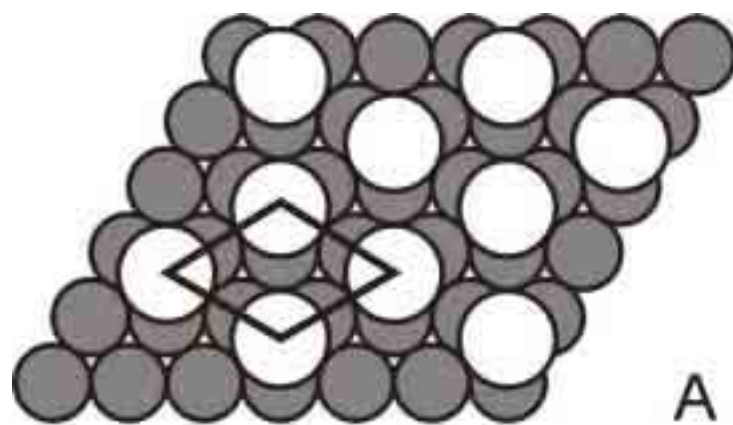
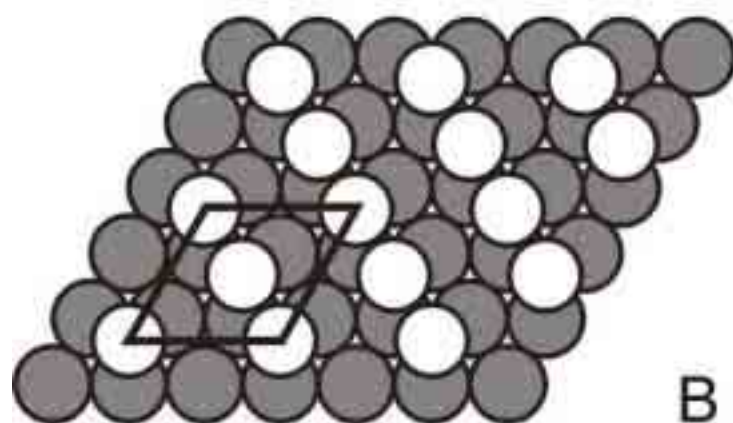


Figure 4.7 Proposed structures for sulfur layers on Au(111). A) $1/3$ ML ($\sqrt{3} \times \sqrt{3}$) $R30^\circ$ structure; B) $1/2$ ML (2X2) structure.



A



B

structure can also be described as a $(1\times\sqrt{3})$. Similar (2×2) structures were formed on Pt(111) [60] and Pd(111) [29] by evaporation and subsequent annealing, but with only 1/4 ML sulfur coverage. At 0.20 V, the S/Au ratio increases sharply, indicating additional oxidative deposition of sulfide, the start of bulk sulfur deposition. In situ STM studies of sulfur layer formation from aqueous solution on Au(111) at comparable potentials found rectangular eight-member ring structures (S_8) with a sulfur coverage just below 1 ML [4, 7, 8, 135]. The S_8 structures reported by Vericat et al. [7, 8] closely resemble the (2×2) model structure in Figure 4.7B, but contain a slightly higher coverage, 0.66 ML. One side of the ring is twice the gold lattice spacing, and the other is slightly larger.

The coverages obtained from the TLEC experiments agree well with the UHV data, indicating approximately 0.30 ML sulfur coverage at potentials where the $(\sqrt{3}\times\sqrt{3})R30^\circ$ was observed. The TLEC data show the increase in sulfur coverage corresponding to bulk sulfur deposition occurring at more negative potentials, -0.30 V versus 0.20 V, and likely a pH effect. Gao et al. observed the same potential shift for bulk sulfur oxidation on Au [139].

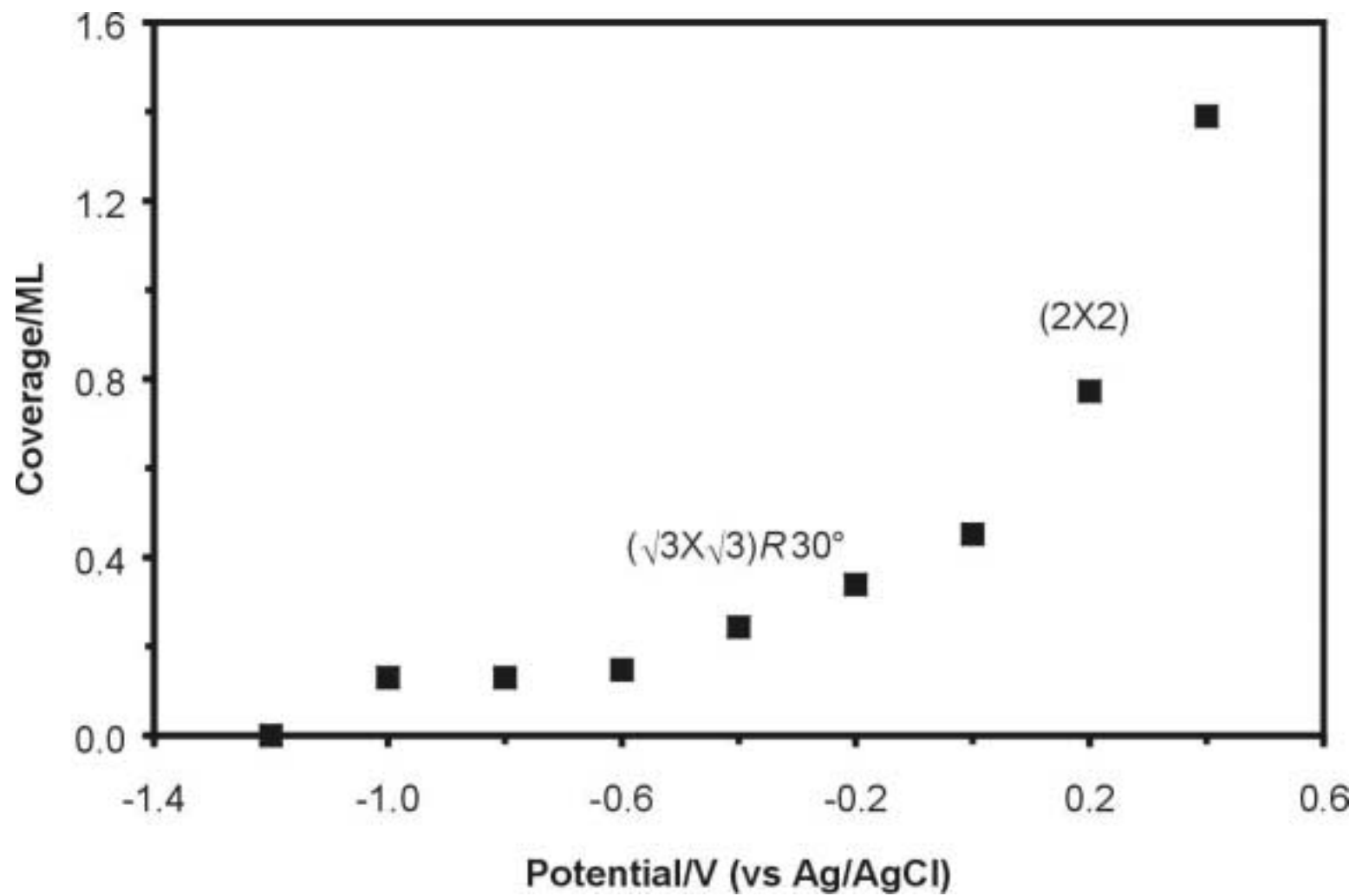
Figure 4.5 shows the K/Au ratios for all immersion potentials. At zero volts and positive, there was no detectable potassium signal in the Auger spectrum, suggesting that a neutral bulk sulfur layer was deposited. In the region of sulfur UPD there was a small amount of potassium, about 0.10 ML, which could be due to a partial charge on the sulfur layer. Sulfur layers deposited on Pt(111) from Na_2S solutions were found to have some anionic character, based on core-level electron energy loss (CEELS) and X-ray photoelectron spectroscopy (XPS) data [16]. Studies of ordered ionic layers on Pt(111)

formed by emersion from K_2S solutions found a $(\sqrt{3} \times \sqrt{3})R30^\circ$ pattern after annealing the electrode to $400^\circ C$, and Auger analysis revealed a strong sulfur signal and a small potassium signal, similar in magnitude to the present study [113, 140]. The adsorbed potassium was attributed to the incomplete neutralization of sulfide ions by oxidative adsorption. The potassium appears to be a result of cation adsorption, which has been well documented in the literature. Cesium adsorption on electrodeposited iodine layers on gold has been reported [112, 141, 142], and in a UHV-EC study by Bravo et al., it was found that cesium adsorbed on an iodine layer at negative potentials [112]. Also, Ohmori et al. have reported the adsorption of sodium and cesium on gold during the electroreduction of nitrate [143]. At more negative potentials, the amount of potassium increased as the sulfur coverage decreased (Table 4.1). Porter and coworkers have reported potassium adsorption at negative potentials on gold, which simultaneously occurred during alkanethiol desorption [144]. The presence of potassium did not affect the $(\sqrt{3} \times \sqrt{3})R30^\circ$ structure for sulfur UPD or the (1×1) for the clean surface at $-1.2 V$. In situ STM studies of similar systems by other groups [5, 7, 8, 44, 135, 136, 145] have not discussed the possibility of adsorbed cations in the $(\sqrt{3} \times \sqrt{3})R30^\circ$ structure. Finally, the potassium may indicate polysulfide adsorption, but it would not fit well with the models of the $(\sqrt{3} \times \sqrt{3})R30^\circ$.

UHV-EC Studies Using Thiosulfate

A series of immersion experiments was also conducted using a $1 \text{ mM Na}_2\text{S}_2\text{O}_3$ solution adjusted to pH 9.7 with KOH. Due to the higher level of electrolyte present, the crystal was rinsed with water after sulfur deposition to minimize the emersion layer [146]. Figure 4.8 shows the sulfur coverage as a function of immersion potential,

Figure 4.8 Graph of the sulfur coverage as a function of immersion potential from 1 mM $\text{Na}_2\text{S}_2\text{O}_3$ in 0.10 mM KOH (pH 9.7).



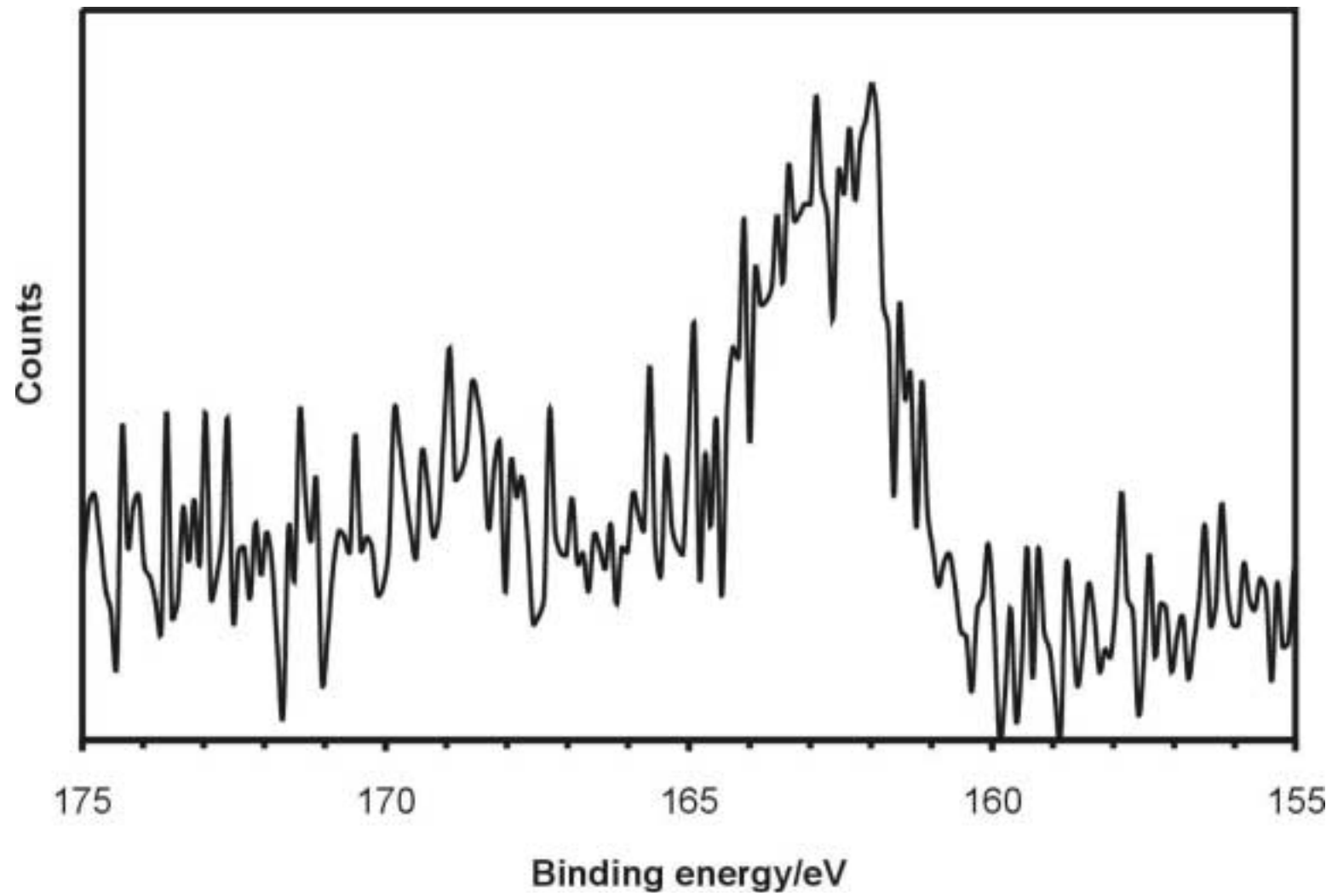
determined from the Auger data [147]. At each potential, the sulfur coverage was somewhat less than obtained in the sulfide solution. The lower values were not a result of rinsing, since the measured sulfur coverage was the same in duplicate experiments using 0.20 mM $\text{Na}_2\text{S}_2\text{O}_3$ in 0.10 mM KOH with no rinsing. At -0.40 V a $(\sqrt{3} \times \sqrt{3})R30^\circ$ LEED pattern was visible, and a faint (2X2) at 0.20 V, in good agreement with the ratios and coverages for the same structures formed in the sulfide solution. The TLEC coverage values are in good agreement, showing the large plateau, and reaching 0.33 ML at more positive potentials.

There was no oxygen signal present in the Auger spectra, indicating that the sulfur was not oxidized by the rinse, and existed as elemental sulfur. An AES study by Freund and coworkers reported similar results for thiosulfate oxidation on gold [125]. XPS analysis of the surface after depositing sulfur at 0.20 V shows a broad sulfur 2p peak centered at 162.0 eV (Figure 4.9), which appears to be split into a doublet, but the high level of noise in the spectrum makes assigning two peaks difficult. Due to spin-orbit coupling, the sulfur 2p peak is split into $2p_{1/2}$ and $2p_{3/2}$ components, producing a doublet [96, 148]. The binding energy is lower than for bulk elemental sulfur (163.6-164.2 eV) [149-151], and is characteristic of metal sulfides such as Cu_2S (161.5 eV) [152] and CdS (161.7 eV) [153]. The results agree well with an XPS study of sulfur layer deposition on gold by Buckley and coworkers [106].

Thiourea

Thiourea was explored as another possible precursor for sulfur atomic layers on Au(111), using a 0.20 mM thiourea solution with KOH to adjust the pH to 8.9. Immersion experiments were performed between -1.20 V and 0.60 V using a two-minute

Figure 4.9 Sulfur 2p XPS spectrum for the Au(111) electrode emersed at 0.20 V from 1 mM Na₂S₂O₃ in 0.10 mM KOH (pH 9.7).



deposition time, and the crystal was not rinsed after emersion. Figure 4.10 shows the sulfur coverage, obtained from the Auger data [147], as a function of deposition potential. A constant sulfur coverage of 0.33 ML was observed between -0.80 V and 0.60V, in agreement with LEED experiments that revealed a $(\sqrt{3}\times\sqrt{3})R30^\circ$ unit cell. At -0.80V and negative, the coverage decreased to 0.10 ML, and a (1X1) was observed by LEED, indicating no ordered sulfur structure [61]. The sulfur coverage was constant for thiourea over a larger potential range than either sulfide or thiosulfate, and the $(\sqrt{3}\times\sqrt{3})R30^\circ$ pattern was observed at coverages similar to those from the sulfide solution. The Auger spectra revealed no detectable nitrogen and carbon signals, only sulfur and gold, suggesting that the gold surface may have catalyzed the decomposition of thiourea molecules as well. An in situ STM study of thiourea on Au(111) [154] reported obtaining images for ordered thiourea and formamidine disulfide layers that slowly converted to a $(\sqrt{3}\times\sqrt{3})R30^\circ$ sulfur layer. Our AES results do not support the formation of ordered thiourea or formamidine disulfide layers on the gold surface; however, since the electrode was emersed and brought to vacuum for analysis, some changes may have occurred. Also, in that study the solution used had a neutral pH, and under basic conditions, thiourea has been found to decompose. For example, in 0.10 M KOH, thiourea undergoes desulfurization, leading to an accumulation of sulfur on gold electrodes [155], and ammoniacal solutions of Cd and thiourea have been used to form CdS by chemical bath deposition (CBD) [156, 157].

Ethanethiolate

The last sulfur precursor used was ethanethiolate, and Figure 4.11 shows a voltammogram for the Au(111) crystal in 0.20 mM $\text{NaSCH}_2\text{CH}_3$ and 1 mM KOH

Figure 4.10 Graph of the sulfur coverage as a function of immersion potential from 0.20 mM thiourea in KOH (pH 8.9).

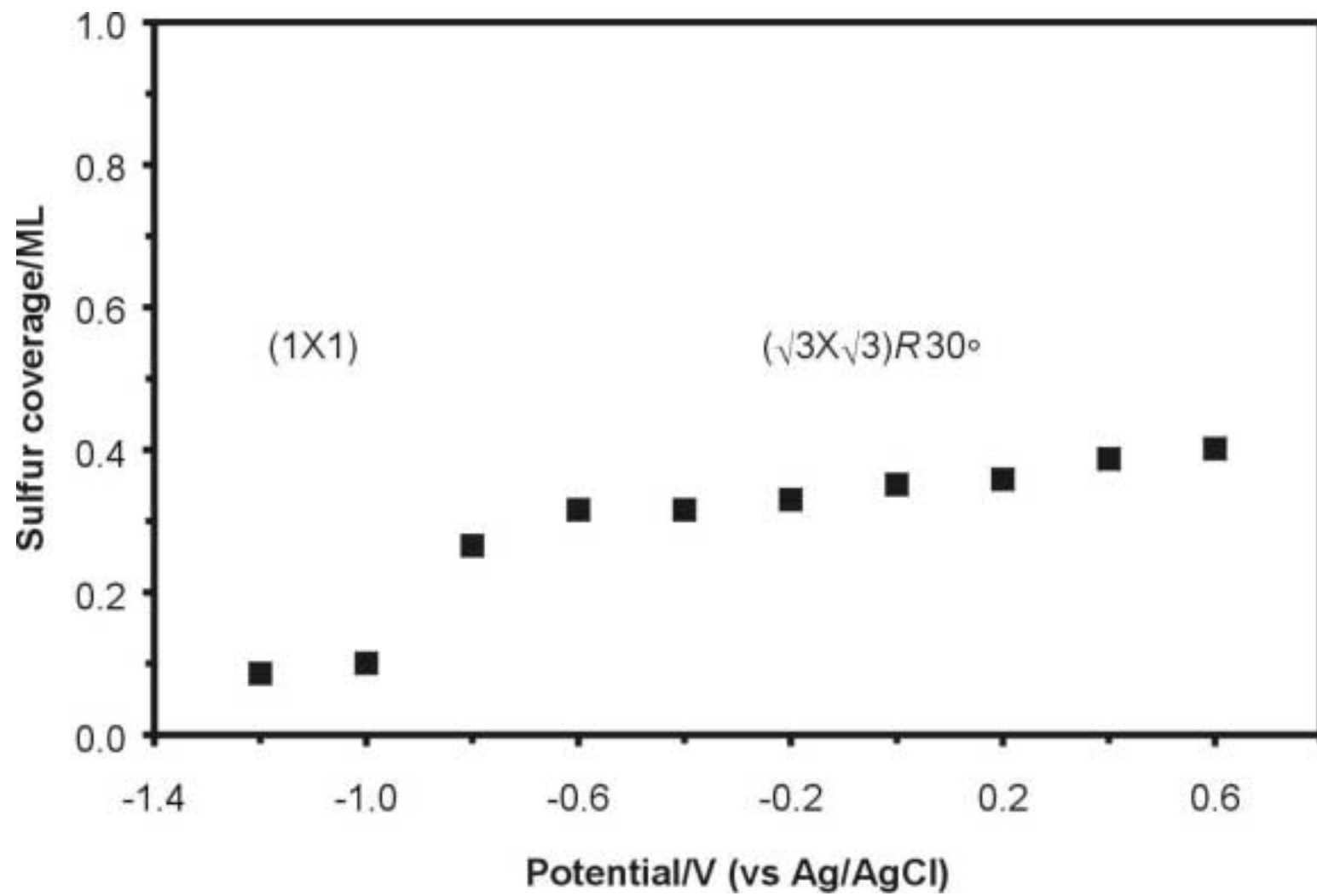
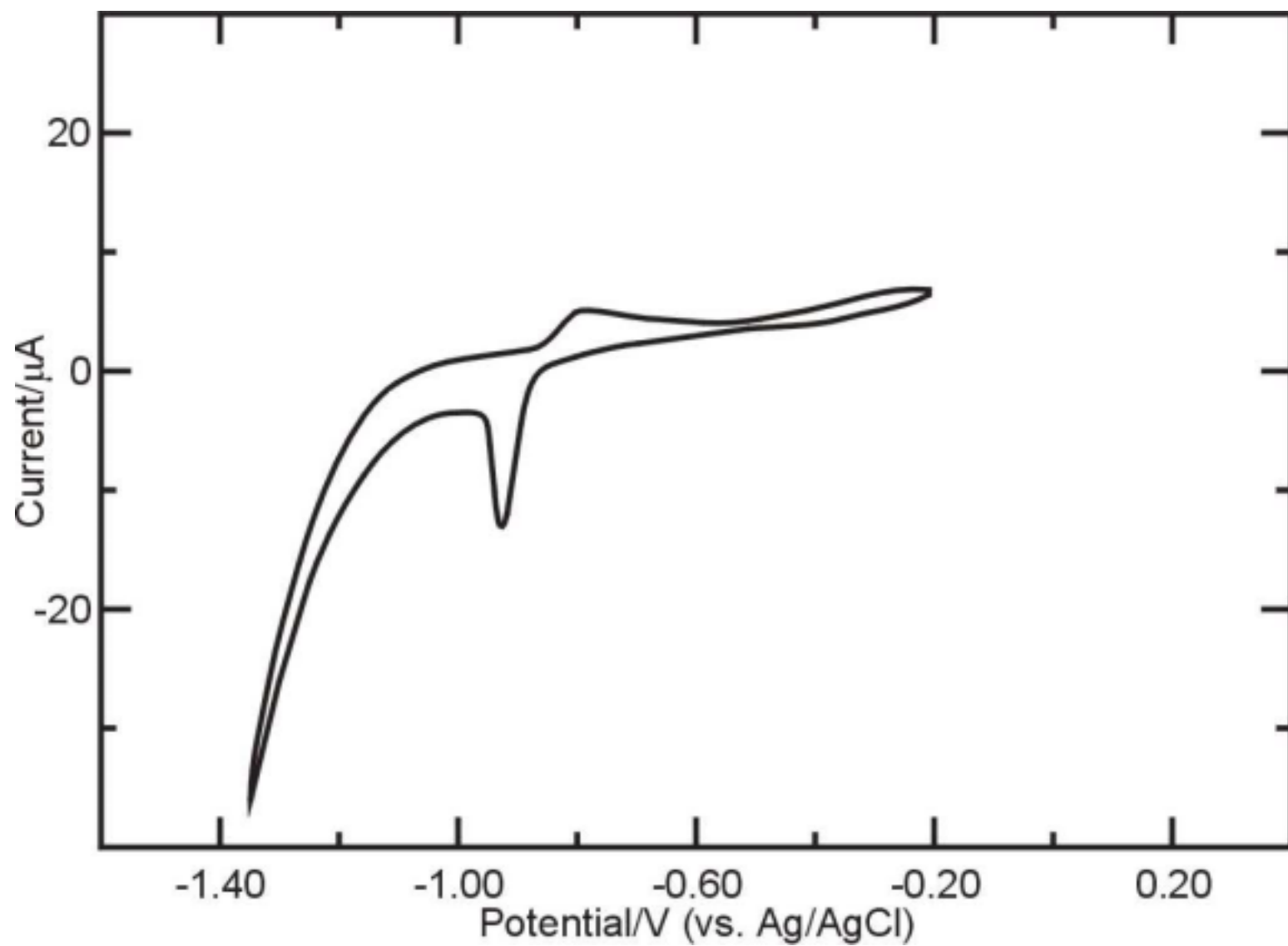


Figure 4.11 Cyclic voltammogram of the Au(111) electrode in 0.20 mM NaSCH₂CH₃ and 1 mM KOH (pH 10.5).



(pH 10.5). The solution was similar to that used by White et al. [158, 159], and is an alternative to the commonly employed solutions of 1 mM ethanethiol dissolved in absolute ethanol used for forming SAMs [54, 160]. The open circuit potential was -0.50 V, and LEED experiments revealed a complex diffraction pattern containing $(\sqrt{3}\times\sqrt{3})R30^\circ$ fractional order spots split into a star pattern and (3×3) spots, shown in Figure 4.12, A-C. In situ STM studies of ethanethiol spontaneously adsorbed on Au(111) revealed a $(\sqrt{3}\times\sqrt{3})R30^\circ$ unit cell [54]. A later LEED and infrared reflection-absorption spectroscopy (IRRAS) study of short chain alkanethiols deposited on Au(111) also found the $(\sqrt{3}\times\sqrt{3})R30^\circ$, but additional spots and streaking were evident in the diffraction pattern [161]. Recently, Rhee and Hyun observed a series of nonequivalent $(\sqrt{3}\times\sqrt{3})R30^\circ$ structures for 2-mercaptoethanol by STM [162]. Kolb and coworkers observed a $(p\times\sqrt{3})$ unit cell (where p is a variable distance for one side of the unit cell) for self-assembled monolayers of ethanethiol on Au(111) using in situ STM [163], which is closely related to the $(\sqrt{3}\times\sqrt{3})R30^\circ$ unit cell. They also observed striped arrays with missing rows. The composite surface structure they observed is similar to tellurium UPD on Au(111), which forms a $1/3$ ML $(\sqrt{3}\times\sqrt{3})R30^\circ$ layer with an array of domain walls produced by some of the tellurium atoms positioned farther apart than the $\sqrt{3}$ spacing [164, 165]. The structure possesses (13×13) periodicity, producing a complex split-spot diffraction. The LEED pattern observed for ethanethiolate is consistent with the literature, but indicates the presence of a more complicated layer. In situ STM studies are currently underway in this lab to determine the atomic structure.

The Auger spectrum for the surface (Figure 4.13) showed a significant sulfur signal (152 eV), and a small carbon signal (272 eV) [147]. Using AES quantitation, the

Figure 4.12 LEED patterns obtained for the Au(111) electrode emersed at -0.50 V from 0.20 mM NaSCH₂CH₃ and 1 mM KOH (pH 10.5). A) 52.0 eV electron beam energy; B) 53.0 eV electron beam energy; C) 18.3 eV electron beam energy.

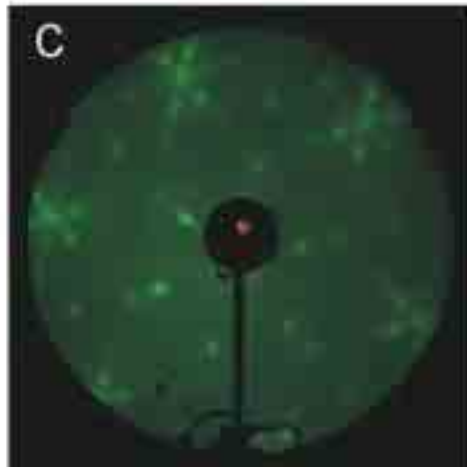
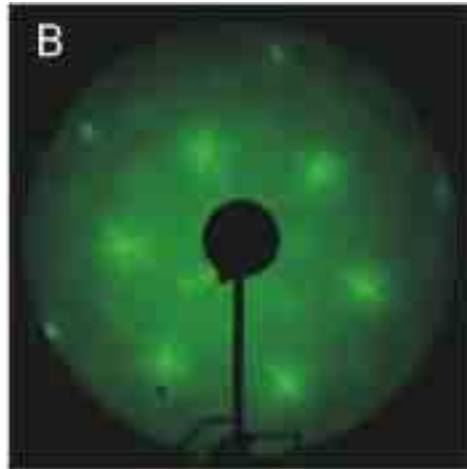
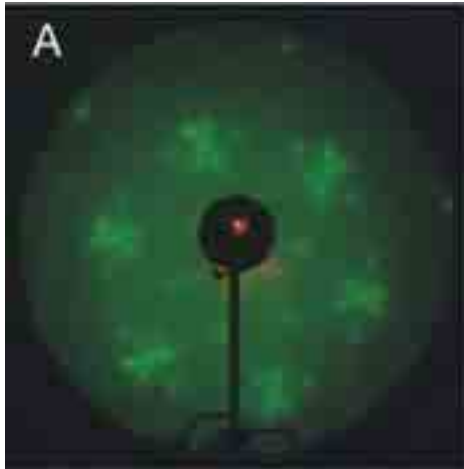
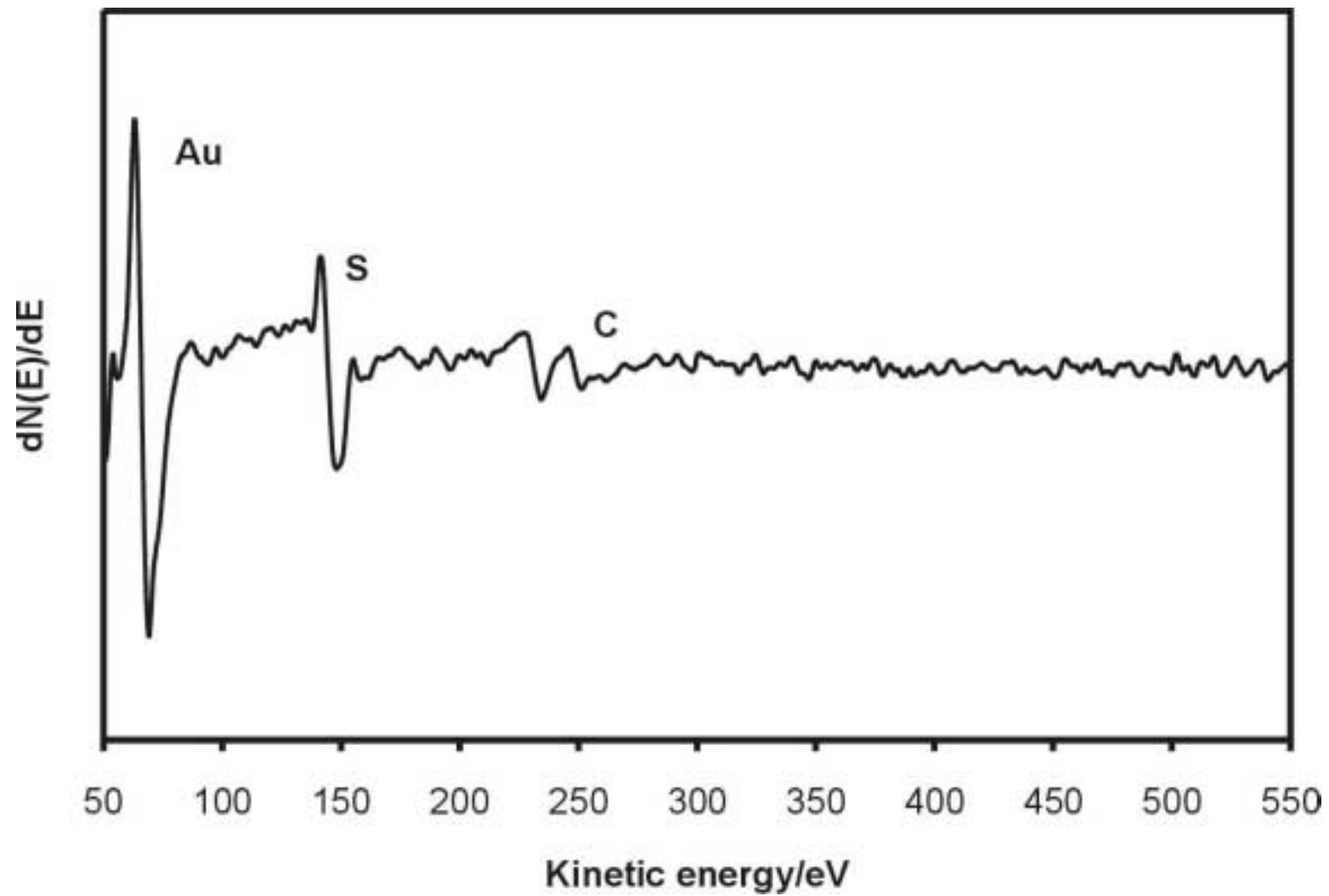


Figure 4.13 AES spectrum of the Au(111) electrode after emersion at -0.50 V from 0.20 mM NaSCH₂CH₃ and 1 mM KOH (pH 10.5).



coverage for sulfur was 0.36 ML, agreeing well with a 1/3 ML sulfur layer, and the carbon coverage was 0.18 ML. XPS analysis revealed a clear carbon signal (Figure 4.14) at a binding energy of 284.3 eV, consistent with aliphatic carbon [166]. The results suggest that a sulfur and ethanethiolate layer is present, possibly due to ethanethiol decomposition to sulfur, which has been reported on Mo(110) [167] and GaAs(100) [168]. The complex LEED pattern observed may arise from the coexisting layers, and both ethanethiol [54] and sulfide [5, 7, 8, 44, 135, 136] adsorbed on Au(111) form $(\sqrt{3}\times\sqrt{3})R30^\circ$ structures.

The sulfur 2p XPS spectrum in Figure 4.15 shows a single peak centered at 161.9 eV binding energy, in good agreement with thiol and sulfide monolayers bound to gold [169]. The binding energy is ~ 1 eV lower than observed for neat thiols and sulfides, caused by Au-S bonding which leads to an increased negative charge on the sulfur atom. There was no indication of a change in the binding energy of the Au 4f_{7/2} peak (~ 84.0 eV) for ethanethiolate adsorption. Other groups using XPS also found no change in the Au 4f_{7/2} peak after SAM adsorption, concluding that the Au(I) peak at 84.3 eV expected for Au-thiol would be only a 5% contribution to the Au 4f_{7/2} peak, making it difficult to discern [166, 170].

Scanning negative from the rest potential, there is a sharp reduction peak at -0.90 V. Similar features were observed in the electrochemical reduction of thiol from gold surfaces in the same potential region [171, 172]. AES showed a decrease in the amount of sulfur, from 0.36 ML to 0.30 ML, and 0.30 ML of potassium was present. It appears that the thiol was incompletely desorbed, as carbon was still detected by XPS. Porter and coworkers have attributed the presence of potassium ions at negative

Figure 4.14 Carbon 1s XPS spectrum for the Au(111) surface after emersion at -0.50 V from 0.20 mM NaSCH₂CH₃ and 1 mM KOH (pH 10.5).

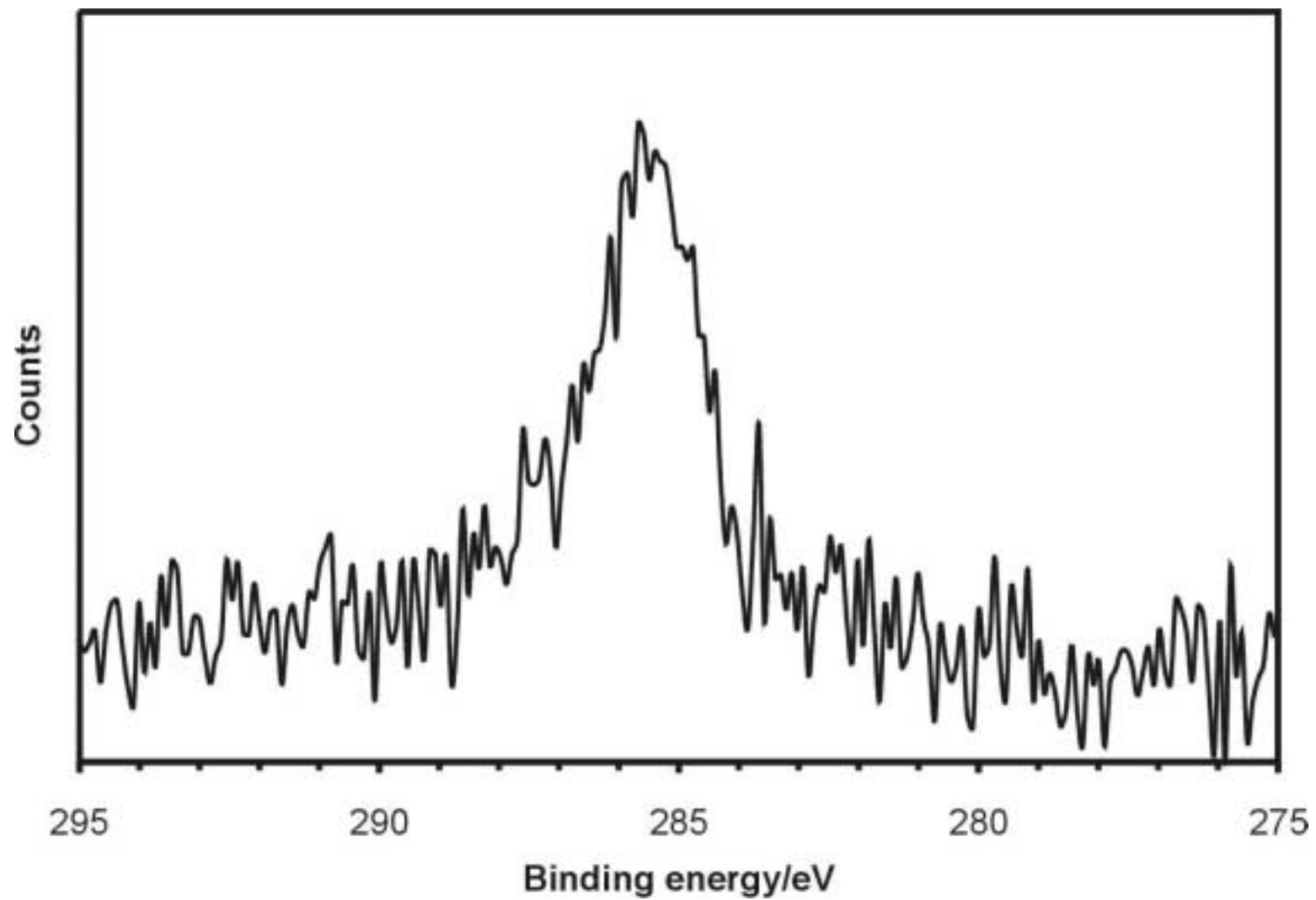
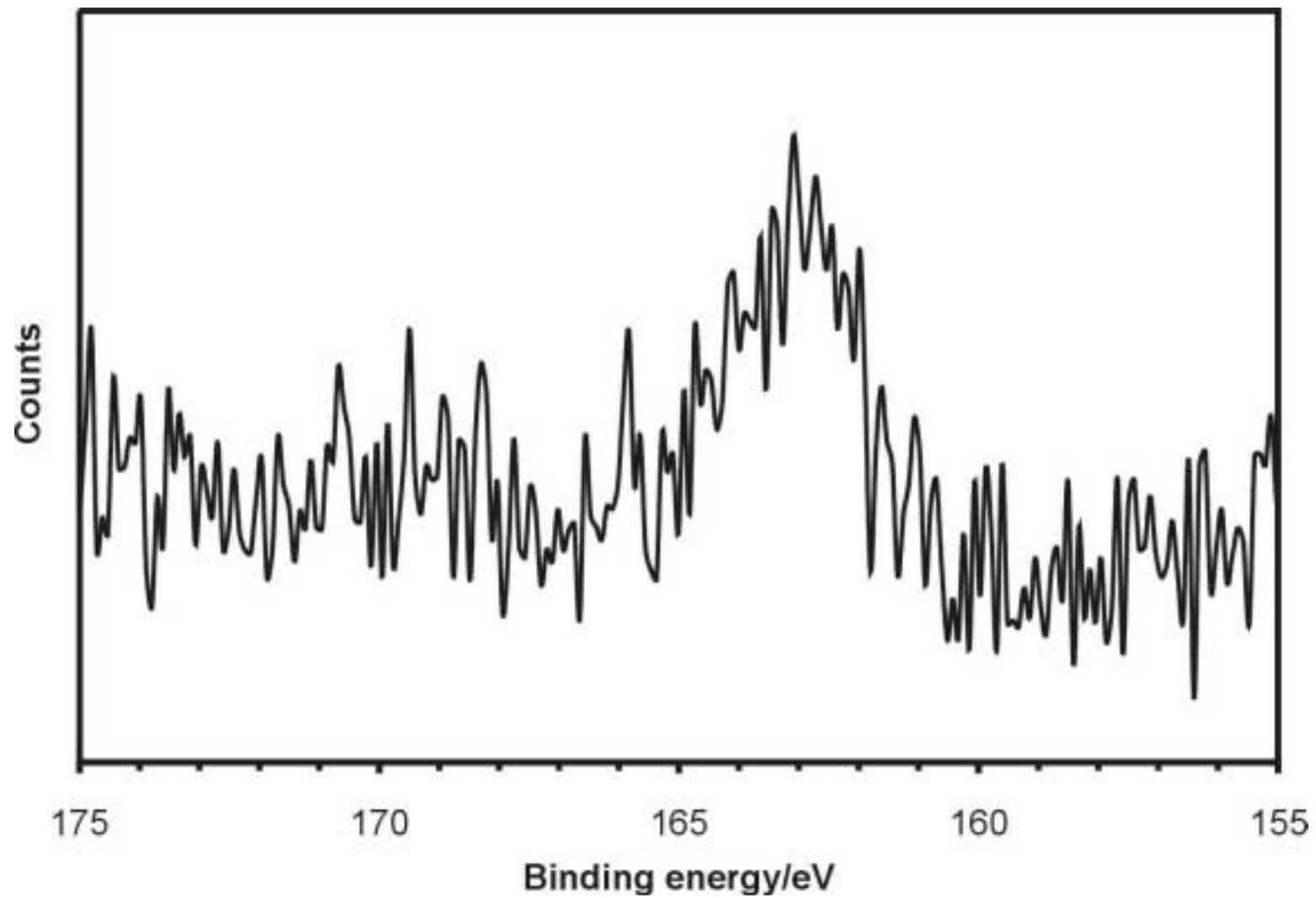


Figure 4.15 Sulfur 2p XPS spectrum for the Au(111) surface after emersion at -0.50 V from 0.20 mM NaSCH₂CH₃ and 1 mM KOH (pH 10.5).



potentials on gold to thiol desorption in a recent EQCM study [144]. Emersing the electrode at -1.0 V revealed a diffuse (1X1) pattern that transformed into a (2X2) during LEED analysis, which was likely caused by the electron beam [93-95]. A similar structural change to a (2X2) was produced by annealing a sulfur layer containing potassium deposited from 0.20 mM K₂S.

Conclusions

Sulfur atomic layers were deposited on polycrystalline and single crystal gold surfaces from alkaline solutions of sulfide, thiosulfate, thiourea, and ethanethiolate under potential control. Oxidative UPD features were identified in the sulfide and thiosulfate voltammetry, and a $(\sqrt{3}\times\sqrt{3})R30^\circ$ unit cell was observed by LEED for sulfur UPD in both solutions. A (2X2) pattern was observed using sulfide and thiosulfate solutions at potentials corresponding to bulk sulfur deposition. There was no indication of oxygen with Auger, confirming that the sulfur signal was due to elemental sulfur. Only a $(\sqrt{3}\times\sqrt{3})R30^\circ$ was observed for thiourea, and no detectable nitrogen or carbon signals were observed with Auger. Indications are that it decomposed at the gold surface and produced a sulfur layer. Ethanethiolate layers appear to undergo partial decomposition upon adsorption, as shown by AES and XPS, to produce a complex LEED pattern containing split- $\sqrt{3}$ and (3X3) spots. More studies are needed to determine the precise surface structure, which is important for fundamental SAM research. Producing the same ordered sulfur monolayers using different sulfur precursors suggest that a large number of compounds may be used as precursors for the formation of sulfur atomic layers in the formation of compound semiconductors by EC-ALE. The large potential

window over which sulfur layers can be deposited from thiosulfate and thiourea solutions would be valuable for the formation of CdS deposits if they also occur on Cd atomic layers.

References

1. M. Kostelitz and J. Oudar, *C. R. Acad. Sci., Ser. C* 271 (1970) 1205.
2. M. Kostelitz and J. Oudar, *Surf. Sci.* 27 (1971) 176.
3. M. Kostelitz, J. L. Domange, and J. Oudar, *Surf. Sci.* 34 (1973) 431.
4. X. P. Gao, Y. Zhang, and M. J. Weaver, *J. Phys. Chem.* 96 (1992) 4156.
5. U. Demir and C. Shannon, *Langmuir* 10 (1994) 2794.
6. V. Bondzie, S. Dixon-Warren, and Y. Yu, *J. Chem. Phys.* 111 (1999) 10670.
7. G. Andreasen, C. Vericat, M. E. Vela, and R. C. Salvarezza, *J. Chem. Phys.* 111 (1999) 9457.
8. C. Vericat, G. Andreasen, M. E. Vela, and R. C. Salvarezza, *J. Phys. Chem. B* 104 (2000) 302.
9. H. Martin, C. Vericat, G. Andreasen, A. H. Creus, M. E. Vela, and R. C. Salvarezza, *Langmuir* 17 (2001) 2334.
10. Y. Berthier, M. Perdereau, and J. Oudar, *Surf. Sci.* 36 (1973) 225.
11. W. Heegemann, E. Bechtold, and K. Hayek, *Proc. Int. Conf. Solid Surf.*, 2nd (1974) 185.
12. W. Heegemann, K. H. Meister, E. Bechtold, and K. Hayek, *Surf. Sci.* 49 (1975) 161.
13. T. E. Fischer and S. R. Kelemen, *Surf. Sci.* 69 (1977) 1.

14. K. Hayek, H. Glassl, A. Gutmann, H. Leonhard, M. Prutton, S. P. Tear, and M. R. Weltoncook, *Surf. Sci.* 152 (1985) 419.
15. K. Hayek, H. Glassl, A. Gutmann, H. Leonhard, M. Prutton, S. P. Tear, and M. R. Weltoncook, *Surf. Sci.* 175 (1986) 535.
16. Y. E. Sung, W. Chrzanowski, A. Zolfaghari, G. Jerkiewicz, and A. Wieckowski, *J. Am. Chem. Soc.* 119 (1997) 194.
17. Y. E. Sung, T. Chrzanowski, A. Wieckowski, A. Zolfaghari, S. Blais, and G. Jerkiewicz, *Electrochim. Acta* 44 (1998) 1019.
18. M. Perdereau and J. Oudar, *Surf. Sci.* 20 (1970) 80.
19. J. E. Demuth, D. W. Jepsen, and P. M. Marcus, *Phys. Rev. Lett.* 32 (1974) 1182.
20. L. Ruan, I. Stensgaard, F. Besenbacher, and E. Laegsgaard, *J. Vac. Sci. Technol., B* 12 (1994) 1772.
21. L. F. Li, D. Totir, G. S. Chottiner, and D. A. Scherson, *J. Phys. Chem. B* 102 (1998) 8013.
22. J. S. Foord and A. E. Reynolds, *Surf. Sci.* 164 (1985) 640.
23. K. C. Wong, W. Liu, M. Saily, and K. A. R. Mitchell, *Surf. Sci.* 345 (1996) 101.
24. H. A. Yoon, M. Salmeron, and G. A. Somorjai, *Surf. Sci.* 395 (1998) 268.
25. F. Maca, M. Scheffler, and W. Berndt, *Surf. Sci.* 160 (1985) 467.
26. C. H. Patterson and R. M. Lambert, *Surf. Sci.* 187 (1987) 339.
27. J. G. Forbes, A. J. Gellman, J. C. Dunphy, and M. Salmeron, *Surf. Sci.* 279 (1992) 68.
28. V. R. Dhanak, A. G. Shard, B. C. C. Cowie, and A. Santoni, *Surf. Sci.* 410 (1998) 321.

29. S. Speller, T. Rauch, J. Bomermann, P. Borrmann, and W. Heiland, *Surf. Sci.* 441 (1999) 107.
30. S. R. Kelemen and T. E. Fischer, *Surf. Sci.* 87 (1979) 53.
31. R. Dennert, M. Sokolowski, and H. Pfnur, *Surf. Sci.* 271 (1992) 1.
32. D. Heuer, T. Muller, H. Pfnur, and U. Kohler, *Surf. Sci.* 297 (1993) L61.
33. D. Jurgens, G. Held, and H. Pfnur, *Surf. Sci.* 303 (1994) 77.
34. T. Muller, D. Heuer, H. Pfnur, and U. Kohler, *Surf. Sci.* 347 (1996) 80.
35. G. A. Somorjai, *J. Catal.* 27 (1972) 453.
36. N. Barbouth and M. Salame, *J. Catal.* 104 (1987) 240.
37. W. T. Owens, N. M. Rodriguez, and R. T. K. Baker, *Catal. Today* 21 (1994) 3.
38. A. Aguinaga, M. Montes, P. Malet, M. J. Capitan, I. Carrizosa, and J. A. Odriozola, *Appl. Catal., A* 110 (1994) 197.
39. I. Touzov and C. B. Gorman, *Langmuir* 13 (1997) 4850.
40. H. Cabibil, J. S. Lin, and J. A. Kelber, *Surf. Sci.* 382 (1997) L645.
41. M. L. Foresti, G. Pezzatini, M. Cavallini, G. Aloisi, M. Innocenti, and R. Guidelli, *J. Phys. Chem. B* 102 (1998) 7413.
42. M. Innocenti, G. Pezzatini, F. Forni, and M. L. Foresti, *J. Electrochem. Soc.* 148 (2001) C357.
43. T. Cecconi, A. Atrei, U. Bardi, F. Forni, M. Innocenti, F. Loglio, M. L. Foresti, and G. Rovida, *J. Electron Spectrosc. Relat. Phenom.* 114 (2001) 563.
44. U. Demir and C. Shannon, *Langmuir* 12 (1996) 6091.
45. A. Gichuhi, B. E. Boone, U. Demir, and C. Shannon, *J. Phys. Chem. B* 102 (1998) 6499.

46. A. Gichuhi, C. Shannon, and S. S. Perry, *Langmuir* 15 (1999) 5654.
47. T. Torimoto, A. Obayashi, S. Kuwabata, H. Yasuda, H. Mori, and H. Yoneyama, *Langmuir* 16 (2000) 5820.
48. T. Torimoto, S. Nagakubo, M. Nishizawa, and H. Yoneyama, *Langmuir* 14 (1998) 7077.
49. T. Torimoto, A. Obayashi, S. Kuwabata, and H. Yoneyama, *Electrochem. Commun.* 2 (2000) 359.
50. R. G. Nuzzo and D. L. Allara, *J. Am. Chem. Soc.* 105 (1983) 4481.
51. R. G. Nuzzo, B. R. Zegarski, and L. H. Dubois, *J. Am. Chem. Soc.* 109 (1987) 733.
52. M. D. Porter, T. B. Bright, D. L. Allara, and C. E. D. Chidsey, *J. Am. Chem. Soc.* 109 (1987) 3559.
53. C. D. Bain, E. B. Troughton, Y. T. Tao, J. Evall, G. M. Whitesides, and R. G. Nuzzo, *J. Am. Chem. Soc.* 111 (1989) 321.
54. C. A. Widrig, C. A. Alves, and M. D. Porter, *J. Am. Chem. Soc.* 113 (1991) 2805.
55. G. M. Whitesides, *Sci. Am.* 273 (1995) 146.
56. G. E. Poirier and E. D. Pylant, *Science* 272 (1996) 1145.
57. A. Ulman, *Chem. Rev.* 96 (1996) 1533.
58. N. Bowden, A. Terfort, J. Carbeck, and G. M. Whitesides, *Science* 276 (1997) 233.
59. G. E. Poirier, *Chem. Rev.* 97 (1997) 1117.
60. H. A. Yoon, N. Materer, M. Salmeron, M. A. VanHove, and G. A. Somorjai, *Surf. Sci.* 376 (1997) 254.

61. G. D. Aloisi, M. Cavallini, M. Innocenti, M. L. Foresti, G. Pezzatini, and R. Guidelli, *J. Phys. Chem. B* 101 (1997) 4774.
62. D. W. Hatchett, X. P. Gao, S. W. Catron, and H. S. White, *J. Phys. Chem.* 100 (1996) 331.
63. D. W. Hatchett and H. S. White, *J. Phys. Chem.* 100 (1996) 9854.
64. X. P. Gao, Y. Zhang, and M. J. Weaver, *Langmuir* 8 (1992) 668.
65. B. W. Gregory and J. L. Stickney, *J. Electroanal. Chem.* 300 (1991) 543.
66. J. L. Stickney, in: A. J. Bard and I. Rubinstein (Eds.), *Electroanalytical Chemistry A Series of Advances*, Marcel Dekker, New York, 1999, p. 75.
67. C. H. L. Goodman and M. V. Pessa, *J. Appl. Phys.* 60 (1986) R65.
68. T. F. Kuech, P. D. Dapkus, and Y. Aoyagi, *Atomic Layer Growth and Processing*, Materials Research Society, Pittsburgh, 1991.
69. M. A. Tischler and S. M. Bedair, *J. Cryst. Growth* 77 (1986) 89.
70. L. Niinisto and M. Leskela, *Thin Solid Films* 225 (1993) 130.
71. D. M. Kolb, in: H. Gerischer and C. W. Tobias (Eds.), *Advances in Electrochemistry and Electrochemical Engineering*, Wiley & Sons, New York, 1978, p. 125.
72. K. Juttner and W. J. Lorenz, *Z. Phys. Chem. (Wiesbaden)* 122 (1980) 163.
73. R. R. Adzic, in: H. Gerischer and C. W. Tobias (Eds.), *Advances in Electrochemistry and Electrochemical Engineering*, 1984, p. 159.
74. B. K. Niece and A. A. Gewirth, *Langmuir* 13 (1997) 6302.
75. S. Z. Zou and M. J. Weaver, *J. Phys. Chem. B* 103 (1999) 2323.

76. L. P. Colletti, B. H. Flowers, and J. L. Stickney, *J. Electrochem. Soc.* 145 (1998) 1442.
77. L. P. Colletti and J. L. Stickney, *J. Electrochem. Soc.* 145 (1998) 3594.
78. B. M. Huang, L. P. Colletti, B. W. Gregory, J. L. Anderson, and J. L. Stickney, *J. Electrochem. Soc.* 142 (1995) 3007.
79. T. E. Lister, L. P. Colletti, and J. L. Stickney, *Isr. J. Chem.* 37 (1997) 287.
80. F. Forni, M. Innocenti, G. Pezzatini, and M. L. Foresti, *Electrochim. Acta* 45 (2000) 3225.
81. G. Pezzatini, S. Caporali, M. Innocenti, and M. L. Foresti, *J. Electroanal. Chem.* 475 (1999) 164.
82. K. Murase, H. Watanabe, S. Mori, T. Hirato, and Y. Awakura, *J. Electrochem. Soc.* 146 (1999) 4477.
83. K. Murase, H. Uchida, T. Hirato, and Y. Awakura, *J. Electrochem. Soc.* 146 (1999) 531.
84. K. Murase, T. Honda, M. Yamamoto, T. Hirato, and Y. Awakura, *J. Electrochem. Soc.* 148 (2001) C203.
85. E. Murase, H. Watanabe, H. Uchida, T. Hirato, and Y. Awakura, *Electrochemistry* 67 (1999) 331.
86. J. L. Stickney, T. L. Wade, and B. H. Flowers, *Abstr. Pap. Am. Chem. Soc.* 217 (1999) 147.
87. T. L. Wade, L. C. Ward, C. B. Maddox, U. Happek, and J. L. Stickney, *Electrochem. Solid State Lett.* 2 (1999) 616.
88. M. P. Soriaga, *Prog. Surf. Sci.* 39 (1992) 325.

89. A. T. Hubbard, *CRC Crit. Rev. Anal. Chem.* 3 (1973) 201.
90. A. T. Hubbard and F. C. Anson, *Electroanal. Chem.* 4 (1970) 129.
91. B. W. Gregory, D. W. Suggs, and J. L. Stickney, *J. Electrochem. Soc.* 138 (1991) 1279.
92. M. P. Soriaga, D. A. Harrington, J. L. Stickney, and A. Wieckowski, in: B. E. Conway, J. O. Bockris, and R. E. White (Eds.), *Modern Aspects of Electrochemistry*, Plenum Press, New York, 1995, p. 1.
93. H. U. Muller, M. Zharnikov, B. Volkel, A. Schertel, P. Harder, and M. Grunze, *J. Phys. Chem. B* 102 (1998) 7949.
94. B. Jager, H. Schurmann, H. U. Muller, H. J. Himmel, M. Neumann, M. Grunze, and C. Woll, *Z. Phys. Chem. (Munich)* 202 (1997) 263.
95. K. Heister, M. Zharnikov, M. Grunze, L. S. O. Johansson, and A. Ulman, *Langmuir* 17 (2001) 8.
96. J. F. Moulder, W. F. Stickle, P. E. Soble, and K. D. Bomben, *Handbook of X-ray Photoelectron Spectroscopy*, Perkin-Elmer Corporation, Eden Prairie, 1992.
97. H. Gerischer, *Z. Elektrochem.* 54 (1950) 540.
98. P. L. Allen and A. Hickling, *Trans. Faraday Soc.* 53 (1957) 1626.
99. N. Ramasubramanian, *J. Electroanal. Chem.* 64 (1975) 21.
100. D. G. Wierse, M. M. Lohrengel, and J. W. Schultze, *J. Electroanal. Chem.* 92 (1978) 121.
101. A. Q. Contractor and H. Lal, *J. Electroanal. Chem.* 96 (1979) 175.
102. C. N. Vanhuong, R. Parsons, P. Marcus, S. Montes, and J. Oudar, *J. Electroanal. Chem.* 119 (1981) 137.

103. I. C. Hamilton and R. Woods, *J. Appl. Electrochem.* 13 (1983) 783.
104. E. Lamypitara, L. Bencharif, and J. Barbier, *Electrochim. Acta* 30 (1985) 971.
105. E. Lamy-Pitara and J. Barbier, *Electrochim. Acta* 31 (1986) 717.
106. A. N. Buckley, I. C. Hamilton, and R. Woods, *J. Electroanal. Chem.* 216 (1987) 213.
107. R. O. Lezna, N. R. Detacconi, and A. J. Arvia, *J. Electroanal. Chem.* 283 (1990) 319.
108. A. Briceno and S. Chander, *J. Appl. Electrochem.* 20 (1990) 506.
109. L. P. Colletti, D. Teklay, and J. L. Stickney, *J. Electroanal. Chem.* 369 (1994) 145.
110. L. G. Sillén, A. E. Martell, and J. Bjerrum, *Stability Constants of Metal-Ion Complexes*, Chemical Society, London, 1964.
111. A. Briceno and S. Chander, *J. Appl. Electrochem.* 20 (1990) 512.
112. B. G. Bravo, S. L. Michelhaugh, M. P. Soriaga, I. Villegas, D. W. Suggs, and J. L. Stickney, *J. Phys. Chem.* 95 (1991) 5245.
113. J. L. Stickney, S. D. Rosasco, G. N. Salaita, and A. T. Hubbard, *Langmuir* 1 (1985) 66.
114. G. N. Salaita, D. A. Stern, F. Lu, H. Baltruschat, B. C. Schardt, J. L. Stickney, M. P. Soriaga, D. G. Frank, and A. T. Hubbard, *Langmuir* 2 (1986) 828.
115. J. L. Stickney, B. W. Gregory, and C. Ehlers, *J. Electrochem. Soc.* 135 (1988) C158.
116. J. L. Stickney and C. B. Ehlers, *J. Vac. Sci. Technol., A* 7 (1989) 1801.
117. C. B. Ehlers, I. Villegas, and J. L. Stickney, *J. Electroanal. Chem.* 284 (1990) 403.

118. G. N. Salaita, F. Lu, L. Laguren-davidson, and A. T. Hubbard, *J. Electroanal. Chem.* 229 (1987) 1.
119. M. L. Foresti, M. Innocenti, H. Kobayashi, G. Pezzatini, and R. Guidelli, *J. Chem. Soc., Faraday Trans.* 92 (1996) 3747.
120. M. L. Foresti, M. Innocenti, F. Forni, and R. Guidelli, *Langmuir* 14 (1998) 7008.
121. F. Johnston and L. McAmish, *J. Colloid Interface Sci.* 42 (1973) 112.
122. E. Fatas, P. Herrasti, F. Arjona, E. G. Camarero, and J. A. Medina, *Electrochim. Acta* 32 (1987) 139.
123. M. G. Aylmore and D. M. Muir, *Miner. Eng.* 14 (2001) 135.
124. N. N. Greenwood and A. Earnshaw, *Chemistry of the Elements*, Pergamon Press, Oxford, 1984.
125. A. M. Pedraza, I. Villegas, P. L. Freund, and B. Chornik, *J. Electroanal. Chem.* 250 (1988) 443.
126. T. Jiang, J. Chen, and S. Xu, in: J. B. Hiskey and G. Warren (Eds.), *Hydrometallurgy: Fundamentals, Technology, and Innovations*, Society for Mining Metallurgy and Exploration, Littleton, 1993, p. 119.
127. J. Y. Chen, T. Deng, G. C. Zhu, and J. Zhao, *Trans. Indian Inst. Met.* 49 (1996) 841.
128. T. Hemmingsen, *Electrochim. Acta* 37 (1992) 2775.
129. A. Gomes, M. I. D. Pereira, M. H. Mendonca, and F. M. A. Costa, *J. Appl. Electrochem.* 25 (1995) 1045.
130. Z. Samec and J. Weber, *Electrochim. Acta* 20 (1975) 403.

131. H. Angerstein-Kozłowska, B. E. Conway, A. Hamelin, and L. Stoicoviciu, *Electrochim. Acta* 31 (1986) 1051.
132. S. Trasatti and O. A. Petrii, *J. Electroanal. Chem.* 327 (1992) 353.
133. R. Woods, D. C. Constable, and I. C. Hamilton, *Int. J. Miner. Process.* 27 (1989) 309.
134. M. S. Zei, D. Scherson, G. Lehmpfuhl, and D. M. Kolb, *J. Electroanal. Chem.* 229 (1987) 99.
135. R. L. McCarley, Y. T. Kim, and A. J. Bard, *J. Phys. Chem.* 97 (1993) 211.
136. X. Gao, Y. Zhang, and M. J. Weaver, *J. Phys. Chem.* 96 (1992) 4156.
137. J. Benard, J. Oudar, N. Barbouth, E. Margot, and Y. Berthier, *Surf. Sci.* 88 (1979) L35.
138. L. Pauling, *The Nature of the Chemical Bond and the Structure of Molecules and Crystals; an Introduction to Modern Structural Chemistry*, Cornell University Press, Ithaca, N.Y., 1960.
139. X. Gao, Y. Zhang, and M. J. Weaver, *Langmuir* 8 (1992) 668.
140. J. L. Stickney, S. D. Rosasco, G. N. Salaita, and A. T. Hubbard, *Abstr. Pap. Am. Chem. Soc.* 188 (1984) 8.
141. D. M. Kolb, D. L. Rath, R. Wille, and W. N. Hansen, *Ber. Bunsenges. Phys. Chem.* 87 (1983) 1108.
142. J. X. Wang, G. M. Watson, and B. M. Ocko, *J. Phys. Chem.* 100 (1996) 6672.
143. T. Ohmori, M. S. El-Deab, and M. Osawa, *J. Electroanal. Chem.* 470 (1999) 46.
144. T. Kawaguchi, H. Yasuda, K. Shimazu, and M. D. Porter, *Langmuir* 16 (2000) 9830.

145. Y. T. Kim, R. L. McCarley, and A. J. Bard, *Langmuir* 9 (1993) 1941.
146. P. N. Ross, in: J. Lipkowski and P. N. Ross (Eds.), *Structure of Electrified Interfaces*, VCH Publishers, Inc., New York, 1993, p. 35.
147. L. E. Davis, N. C. MacDonald, P. W. Palmberg, G. E. Riach, and R. E. Weber, *Handbook of Auger Electron Spectroscopy*, Physical Electronics Industries, Inc., Eden Prairie, 1976.
148. D. Briggs and M. P. Seah, eds., *Practical Surface Analysis*, John Wiley and Sons, Ltd., Chichester, 1983.
149. B. J. Lindberg, K. Hamrin, G. Johansson, U. Gelius, A. Fahlman, C. Nordling, and K. Siegbahn, *Phys. Scr.* 1 (1970) 286.
150. J. R. Mycroft, G. M. Bancroft, N. S. McIntyre, J. W. Lorimer, and I. R. Hill, *J. Electroanal. Chem. Interfacial Electrochem.* 292 (1990) 139.
151. S. C. Termes, A. N. Buckley, and R. D. Gillard, *Inorg. Chim. Acta* 126 (1987) 79.
152. L. S. Johansson, J. Juhanaja, K. Laajalehto, E. Suoninen, and J. Mielczarski, *Surf. Interface Anal.* 9 (1986) 501.
153. V. G. Bhide, S. Salkalachen, A. C. Rastogi, C. N. R. Rao, and M. S. Hegde, *J. Phys. D: Appl. Phys.* 14 (1981) 1647.
154. O. Azzaroni, G. Andreasen, B. Blum, R. C. Salvarezza, and A. J. Arvia, *J. Phys. Chem. B* 104 (2000) 1395.
155. P. J. D. Vandeberg, *J. Electroanal. Chem.* 362 (1993) 129.
156. D. Lincot, B. Mokili, R. Cortes, and M. Froment, *Microsc. Microanal. Microstruct.* 7 (1996) 217.
157. D. Lincot, R. Ortégaborges, and M. Froment, *Philos. Mag. B* 68 (1993) 185.

158. K. J. Stevenson, D. W. Hatchett, and H. S. White, *Isr. J. Chem.* 37 (1997) 173.
159. D. W. Hatchett, K. J. Stevenson, W. B. Lacy, J. M. Harris, and H. S. White, *J. Am. Chem. Soc.* 119 (1997) 6596.
160. T. T. T. Li and M. J. Weaver, *J. Am. Chem. Soc.* 106 (1984) 6107.
161. L. H. Dubois, B. R. Zegarski, and R. G. Nuzzo, *J. Chem. Phys.* 98 (1993) 678.
162. M. Hyun and C. K. Rhee, *Bull. Korean Chem. Soc.* 22 (2001) 213.
163. H. Hagenstrom, M. A. Schneeweiss, and D. M. Kolb, *Langmuir* 15 (1999) 2435.
164. D. W. Suggs and J. L. Stickney, *J. Phys. Chem.* 95 (1991) 10056.
165. T. A. Sorenson, K. Varazo, D. W. Suggs, and J. L. Stickney, *Surf. Sci.* 470 (2001) 197.
166. M. C. Bourg, A. Badia, and R. B. Lennox, *J. Phys. Chem. B* 104 (2000) 6562.
167. J. T. Roberts and C. M. Friend, *J. Phys. Chem.* 92 (1988) 5205.
168. N. K. Singh and D. C. Doran, *Surf. Sci.* 422 (1999) 50.
169. C. J. Zhong, R. C. Brush, J. Anderegg, and M. D. Porter, *Langmuir* 15 (1999) 518.
170. F. Bensebaa, Z. Yu, Y. Deslandes, E. Kruus, and T. H. Ellis, *Surf. Sci.* 405 (1998) L472.
171. M. E. Vela, H. Martin, C. Vericat, G. Andreassen, A. H. Creus, and R. C. Salvarezza, *J. Phys. Chem. B* 104 (2000) 11878.
172. D. Hobara, M. Yamamoto, and T. Kakiuchi, *Chem. Lett.* (2001) 374.

CHAPTER 5
CONCLUSIONS AND FUTURE STUDIES

Electrochemical atomic layer epitaxy (EC-ALE) is a method developed to form compound semiconductor thin films by electrodepositing each element of the material from a separate solution, in a cycle. Well-ordered atomic layers of each element are formed by underpotential deposition (UPD). By controlling growth at the atomic level, high quality compound semiconductors can be formed. This is facilitated in EC-ALE by controlling the electrode potential and solution composition, which affects the structure and composition of the deposited atomic layers. EC-ALE is a low cost alternative to high vacuum methods such as molecular beam epitaxy (MBE) [1] and metalorganic vapor phase epitaxy (MOVPE) [2], and offers more control parameters than chemical bath deposition (CBD) [3] methods.

The electrodeposition of atomic layers of cadmium, tellurium, sulfur, and monolayers of cadmium telluride on gold electrodes from aqueous solutions has been studied by cyclic voltammetry to determine the optimal solution compositions and electrode potentials required for the UPD of these elements and the formation of cadmium telluride. The structure and composition of cadmium, tellurium, and sulfur atomic layers, as well as cadmium telluride monolayers on Au(111) were examined using surface sensitive techniques: Auger electron spectroscopy (AES), low energy electron diffraction (LEED), X-ray photoelectron spectroscopy (XPS), and scanning tunneling microscopy (STM). These studies were performed in order to improve our understanding of the EC-ALE process, and to facilitate improved control over compound growth at the atomic scale.

In the two-step EC-ALE deposition of CdTe monolayers on Au(111), $(\sqrt{7} \times \sqrt{7})R19.1^\circ$ -CdTe and (3X3)-CdTe structures were observed by LEED. Results from

AES showed that the stoichiometry of the $(\sqrt{7}\times\sqrt{7})R19.1^\circ$ -CdTe monolayer was 1:1, and 2:1 for the (3×3) -CdTe monolayer. Both structures were formed using either cadmium or tellurium as a first layer. The highest quality (3×3) was formed using a three-step process: beginning with cadmium, then tellurium, and finally cadmium again. The highest quality $(\sqrt{7}\times\sqrt{7})R19.1^\circ$ was formed starting with a cadmium atomic layer. In situ STM showed that depositing cadmium on a $1/3$ ML tellurium layer resulted in the formation of clusters of UPD Cd, and CdTe did not completely cover the gold surface. These studies demonstrated how stoichiometry affects the structure and morphology of CdTe monolayers on Au(111).

Studies of cadmium electrodeposition on Au(111) in chloride, sulfate, iodide, acetate, and perchlorate solutions showed that ordered atomic layers were formed during cadmium UPD. Surface analysis showed the layers contained coadsorbed anions that influenced the structures observed by LEED and protected the cadmium from spontaneous oxidation during removal from solution. These layers can be used in the EC-ALE formation of CdTe, CdSe, and CdS compound semiconductors.

The formation of sulfur atomic layers on polycrystalline and (111) gold surfaces from alkaline solutions of sulfide, thiosulfate, thiourea, and ethanethiolate was studied using a thin layer electrochemical cell (TLEC) and UHV-EC techniques. A $1/3$ ML $(\sqrt{3}\times\sqrt{3})R30^\circ$ sulfur layer was formed using sulfide, thiosulfate, and thiourea solutions, over a range of electrode potentials. These sulfur layers can be used to form different sulfur-containing compound semiconductor materials, such as CdS and CuInS_2 . For ethanethiolate, a complex $(\sqrt{3}\times\sqrt{3})R30^\circ$ split-spot pattern with some (3×3) intensity was

observed with LEED, which should be related to the structures of alkanethiol self-assembled monolayers (SAMs).

Future Studies

The UHV-EC study of CdTe monolayers on Au(111) provided new information about the stoichiometry of the structures formed, and the effect of using each element as the first layer. An atomic level description of the structural changes that accompany the stoichiometric changes in CdTe monolayers can be obtained using in situ STM. A flow cell has been constructed for the STM that will provide sufficient flexibility in changing solutions; so that multiple layers can be formed and studied during deposition. Similar UHV-EC studies of CdTe formation should be performed on Au(100) and Au(110), as well as the low index planes of copper. Ordered structures for Cd UPD have been reported on Cu(111) [4], and Te deposition on Cd has been demonstrated in the work presented here. Additionally, the formation of other Te-containing compounds can be studied. Some preliminary experiments in this lab have shown that ZnTe electrodeposition on Au(111) forms a $(\sqrt{7} \times \sqrt{7})R19.1^\circ$ unit cell.

The study of Cd atomic layer formation has shown that metal layers are not oxidized during emersion, and their structure depends on coadsorbed anions. In situ STM studies are necessary to verify the unit cells observed by LEED and determine the positions of cadmium and anions in the unit cell. To date, only Cd UPD from sulfate electrolytes has been investigated [5-7]. UHV-EC should be used to study the electrodeposition of other metals such as zinc and indium, in different electrolytes. A few experiments have been conducted for both metals, where anions were detected by

AES and ordered structures were observed by LEED. XPS again showed no evidence of metal layer oxidation. The quartz crystal microbalance can be used as another measure of the coverage for cadmium and coadsorbed anions. Additionally, the cadmium solutions can be used in an EC-ALE automated flow cell deposition system to form thin films of CdTe or other cadmium-containing compound semiconductors.

The sulfur studies demonstrated that ordered sulfur layers were formed using sulfide, thiosulfate, and ethanethiolate. An in situ STM study of these systems will provide atomic level information on the sulfur layers, including possible verification of the (2X2) sulfur structure and the complex ethanethiolate structure. An in situ STM study of thiourea layers on Au(111) has been reported [8]. The sulfur layers should be used to form CdS and ZnS on Au(111), which can be studied using UHV-EC.

Thiosulfate and thiourea have been shown to undergo decomposition on gold surfaces and form a sulfur layer. In order to use these sulfur sources, however, it will have to be determined if decomposition occurs on a cadmium coated gold surface, since EC-ALE requires the alternated deposition of cadmium and sulfur to form CdS. UHV-EC can be used to determine what structures will be formed for CdS and ZnS using the metal or chalcogenide as the first layer, and after depositing multiple layers. The results can be compared with in situ STM studies by Shannon et al. [9-11]. Additionally, if these experiments are successful, they can be used in the automated flow cell to deposit much thicker CdS and ZnS thin films.

References

1. A. T. S. Wee, Z. C. Feng, H. H. Hng, K. L. Tan, R. F. C. Farrow, and W. J. Choyke, *J. Phys.: Condens. Matter* 7 (1995) 4359.
2. M. R. Czerniak and P. L. Anderson, *S. Afr. J. Sci.* 84 (1988) 645.
3. D. S. Boyle, A. Bayer, M. R. Heinrich, O. Robbe, and P. O'Brien, *Thin Solid Films* 361 (2000) 150.
4. C. Stuhlmann, Z. Park, C. Bach, and K. Wandelt, *Electrochim. Acta* 44 (1998) 993.
5. J. C. Bondos, A. A. Gewirth, and R. G. Nuzzo, *J. Phys. Chem.* 100 (1996) 8617.
6. B. K. Niece and A. A. Gewirth, *Langmuir* 13 (1997) 6302.
7. S. J. Hsieh and A. A. Gewirth, *Langmuir* 16 (2000) 9501.
8. O. Azzaroni, G. Andreasen, B. Blum, R. C. Salvarezza, and A. J. Arvia, *J. Phys. Chem. B* 104 (2000) 1395.
9. U. Demir and C. Shannon, *Langmuir* 10 (1994) 2794.
10. U. Demir and C. Shannon, *Langmuir* 12 (1996) 6091.
11. A. Gichuhi, B. E. Boone, U. Demir, and C. Shannon, *J. Phys. Chem. B* 102 (1998) 6499.